Ministério da Saúde

FIOCRUZ
Fundação Oswaldo Cruz

INSTITUTO OSWALDO CRUZ
Pós-Graduação em Biologia Celular e Molecular

PAPEL DOS CORPÚSCULOS LÍPIDICOS NA RESPOSTA ANTIBACTERIANA

FILIPE SANTOS PEREIRA DUTRA

RIO DE JANEIRO
2020

Ministério da Saúde

FIOCRUZ
Fundação Oswaldo Cruz

INSTITUTO OSWALDO CRUZ
Pós-Graduação em Biologia Celular e Molecular

FILIPE SANTOS PEREIRA DUTRA

Papel dos corpúsculos lipídicos na resposta antibacteriana

Tese apresentada ao Instituto Oswaldo Cruz como parte dos requisitos para obtenção do título de Doutor em Biologia Celular e Molecular.

Orientadora: Profa. Dra. Patrícia Torres Bozza

RIO DE JANEIRO
2020

Santos Pereira Dutra, Filipe.

Papel dos corpúsculos lipídicos na resposta antibacteriana / Filipe Santos Pereira Dutra. - Rio de janeiro, 2020.
247 f.

Tese (Doutorado) – Instituto Oswaldo Cruz, Pós-Graduação em Biologia Celular e Molecular, 2020.

Orientadora: Patrícia Torres Bozza.

Bibliografia: f. 69-92

1. Corpúsculos lípidicos. 2. Sepse. 3. antibacterano. 4. LTB4. 5. inflamação. I. Título.

Elaborada pelo Sistema de Geração Automática de Ficha Catalográfica da Biblioteca de Manguinhos/ICICT com os dados fornecidos pelo(a) autor(a).

Ministério da Saúde

FIOCRUZ
Fundação Oswaldo Cruz

INSTITUTO OSWALDO CRUZ
Pós-Graduação em Biologia Celular e Molecular

AUTOR: Filipe Santos Pereira Dutra

PAPEL DOS CORPÚSCULOS LÍPIDICOS NA RESPOSTA ANTIBACTERIANA

ORIENTADORA: Profa. Dra. Patrícia Torres Bozza

Aprovada em: 23 / 09 / 2020

EXAMINADORES:

Prof. Dr. Flavio Alves Lara – IOC/FIOCRUZ (Presidente)

Prof. Dra. Valéria de Matos Borges – Fiocruz/BA (Membro titular)

Prof. Dr. José Carlos Farias Alves Filho – USP/SP (Membro titular)

Prof. Dr. Heitor Affonso de Paula Neto - UFRJ/RJ (Suplente)

Prof. Dra. Roberta Olmo-Pinheiro – IOC/FIOCRUZ (Suplente e revisora)

Rio de Janeiro, 20 de outubro de 2020

Agradecimentos

Primeiramente, um enorme agradecimento à minha orientadora Dra Patricia Bozza, pela oportunidade, pela confiança, pela atenção e disposição ao longo de toda essa etapa acadêmica.

Às pesquisadoras Dra Luciana Souza-Moreira e Dra Ana Paula Teixeira Monteiro, pela ajuda, pela atenção e ensinamentos indispensáveis sem a qual não teria sido possível a realização desse trabalho.

À futura Dra Ellen Kiarely, minha parceira de bancada, de experimento e de viagem. Agradeço por toda ajuda indispensável; pela convivência durante as longas jornadas dos experimentos, pelas conversas e pelo companheirismo dentro e fora do laboratório.

À Dra Patricia Alves Reis, pelas ideias que iluminaram esse trabalho, pela sabedoria e truques de mágica que só uma grande pesquisadora poderia ter.

À Dra Livia Teixeira disposição e companheirismo durante todos os experimentos, pela convivência, pela conversa, pelo companheirismo dentro e fora do laboratório (e pelas comilanças).

Aos ICs que se dedicaram a esse projeto, Felipe Ferraro e Taynná Goldara, que me ensinaram muito como ser um pesquisador melhor.

Aos amigos que adquiri no laboratório de Imunofar: Ester, Tathiany, Tamirinha, Maria Fernanda, Lohanna, Érica, Milena, Mayara, Isaclaudia, Emílio, Vinicius, Suelen e Julia.

Aos demais colegas e membros do laboratório de Imunofarmacologia, que me ajudaram e que foram atenciosos, pois sem ajuda não se chega a lugar nenhum.

A todos os colegas e amigos que adquiri ao longo dessa jornada no Instituto Oswaldo Cruz e nas demais unidades da Fundação Oswaldo Cruz.

Às secretárias que possibilitaram que tudo desse certo, Julimar, da Secretaria Academica da BCM, e Rose Branco, do laboratório de Imunofarmacologia.

A minha família e a todos que acreditaram em mim.

E por fim, mas não menos importante ao Human Frontiers of Science Program e ao CNPq, sem os quais não teria sido possível a realização desse trabalho.

Muito obrigado!

"A simplicidade é o último grau de sofisticação"

Leonardo da Vinci

Ministério da Saúde

FIOCRUZ
Fundação Oswaldo Cruz

INSTITUTO OSWALDO CRUZ

PAPEL DOS CORPÚSCULOS LIPÍDICOS NA RESPOSTA ANTIBACTERIANA

RESUMO

TESE DE DOUTORADO

Filipe Santos Pereira Dutra

A sepse é uma disfunção orgânica ameaçadora à vida, secundária à resposta desregulada do organismo à infecção. Estudos recentes indicam que a reprogramação do metabolismo lipídico é crucial para sobrevivência à sepse bacteriana, desempenhando papéis centrais, tanto no combate à infecção sistêmica como na manutenção do suporte das funções vitais. No nível intracelular, o aumento da biogênese de corpúsculo lipídicos (CLs) foi demonstrado em pacientes sépticos e em modelos experimentais de sepse. CLs são organelas dinâmicas e complexas que fornecem a todas as células eucarióticas substratos lipídicos. Apesar de diversos patógenos estimularem a biossíntese dessa organela como parte de suas estratégias de evasão do sistema imune ou para a obtenção de uma fonte de energia e nutrientes, muitos detalhes sobre a interação patógeno / CLs ainda são desconhecidos. Resultados recentes vêm demonstrando uma outra face desta interação patógeno-hospedeiro, indicando que os CL podem também participar ativamente na resposta pró-hospedeiro, inclusive apresentando atividade antibacteriana em drosophilas. No entanto, a participação de CLs na atividade antibacteriana não foi explorada em mamíferos. Nosso objetivo neste trabalho foi analisar a participação dos CLs na resposta antibacteriana. Para isso foram realizados experimentos in vitro, em macrófagos estimulados com *E. coli e*, experimentos in vivo no modelo de sepse experimental induzido pela ligação cecal e perfuração (CLP). Nossos dados mostram que a modulação da quantidade dessa organela afeta a capacidade de *killing* dos macrofagos frente à *E. coli*. Além de elevar o número de bacterias viáveis intracelulares, a redução do acúmulo de CL em macrófagos é acompanhada pela redução da produção de PGE_2, lactato e óxido nitrico. Esses achados in vitro foram corroborados in vivo no modelo de CLP. Observamos que a inibição da biogênese de CLs nos leucócitos peritoneais resulta no aumento da carga bacteriana tanto local como sistêmica. Diferente do observado in vitro, nesse modelo nós observamos que a inibição da biogenese de CL afetou principalmente a quantidade dos mediadores inflamatórios do eixo LTB_4/IL-6 no início da infecção. Além disso, nós observamos que os CLs hepáticos induzidos pela sepse atuam na resposta antibacteriana autonôma das células, apresentando uma atividade antibacteriana direta, principalmente devido ao seu conteúdo proteico. Nesse contexto. diferente ao observado em *Drosophila*, os CLs não compartimentalizam histonas. Em vez disso, observamos a presença de catelicidina e HMGB-1 (*High mobility group Box-1*), duas proteinas antibacterianas nos CL, juntamente com a viperina, uma proteina antiviral, sugerindo que essa organela seja central na resposta pró-hospedeiro das células. Em conjunto, nossos dados destacam que os CLs são centrais na resposta imune inata frente a infecções por bactérias extracelulares em mamíferos.

Ministério da Saúde

FIOCRUZ
Fundação Oswaldo Cruz

INSTITUTO OSWALDO CRUZ

PAPEL DOS CORPÚSCULOS LIPÍDICOS NA RESPOSTA ANTIBACTERIANA

RESUMO/ABSTRACT

TESE DE DOUTORADO

Filipe Santos Pereira Dutra

Sepsis is a life-threatening organ dysfunction caused by a dysregulated host response to infection. Recent studies indicate that lipid metabolism reprogramming is crucial for the survival of bacterial sepsis, playing central roles both in systemic infection control and in the maintenance of support of vital functions. At the intracellular level, the increased lipid droplet (LDs) biogenesis has been demonstrated in septic patients and experimental models of sepsis. LDs are dynamic and complex organelles that provide all eukaryotic cells with lipid substrates. Although several pathogens stimulate the biosynthesis of this organelle as part of their strategies to evade the immune system or to obtain a source of energy and nutrients, many details about the pathogen / LDs interaction are still unknown. Recent results have shown another side of this pathogen-host interaction, indicating that LD can also participate actively in the pro-host response, including showing antibacterial activity in drosophilas. However, the participation of LDs in antibacterial activity was not explored in mammals. Our objective in this work was to analyze the participation of LDs in the antibacterial response. For that, so many experiments were carried out in vitro, with macrophages infected with E. coli, as in vivo experiments in the experimental sepsis model induced by the cecal connection and perforation (CLP). Our data show that modulation of the amount of this organelle affects the killing capacity of macrophages. In addition to increasing the number of viable intracellular bacteria, the reduction in LD accumulation in macrophages is accompanied by a decrease in the synthesis of PGE2, lactate, and nitric oxide. These in vitro findings have collaborated in vivo on the CLP model. We observed that the inhibition of LD biogenesis in peritoneal leukocytes results in increased both local and systemic bacterial load. Unlike in vitro, in this model, we observed that the inhibition of LD biogenesis mainly affected of inflammatory mediators of the LTB4 / IL-6 axis at the beginning of the infection. Also, we observed that hepatic LDs induced by sepsis act on the autonomous antibacterial response of cells, presenting a direct antibacterial activity, mainly due to their protein content. Different from Drosophila, mammals LDs do not compartmentalize histones. Instead, we observed the presence of cathelicidin and HMGB-1 (*High mobility group Box-1*), two antibacterial proteins on LD, together with viperine, an antiviral protein, suggesting that this organelle is central to the autonomous pro-host response of cells. Together, our data highlight that LDs are also central to the innate immune response to infections by extracelular bacterial in mammals.

Sumário

1. INTRODUÇÃO 1
1.1. Sepse 1
1.2. Inflamação e infecções bacterianas 2
1.3. Imunometabolismo nas infecções bacterianas e na sepse 5
1.4. Os corpúsculos lipídicos 8
1.5. Biogênese de CLs nos leucócitos 9
1.6. Corpúsculos lipídicos na inflamação e infecção 10
1.7. Corpúsculos lipídicos na infecção bacteriana 13
2. JUSTIFICATIVA E HIPÓTESE 17
3. OBJETIVOS 18
3.1. Objetivo geral 18
3.2. Objetivos específicos: 18
4. METODOLOGIA 19
4.1. Animais 19
4.2. Diferenciação dos macrófagos a partir de medula óssea murina 19
4.3. Pré-tratamentos in vitro 20
4.4. Cultura da *Escherichia coli* 20
4.5. Infecção por *Escherichia coli* (Ensaio de proteção a gentamicina) 20
4.6. Marcação de CLs e microscopia confocal 21
4.7. Dosagem de lactato 21
4.8. Dosagem de óxido nítrico 21
4.9. Mensuração dos mediadores inflamatórios lipídicos no sobrenadante celular 22
4.10. Dosagem de citocinas 22
4.11. Determinação da atividade da enzima lactato desidrogenase (LDH) 22
4.12. Modelo de Sepse experimental (CLP) 23
4.13. Tratamento com inibidor da DGAT-1 23
4.14. Avaliação do escore clínico de gravidade da sepse 24
4.15. Coletas das amostras 25
4.16. Quantificação da carga bacteriana 26
4.17. Análises dos parâmetros celulares (leucometria) e quantificação dos CLs 26
4.18. Avaliação dos triglicerídeose colesterol no sangue 26
4.19. Dosagem de 8-Isoprostano e LTB4 no lavado peritoneal 27
4.20. Contagem total e diferencial do sangue 27
4.21. Análise histológica do fígado 27
4.22. Cromatografia em camada fina (TLC) 27

4.23. Determinação das substâncias reativas ao ácido tiobarbitúrico (TBARS) 28
4.24. Determinação total de grupos tiólicos 28
4.25. Determinação da atividade da Mieloperoxidase 29
4.26. Isolamento de corpúsculo lipídicos por fracionamneto celular 29
4.27. Ensaio de antividade antibacteriana in vitro 30
4.28. Western blotting 31
4.29. Análise estatística 32
5. RESULTADOS 33
5.1. Modulação da quantidade de CLs afeta a capacidade de *killing* de macrófagos 33
5.2. CLs interage com bactérias internalizadas 35
5.3. Inibição do acúmulo de CLs afeta a resposta inflamatória dos macrófagos 37
5.4. A inibição da biogênese de CLs afeta a carga bacteriana in vivo. 39
5.5. Tratamento com A922500 eleva a bacteremia nos animais sépticos, mas não interfere na dislipidemia. 41
5.6. O metabolismo lipídico hepático não está envolvido na disseminação da infecção no inicio da sepse. 43
5.7. O papel protetor do CLs frente à infecção bacteriana perdura no tempo 24h após a cirurgia. 45
5.8. O papel imunometabólico dos CLs é mais proeminente em tempos mais precose durante a sepse 47
5.9. Inibição da enzima DGAT-1 não interfere na sobrevivência e nem na gravidade da sepse 49
5.10. CLs de macrofágos murinos não compartimentalizam histonas 51
5.11. CLs hepáticos induzidos pela sepse apresentam atividade antibacteriana 53
5.12. A atividade antibacteriana das proteínas de CLs é dependente da dose e do tempo 55
5.13. CLs compartimentalizam proteínas pró-hospedeiro 57
6. DISCUSSÃO 59
7. CONCLUSÕES 68
8. REFERÊNCIAS BIBLIOGRÁFICA 69
Anexos 93

LISTA DE ABREVIATURAS

ACAT acil-CoA:colesterol aciltransferase

AO ácido oléico

BPKA Ensaio de morte bacteriana em placa, do inglês *bacterial plate killing assay*

CAMP catelicidina, do inglês *Cathelicidin* antimicrobial peptides

CCL2 Ligante 2 de Quimiocina com Motivo C-C do inglês *chemokine (C-C motif) ligand 2*

CL corpúsculo lipídico

CLP ligadura e perfuração cecal, do inglês *cecal ligation and puncture*

COX ciclo-oxigenase

DGAT Diacilglicerol O-Aciltransferase

EDTA ácido etilenodiamino tetra-acético

EGTA ácido etileno glicol-bis-(ß-aminoetil eter)-NN'-tetra acético

FASN: ácido graxo sintase, do inglês Fatty acid synthase

GFP proteína verde fluorescente, do inglês *green fluorescent protein*

HIF fatores induzíveis por hipóxia, do inglês *Hypoxia-inducible factors*

IFN interferons

HMGB-1 proteína caixa 1 do grupo de alta mobilidade, do inglês *High mobility group box 1 protein*

H1 histona 1

H2a histona 2a

H2b histona 2b

IL-1β Interleucina 1β

IL-6 Interleucina 6

IL-10 Interleucina 10

iNOS óxido nítrico sintase induzível, do inglês *inducible nitric oxide synthase*

Irgm proteína da família M GTPase relacionada à imunidade, do inglês *Immunity-related GTPase family M protein*

LDH Lactato desidrogenase, do inglês *Lactate dehydrogenase*

LOX lipoxigenase

LPS lipopolissacarídeo

LTB_4 leucotrieno B_4

LXR receptor X do fígado, do inglês liver X receptor

MDA malonaldeídeido

MCP-1 proteína quimioatraente de monócitos-1, do inglês *Monocyte Chemoattractant Protein-1*

MΦ macrófagos

NO óxido nítrico, do inglês *nitric oxide*

ORO *Oil red O*

Plin2 perilipina 2

Plin3 perilipina 3

Plin5 perilipina 5

PGE_2 prostaglandina E_2

PPAR receptores ativados por proliferador de peroxissoma, do inglês *peroxisome proliferator-activated receptor*

SPN sobrenadante pós-núcleo

SREBP proteína de ligação ao elemento regulador de esterol, do inglês *Sterol regulatory element-binding proteins*

TLR receptores semelhantes a Toll, do inglês *Toll-like receptor*

TBARS substâncias reativas ao ácido tiobarbitúrico, do inglês *Thiobarbituric acid reactive substances*

1. INTRODUÇÃO

1.1. A sepse

A sepse é um grave problema de saúde pública, que se desenvolve a partir de uma resposta desregulada do hospedeiro à uma infecção associada à uma disfunção orgânica aguda (CECCONI *et al.*, 2018). Apesar da sepse poder ser desencadeada por uma infecção causada por qualquer tipo de microorganismo invasor, a grande maioria dos casos de sepse estão associadas à infecções bacterianas, em especial bactérias Gram-negativas, sendo os principais agentes etiológicos a *Escherichia coli, Klebsiella pneumoniae, Pseudomonas aeruginosa* e *Enterobacter* sp. (BARROS; MAIA; MONTEIRO, 2016; CECCONI *et al.*, 2018; LOBO *et al.*, 2019). A sepse é a principal causa de morte nas Unidades de Tratamento Intensivo (FLEISCHMANN *et al.*, 2016), sendo a ela atribuídos cerca de 49 milhões de casos e 11 milhões de óbitos em todo o mundo somente no ano 2017 (RUDD *et al.*, 2020). Apesar dos inúmeros avanços nos últimos anos no diagnóstico e no tratamento, a sepse continua apresentando uma alta mortalidade, superior a 25 %, chegando à cerca de 50 % na presença de choque séptico, condição mais grave na evolução da sepse (HOTCHKISS; MONNERET; PAYEN, 2013; LUHR *et al.*, 2019; VINCENT *et al.*, 2014), principalmente em países subdesenvolvidos (RUDD *et al.*, 2020). No Brasil, a taxa de mortalidade de pacientes com sepse foi de 30% segundo dados do projeto UTIs Brasileiras (LOBO *et al.*, 2019). O impacto da sepse não se restringe à fase aguda da doença, na fase subsequente à alta hospitalar os sobreviventes ainda enfrentam uma redução da qualidade e da expectativa de vida (QUARTIN *et al.*, 1997; WESTPHAL *et al.*, 2012; WINTERS *et al.*, 2010)

A definição de sepse sofreu constantes alterações no decorrer dos anos, segundo o último consenso internacional (Sepse-3) ela passou a ser definida como uma disfunção orgânica ameaçadora à vida secundária à resposta desregulada do organismo à infecção (SINGER *et al.*, 2016). Já o choque séptico passou a ser definido como uma forma generalizada de falência circulatória aguda ameaçadora à vida, associada à utilização inadequada de oxigênio pelas células (SINGER et al., 2016). Com a mudança no entendimento sobre a sepse também houve alteração no diagnóstico de sepse. Com base no Sepse-3, o diagnóstico clínico da sepse passou a embasar a disfunção orgânica através da variação de dois ou mais pontos no escore *Sequential Organ Failure Assessment* (SOFA), e não mais na presença dos critérios da síndrome da resposta

inflamatória sistêmica (SRIS) (MACHADO *et al.*, 2016; SINGER *et al.*, 2016). Com essa nova definição, a sepse deixou de ser classificada como uma doença essencialmente inflamatória (MACHADO et al., 2016; VAN WYNGENE et al., 2018). A heterogeneidade presente nos pacientes sépticos e critérios muito abrangentes pode explicar o motivo que diversos ensaios clínicos falharam nos últimos anos (REINHART et al., 2012; VAN WYNGENE et al., 2018), inclusive utilizando a proteína C reativa humana recombinante (Drotrecogin-α)(HECKSHER; LACERDA; MACIEL, 2008). A compreensão de que a sepse é um distúrbio complexo é reforçada por diversos estudos que destacam a contribuição da coagulação, do sistema complemento, da composição microbiana, da termorregulação, do ciclo circadiano e do metabolismo, além da inflamação sistêmica, na patofisiologia da sepse (CLAUSHUIS *et al.*, 2016; COHEN *et al.*, 2015; HEIPERTZ *et al.*, 2018; NOGUEIRA *et al.*, 2007; O'CALLAGHAN *et al.*, 2012; RANNIKKO *et al.*, 2017; SCHIEBER; AYRES, 2016; SHARMA *et al.*, 2019; STRNAD *et al.*, 2017; VAN WYNGENE; VANDEWALLE; LIBERT, 2018).

Durante o processo infeccioso diversas adaptações fisiológicas são feitas no organismo hospedeiro, tanto para combater o patógeno como para limitar o dano desse processo aos tecidos (MCCARVILLE; AYRES, 2018; SCHNEIDER; AYRES, 2008). Do ponto de vista ecológico e fisiológico a atuação do sistema imunológico no processo infeccioso pode ser dividido em dois processos biológicos distintos; a resistência à infecção, relacionada à capacidade de detecção e eliminação dos patógenos e, a tolerância à doença, que agrupa diversas adaptações que promovem a minimização do danos aos tecidos (SCHNEIDER; AYRES, 2008; SOARES; TEIXEIRA; MOITA, 2017). Uma resposta adequada a um processo infeccioso é dependente de um delicado equilíbrio entre esses dois processos biológicos (SOARES; TEIXEIRA; MOITA, 2017; WANG; LUAN; MEDZHITOV, 2019; WEIS *et al.*, 2017). A quebra desse delicado equilíbrio esta fortemente associado com a fisiopatologia da sepse e com a falência múltipla de orgãos (SOARES; TEIXEIRA; MOITA, 2017; WEIS *et al.*, 2017).

1.2. Inflamação e infecções bacterianas

Os mecanismos envolvidos no processo de resistência do organismo à infecção são os mecanismos imunológicos mais bem caracterizados, sendo profundamente associados com a resposta inflamatória induzida pela infecção. Alterações nesses

processos levam à perda do controle do processo infeccioso, levando ao aumento e a disseminação dos patógenos no organismo (MCCARVILLE; AYRES, 2018; WANG; LUAN; MEDZHITOV, 2019; WEIS *et al.*, 2017). A resposta inflamatória induzida pela infecção é composta tipicamente por quatro componentes principais: indutores inflamatórios, sensores que os detectam, mediadores inflamatórios induzidos pelos sensores e tecidos-alvo afetados pelos mediadores inflamatórios. Para cada tipo de reposta inflamatória, os componentes podem ser apresentados de múltiplas formas e as diferentes combinações desses elementos irão desencadear vias inflamatórias distintas (MEDZHITOV, 2010).

No caso especifico das infecções bacterianas, em geral, o desencadeamento da resposta inflamatória começa pela detecção de padrões moleculares associados aos patógenos (PAMPs) por receptores do sistema imune inato, expressos nos macrófagos residentes ou em monócitos patrulheiros, sendo os receptores semelhantes ao Toll (TLRs) alguns dos mais estudos. O reconhecimento de patógenos por essa família de receptores leva à produção de citocinas pró-inflamatórias (TNF-α, IL-1β, IL-6) e de quimiocinas (CCL2/MCP1 e CXCL8), bem como a síntese de prostaglandinas. Esses mediadores inflamatórios coordenam tanto a resposta inflamatória local como a sistêmica aos produtos microbianos, atuando nos tecidos-alvos e também nos vasos sanguíneos locais, induzindo a vasodilatação, o recrutamento e a translocação de neutrófilos, além do extravazamento do plasma para o tecido infectado (JANEWAY; MEDZHITOV, 2002; MEDZHITOV, 2008, 2010; PECCHI *et al.*, 2009).

Os neutrófilos recrutados, assim como os macrófagos residentes e os mastócitos teciduais são os grandes responsáveis pela eliminação dos patógenos invasores (MEDZHITOV, 2010). Os fagócitos profissionais dispõem de uma ampla gama de mecanismos microbicidas extremamentes eficientes para eliminação dos agentes invasores (MURRAY; WYNN, 2011; SOEHNLEIN; LINDBOM, 2010). No sítio da infecção, tanto os neutrófilos como os macrófagos fagocitam os microrganismos, produzem espécies reativas de oxigênio e nitrogênio, e secretam diversos peptídeos e moléculas antimicrobianas, como os peptídeos da família das catelicidinas (MURRAY; WYNN, 2011; SOEHNLEIN; LINDBOM, 2010; VAN HARTEN *et al.*, 2018). Esse processo pode ser auxiliado por componentes proteicos do plasma, principalmente anticorpos, proteínas do sistema complemento e proteínas de fase aguda (MEDZHITOV, 2010).

Ao nível intracelular, as bactérias fagocitadas são eliminadas principalmente pelas diversas enzimas e proteínas antimicrobianas contidas nos lisossomos ou nos grânulos citoplasmáticos dos fagócitos, entre elas lipases, proteases, lisozima, hidrolases, muramidase, mieloperoxidase e proteínas catiônicas (COWLAND; BORREGAARD, 2016; GAJDA; BUGLA-PŁOSKOŃSKA, 2014; O'NEILL; KISHTON; RATHMELL, 2016; SONAWANE *et al.*, 2011). Em conjunto à ação dessas proteínas antimicrobianas, há a produção de espécies reativas de oxigênio, como o ânion superóxido (O_2^-), o peróxido de hidrogênio (H_2O_2) e o ácido hipocloroso (HOCl), produzidos respectivamente pela ação da NADPH-oxidase, superóxido dismutase e mieloperoxidase, respectivamente (DUPRÉ-CROCHET; ERARD; NÜBE, 2013; JOSEPH *et al.*, 2017). A produção destas espécies reativas de oxigênio é desencadeada pela ativação do sistema da NADPH oxidase, que se organiza na membrana dos vacúolos fagocitários, resultando em um grande consumo de oxigênio pelos fagócitos (explosão respiratória), essencial para o controle da infecção (ABDELMAGEED; EL-AWADY; SUDDEK, 2016; ATASHI; MODARRESSI; PEPPER, 2015; DUPRÉ-CROCHET; ERARD; NÜBE, 2013; GAJDA; BUGLA-PŁOSKOŃSKA, 2014; JANN *et al.*, 2011; KONG *et al.*, 2010; SONAWANE *et al.*, 2011; XU *et al.*, 2016). Entre as espécies reativas de oxigênio e nitrogênio, merece destaque o óxido nitrico (NO), essencial para o controle da infecção bacteriana, tanto como um agente antibacteriano, como um importante mediador pro-inflamatório (MURRAY; WYNN, 2011; SOEHNLEIN; LINDBOM, 2010).

Dependendo da sua concentração, os mediadores pró-inflamatórios induzidos no sítio da infecção podem ter efeitos sistêmicos, induzindo a produção de proteínas de fase aguda, como proteína C reativa e fatores de coagulação pelos hepatócitos. Ao nível sistêmico, o fígado é um órgão central na detecção, captura e eliminação de patógenos que estejam presentes na circulação sanguínea (KUBES; JENNE; SNYDER, 2018; YAN; LI; LI, 2014), e alterações nesse órgão reduzem a capacidade do organismo de lidar com as infecções sistêmicas (CANABAL; KRAMER, 2008). Por fim, as citocinas inflamatórias também agem sobre o endotélio cerebral, induzindo a produção local de prostaglandinas, incluindo a PGE_2, a principal prostaglandina pró-inflamatória. Por sua vez, a PGE_2 induz populações específicas de neurônios do sistema nervoso central a promover o chamado comportamento doentio (*sickness behavior*): febre, anorexia, fadiga, sonolência e retraimento social (MEDZHITOV, 2010; PECCHI *et al.*, 2009).

1.3. Imunometabolismo nas infecções bacterianas e na sepse

Para o correto desencadeamento e a manutenção da resposta inflamatória essencial para controle da infecção é necessário a realocação de recursos metabólicos (energia e metabólitos) no hospedeiro (WANG; LUAN; MEDZHITOV, 2019). A interação do processo inflamatório com o metabolismo é um fenômeno complexo e multifacetado, que deve ser precisamente regulado para apoiar as funções biológicas tanto no nível celular, tecidual e organizacional (WANG; LUAN; MEDZHITOV, 2019). Os efeitos metabólicos da infecção influenciam inúmeras vias bioquímicas e diversos mecanismos moleculares do hospedeiro, dando suporte aos sistemas de defesa utilizados pelo organismo para controlar ou eliminar os agentes patogênicos (BEISEL, 1975). A alocação de recursos metabólicos durante a resposta inflamatória envolve tanto processos biossintéticos que consomem energia (anabolismo) como aqueles que geram energia (catabolismo) (WANG; LUAN; MEDZHITOV, 2019). Estudos recentes indicam que alterações no metabolismo durante a infecção desempenham papéis centrais tanto no combate à infecção sistêmica como na manutenção do suporte das funções vitais, especialmente diante da baixa ingestão energética de pacientes em estado grave (ENGLERT e ROGERS, 2016; WANG et al., 2016).

Em resposta à infecção bacteriana sistêmica, o organismo ativa um estado hipercatabólico (WANG *et al.*, 2016), mobilizando suas reservas energéticas, o que culmina em uma reprogramação metabólica de todos os macronutrientes (SAMRA; SUMMERS; FRAYN, 1996; VAN WYNGENE; VANDEWALLE; LIBERT, 2018). Essas respostas metabólicas sistêmicas são iniciadas e moduladas pela liberação de mediadores endógenos, hormônios e também por estímulos do sistema nervoso central. A magnitude dessas alterações metabólicas pode ser influenciada pela gravidade e duração da doença (BEISEL, 1975; VAN WYNGENE; VANDEWALLE; LIBERT, 2018). Apesar de clinicamente os efeitos metabólicos mais visíveis de uma doença infecciosa serem os catabólicos (BEISEL, 1975), os mediadores inflamatórios induzidas pela infecção tendem a ativar processos anabólicos nas células do sistema imunológico, igualmente importantes para o sucesso dos mecanismos defensivos do hospedeiro (BEISEL, 1975; WANG; LUAN; MEDZHITOV, 2019).

A reprogramação metabólica das células imunes está intimamente relacionadas as diferentes funções e atividades que essas células desempenham na homeostase e na inflamação, em especial no caso dos macrófagos, células dendríticas e células T (BEISEL,

1975; WANG; LUAN; MEDZHITOV, 2019). Durante processos infecciosos, a ativação dos TLRs induz as células T efetoras e os macrófagos a adquirirem metabolismo glicolítico e anabólico. Em contrapartida, alguns mediadores anti-inflamatórios promovem programas metabólicos nessas células que não são suportivos à resposta pró-inflamatória (O'NEILL; KISHTON; RATHMELL, 2016). A desregulação desses processos está subjacente à muitas doenças humanas modernas, como diabetes, obesidade e na própria sepse (BEISEL, 1975; WANG; LUAN; MEDZHITOV, 2019).

Em diversas análises sistemáticas de alterações fisiopatológicas induzidas pela sepse, o metabolismo lipídico vem emergindo como um dos mais profundamente remodelados. Como fruto de um desbalanço energético sistêmico, diversas alterações da homeostase lipídica acontecem durante a sepse **(Figura 1)**, entre elas: o aumento da lipólise no tecido adiposo, a diminuição da β-oxidação nos tecidos periféricos, a diminuição da cetogênese, dislipidemia, aumento da lipotoxidade, disfunção mitocondrial, esteatose, desregulação da síntese de mediadores inflamatórios e aumento da peroxidação lipídica (HENRICH *et al.*, 2013; LEE *et al.*, 2013; LORENTE *et al.*, 2013; PACHECO *et al.*, 2002, 2007; SAMRA; SUMMERS; FRAYN, 1996; VAN WYNGENE; VANDEWALLE; LIBERT, 2018; WARE *et al.*, 2011; WEIS *et al.*, 2017). Resultados recentes, através de abordagens metabolômicas e proteômicas, apontaram as alterações no metabolismo lipídico como a principal adaptação de pacientes sépticos e importantes preditores da mortalidade (LANGLEY *et al.*, 2013; ROGERS *et al.*, 2014; SHARMA *et al.*, 2019).

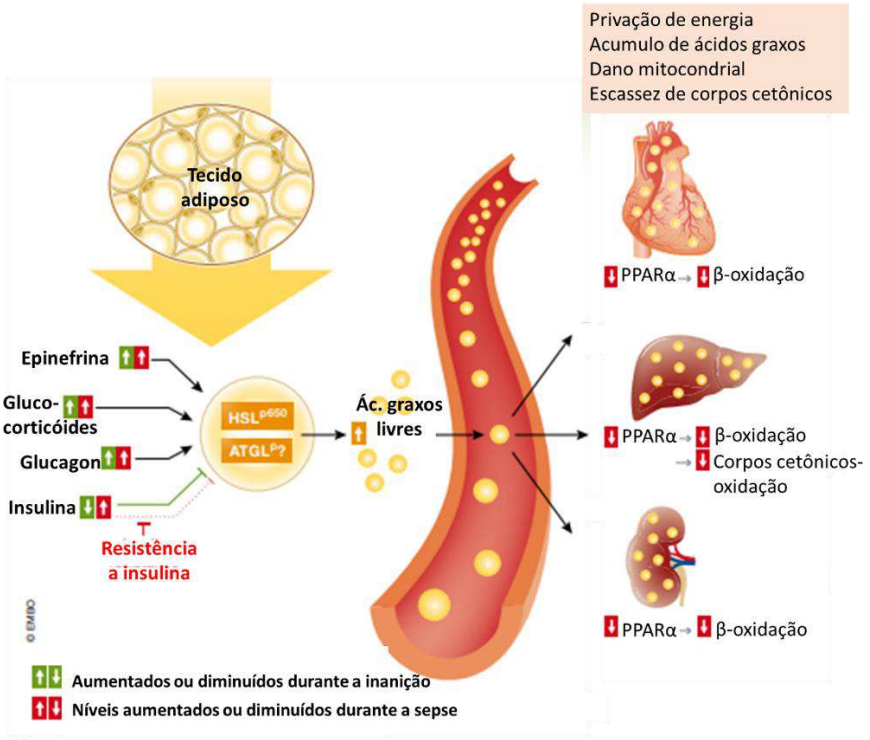

Figura 1: A **sepse induz um remodelamento do metabolismo lipídico.** Durante a sepse diversas alterações ocorrem no metabolismo lipídico. (Adaptado de VAN WYNGENE *et al.*, 2018). Em virtude da privação energética há uma reprogramação metabolica sistêmica, desencadeada pelo liberação de hormônios hiperglicemiantes, como o glucagon, glucocorticóides e epinefrina, e diferente da inanição, há também o aumento dos níveis de insulina durante a sepse. A presença desses hormônios leva a ativação das lipases (HSL e ATGL) nas células do tecido adiposo e a liberação de ácidos graxos para corrente sanguínea, levando a lipimia nos pacientes sépticos. Esse excesso de lipideos circulantes são armazenados em diversos tecidos, na sua forma esterificada (os triglicerídeos), levando a esteatose ou degeneração gordurosa, principalmente no fígado, rim e coração.

Os lipídios são a principal fonte de energia em pacientes com infecções, e, adaptações no metabolismo lipídico são um requisito crucial para sobrevivência à sepse bacteriana em modelos experimentais (GARRIDO; FIGUEIREDO; SILVA, 2004; SAMRA; SUMMERS; FRAYN, 1996; WANG *et al.*, 2016). Os lipídios formam a classe mais diversa das biomoléculas, com papéis chaves na fisiologia dos sistemas vivos, tanto na homeostase quanto em situações patológicas. Além de atuar como componentes estruturais das membranas celulares, os lipídios são fontes de energia e também moléculas sinalizadoras em processos inflamatórios e infecciosos (PEREIRA-DUTRA *et al.*, 2019; TENG; ANG; GUAN, 2017; VAN MEER; VOELKER; FEIGENSON, 2008).

No nível celular, a dislipidemia induzida pela sepse também leva ao acúmulo ectópico de ácidos graxos e triglicerídeos através do aumento da quantidade de corpúsculos lipídicos (CLs) em tecidos não adiposos (LEE *et al.*, 2013; PACHECO *et al.*, 2002, 2007), quadro clinicamente conhecido como *esteatose* ou degeneração gordurosa.

Na célula as organelas centrais na homeostase lipídica, são os CLs ou gotículas lipídicas, (BOZZA *et al.*, 2009; FARESE; WALTHER, 2009).

1.4. Os corpúsculos lipídicos

Os CLs são organelas complexas e dinâmicas derivadas do reticulo endoplasmático, formadas por um núcleo de lipídeos neutros (ésteres de colesterol e triacilgliceróis) envoltos por uma monocamada de fosfolipídios associada a um conteúdo proteico diversificado (FARESE; WALTHER, 2009; MELO *et al.*, 2011a). O tamanho, a função e constituição lipídica e proteica dos CLs são dependentes do tipo e do estágio celular (POL; GROSS; PARTON, 2014; WALTHER; FARESE, 2012; WELTE, 2015).

Apesar do conteúdo protéicos dos CLs ser dependente do tipo celular, a montagem e a biogênese dessas organelas é dependente de proteínas estruturais pertencentes a família das perilipinas, um conjunto de 5 proteínas (BRASAEMLE, 2007; ITABE *et al.*, 2017), sendo as mais conhecidas a Perilipina-2 (Plin2/ADRP) (GAO; SERRERO, 1999; HUANG *et al.*, 2014; SILVA *et al.*, 2009) e a Perilipina-3 (Plin3/TIP47) (FAN *et al.*, 2013; PLOEN *et al.*, 2013). Além disso, as diferentes perilipinas vêm sendo associadas com as diferentes funções dos CLs nos diferentes tipos celulares (ITABE *et al.*, 2017).

Nas últimas décadas os CLs deixaram de ser vistos apenas como um depósito inerte de lipídios e passaram a ser caracterizados como uma plataforma celular envolvida em diversos processos celulares. Além disso, CLs são estruturas centrais na homeostase lipídica e energética, na biossíntese das membranas celulares, na proteção da lipotoxicidade e na sinalização celular (FUJIMOTO; OHSAKI, 2006; FUJIMOTO; PARTON, 2011; OLZMANN; CARVALHO, 2019; SAKA; VALDIVIA, 2012; VIKTOROVA *et al.*, 2018; WELTE, 2015; WILFLING *et al.*, 2013). Além disso, diversas evidências vêm demonstrando que os CLs são importantes sítios de compartimentalização tanto de vias de sinalização como do metabolismo, principalmente as do metabolismo lipídico (DUCHARME; BICKEL, 2008) e da síntese de eicosanóides (BOZZA *et al.*, 1998, 2011).

1.5. Biogênese de CLs nos leucócitos

Apesar dos CLs serem virtualmente presentes em todos os tipos de celulares, o aumento no tamanho e no número de CLs nas células envolvidas em processos infecciosos e inflamatórios ocorrem com tanta frequência que os CLs vêm sendo considerados marcadores estruturais da inflamação (ROINGEARD; MELO, 2017). A biogênese de CLs nos leucócitos é um processo rápido e altamente regulado, cujos mecanismos e vias de sinalização mobilizadas dependem do agente infeccioso e do tipo celular envolvido (BOZZA; MAGALHÃES; WELLER, 2009).

Embora os mecanismos moleculares que governam a biogênese dos CLs durante a inflamação e infecção ainda sejam incompletos, sabemos que é um processo complexo envolvendo multiplos mecanismos, como o aumento da captação lipídica, inibição da lipólise, síntese *de novo* de lipídeos, diminuição da β-oxidação, remodelamento lipidico e/ou autofagia (BOSCH; PARTON; POL, 2020; MELO *et al.*, 2011a). Além disso, foi demonstrado que esse fenômeno depende não apenas da interação direta entre o patógeno e as células hospedeiras, mas também dos mecanismos indiretos de amplificação de sinal por meio tanto de componentes do agente patogênico e / ou citocinas e quimiocinas geradas pelo hospedeiro (D ' AVILA et al., 2008; MATTOS et al., 2010, 2011a, 2011b; PACHECO et al., 2002, 2007; PEYRON et al., 2008).

Principalmente nas células da imunidade inata, a biogênese dos CLs pode ser desencadeada pelo reconhecimento dos padrões moleculares associados a patógenos (PAMPS) pelos receptores de reconhecimento de padrões (PRRs) (VALLOCHI *et al.*, 2018). Entre os PRRs destaca-se a família de receptores TLRs, uma família de onze proteínas em humanos, cuja ativação está associada à modulação de centenas de genes inflamatórios e à ativação dos leucócitos (AKIRA; TAKEDA, 2004). Após a estimulação por ligantes ou agonistas, a sinalização via TLRs promove profundas alterações no metabolismo celular, como o aumento da glicólise, diminuição da β-oxidação e aumento da esterificação dos ácidos graxos na forma de triglicerídeos nos CLs (FEINGOLD *et al.*, 2010, 2012; HUANG *et al.*, 2014). Além disso, a ativação da sinalização dos TLRs induz o aumento da expressão de várias enzimas envolvidas na síntese de triglicerídeos e / ou ésteres de colesterol, como ácido graxo sintase (FASN), diacilglicerol O-aciltransferase (DGAT-1 e DGAT-2) e acil-CoA: colesterol O-aciltransferases (ACAT1 e ACAT2) (HU; BINNS; REESE, 2017; HUANG *et al.*, 2014; NICOLAOU *et al.*, 2012). Quando a síntese lipídica de novo é inibida, a biogênese de CLs a jusante da ativação do TLRs é gravemente

comprometida (D'AVILA *et al.*, 2011; MATTOS *et al.*, 2011b). A participação da sinalização por TLRs na biogênese de CLs vem sendo reportada em diversas infecções, principalmente nas de origem bacteriana (PEREIRA-DUTRA *et al.*, 2019).

As vias a jusante a ativação dos TLRs envolvidas na biogênese dos CLs ainda envolvem a ativação de diversos fatores de transcrição e receptores nucleares, incluindo reguladores mestres do metabolismo lipídico, como receptores ativados por proliferador de peroxissoma (PPARs), receptor hepático X (LXR), proteína de ligação e elemento regulador de esterol (SREBPs) e fatores induzidos por hipoxia (HIF) (ALMEIDA *et al.*, 2009, 2014; CAO *et al.*, 2007; CASTRILLO *et al.*, 2003; KNIGHT *et al.*, 2018; MCRAE *et al.*, 2016; MEI *et al.*, 2009; SYED; SIDDIQUI, 2011; SZATMARI *et al.*, 2007; SZELES; TOROCSIK; NAGY, 2007). Membros da subfamília de PPARs, LXR e SREBPs são importantes sensores do ambiente lipídico intracelular e modulam a expressão de genes-chaves no metabolismo lipidico, como os envolvidos na captação de ácidos graxos, síntese lipídica, as enzimas lipolíticas e a biogênese dos CL (PAWLAK; LEFEBVRE; STAELS, 2015; SZATMARI *et al.*, 2007).

Durante o processo infeccioso, a biogênese dos CLs não depende exclusivamente da interação direta entre patógenos e a célula hospedeira, mas também por mecanismos indiretos de amplificação da resposta inflamatória (D'AVILA *et al.*, 2011). Além disso, existe uma grande intercessão entre a resposta inflamatória e a biologia dos CLs. Várias das moléculas produzidas durante a resposta inflamatória atuam de maneira parácrina, induzindo a formação dos CLs, incluindo mediadores lipídicos, citocinas e quimiocinas (BOZZA *et al.*, 2009).

1.6. Corpúsculos lipídicos na inflamação e infecção

Os eicosanóides são importantes mediadores inflamatórios lipídicos derivados da oxigenação enzimática do ácido araquidônico pelas vias da ciclooxigenase (COX) e lipoxigenase (LOX). Os eicosanóides atuam em diversos processos celulares, desde a homeostase tecidual ao processo inflamatório (BANNENBERG *et al.*, 2007; HAMILTON *et al.*, 2018). Diversos estudos vem demostrando que a orquestração de cada mediador lipídico por seu tempo, duração e magnitude é essencial para a homeostase e proteção contra infecções (BANNENBERG *et al.*, 2007; HAMILTON; *et al.*, 2018). Nesse contexto, a compartimentalização de maquinaria de síntese dos eicosanóides é um

componente crucial na regulação da síntese e no delineamento de ações funcionais intracelulares e extracelulares dos eicosanóides (BANDEIRA-MELO *et al.*, 2017; WELLER, 2016).

Diversas evidências vêm demonstrando que os CLs são um dos principais locais de síntese de eicosanóides, principalmente durante processos inflamatórios e infecciosos (BOZZA *et al.*, 2009; MELO *et al.*, 2011a). A atuação dos CLs como plataforma de síntese de eicosanóides foi evidenciada primeiramente pela compartimentalização de toda a maquinaria enzimática para a síntese no proteoma associado a essa organela, incluindo a fosfolipase A2 (PLA2), as principais quinases ativadoras envolvidas na via de mobilização do ácido araquidônico (ERK1 / 2, p85 e p38) e as principais enzimas formadoras de eicosanóides (COX-1, COX-2, 5-LOX, 15-LOX, proteína de ativação de 5-LO, PGE-sintase e LTC4-sintase) (BOZZA *et al.*, 1997; MAGALHAES *et al.*, 2018; SILVA *et al.*, 2009; YU *et al.*, 1998). A presença de todos esses componentes possibilita que os CLs sejam capazes de rápida mobilização do ácido araquidônico para produzir prostaglandinas e leucotrienos (MELO *et al.*, 2006; WELLER, 2016).

A atuação dos CLs como local de síntese de eicosanóides já foi demonstrada experimentalmente para o leucotrieno C_4 (LTC_4) (BANDEIRA-MELO *et al.*, 2001; SILVA *et al.*, 2009), leucotrieno B_4 (LTB_4) (PACHECO *et al.*, 2007; SILVA *et al.*, 2009), prostaglandina E_2 (PGE_2) (D'AVILA *et al.*, 2006, 2011), prostaglandina D_2 (PGD_2) (LUNA-GOMES *et al.*, 2011) e eoxina C_4 (EXC_4) (MAGALHAES *et al.*, 2018). Além disso, dados de eicosanômica sugerem ainda que os CLs sejam locais de síntese da lipoxina B_4 (LXB_4) (KNIGHT *et al.*, 2018) e da prostaglandina F2α (PGF2α) (ARAÚJO-SANTOS *et al.*, 2014; KNIGHT *et al.*, 2018).

Como plataforma para a síntese de mediadores lipídicos, os CLs desempenham um papel importante na sobrevivência de patógenos e na resposta efetiva do hospedeiro à infecção, principalmente através do equilíbrio entre a produção de PGE_2 e LTB_4 (BOZZA *et al.*, 2011; PETERS-GOLDEN *et al.*, 2005). Em geral, a participação de CLs como local de síntese de PGE_2 tem sido associada à indução de um fenótipo anti-inflamatório em macrófagos, favorecendo a inibição da atividade de *killing*, além da regulação negativa de citocinas do tipo Th1 e aumentando a produção de IL-10, favorecendo a proliferação e disseminação de diversos patógenos (ALMEIDA *et al.*, 2009; D'AVILA *et al.*, 2008; MATTOS *et al.*, 2011a; TOLEDO *et al.*, 2016). Em contraste, a síntese de LTB_4, um mediador pró-inflamatório, também foi relatada nos CLs durante a resposta fortemente pró-inflamatória (PACHECO *et al.*, 2007). A geração de

LTB_4 durante a infecção contribui para o *killing* de parasitas (SEREZANI *et al.*, 2006; TAVARES *et al.*, 2016) e no controle da infecção bacteriana (LI *et al.*, 2015), principalmente através da recrutamento e a ativação de células efetoras (PETERS-GOLDEN *et al.*, 2005).

Os CLs também estão envolvidos no ciclo de infecção, patogênese, sobrevivência e multiplicação de diversos patógenos, que estimulam a biossíntese dessa organela. Essa relação oportunista de estímulo da biossíntese pode ser tanto para a obtenção de uma fonte de energia ou como parte dos mecanismos de evasão do sistema imune, principalmente através da usurpação dessa organela como uma plataforma de síntese de eicosanóides (FARESE; WALTHER, 2009; SAKA; VALDIVIA, 2012). Essa relação patógeno-hospedeiro envolvendo os CLs já foi constatada para diferentes organismos pelo nosso grupo de pesquisa, a exemplo do *Mycobacterium leprae* (MATTOS *et al.*, 2011a, 2011b), *Microbacterium bovis* BCG (D'AVILA *et al.*, 2008), virus da dengue (CARVALHO *et al.*, 2012; MARTINS *et al.*, 2012; SAMSA *et al.*, 2009), *Toxoplasma gondii* (GOMES *et al.*, 2014; MOTA *et al.*, 2014) e *Tripanosoma cruzi* (D'AVILA *et al.*, 2011).

Em contrapartida, estudos recentes vêm desmonstrando uma forte associação dos CLs com a eficiência das respostas mediadas pelos interferons. Os CLs participam tanto como uma plataforma integradora das vias de sinalização quanto na efetividade da resposta mediada pelos interferons (MONSON *et al.*, 2020, 2018; SAKA; VALDIVIA, 2012; SEO; YANEVA; CRESSWELL, 2011). Nesse contexto, proteínas chaves na inibição da infecção viral (viperina) (HINSON; CRESSWELL, 2009) e na resposta antiparasitária (IRGM) (HALDAR *et al.*, 2013) se acumulam nos CLs após estimulação com interferon **(Figura 2)**.

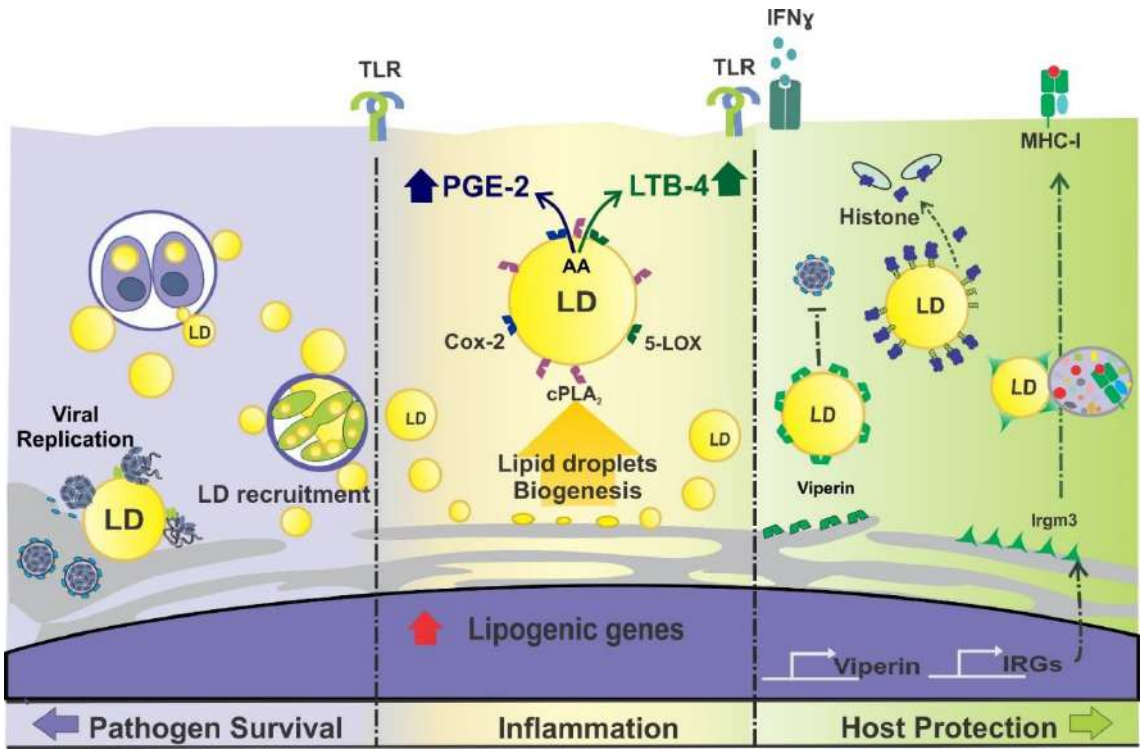

Figura 2: Corpúsculo lipidicos são centrais na resposta inflamatória tanto pró-patógeno como na resposta protetiva ao hospdeiro. Cl são estruturas centrais na resposta inflamatória, sendo local de sintese tanto de protaglandina E2 via cicloxigenase 2, e/ou de leucotrieno B4 (LTB_4) via 5-lipoxigenase, dois mediadores centrais tanto na reposta pró-hospedeiro como na sobrevivência dos patógenos. Entre as funções dos CL associadas a sobrevivência dos patógenos estão a usurpação dessa organela como uma plafatorma de replicação e de montagem das partículas virais, e utilização dessa organela como fonte de energia por protozoários e bactérias patogênicas intracelulares. Por outro lado, o remodelamento proteíco dessa organela principalmente devido a ação das vias de interfone, levam a presença de proteínas antivirais (viperina) e antiparasitárias (Irgm-3), sedo que esta está associada também com a apresentação antigênica via complexo de imunocompartibilidade I (MHC-I). Além disso a presença de histonas nos CL foi fortemente associada à atividade antibcateriana dessa organela.

1.7. Os CL na infecção bacteriana

Ao longo da evolução patógeno-hospedeiro, bactérias patogênicas adquiriram um eficiente conjunto de adaptações que dão suporte aos eventos cruciais na infecção, incluindo sobrevivência bacteriana, replicação e evasão da resposta imunológica do hospedeiro (COLONNE; WINCHELL; VOTH, 2016; TENG; ANG; GUAN, 2017). Para que a infecção e a replicação bacteriana ser bem-sucedidas, várias bactérias patogênicas desenvolveram diversos mecanismos que subvertem diversas funções celulares, incluindo o metabolismo do hospedeiro (COLONNE; WINCHELL; VOTH, 2016; SAMANTA *et al.*, 2017; TENG; ANG; GUAN, 2017). Alterações na homeostase lipídica e a indução da

biogênese dos CLs nas células do hospedeiro são fenômenos recorrentes após a infecção bacteriana, tanto em modelos experimentais como em humanos (BOZZA et al., 2009; BOZZA; MAGALHÃES; WELLER, 2009; PACHECO et al., 2002; ROINGEARD; MELO, 2017).

A subversão dos CLs por bactérias patogênicas para completar seu próprio ciclo de vida tem sido relatada para várias bactérias intracelulares, como *M. tuberculosis* (PEYRON *et al.*, 2008; RUSSELL *et al.*, 2009), *M. bovis* (D'AVILA *et al.*, 2006), *M. leprae* (MATTOS *et al.*, 2011b) *Chlamydia trachomatis* (COCCHIARO *et al.*, 2008) e *C. pneumoniae* (CAO *et al.*, 2007). A inibição do metabolismo lipídico e a interferência na homeostase dos CLs afetam a sobrevivência e/ou a replicação dessas bactérias dentro da célula hospedeira (DANIEL *et al.*, 2011; KUMAR; COCCHIARO; VALDIVIA, 2006; MATTOS *et al.*, 2010). Assim como observado para outras classes de pátogenos, o acúmulo de CLs durante a infecção bacteriana geralmente está associado a um mecanismo para obter um recurso energético do hospedeiro, bem como a uma estratégia de escape do sistema imunológico através da geração de eicosanóides (BOZZA *et al.*, 2011; GOMES *et al.*, 2014; MELO *et al.*, 2011a; ROINGEARD; MELO, 2017) **(Figura 3)**.

Embora os CLs geralmente sejam frequentemente associados a uma resposta anti-inflamatória, vários estudos vêm demonstrando a presença de CLs também em ambientes pró-inflamatórios (NICOLAOU; GOODALL; ERRIDGE, 2012; PACHECO *et al.*, 2002; QADRI, 2004). Na sepse, alterações no metabolismo lipídico são frequentemente observadas na forma de acúmulo de CLs em vários tipos de células in vivo e in vitro, inclusive em leucócitos de pacientes sépticos (PACHECO *et al.*, 2002). O acúmulo de colesterol éster nos macrófagos, provavelmente nos CLs, foi observado tanto para bactérias Gram-negativas (*Acinetobacter baumannii*, *Escherichia coli*, *Klebsiella pneumoniae*, *Pseudomonas aeruginosa*, *P. diminuta*, and *Proteus vulgaris*) como bactérias Gram-positivas (*Staphylococcus aureus*, *S. epidermidis*, and *Streptococcus salivarius*). E esse acúmulo de lipídeos é um processo altamente regulado, envolvendo principalmente TLR-2, TLR-4 e TLR-5, sendo acompanhado pela secreção da IL-6, uma citocina pró-inflamatória (NICOLAOU; GOODALL; ERRIDGE, 2012).

Recentemente KNIGHT e colaboradores (2018) propuseram que a formação de CLs em macrófagos não seria simplesmente um processo induzido pelo *M. tuberculosis*, mas seria resultado de uma reprogramação glicolítica dependente da sinalização por interferon-γ (IFN-γ) e pelo fator induzido por hipóxia 1- α (HIF1-α) nos macrófagos

murinos. Além disso, neste mesmo trabalho, os CLs induzidos por IFN-γ atuavam como uma plataforma importante para a produção de uma ampla-gama de eicosanóides, especialmente LXB_4 e PGE_2, mediadores protetivos ao hospedeiro (KNIGHT *et al.*, 2018). No entanto, a presença de IFN-γ sozinha não foi suficiente para induzir o acúmulo de CLs, exigindo um segundo sinal via TLR2 (KNIGHT *et al.*, 2018), que não exclui o *M. tuberculosis* como possível indutor dessa biogênese. Curiosamente, neste modelo, *M. tuberculosis* foi capaz de adquirir lipídios no hospedeiro na ausência de CLs, mas não na presença dos CLs induzidos por IFN-γ (KNIGHT *et al.*, 2018). Embora pareça contraditório com a literatura atual, a indução dos CLs como resposta do hospedeiro não pode ser subestimada, o que nos leva a sugerir que a indução dos CLs possa ter sido uma resposta inicialmente protetora para o hospedeiro, mas que ao longo da evolução patógeno-hospedeiro alguns patógenos podem ter usurpado essa resposta.

Ainda neste contexto, uma importante mudança de paradigma na interação bactéria/CLs foi a participação dos CLs na atividade antibacteriana reportado por ANAND e colaboradores (2012). Ensaios *in vitro* a partir de CLs purificados de embriões de *Drosophila melanogaster* apresentavam atividade antibacteriana *in vitro* contra *S. epidermidis* e *E. coli*. Neste mesmo trabalho foi constatado que esta resposta antimicrobiana era devido ao conteúdo proteico dessa organela (principalmente devido a ação das histonas) e não devido aos lipídios (ANAND *et al.*, 2012). Apesar de ser uma proteína catiônica canonicamente envolvida na formação e manutenção de nucleossomos (SILK *et al.*, 2017), as histonas são citotóxicas in vitro e in vivo quando localizadas no ambiente extracelular ou quando em excesso no citoplasma, além disso, apresentam uma forte capacidade de matar bactérias (CHEN *et al.*, 2014; PATAT *et al.*, 2004; SILK *et al.*, 2017). A compartimentalização de histonas em CLs foi detectada pela primeira vez durante a oogênese de *D. melanogaster* (CERMELLI *et al.*, 2006) e envolve a participação da proteína Jabba, que interage fisicamente com histonas através de uma interação eletrostática fraca (LI *et al.*, 2012). Embriões de drosophilas mutantes para a proteína Jabba apresentam uma drástica redução nos estoques de histonas e uma maior sucetibilidade à infecção bacteriana (ANAND et al., 2012). Além disso, em camundongos expostos ao LPS foi visualizado o aumento da presença da histona H1 nos CL hepáticos, sugerindo que esse aumento pode estar envolvido em algum tipo de resposta antimicrobiana (ANAND *et al.*, 2012). Entretanto o mecanismo e natureza da interação de CLs com as histonas em mamíferos é desconhecido, pois não há nenhuma proteína homóloga à jabba de *D. melanogaster.*

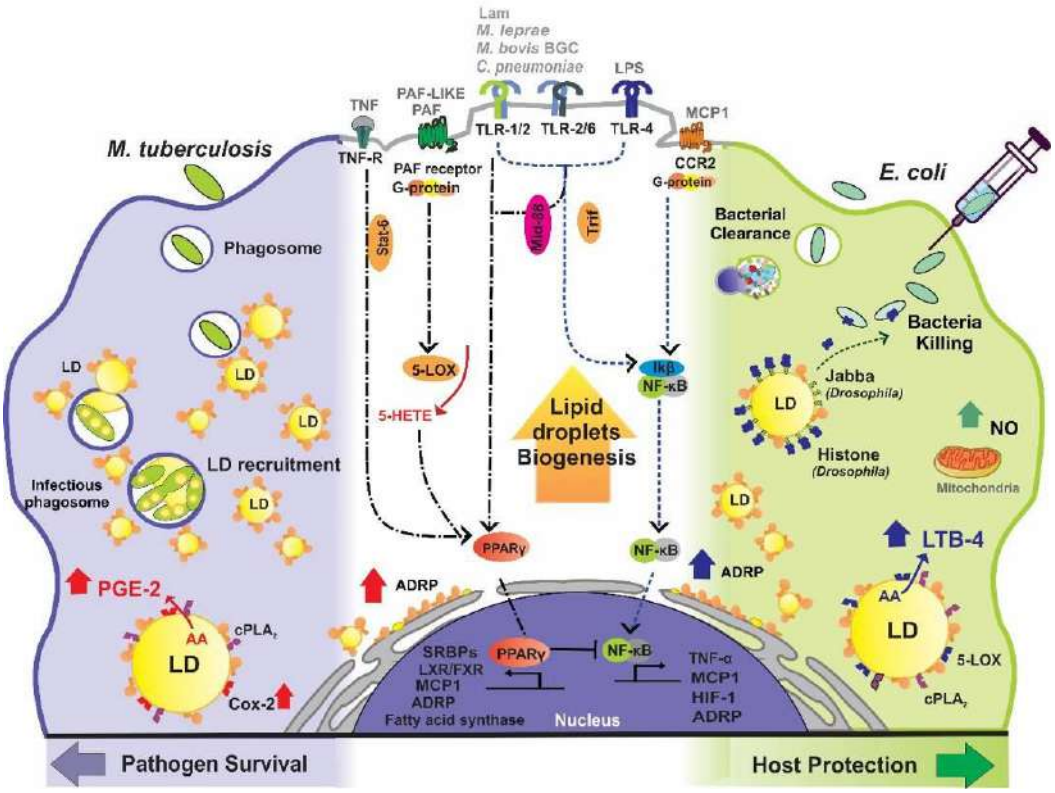

Figura 3: Participação dos corpúsculos lipídicos nas infecções bacterianas. A biogênese de CLs é um processo altamente regulado, envolvendo diversos receptores da imunidade inata, incluindo TLRs, que reconhecem bactérias ou partes de bactérias, além de citocinas. A ativação dos receptores dessas moléculas se inicia após uma complexa cascata de sinalização que culmina na ativação de fatores de transcrição que induzem direta ou indiretamente a ativação de vários genes lipogênicos. Algumas bactérias recrutam os CLs para as proximidades dos endossomos, tendo acesso ao conteúdo dos CLs, que servem como uma fonte nutricional para a sobrevivência e proliferação de bactérias patogênicas. Além disso, os CLs também são atores importantes na imunidade inata. A interação patógeno-hospedeiro leva à biossíntese e secreção de mediadores inflamatórios como a prostaglandina E_2 (PGE_2) através das vias da ciclo-oxigenase (COX-2) derivada do ácido araquidônico (AA). A PGE_2 pode inibir potencialmente a resposta Th1, favorecendo a proliferação de patógenos. Por outro lado, os CL também participam na imunidade inata, armazenando proteínas antibacterianas, como as histonas. Além disso, os LDs também são um local para a produção de leucotrieno B_4 (LTB_4), um mediador pró-inflamatório derivado do AA, associada à eliminação do patógeno (Fonte: PEREIRA-DUTRA *et al.*, 2019).

2. JUSTIFICATIVA E HIPÓTESE

Apesar dos CLs serem subvertidos durante a infecção por alguns patógenos intracelulares, a presença dessa organela em uma vasta gama de processos inflamatórios pode ser um indicio da existência de uma outra face dessa interação patógeno-hospedeiro. A exemplo do que acontece em *Drosophila*, nossa hipótese nesse trabalho é que os CLs também participam dos processos de resistência a algumas infecções bacterianas, tanto através do acúmulo de proteínas antibacterianas em seu proteoma, como local de síntese de LTB_4 **(Figure 4)**. O presente trabalho justifica-se pela ausência de informação sobre o papel dessa organela em diversas infecções bacterianas, principalmente nas desencadas por bactérias extracelulares. Em um contexto em que é cada vez mais comum a resistência bacteriana aos antibióticos, a melhor compreensão de mecanismos de defesa do hospeiro pode fornecer novas estratégias para o controle das infecções bacterianas. Uma vez que todas as células virtualmente possuem CLs, a participação dessa organela na resposta imune pode torná-la um promissor alvo para futuras intervenções terapêuticas.

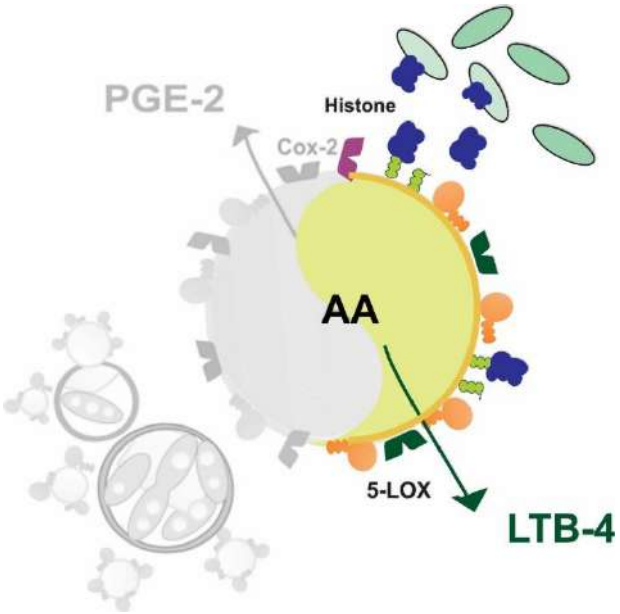

Figure 4: Hipótese do papel protetor dos corpúsculos lipidicos durante a infecção. Em contrapatida a subversão dos CL pelas bactérias intracelulares como fonte de energia e como uma imunoplataforma de supressão da resposta imune do tipo Th1 através da produção de PGE_2, nossa hipótese nesse trabalho é que os CL possuem atividade antibacteriana, principalmente através da presença de histonas em seu proteoma. Além disso como local de síntese de LTB_4 , ao CL também podem atuar como um importante regulador da resposta imune inata frente a infecções bacterianas.

2. OBJETIVOS

2.1. Objetivo geral

O objetivo geral do presente estudo é avaliar a participação dos corpúsculos lipídicos nos mecanismos de resistência à infecção bacteriana.

2.2. Objetivos específicos:

- Caracterizar a participação dos CLs na resposta antibacteriana e inflamatória in vitro durante a infecção à *E. coli* em macrófagos
- Caracterizar o papel dos CLs na resposta antibacteriana e inflamatória durante a sepse experimental.
- Caracterização dos CLs como uma plataforma autônoma na resposta antibacteriana.
- Identificação de proteínas antibacteriana e pró-hospedeiro nos CLs de macrófagos e no fígado.

3. METODOLOGIA

3.1. Animais

Nesse trabalho foram utilizados camundongos C57BL/6 machos com 6-8 semanas de idade, pesando entre 20 e 30g, fornecidos pelo Instituto de Ciências e Tecnologia em Biomodelos (ICTB/Fiocruz). Durante os experimentos, os animais foram mantidos no Centro de Experimentação Animal do Pavilhão Hélio e Peggy Pereira (HPP) do Instituto Oswaldo Cruz (IOC/Fiocruz). Os animais foram mantidos em temperatura constante (25°C), com ciclo de 12 h claro/escuro e livre acesso de água e comida. Os protocolos utilizados neste estudo foram aprovados pelo Comitê de ética no uso de animais de laboratório da Fundação Oswaldo Cruz (CEUA / FIOCRUZ), sob licença número CEUA- L025/15.

3.2. Diferenciação dos macrófagos a partir de medula óssea murina

Os macrófagos derivados da medula óssea (BMDM) foram obtidos através da diferenciação de células isoladas do fêmur e da tíbia de C57/BL6 foram cultivadas por 7 dias em meio RPMI-1640 suplementado com 18 % (v/v) sobrenadante L929, 20% (v/v) soro fetal bovino inativado pelo calor, 1% (v/v) de L-glutamina e 1% (v/v) de penicilina-estreptomicina, conforme descrito anteriormente por ASSUNÇÃO e colaboradores, (2017). Após 7 dias de diferenciação, os sobrenadantes foram descartados e os macrófagos já diferenciados foram removidos das placas por lavagem com PBS gelado (27 mM KCl, 20 mM KH_2PO_4, 137 mM NaCl, 100 mM $NaHPO_4$, pH 7,4), contados e plaqueados em placas de 24 poços (1×10^5 células/poço) ou placas de 12 poços (5×10^5 células/ poço). O meio utilizado para plaqueamento foi RPMI 1640 suplementado com 10% (v/v) de SFB e 1% de L-glutamina. As células plaqueadas foram mantidas em repouso na estufa por 24 horas antes do início da infecção.

3.3.Pré-tratamentos in vitro

Para avaliar o papel dos CLs na resposta antibacteriana, macrófagos foram pré-tratados com 40μM de ácido oléico (Sigma, EUA), adicionados à cultura 16h antes da infecção. Já o tratamento com a droga A922500 foi adicionado à cultura 30 min antes da infecção, permanecendo por todo o tempo do experimento.

3.4. Cultura da *Escherichia coli*

Nos experimentos *in vitro* utilizou-se uma cepa de *Escherichia coli* patogênica (ATCC 25922), pertencentes ao nível 2 de biossegurança, oriundas da Coleção de Enteropatógenos Bacterianos do Instituto Oswaldo Cruz. Mantidas sob congelamento em -80°C. Para infecção utilizou-se bactérias na fase estacionária, obtidas a partir de pré-inóculos cultivados no meio de cultura Luria Bertani (LB; Kasvi, Brasil) líquido, e incubado a 37°C por 16h com agitação constante. No dia seguinte, as bactérias foram purificadas e realiza-se a leitura por espectrofotometria na Densidade Optica em 600 nm (OD_{600}).

3.5. Infecção por *Escherichia coli* (Ensaio de proteção a gentamicina)

Para avaliar a internalização e sobrevivência intracelular da *E. coli* foi realizado o ensaio de proteção com gentamicina com base no método descrito por LISSNER e colaboradores (1983), com algumas modificações. No dia da infecção removeu-se o sobrenadante das placas previamente plaqueadas com macrófagos, e as células foram infectadas com *E. coli* em um MOI (multiplicidade de infecção) de 100, e incubados por 1h a 37°C e 5% de CO_2. Uma hora após a infecção a 37°C, o meio de cultura foi descartado e as células foram lavadas com PBS com 100 μg / mL de gentamicina três vezes. Adicionou-se RPMI suplementado com 100 μg / mL de gentamicina em cada poço para matar as bactérias extracelulares e a incubação foi continuada por mais 1 h. Após a incubação, os meios foram removidos novamente e um meio fresco sem gentamicina foi adicionado pelo restante do tempo do experimento. Para enumeração bacteriana, nos momentos indicados, as células foram lavadas três vezes com PBS e lisadas com solução de saponina a 5%. As unidades formadoras de colônias (UFC) foram contadas através da

diluição apropriada em placas de agar triptona de soja (TSA; Kasvi, Brasil). Todos os experimentos foram realizados em triplicata.

3.6. Marcação de CLs e microscopia confocal

Para a quantificação dos CLs, as células foram fixadas com 4% de paraformaldeído e os CLs foram corados com 0,3% de Oil Red O (diluído em isopropanol 60%) por 2 min em temperatura ambiente, como descrito anteriormente (MELO *et al.*, 2011b). Os núcleos das células foram marcados com DAPI (ThermoFisher Scientific, EUA), e como meio de montagem foi utilizado o meio Fluoromount G (ThermoFisher Scientific, EUA) para a microscopia confocal. As imagens foram capturadas pelo microscópio FluoView FV10i da OLYMPUS, da plataforma de microscopia do INCA. Os CLs foram quantificados a partir de um mínimo de 100 células de 5 campos diferentes pelo software ImageJ (https://imagej.nih.gov/ij/index.html).

3.7. Dosagem de lactato

Para dosagem de lactato no sobrenadante das culturas utilizou-se o lactato enzimático (Labtest, Brasil), conforme as instruções do fabricante. Brevemente, as amostras foram diluídas em água destilada (10X), e em placas de 96 poços pipetou-se 2 µl das diluições dos sobrenadantes, seguido por 200 uL da reação de trabalho do kit. Após incubação de 5 min a 37°C, a leitura no espectrofotômetro foi realizada a 550 nm. Como curva-padrão utilizou-se uma solução de lactato (Labtest, Brasil) na concentração inicial de 60 mg/dL.

3.8. Dosagem de óxido nítrico

Para a dosagem do óxido nítrico (NO) nos sobrenadantes de cultura e no sobrenadante dos lavados peritoneais foi utilizada a reação colorimétrica de Griess, que consiste na detecção de nitrito (NO_2^-), produto estável da oxidação do NO. Em placa de 96 poços, pipetou-se 25µL dos sobrenadantes, seguido do mesmo volume do reagente de Griess (composto 1:1 de sulfanilamida 1% diluída em H_3PO_4 2,5% e de N-1-naphtylethtylenodiamina, também diluído em solução de H_3PO_4 a 2,5%). Após incubação

de 10 minutos ao abrigo da luz, a leitura no espectrofotômetro foi realizada a 450 nm. Como curva-padrão utilizou-se uma solução de nitrito de sódio ($NaNO_2$) na concentração inicial de 200uM, diluído em meio de cultura fresco.

3.9. Mensuração dos mediadores inflamatórios lipídicos no sobrenadante celular

Para a determinação das concentrações de mediadores lipídeos prostaglandina E_2 (PGE_2) e leucotrieno B_4 (LTB_4) nos sobrenadantes de cultura foi utilizado kits de ensaio imunoenzimátio (EIA), utilizando-se kits comerciais (Cayman, EUA), conforme as orientações do fabricante.

3.10. Dosagem de citocinas

A determinação das concentrações de IL-1β, IL-6, IL-10, MCP-1/CCL2 e TNF-α no sobrenadante da cultura celular foram realizados por meio de ELISA, utilizando-se kits comerciais (BD biosciences), conforme as orientações do fabricante. As concentrações de IL-1β, IL-6, IL-10, IL-12p70, TNF-α, MCP-1, KC, IFN-γ no sobrenadante dos lavados peritoneais foram quantificados através da técnica de Luminex utilizando-se kits comerciais (BD biosciences). Todas as análises foram realizadas na subunidade Luminex-*RPT03C* da Rede de Plataformas PDTIS (FIOCRUZ/RJ).

3.11. Determinação da atividade da enzima lactato desidrogenase (LDH)

Para a determinação da atividade da enzima lactato desidrogenase (LDH) no sobrenadante da cultura celular foi utilizado o ensaio de citotoxicidade não-radioativo CytoTox 96 (Promega, EUA), conforme as orientações do fabricante. Os resultados foram expressos em atividade relativa, a partir do percentual em relação a atividade de células lisadas com 0,1% de Triton X-100.

3.12. Modelo de Sepse experimental (CLP)

Para a indução da sepse experimental, utilizarmos o modelo de ligação e perfuração do ceco (CLP) para induzir uma peritonite polimicrobiana grave, conforme descrito por REIS e colaboradores (2017). Para induzir a sepse polimicrobiana, camundongos C57BL/6 foram anestesiados intraperitonealmente com 112,5 mg/kg de ketamina (Cristália, Brasil) e 10 mg/kg de xilazina (Syntec, Brasil). Após anestesiados, a cavidade abdominal foi aberta, o ceco foi exposto e ligado com linha de algodão (4.0), abaixo da junção ileocecal. Em seguida, o ceco foi perfurado 4 vezes com uma agulha de 21G, e uma pequena quantidade de material fecal foi extravasada antes da recolocação do ceco na cavidade abdominal (grupo CLP). O abdômen foi suturado com agulha de nylon (3.0), e após o procedimento cirúrgico, os animais receberam 1,0 mL de solução salina (0,9% NaCl) por via subcutânea para reposição volêmica. Como controle foram utilizados animais falsos operados (grupo Sham), submetidos à cirurgia, com a exposição do ceco, mas sem a ligação e a perfuração. Após o procedimento cirúrgico, os animais também receberam 1,0 mL de solução salina. Nos experimentos de sobrevida, após 6h e 24h da cirurgia, todos animais foram tratados intraperitonealmente com antibiótico Meropenem (75 mg/kg; Merck, EUA), e acondicionados em caixas apropriadas para a observação diária.

3.13. Tratamento com inibidor da DGAT-1

Parte dos animais dos grupos CLP e Sham foram pré-tratados com A922500 (Sigma, EUA), um inibidor da diacilglicerol aciltransferase-1 (DGAT-1). Para isso a molécula foi dissolvida em DMSO e armazenada a -20°C. No dia dos experimentos a solução estoque foi diluída em solução salina. Uma hora antes da cirurgia, os animais foram pré-tratados com A922500 (3 mg/kg, via intragástrica) ou solução salina mais 0,05% de DMSO (via intragástrica) **(Figura 5A)**. Nos experimentos de 24h, os animais receberam uma segunda administração do inibidor 6h após a cirurgia **(Figura 5B)**. Por fim, nos experimentos de análise de sobrevida o inibidor A922500 também foi administrada 6h e 24h após a cirurgia, concomitantemente a administração do antibiótico **(Figura 5C)**. A concentração do inibidor e forma de administração do A922500 foi escolhida em função do estudos prévios que validaram a molécula (KING *et al.*, 2009, 2010).

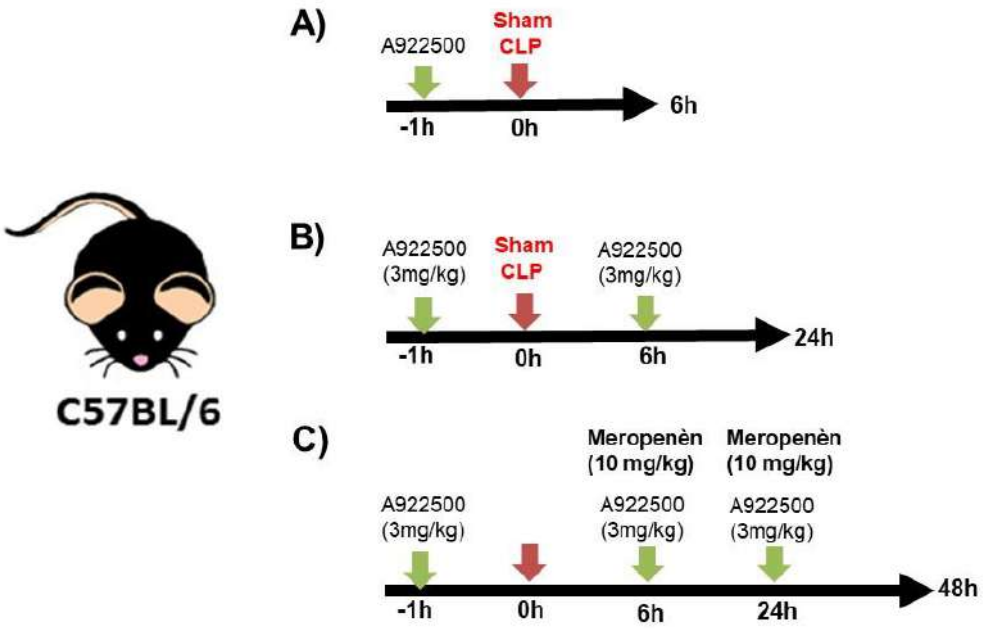

Figura 5: Esquemas representativos dos tratamentos com A922500 durante a sepse, nos experimentos de sobrevida e escore clínico

3.14. Avaliação do escore clínico de gravidade da sepse

Entre 6h e até 48h após a cirurgia foi avaliado a progressão da sepse através de um escore derivado do protocolo SHIRPA (SmithKline Beecham, Harwell, Imperial College and Royal London Hospital Phenotype Assessment) (ROGERS *et al.*, 1997), com as adaptações de REIS e colaboradores (2017). Foram avaliados tanto parâmetros físicos como comportamentais indicadores de gravidade. Nesse trabalho foram avaliadas as seguintes variáveis: piloereção, abdômen contraído, alterações de locomoção, frequência respiratória, lacrimação, fechamento de pálpebras, força ao agarrar, tônus corporal, temperatura corporal, o interesse pelo ambiente, perda da atividade motora e alterações nas fezes. Para cada alteração dos parâmetros foi acumulado 1 ponto no escore total. Para a confirmação do quadro séptico foi considerado um escore acima de 4 pontos. Os animais controles (grupo *Sham*) também foram submetidos a avaliação clínica dos mesmos parâmetros já citados, de modo a confirmar a ausência de interferências externas no experimento.

3.15. Coletas das amostras

Após 6h e 24h da indução de sepse, os animais foram eutanasiados por meio de uma dose letal do anestésico inalatório Isofurano (5%), e foi feita a coleta das amostras biológicas:

Punção ocular para obtenção de sangue

O sangue foi coletado por via ocular, com o auxílio de uma pinça, e alocado em microtubos. Após a coagulação, o sangue foi centrifugado a 2500 rpm por 10min a 4°C, o soro foi coletado e armazenado a -80°C para as análises posteriores.

Lavado peritoneal

Após a coleta do sangue, as cavidades peritoneais foram abertas e lavadas com 3 mL de PBS estéril no fluxo laminar. A suspensão celular foi diluída 40X em solução de Turk (2% CH2COOH, 0,1% de cristal violeta) e quantificada em câmeras de Neubauer. Alíquotas contendo 1 x 10^4 células foram citocentrifugadas a 500 x g por 5 min para a confecção dos citoesfregaços. As lâminas contendo os citoesfregaços foram fixadas em 4% de paraformaldeído por 16h a 4°C, para posterior contagem total e diferencial de células, e coloração e quantificação dos corpúsculos lipídicos. O restante do lavado peritoneal foi então centrifugado a 500 x g por 10min a 4°C, e as frações dos sobrenadantes foram coletadas e armazenadas a -80°C para posterior análises.

Coleta do Fígado

Em seguida a obtenção do lavado peritoneal, os animais foram perfundidos com solução de salina (0,9% NaCl). Após perfusão, o fígado foi coletado e a vesícula biliar descartada. Os lóbulos menores foram imediatamente fixados em solução de 4 % de paraformadeído, para análises histológicas. E os lóbulos maiores foram imediatamente congelados em gelo seco e armazenados a -80ºC para futuras análises bioquímicas.

3.16. Quantificação da carga bacteriana

A quantificação do número de unidades formadoras de colônias bacterianas foi realizada da diluição do lavado peritoneal em PBS, e 100 µL dos lavados foram plaqueados em placa de Ágar Triptona de Soja (TSA, Kasvi, Brasil) e incubadas na estufa a 37°C por 16 h para posterior contagem manual de unidades formadoras de colônias (UFC). Para a quantificação da carga bacteriana no sangue, 20 uL de soro foram plaqueados em em placa de Ágar Triptona de Soja (TSA, Kasvi, Brasil) e incubadas na estufa a 37°C por 16 h para posterior contagem manual de unidades formadoras de colônias (UFC).

3.17. Análises dos parâmetros celulares (leucometria) e quantificação dos CLs

As suspensões de células do lavado peritoneal foram citocentrifugadas (400 x g/5 min) em lâmina de vidro e fixadas em paraformaldeido a 4%, durante 20 minutos. Para coloração das células, as células foram coradas com 0,3% de Oil Red O (ORO, diluído em isopropanol 60%) por 2 min em temperatura ambiente. Após isso, as células foram lavadas 1 vez em isopopanol e 3 vezes em água e mergulhadas, e então coradas com Hematoxilina de Meyer (Merck, Alemanha) durante 4 minutos. As lâminas foram montadas utilizando meio de montagem Fluoroumont G. Após a coloração com ORO, foram quantificados o número de CLs de 50 células consecutivas no microscópio Olympus BX 41, utilizando objetiva de 100x. Para a análise diferencial de leucócitos foram contadas 100 células consecutivas por citocesfregaço em microscópio de luz, com objetiva (aumento de 100x) de imersão em óleo. A quantidade de cada tipo celular foi calculada a partir da porcentagem encontrada com relação ao número total de células.

3.18. Avaliação dos triglicerídeos e colesterol no sangue

As concentrações de triglicerídeos totais e de colesterol total foram determinados a partir do soro dos animais, utilizando os kits Triglicérides Liquiform (Labtest, Brasil) e de Colesterol Liquiform (Labtest, Brasil), respectivamente, conforme as instruções do fabricante.

3.19. Dosagem de 8-Isoprostano e LTB4 no lavado peritoneal

As concentrações de 8-Isoprostano e LTB_4 foram determinados diretamente dos sobrenadantes dos lavados peritoneais utilizando-se kits comerciais (Cayman, EUA), conforme especificado pelo fabricante.

3.20. Contagem total e diferencial do sangue

Alíquotas de sangue total foram diluídas 40X em solução de Turk (2% CH_2COOH, 0,1% de cristal violeta) e o número total de leucócitos foi quantificado em câmeras de Neubauer. A análise diferencial de leucócitos foi realizada a partir de esfregaços sanguíneos corados pelo método Panótico Rápido (Laborclin, Brasil). Foram contadas 100 células consecutivas por esfregaço em microscópio de luz, com objetiva (aumento de 100x) de imersão em óleo. A quantidade de cada tipo celular foi calculada a partir da porcentagem encontrada com relação ao número total de células.

3.21. Análise histológica do fígado

Para a análise histológica, os lóbulos menores do fígado de animais controle e sépticos foram fixados em paraformaldeído 3,7% a 4°C por 24h. Após a fixação, foi realizado processamento histológico através de desidratação em série alcoólica crescente de etanol, passando por álcool 80%, 85%, 90%, 95% e etanol absoluto. Posteriormente, as amostras foram diafanizadas em xilol, seguida pela impregnação e inclusão em parafina a 56 °C. Os blocos foram cortados em micrótomo à espessura de 5 μm e as lâminas foram coradas com hematoxilina e eosina para análise morfológica. Os cortes histológicos foram fotografados em microscópio Olympus BX41, no aumento de 200 vezes.

3.22. Cromatografia em camada fina (TLC)

Para a análise da composição lipídica, 5 mg de tecido foram maceradas em 500 μL de água destiladas. A extração dos lipídeos hepáticos foi feita pelo método de Bligh-Dyer e analisadas por TLC em placas de sílica gel 60 (Merck) aplicando 1 mg de tecido

hepático, de acordo com HORWITZ; PERLMAN (1987). Para identificar lipídios neutros, as placas foram desenvolvidas em hexano-éter etílico-ácido acético (60: 40: 1, em volume) até a frente do solvente atingir a linha superior. Os lipídios neutros foram identificados por comparação com os lipídios padrão (1 mg / ml): colesterol (CE), éster de colesterol (C), ácido graxo (FA), monoacilglicerol (MAG), diacilglicerol (DAG), triacilglicerol (TAG), obtido da Sigma (EUA). Para visualização dos lipídios, as placas de TLC foram coradas por pulverização com reagente de Charring (3% de CuSO4 e 8% de H3PO4 (v / v) e aquecidas a 110 ° C por 10 min. Cada mancha lipídica foi identificada por comparação com um padrão lipídico (Sigma-Aldrich, EUA) executado em paralelo. Os níveis de triglicerídeos e colesterol éster foram quantificados através de densitometria a partir de imagens digitais das placas de sílica, utilizando o programa ImageJ.

3.23. Determinação das substâncias reativas ao ácido tiobarbitúrico (TBARS)

As espécies reativas de ácido tiobarbitúrico (TBARS), um índice de peroxidação lipídica, foram determinadas de acordo com o método descrito por Buege and Aust (1978) com algumas modificações. O ácido tricloroacético e ácido tiobarbitúrico foram adicionados às amostras, os quais foram incubados durante 25 min a 100°C. A curva de calibração foi realizada utilizando 1,1,3,3-tetrametoxipropano. A absorbância foi lida a 535 nm e os resultados foram expressos como nmol de TBARS / mg de proteína. A determinação proteica foi realizada pelo método de Bradford (Bio-Rad Laboratories, EUA), conforme as orientações do fabricante e utilizando albumina bovina como padrão.

3.24. Determinação total de grupos tiólicos

O conteúdo total de tiol foi determinado pelo método de DTNB (ácido 5,5 '-ditiobis-2-nitrobenzóico), descrito por Aksenov and Markesbery (2001) com algumas modificações. A quantidade de TNB formada foi determinada a 412 nm. Os resultados foram expressos como nmol de TNB / mg de proteína. A determinação proteica foi realizada pelo método de Bradford (Bio-Rad Laboratories, EUA), conforme as orientações do fabricante e utilizando albumina bovina como padrão.

3.25. Determinação da atividade da Mieloperoxidase

Para esta análise, o fígado dos animais foi pesado, e 50 mg de tecido hepático foi macerada em 100 µL de solução de homogeneização (PBS-EDTA 5 µM + Brometo de cetildimetilamônio 0,5% (HTAB). Após a homogeneização, as amostras foram centrifugadas a 4°C por 4000 rpm durante 15 min. O sobrenadante das amostras foi recolhido e novamente centrifugado a 4ºC por 1200 rpm durante 15 min. Em placas de 96 poços de fundo curvo, 50 µL do sobrenadante de cada amostra foi adicionado à 50 µL da solução de homogeneização e 50 µL de solução de o-dianisidina (0,68 mg/mL), e incubados a 37°C protegido da luz. Após 30 min, foram adicionados 50 µL de peróxido de hidrogênio (H_2O_2 0,006%) por poço e incubou-se por mais 10 min a 37°C. Para a leitura no espectrofotômetro, 200 µL da reação foram transferidos para uma placa de fundo chato, e a leitura foi realizada a 460 nm. O cálculo foi realizado a partir do valor da absorvância/peso das amostras hepaticas.

3.26. Isolamento de corpúsculo lipídicos por fracionamento celular

Purificação de corpúsculo lipídicos de macrófagos

Após a diferenciação, 1 x10^8 macrófagos murinos foram plaqueados em garrafas de cultura de 175cm^2, na desidade de 25 x 10^7 células/placa, em RPMI 1640 suplementado com 10% (v/v) de SFB e 1% de L-glutamina. No dia seguinte ao plaqueamento, os macrófagos foram estimulados com 500ng/mL de LPS sorotipo 0111:B4 (Sigma-Aldrich, EUA) e 10ng/mL de interferon γ murino recombinante (Peprotech, EUA). Após 24h de estímulo, as células foram ressuspensas com PBS gelado e com o auxilio do *cell scraper*. As células foram centrifugadas a 500xg por 10 min a 4°C, e ressuspendidas no tampão de TEE-KCl (25 mM Tris/HCl, 100 mM KCl, 1 mM EDTA e 5 mM EGTA, pH 7,4), suplementado com inibidores de proteases (Complete™ protease inhibitor cocktail, Roche) e fosfatases (PhosSTOP™, Merk). A suspensão celular foi cavitada em nitrogênio (700 psi), por 15 min no gelo. Após a lise, as células foram centrifugadas a 500 xg por 10 minutos a 4 ° C. O sobrenadante pós-núcleo (SPN) foi utilizado para a análise de *Western blot* ou purificação dos CLs. Para purificar os CLs, após a mistura de 3 mL do SPN com 3 mL de sacarose 1,08 M, um

gradiente descontínuo de sacarose foi preparado por camadas de 2 mL de soluções de sacarose a 0,27 M e 0,135 M, e uma camada adicional de 2 mL de Top solution (Tris-HCl 25 mM, pH 7,5, EDTA 1 mM e EGTA 5 mM). Após centrifugação a 150.000 xg por 1 hora a 4 ° C (rotor SW-41Ti, Beckman Coulter), a fração de CLs no topo do gradiente foi recuperada. As proteínas dos CLs foram precipitadas adicionando 10 volumes de acetona gelada e mantidas durante a noite a -20 ° C. As amostras foram centrifugadas a 4300 xg durante 1 hora a 4 ° C, o sobrenadante foi removido e o sedimento foi seco ao ar. O sedimento resultante utilizado para análise por Western blot foi ressuspensa em Tris 0,1 mM pH 8,0, sonicada e a concentração de proteínas foi quantificada pelo kit de quantificação de proteínas Bradford (Bio-Rad Laboratories, EUA), conforme as orientações do fabricante e utilizando albumina bovina como padrão.

Purificação de corpúsculo lipídico hepático

Após a perfusão hepática com solução salina (NaCl 0,9% e EDTA 0,1%), o fígado foi colocado em uma placa de Petri, picado com bisturi e transferido para um macerador de tecidos do tipo Dounce juntamente com 3 volumes (1 g / 3 ml) de tampão de homogeneização (Tris-HCl 25 mM, pH 7,5, KCl 100 mM, EDTA 1 mM e EGTA 5 mM), suplementado com inibidores de proteases (Complete™ protease inhibitor cocktail, Roche) e fosfatases (PhosSTOP™, Merk). Após a maceração, o homogenato de fígado foi centrifugado a 500 xg por 10 minutos a 4 ° C. O sobrenadante pós-núcleo (SPN) resultante foi coletado e utilizado para Western blot ou purificação de CLs. Para purificar os CLs, foi seguido o mesmo protocolo descrito acima.

3.27. Ensaio de antividade antibacteriana in vitro

Ensaios de formação de colônias foram realizados para avaliar a capacidade antibacteriana dos CLs. Para isso, *E. coli* cresceram exponencialmente no caldo Luria-Bertani (LB) a 37 ° C até atingir OD_{600} = 1. Após, as bactérias foram então centrifugadas, lavadas, ressuspendidas com 10 mM (pH 7,4) suplementado com 0,01 volume (1% v / v) de meio LB em microtubos. Alicotas de 100 µL da suspensão bacteriana foram incubados com 25-100 µg de proteína CL por 16h a 37 ° C em agitação. Em alguns experimentos, 100 µL CLs intactos obtidos do gradiente de sacarose foram usadas no ensaio. Após a incubação, as amostras foram diluídas em 6 ou 8 diluições seriadas (1/10) consecutivas

com Tris-HCl 10 mM (pH7.4) e plaqueadas em triplicado em placas de agar LB. As bactérias viavéis foram quantificadas em UFC / mL em placas após incubação por 16h a 37 ° C.

3.28. *Western blotting*

Para as análises de *Western blotting* nesse trabalho foram utilizadas principalmente extratos proteicos obtidos após a ressuspensão das proteínas oriundas dos gradientes de sacarose. Os extratos foram desnaturados a 100°C por 5min na presença de tampão de amostra 4x (Tris-HCl 187,5 mM pH 6,8, SDS 6%, glicerol 30 % (Invitrogen), β- mercaptoetanol 10 %(Sigma) e de azul de bromofenol 0,03%). As amostras foram submetidas à eletroforese (em gel de acrilamida 12%) no sistema SDS-PAGE com a aplicação de 100 V por 4 h, e então transferidas para membrana de nitrocelulose (GE Healthcare) utilizando tampão de transferência (Tris 25 mM, glicina 192 mM pH 8 e 20 % de metanol). A transferência foi realizada a 15 V por 40 minutos em sistema semi-seco (Trans-Blot Semi Dry, GE). Após as transferências as membranas foram incubadas com solução bloqueadora de leite a 5 % em TBS/T (Tris-HCl 5 mM pH 7,4, NaCl 15 mM e 0,1% Tween 20). Posteriormente, as membranas foram incubadas com os anticorpos primários (Tabela 1) por 16h a 4°C. Após incubação, as membranas foram lavadas 3 x com TBS-T, e então incubadas com anticorpos segundários apropriados conjugados com peroxidase (HRP) por 1h à temperatura ambiente. Para a revelação, as membranas foram expostas à mistura dos reagentes ativadores de peroxidase (*Luminol, Super Signal West Pico Chemiluminescent Substrate*, Pierce) em temperatura embiente por cerca de 5 min. A quimioluminescência foi detectada por exposição a filme radiográfico (GE Healthcare) em um cassete para exposição apropriado. Após a exposição, os filmes foram revelados e fixados.

Tabela 1: Lista de anticorpos utilizados nesse trabalho

Anticorpo	Marca	Catalogo	Diluição
anti-H2A	Santa Cruz	sc-10807	1/1000
anti-H2B	Santa Cruz	sc10808	1/1000
anti-catelicidina	Abcan	ab180760	1/500
anti-viperina	Cell signalling	13996S	1/1000
anti-HMGB-1	Proteintech	10829-1-AP	1/500
anti-ADRP/Plin2	Proteintech	15294-1-AP	1/2000

3.29. Análise estatística

Os dados dos experimentos in vivo foram expressos como mediana ± interquatil, enquanto que os dos experimentos in vitro como média ± desvio padrão. Para avaliação estatística das curvas de sobrevida foi utilizado o teste de Log-rank (Mantel-Cox), já para as demais análises estatísticas foi utilizado o Teste t de Student ou ANOVA one-way seguido pelo teste post-hoc de Tukey, conforme o indicado. Foi consierado como estatisticamente significativo de $p \leq 0,05$.

4. RESULTADOS

4.1. Modulação da quantidade de CLs afeta a capacidade de *killing* de macrófagos

A biogênese de CLs é um fenômeno altamente regulado, envolvendo a participação de TLRs, sendo um fenômeno recorrente em diversas infecções bacterianas, tanto in vitro como in vivo (BOZZA; MAGALHÃES; WELLER, 2009); entretanto, o papel dessa organela, principalmente durante a infecção por bactérias extracelulares ainda não foi esclarecido. Para investigar o papel do CLs na resposta antibacteriana conduzimos experimentos in vitro com macrófagos murinos e avaliarmos se a modulação do acúmulo de CLs afetaria a capacidade de macrófagos de eliminar a *E. coli*, uma bactéria extracelular.

Nossa primeira estratégia experimental foi estimular a biogênese de CLs através do pré-tratamento dos macrófagos derivados da medula com 40 µM de ácido oléico (AO) por 16h antes da infecção. Observamos que essa estratégia elevou significativamente a quantidade de CLs nos macrófagos tanto na primeira hora pós-infecção como em 24h **(Figura 6A-B)**. Além disso, essa estratégia também levou a uma diminuição da carga bacteriana intracelular nos macrófagos pré-tratados com ácido oleico em comparação aos macrófagos expostos ao veículo em ambos os tempos analisados **(Figura 6C)**.

Se o aumento da quantidade de CLs diminui a carga bacteriana, nosso próximo passo foi avaliar se a inibição da biogênese de CLs teria um impacto inverso sobre a carga bacteriana. Para isso, utilizamos um inibidor da enzima DGAT-1 (A922550), responsável pela última etapa da síntese de triglicerídeos. Apesar do tratamento com A922500 inibir de forma parcial a biogênese de CLs em 24h **(Figura 6D-E)**, o tratamento levou ao aumento significativo da carga bacteriana intracelular em 24h **(Figura 6F)**. Esse conjunto de dados sugere a participação dos CLs na atividade antibacteriana.

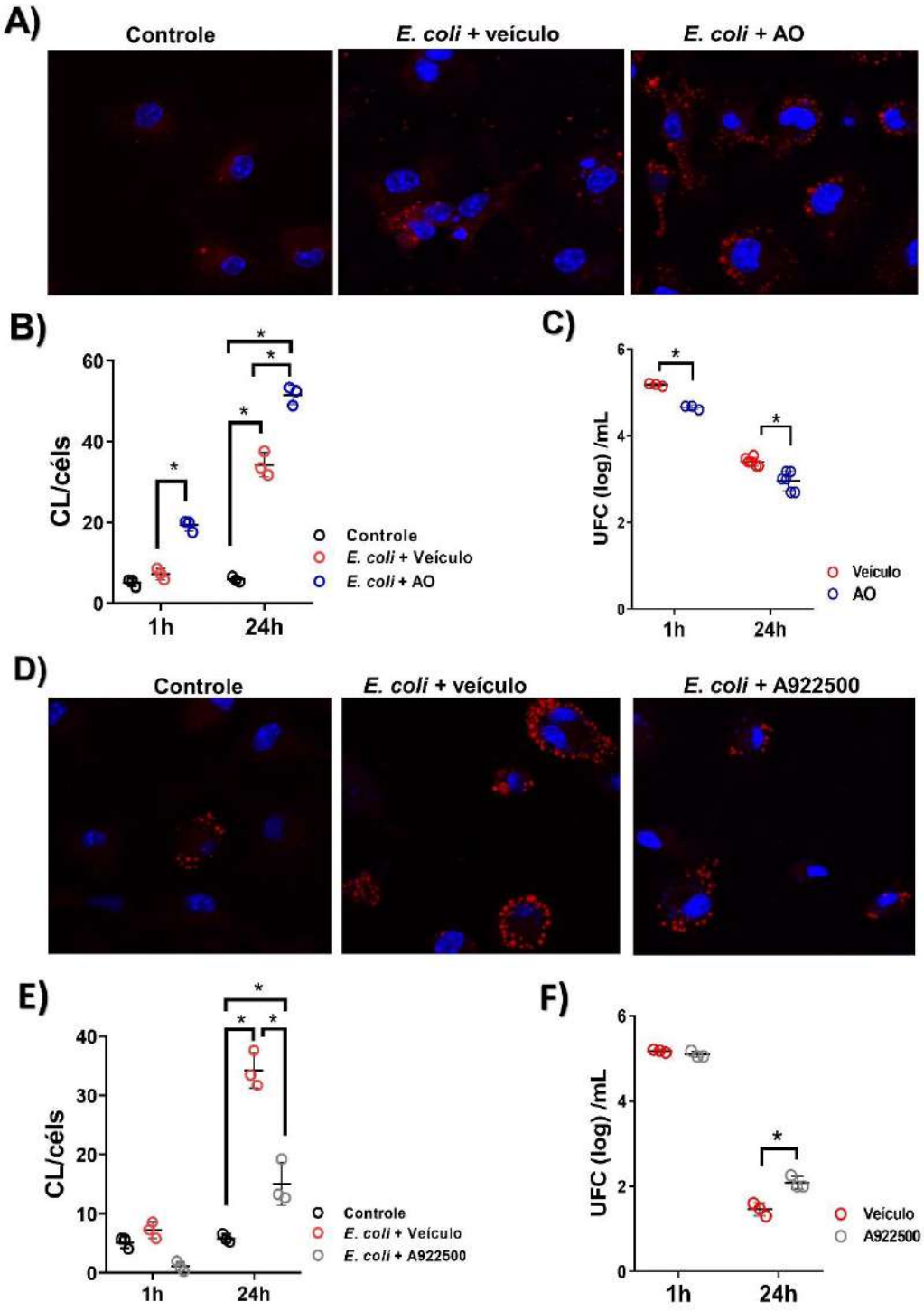

Figura 6: Modulação da biogênese de CLs afeta a capacidade de killing dos macrófagos. Macrófagos BMDM com ou sem pré-tratamento com **(A-C)** 40 µM de ácido oleico (AO) or **(E-F)** 5 µM de A922500 foram infectadas com *E. coli* (MOI de 100). **(A)** Imagens representativas de 24h pós-infecção de macrófagos intectados com *E. coli* com ou sem pré-tratamento com ácido oleico. CL foi marcado com ORO (vermelho) e o núcleo foi marcado por DAPI (azul). Barra de escala: 10 µm. **(B)** Quantificação dos CLs nos macrófagos 1h e 24h pós-infecção por *E. coli*. (n=3) **(C)** Cinética de internalização (n=3) e sobrevivência (n=6) da *E. coli* dentro dos macrofagos. **(D)** Imagens representativas de 24h pós-infecção de macrófagos intectados com *E. coli* com ou sem pre-tratamento com A922500. CLs foram marcados com ORO (vermelho) e o núcleo foi marcado por DAPI (azul). **(E)** Quantificação dos CLs nos macrófagos 1h e 24h pó-infecção por *E. coli*. (n=3) **(F)** Cinética de internalização e sobrevivência da *E. coli* dentro dos macrófagos (n=3). Cada ponto representa a média de um experimento independente. A análise estatística foi feita usando o teste ANOVA One-way seguida do pós-teste de Turkey. * significa $p < 0,05$.

4.2. CLs interagem com bactérias internalizadas

Nosso próximo passo foi avaliar se durante a infecção por *E. coli* haveria interação dos CLs com as bactérias. Através microscopia confocal observamos que de fato havia interação bactéria/CLs e, em uma frequência relativamente comum nessas células, sendo que parte dos CLs ficam nas proximidades das bactérias **(Figura 7A-B)**. Quando analisamos os macrófagos tratados com ácido oléico, nas mesmas condições, observamos que houve aumento dessa interação e do número de CLs nas proximidades das bactérias **(Figura 7B)**.

Nós nos perguntamos se essa interação bactéria/CLs poderia indicar que os CLs teriam propriedades antibacterianas. Para testar essa hipótese, tentamos mimetizar a interação CLs e bactérias in vitro. Nós crescemos *E. coli* até a fase estacionária. Em paralelo, purificamos os CLs de macrófagos estimulados com LPS e interferon- γ (IFN-γ), um clássico indutor de CLs. Em virtude das limitações impostas pelo modelo em relação a quantidade de amostra, escolhemos o método de Ensaio de morte bacteriana por placas (BPKA), conforme o desenho experimental na **Figura 7C**. Após 16h de incubação à 37°C, as amostras foram diluídas e plaqueadas e no dia seguinte as colônias contadas. Apesar de observarmos que os CLs purificados de macrófagos estimulados com LPS+INF apresentaram uma redução no número de bactérias viáveis em relação ao controle negativo (**Figura 7D-F**), não observamos diferenças significativas quanto aos CL purificados das células expostas ao veículo (que apresentam uma baixa quantidade CL) em relação a amostras tratadas com LPS+IFN (que apresentam uma grande quantidade de CLs) (**Figura 7D-F**).

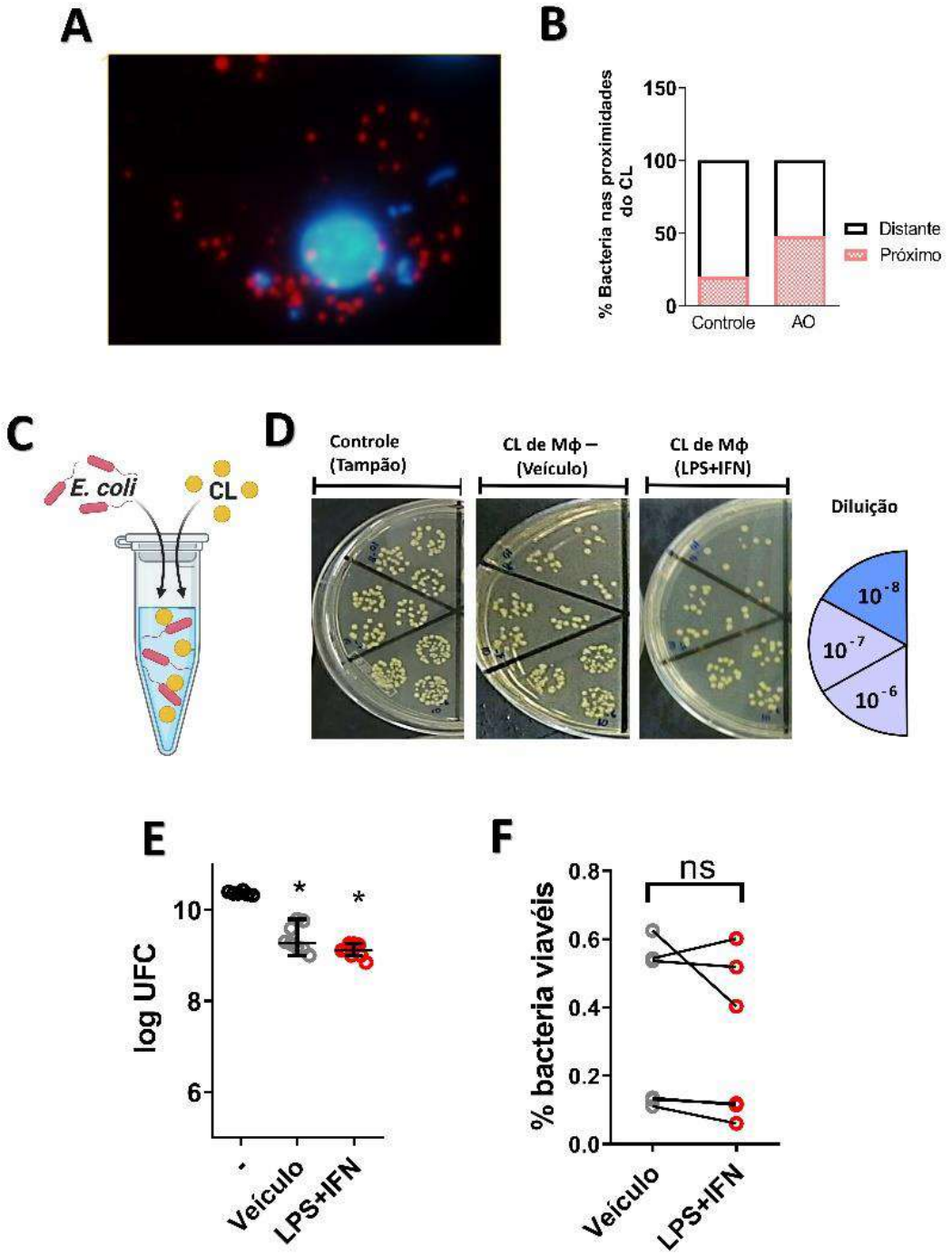

Figura 7: Bactérias interagem com CLs em macrófagos. Os macrófagos BMM foram infectados durante 1 h com *E. coli* (MOI 5). **(A)** Imagem representativa da interação bactéria/CLs. Após 24h as células foram fixadas e coradas com Oil Red O para detectar CLs (vermelho) e DAPI (azul) para marcar o DNA. **(B)** Percentuais de bactérias nas proximidades e distantes dos CLs (n=100 bactérias) em macrófagos com e sem pré-tratamento com ácido oleico (AO). (n=3) **(C)** Desenho experimental do ensaio de morte bacteriana em placa. **(D)** Imagens representativas do ensaio de morte celular em placa. **(E-F)** Quantificação do número UFC no ensaio de morte celular em placa (n=9/grupo). (F) Quantidade de bactérias viáveis nas amostras em relação ao controle negativo (Tampão salino) (N=6/grupo). *Cada ponto representa* um experimento independente. A análise estatística foi feita usando o teste ANOVA One-way seguida do pós-teste de Turkey. * significa $p < 0,05$ e ** significa $p < 0,01$. CL de Mφ: corpúsculos lipídicos purificados de macrófagos controle (veículo) ou estimulados com LPS+IFN. Controle negativo: Bacterias + tampão salino.

4.3. Inibição do acúmulo de CLs afeta a resposta inflamatória dos macrófagos

Como a participação dos CLs no processo inflamatório é algo recorrente na literatura, nós avaliamos o papel dos CLs na ativação dos macrófagos. Como estratégia experimental nós utilizamos o inibidor A922500 e avaliamos parâmetros relacionados à ativação e inflamação dos macrófagos. Primeiramente nós avaliamos dois marcadores metabólicos clássicos de ativação pró-inflamatória de macrófagos, a produção de óxido nítrico (NO) e de lactato. Assim como o esperado, a infecção por *E. coli* estimulou a produção de óxido nítrico (NO) **(Figura 8A)** e ao aumento dos níveis de lactato **(Figura 8B)**, e de forma expressiva a inibição do acúmulo de CLs foi acompanhada pela diminuição desses marcadores, indicando que a modulação do metabolismo lipídico também modula outras vias metabólicas além da síntese e oxidação de ácidos graxos.

Nosso próximo passo foi avaliar a produção de mediadores inflamatórios e a atuação dos CLs como uma plataforma de síntese desses mediadores. Para isso foi analisado se a infecção por *E. coli* induziria a produção de leucotrieno B_4 (LTB_4) e de prostaglantina E_2 (PGE_2). Observamos que a infecção por *E. coli* induziu apenas a produção de PGE_2 **(Figura 8C-D)** e, o tratamento com A922500 provavelmente inibiu de forma parcial a produção desse mediador.

Por fim, fizemos um experimento piloto para verificar se os CLs poderiam também modular outros mediadores inflamatórios. Para isso nós avaliamos a produção de IL-1β **(Figura 8E)**, IL-6 **(Figura 8F)**, IL-10 **(Figura 8G)**, MCP1/CCL2 **(Figura 8H)** e TNF-α **(Figura 8I)**. Nossos dados preliminares indicam que a infecção por *E. coli* induziu a produção principalmente de citocinas pró-inflamatórias, e que a inibição do acúmulo de CLs parece afetar a produção de MCP-1/CCL2, TNF-α e IL-1β **(Figura 8)**. Nós também avaliamos se essa modulação imunometabólica também impactaria na sobrevivência celular. Nós observamos que a infecção por *E. coli* elevou os níveis da enzima lactato desidrogenasse no sobrenadante da cultura. E o tratamento com inibidor da DGAT-1 elevou ainda mais os níveis desse marcador (**Figura 8J**), que pode estar relacionado com o provável aumento de IL-1β nas células tratadas.

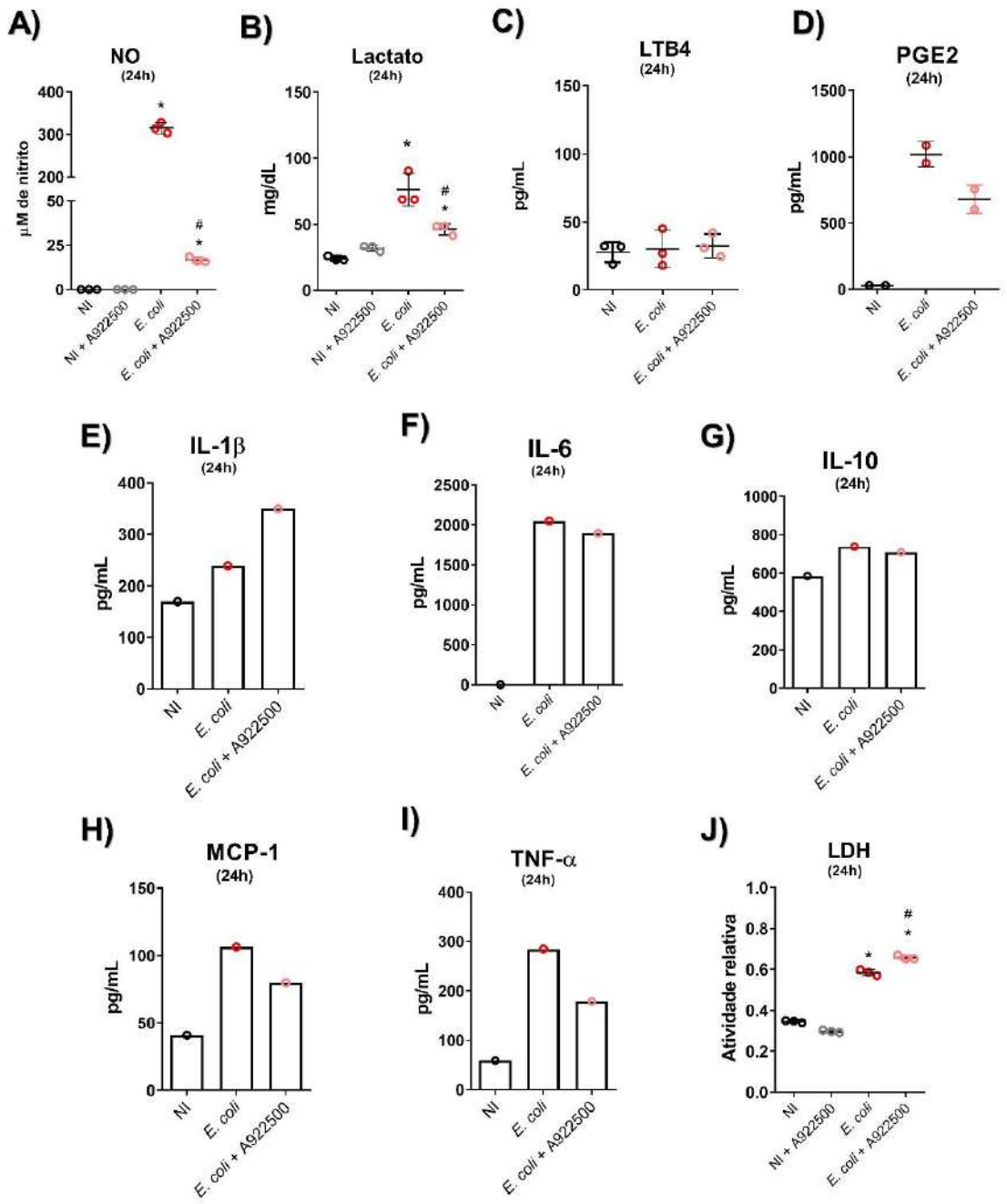

Figura 8: CLs são uma plataforma imunometabólica central na resposta pro-inflamatória de macrófagos. Macrófagos BMDM com ou sem pré-tratamento com 5 µM de A922500 foram estimuladas com *E. coli* (MOI de 100). **(A)** Concentração de óxido nítrico no sobrenadante celular após 24h da infecção, determinado pelo método de Griess. (n=3) **(B)** Nivéis de lactato no sobrenadante celular após 24h da infecção, determinado pelo método de lactato enzimático. (n=3) **(C)** Concentração de LTB_4 (n=3) e **(D)** PGE_2 (n=2) no sobrenadante celular após 24h da infecção, determinados pelo método de ensaio imuno enzimático (EIA). **(E-I)** Determinação da concentração de citocinas e quimiocinas no sobrenadante celular após 24h da infecção, determinado pelo método de ELISA (n=1). **(J)** Atividade enzimática da enzima Lactato desidrogenase (LDH) no sobrenadante celular após 24h da infecção (n=3). Cada ponto representa a média de um experimento independente. A análise estatística foi feita usando o teste ANOVA One-way seguida do pós-teste de Turkey.* significa $p < 0,05$ em relação ao controle não infectado (NI), e # significa $p < 0,05$ em relação ao grupo infectado com *E.coli* mais veículo.

4.4. A inibição da biogênese de CLs afeta a carga bacteriana in vivo.

Com base nos nossos resultados in vitro, nos perguntamos se os CLs também participariam da resposta antibacteriana in vivo. Como modelo experimental nós utilizamos o modelo de ligação cecal com perfuração (CLP), e avaliamos o impacto da inibição da biogênese de CLs na carga bacteriana nos tempos de 6h e 24h. Assim como esperado, a sepse induziu o aumento da biogênese de CLs nos leucócitos peritoniais nas primeiras 6h pós-cirurgia, e o tratamento com o inibidor A92500 aboliu essa biogênese (**Figura 9A-B).** Diferente dos experimentos in vitro, durante a sepse observamos um grande aumento da produção de LTB_4, e o tratamento com inibidor reverteu esse aumento **(Figura 9C)**. Apesar de dados anteriores no nosso grupo reportarem a associação entre CLs e isoprostano (Anexo 4), no tempo inicial da sepse não foi visto uma correlação entre esses dois fenômenos **(Figura 9D)**. Como o tratamento com A922500 impactou de forma expressiva a produção de LTB_4, nós avaliamos se isso teria impacto na migração de neutrófilos para o sitio da infecção. Diferente ao esperado, nesse tempo nós não observamos um aumento significativo de número de neutrófilos no peritônio dos animais CLP em relação ao grupo Sham **(Figura 9E)** e, consequentemente, nenhuma diferença foi observada entre o grupo CLP e CLP tratado com A922500. Resultado similar foi observado para os leucócitos mononucleados **(Figura 9F)**.

Por fim, nós avaliamos se a inibição da biogênese de CLs pelo tratamento com A922500 levou ao aumento da carga bacteriana no sitio de infecção. Nossos resultados mostram que a inibição da biossíntese de CLs foi acompanhada por um aumento significativo na carga bacteriana já nas primeiras 6h após a sepse **(Figura 9G-H)**. Este conjunto de resultados colaboram com a nossa hipótese que os CLs nos leucócitos estejam envolvidos no processo de resistência à infecção bacteriana.

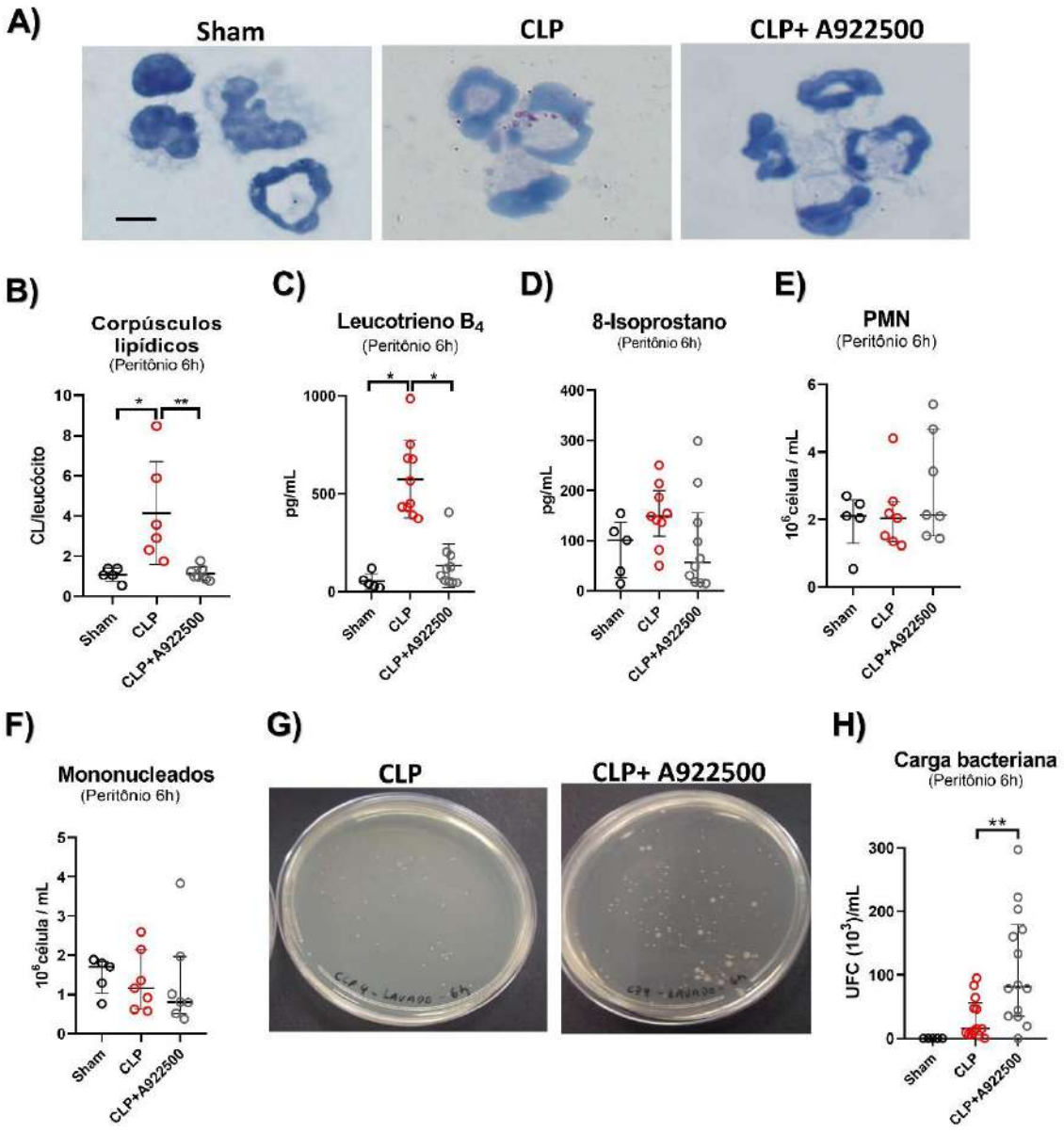

Figura 9: Inibição da biogênese de CLs nos leucócitos peritoneais aumenta a carga bacteriana durante as primeiras horas da sepse. Camundongos C57Bl/6 foram pretratados com A922500 (3mg/kg, i.g.) ou veículo. Após 1h, os animais foram submetidos à CLP e eutanasiados após 6h da cirurgia. **(A)** Imagens representativas dos leucócitos peritoneais após 6h da indução da sepse, corados com hematoxilina de Meyer (núcleos) e ORO (CLs). Barra de escala: 10 µm. **(B)** Quantificação do número de CLs por células, a partir da contagem de CLs em 50 leucócitos peritoneais consecutivos (sham=5, CLP=7, CLP+A922500=7). **(C)** Concentração de LTB_4 e **(D)** 8-isoprostano no sobrenadante do lavado peritoneal após 6h da cirurgia, determinados pelo método de ensaio imuno enzimático (EIA) (sham=5, CLP=10, CLP+A922500=10). Leucometria dos leucócilos **(E)** polimorfonucleares (PMN) e **(F)** mononucleados presentes no lavado peritoneal após 6h da cirurgia. (sham=5, CLP=7, CLP+A922500=7) **(G)** Imagens representativas da carga bacteriana presente no lavado peritoneal no tempo de 6h pós-cirurgia. **(H)** Quantificação das unidades formadoras de colônia (CFU) no peritônio após 6h da indução da sepse (sham=10, CLP=14, CLP+A922500=14). Cada ponto representa um animal. A análise estatística foi feita usando o teste ANOVA One-way seguida do pós-teste de Turkey.* significa $p < 0,05$ e ** significa $p<0,01$.

4.5. O tratamento com A922500 eleva a bacteremia nos animais sépticos, mas não interfere na dislipidemia.

Com base nos resultados anteriores, nós nos perguntamos se o tratamento com A922500 também teria impacto sistêmico, favorecendo a disseminação da infecção. Para isso nós analisamos a carga bacteriana presente no sangue dos animais. Apesar da carga bacteriana no sangue ser baixa no tempo de 6h nos animais sépticos, o tratamento com A922500 apresentou um aumento significativo na bacteremia, de cerca de duas vezes em comparação aos animais sépticos controle **(Figura 10A-B)**. Como houve um aumento da bacteremia nos animais tratados com A922500, nós avaliamos se haveria uma diferença na quantidade e na composição dos leucócitos circulantes nesses animais. Nós observamos que em ambos os grupos CLP houve uma diminuição do número de neutrófilos **(Figura 10C)** e não foi observada nenhuma alteração no número de monócitos circulantes **(Figura 10D).** Esses dados corroboram com o resultado anterior de que o tratamento com A922500 não intefere na migração celular.

Nós avaliamos se o tratamento com o inibidor da DGAT-1 também afetaria a dislipidemia associada à sepse. Observamos, conforme é bem documentado na literatura, aumento dos níveis de triglicerídeos circulantes nos animais sépticos. O tratamento com A922500 não interferiu nesse processo **(Figura 10E)**. Em relação a concentração de colesterol total no sangue, nenhuma diferença significativa foi observada entre os grupos **(Figura 10F).**

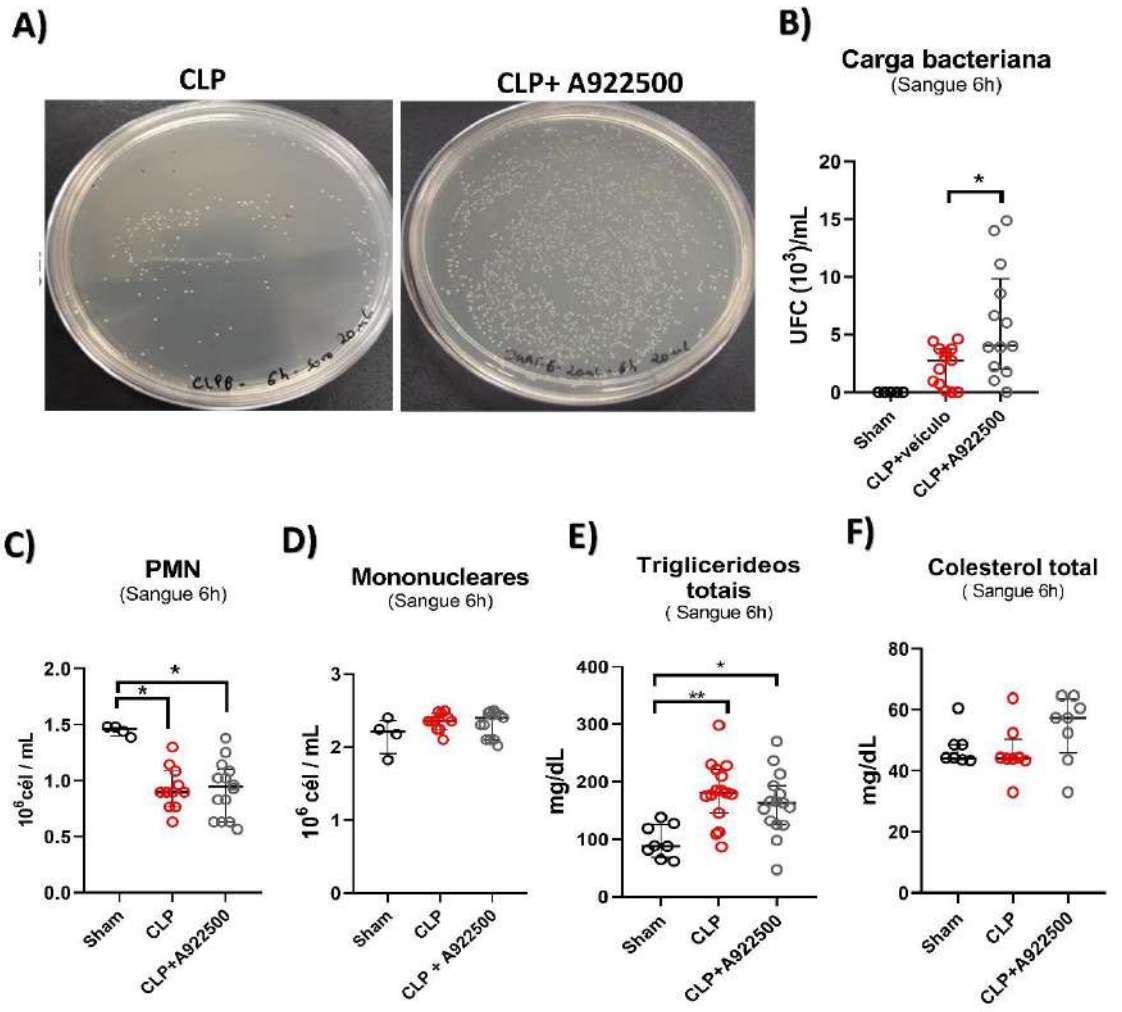

Figura 10: Animais sépticos tratados com A922500 apresentam uma elevação da bacteremia, mas esse fenômeno não está associado a migração celular e nem a dislipidemia. Camundongos C57Bl/6 foram pretratados com A922500 (3mg/kg, i.g.) ou veiculo. Após 1h, os animais foram submetidos à CLP e eutanasiados após 6h da cirurgia **(A)** Imagens representativas da carga bacteriana presente no soro no tempo de 6h pós-cirurgia. **(B)** Quantificação das unidades formadoras de colônia (CFU) no soro após 6h da indução da sepse. (sham=5, CLP=14, CLP+A922500=14) **(C-D)** Leucometria dos leucócilos **(C)** polimorfonucleares (PMN) e **(D)** mononucleados presentes no sangue após 6h da cirurgia. (sham=4, CLP=10, CLP+A922500=10) **(E-F)** Determinação bioquímica dos níveis de **(E)** triglicerideos totais (sham=8, CLP=14, CLP+A922500=14) e **(F)** colesterol total (sham=7, CLP=8, CLP+A922500=8) no soro de animais sépticos tratdos e não tratados com A922500. Cada ponto representa um animal. A análise estatística foi feita usando o teste ANOVA One-way seguida do pós-teste de Turkey.* significa $p < 0,05$ e ** significa $p<0,01$.

4.6. O metabolismo lipídico hepático não está envolvido na disseminação da infecção no inicio da sepse.

Na sepse muitas vezes são observados o acúmulo de CLs em diversas células e tecidos, como macrófagos, neutrófilos, além do fígado, tanto em modelos experimentais como em amostras de pacientes sépticos (GAROFALO *et al.*, 2019; PACHECO *et al.*, 2007). No nível sistêmico, o fígado é o principal orgão na resposta sistêmica à infecção. Apesar de ser bem caracterizado o acúmulo de CLs em diversos órgãos, o papel dessa organela em resposta à infecção ainda não é conhecido. Para avaliar se a maior disseminação da infecção estaria relacionada à modulação da quantidade de CLs hepático pelo tratamento com A922500, avaliamos a esteatose por duas técnicas diferentes. Diferente ao reportado em tempos mais tardios, nós não observamos nas histologias o aumento da esteatose hepática nos animais sépticos no tempo de 6h após cirurgia (**Figure 11A**). Para confirmar essa análise, extraímos os lipídios neutros presentes no fígado e fizemos uma cromatografia em camada delgada, e não observamos diferenças significativas na quantidade de lipídeos neutros entre o grupo controle (sham) e o grupo CLP **(Figure 11B-D)**. Além disso, nenhuma diferença significativa foi observada em nenhum dos lipídeos neutros analisados entre os grupos CLP e os CLP tratados com o inibidor **(Figure 11B-D)**.

Dados recentes do nosso grupo **(Anexo 4)** mostraram que o tratamento com A922500 foi capaz de inibir o estresse oxidativo no fígado no tempo de 48h. Para avaliar se no nosso modelo a modulação do estresse oxidativo no fígado estaria relacionado à maior disseminação da infecção, nós avaliamos as concentrações de malonaldeído hepático (MDA, um marcador de estresse oxidativo lipídico) e de sulfidrilas (um marcador do estresse oxidativo ao nível de proteína). Diferente ao que vem sendo reportado para tempos tardios da sepse, no tempo de 6h não foi observado aumento do estresse oxidativo nos animais sépticos **(Figure 11E-F)**. O tratamento com A922500 não mudou esse fenômeno. Por fim, avaliamos ainda a atividade da mieloperoxidase, um marcador de infiltração de neutrófilos aos tecidos. Observamos que apesar da sepse induzir ao aumento significativo dessa enzima no fígado, não foi observado diferenças significativas em relação grupo tratado com A922500 **(Figure 11G)**. Apesar de negativos, esse conjunto de resultados reforça que a disseminação da infecção não está relacionada a modulação sistêmica da resposta a infecção.

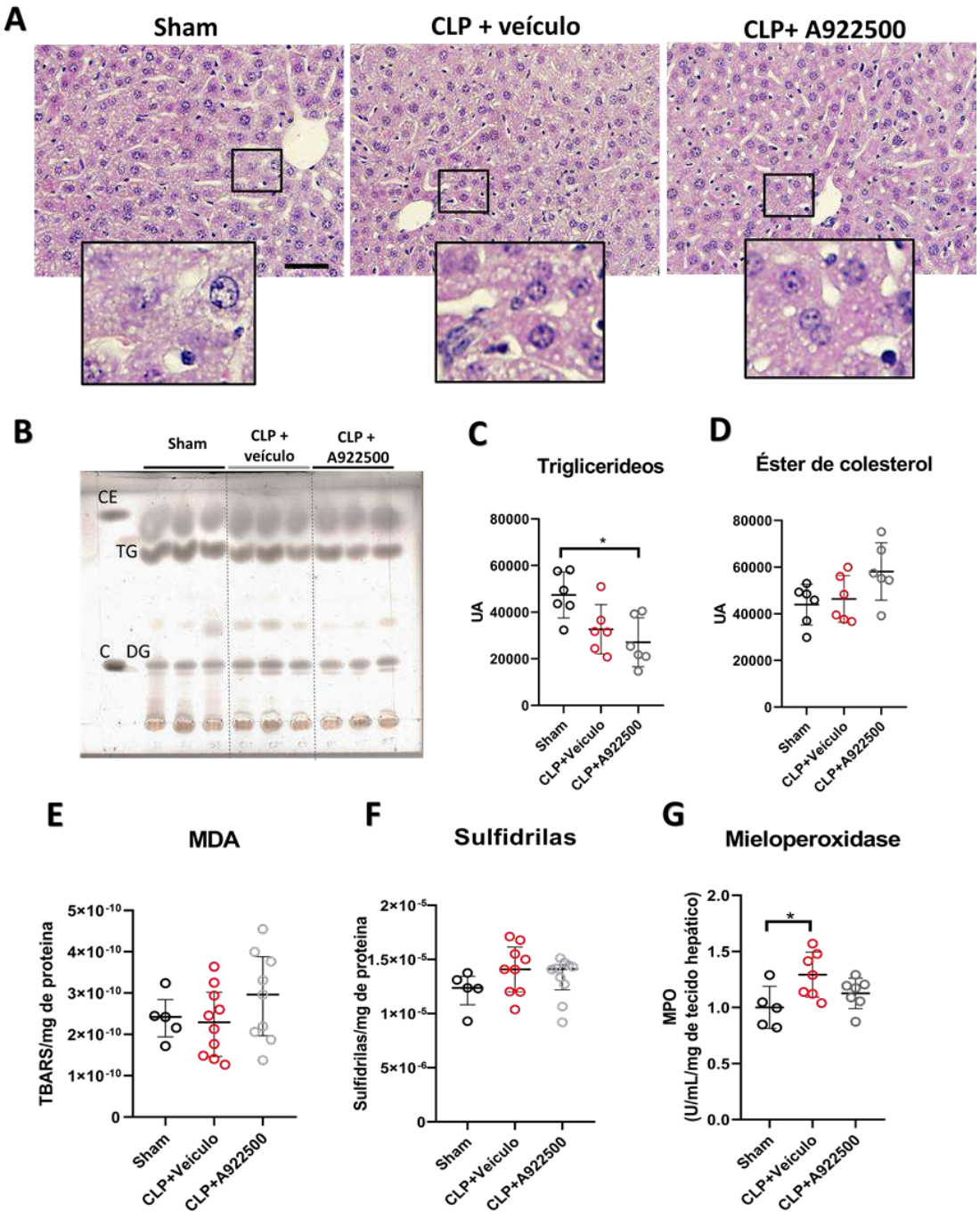

Figure 11: Tratamento com A922500 não interfere no metabolismo lipídico hepático nos tempos iniciais da sepse. Camundongos C57Bl/6 foram pré-tratados com A922500 (3mg/kg, i.g.) ou veículo. Após 1h, os animais foram submetidos à CLP e eutanasiados após 6h da cirurgia **(A)** Cortes histológicos de fígado corado por Hematoxilina-Eosina. **(B)** Imagem representativa de cromatografia em camada delgada evidenciando lipídios neutros do fígado dos animais séticos e controle. CE: colesterol ester, C: colesterol, TG: triglicerídeos, DG: diacilglicerídeos **(C-D)** Densiometria da quantidade hepática de **(C)** triglicerídeos e de **(D)** colesterol ester (n=6). **(E)** Avaliação da quantidade de malonaldeído (MDA) através da determinação dos niveis de substâncias reativas ao ácido tiobarbitúrico (TBARS) no fígado de animais sépticos tratados e não tratados com A922500. (Sham=5, CLP=10, CLP+A922500=10) **(F)** Conteúdo tiólico total no fígado de animais sépticos tratados e não tratados com A922500 (Sham=5, CLP=10, CLP+A922500=10) (G) Avaliação da atividade de mieloperoxidase hepático no fígado de animais sépticos tratados e não tratados com A922500 (Sham=5, CLP=7, CLP+A922500=7). Cada ponto representa uma amostra. A análise estatística foi feita usando o teste ANOVA One-way seguida do pós-teste de Turkey.* significa $p < 0,05$ e ** significa $p < 0,01$.

4.7. O papel protetor do CLs frente à infecção bacteriana perdura no tempo 24h após a cirurgia.

Nosso próximo passo foi avaliar se a participação dos CLs na resposta antibacteriana seria um fenômeno transitório ou se continuaria ao longo do tempo da infecção. Para isso, nós avaliamos se o tratamento conseguiria inibir o acúmulo de de CLs no tempo de 24h. Assim como vem sendo reportado pelo nosso grupo, observamos que a sepse induziu um acúmulo expressivo de CLs nesse tempo analisado, e o tratamento com A922500 foi capaz de inibir significativamente esse fenômeno **(Figura 12A-B)**. Além disso, observamos que a sepse induziu a migração de neutrófilos para a cavidade peritoneal, e o tratamento com A922500 não impactou a migração de neutrófilos para o sítio da infecção **(Figura 12C)**. Assim como observado no tempo de 6h, não houve alteração na quantidade de macrófagos no lavado peritoneal entre os grupos analisados **(Figura 12D)**.

Por fim, investigamos se a participação dos CLs no processo de resistência continuaria no tempo de 24h. Nossos dados preliminares mostram que o papel protetor dos CLs parece perdurar também em tempos mais tardios. Observamos que a carga bacteriana nos animais tratados com A922500 foi maior do que a dos animais sépticos não tratados **(Figura 12E-F)**.

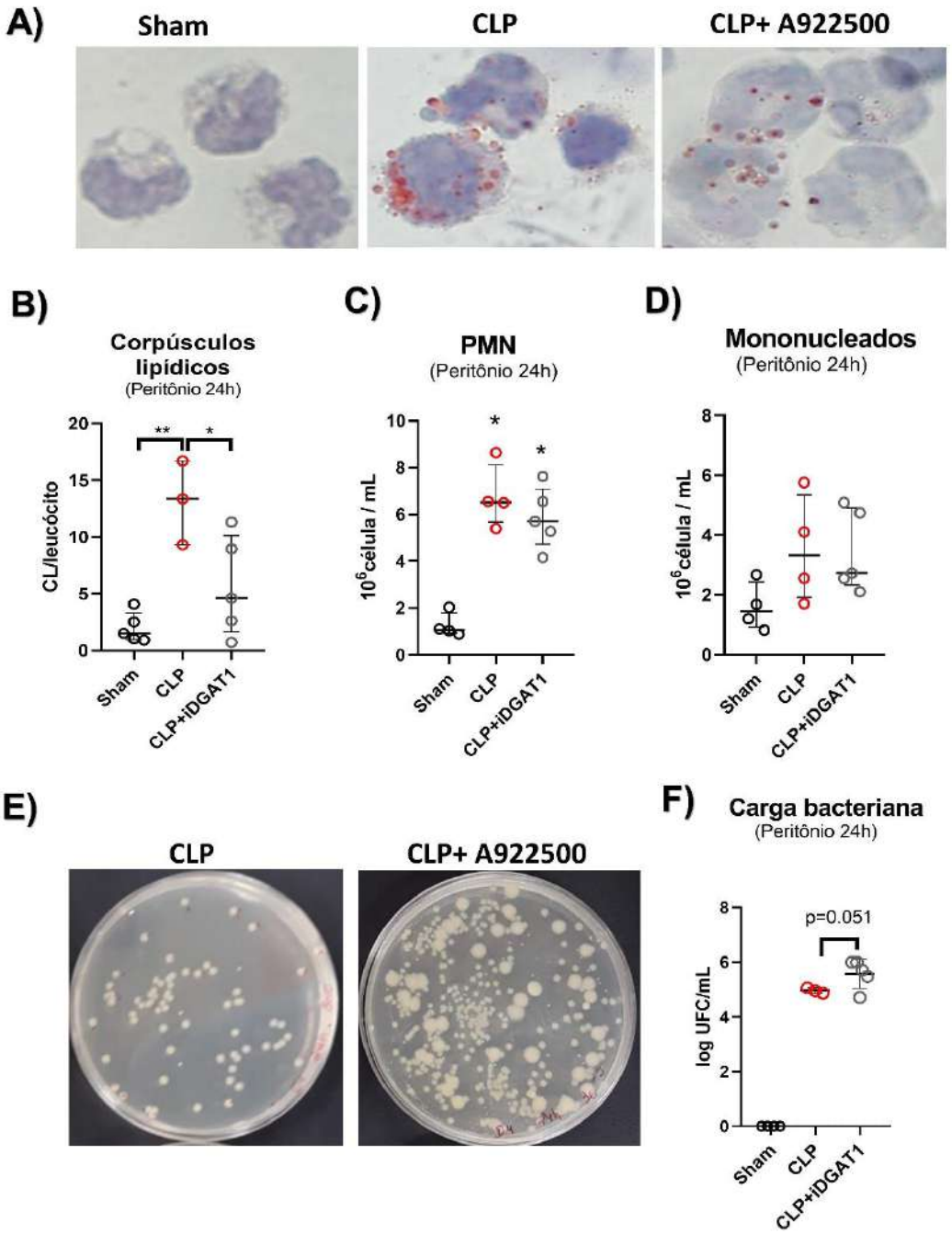

Figura 12: Inibição da biogênese de CLs nos leucócitos peritoneais aumenta a carga bacteriana no peritôneo dos animais sépticos. Camundongos C57Bl/6 foram pretratados com A922500 (3mg/kg, i.g.) ou veículo. Após 1h, os animais foram submetidos à CLP. No tempo de 6h após a cirurgia os animais receberam uma segunda dose do tratamento com A922600, e foram eutanasiados após 24h da cirurgia **(A)** Imagens representativas dos leucócitos peritoneais após 24h da indução da sepse, corados com hematoxilina de Meyer (núcleos) e ORO (CLs). Barra de escala: 10 µm. **(B)** Quantificação do número de CLs por células, a partir da contagem de CLs em 50 leucócitos peritoneais consecutivos. Leucometria dos leucócilos **(C)** polimorfonucleares (PMN) e **(D)** mononucleados presentes no lavado peritoneal após 24h da cirurgia. **(E)** Imagens representativas da carga bacteriana presente no lavado peritoneal no tempo de 24h pós-cirurgia. **(F)** Quantificação das unidades formadoras de colônia (CFU) no peritônio após 24h da indução da sepse. Cada ponto representa um animal. A análise estatística foi feita usando o teste ANOVA One-way seguida do pós-teste de Turkey.* significa $p < 0,05$. ($Sham_{24h}$=5, CLP_{24h}=4, $CLP+A922500_{24h}$=6)

4.8. O papel imunometabólico dos CLs proeminente durante a sepse

Para melhor compreender a participação dos CLs nos mecanismos de resistência à infecção, nos avaliamos a influência da inibição da biogênese dos CLs no processo inflamatório. Para isso avaliamos a secreção de oito citocinas e quimiocinas, tanto pró-inflamatórias quanto antiinflamatórias, presentes no lavado peritoneal dos animais sépticos. Nós observamos que em ambos os tempos analisados houve um intenso processo inflamatório, com aumento de praticamente todas as citonas/quimiocinas analisadas, sendo que em 24h o processo inflamatório no geral foi mais exacerbado **(Figura 13)**.

Em uma análise mais cuidadosa, nós observamos que no tempo de 6h após a indução da sepse houve um aumento significativo nos níveis de praticamente todas as citocinas analisadas, com exceção da IL-12 (**Figura 13A)**. Nós observamos que a inibição da biossíntese de CLs foi acompanhada pela inibição significativa dos níveis de IL-6 **(Figura 13B)**) e KC **(Figura 13C)**, e por uma perturbação nos níveis dos IFN-γ (**Figura 13D)** e MCP-1/CCL2 **(Figura 13E)**, apesar dos níveis dessas últimas não serem significativas em relação ao grupo CLP.

Já em 24h, a inibição do acúmulo de CLs teve menos impacto no acúmulo dos mediadores inflamatórios na peritôneo, apesar da resposta inflamatória ser mais intensa nesse tempo. Nesse tempo só foi observado que a inibição do acúmulo de CLs foi acompanhada da redução significativa dos níveis de MCP-1/CCL2 (**Figura 13D)**. E, em nenhum dos tempos analisados foi visto uma relação entre o acúmulo de CLs com os níveis de IL-1β (**Figura 13F)**, IL-10 (**Figura 13G)** e TNF-α (**Figura 13H)**, indicando que o papel dos CLs na resposta inflamatória é especifico e coordenado.

Por fim, avaliarmos o papel dos CLs na produção de óxido nítrico (NO) no lavado peritoneal. Apesar de não ter sido possível detectar NO no tempo de 6h, a inibição do acúmulo de CLs foi acompanhada pela diminuição da produção NO no tempo de 24h (**Figura 13I)**, indicando que os CLs afetam uma das vias mais clássicas relacionadas à atividade antibacteriana dos leucócitos.

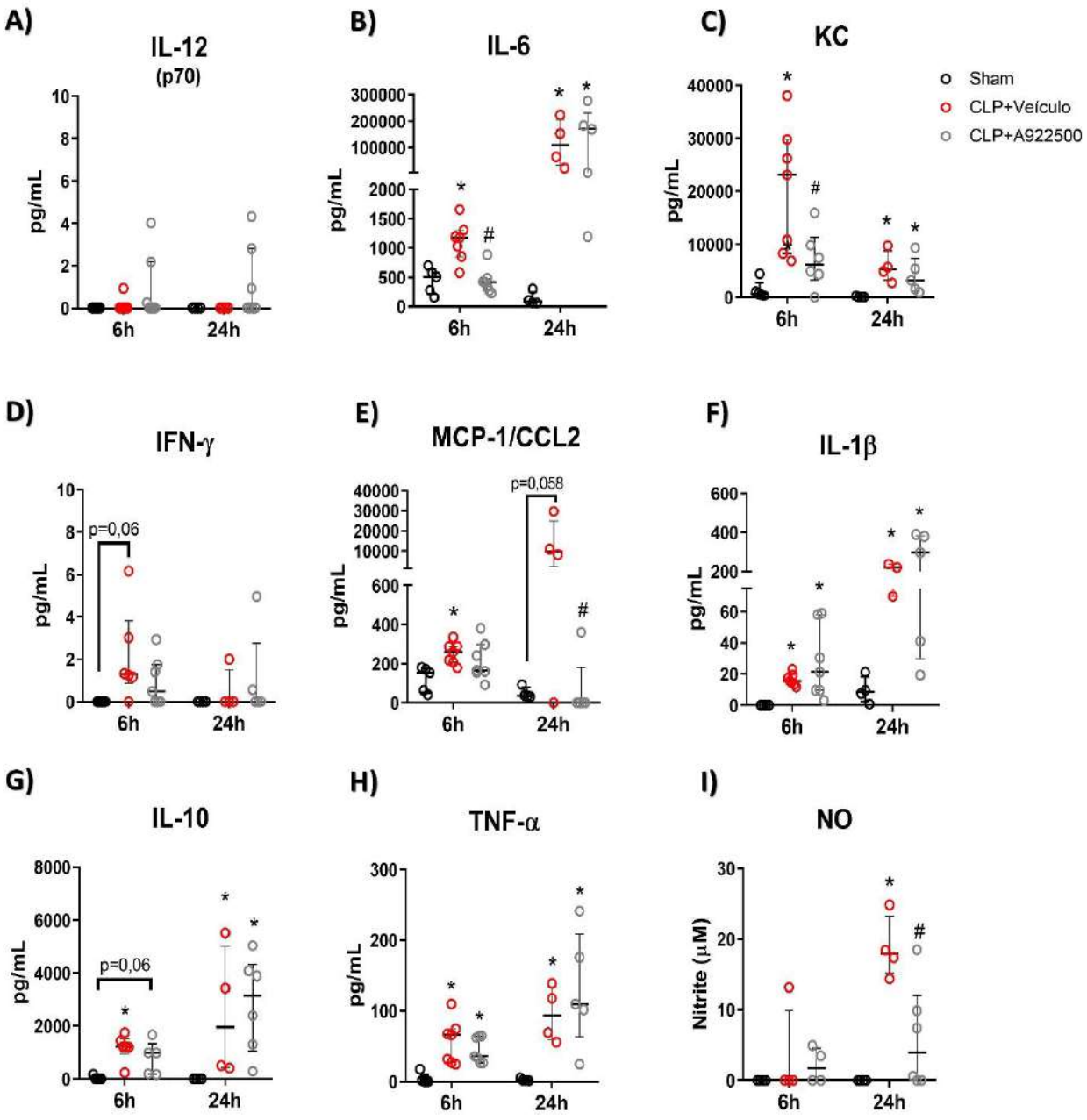

Figura 13: O papel imunometabólico na inflamação induzida pela sepse é proeminente durante. Camundongos C57Bl/6 foram pretratados com A922500 (3mg/kg, i.g.) ou veículo. Após 1h, os animais foram submetidos à CLP. Os grupos de 24h receberam uma segunda dose do tratamento com A922600 ou veículo **(A-H)** Determinação das concentrações de citocinas e quimiocinas no sobrenadante lavado peritoneal após 6h e 24h após a indução da sepse. Todas as citocinas analisadas foram quantificadas através da técnica de Luminex. **(I)** Concentração de óxido nítrico no sobrenadante do lavado peritoneal após 6h e 24h da indução da sepse, determinado pelo método de Griess. Cada ponto representa um animal analisado. A análise estatística foi feita usando o teste ANOVA One-way seguida do pós-teste de Turkey.* significa $p < 0,05$ em relação ao controle não infectado (NI), e # significa $p < 0,05$ em relação ao grupo CLP mais veículo. ($Sham_{6h}$=5, CLP_{6h} =6, $CLP+A922500_{6h}$ =7, $Sham_{24h}$=5, CLP_{24h}=4, $CLP+A922500_{24h}$=6)

4.9. Inibição da enzima DGAT-1 não interfere na sobrevivência e nem na gravidade da sepse

Por fim, nós verificamos se o tratamento com A922500 influenciaria na sobrevida e na gravidade da sepse além do controle da carga bacteriana. Para isso, todos os animais receberam 1h antes da cirurgia uma dose via intragástrica do inibidor ou do veículo, com reforço em 6h e 24h. Para essas análises os animais foram tratados com antibiótico, nos tempos de 6h e 24h após a cirurgia. Observamos que em 6h após cirurgia não houve mortalidade em nenhum dos grupos. Já em 24h, observamos uma mortalidade de 50% no grupo CLP e de 70% no grupo CLP tratado com A922500. Em 48h, a mortalidade subiu em ambos grupos, atingindo 80% no grupo CLP e 90% no grupo CLP tratado com A922500. Não foram observadas diferenças estatísticas entre os grupos CLP. O grupo de animais *sham* e *sham* tratado com A922500 não apresentaram mortalidade, apresentando 100% de sobrevivência ao longo de todo experimento **(Figura 14A)**.

Concomitantemente, nós avaliamos se o tratamento com o inibidor seria capaz de modificar a gravidade da sepse. Para isso foi realizado a avaliação do escore clínico nos camundongos de todos os grupos ao longo do tempo, através dos parâmetros característicos do quadro infeccioso. Nas primeiras 6h já observamos a caracterização do quadro séptico nos camundongos CLP, que se agravou em 24h, atingindo escore acima de 9, compatível com o choque séptico, que se manteve até 48h **(Figura 14B)**. E assim como na mortalidade, não foi observado diferenças significativas entre os grupos CLP e CLP tratado com A922500 em nenhum dos tempos analisados. Além disso, os grupos *Sham* e *Sham* tratado com A922500 apresentaram escore zero durante todo período analisado.

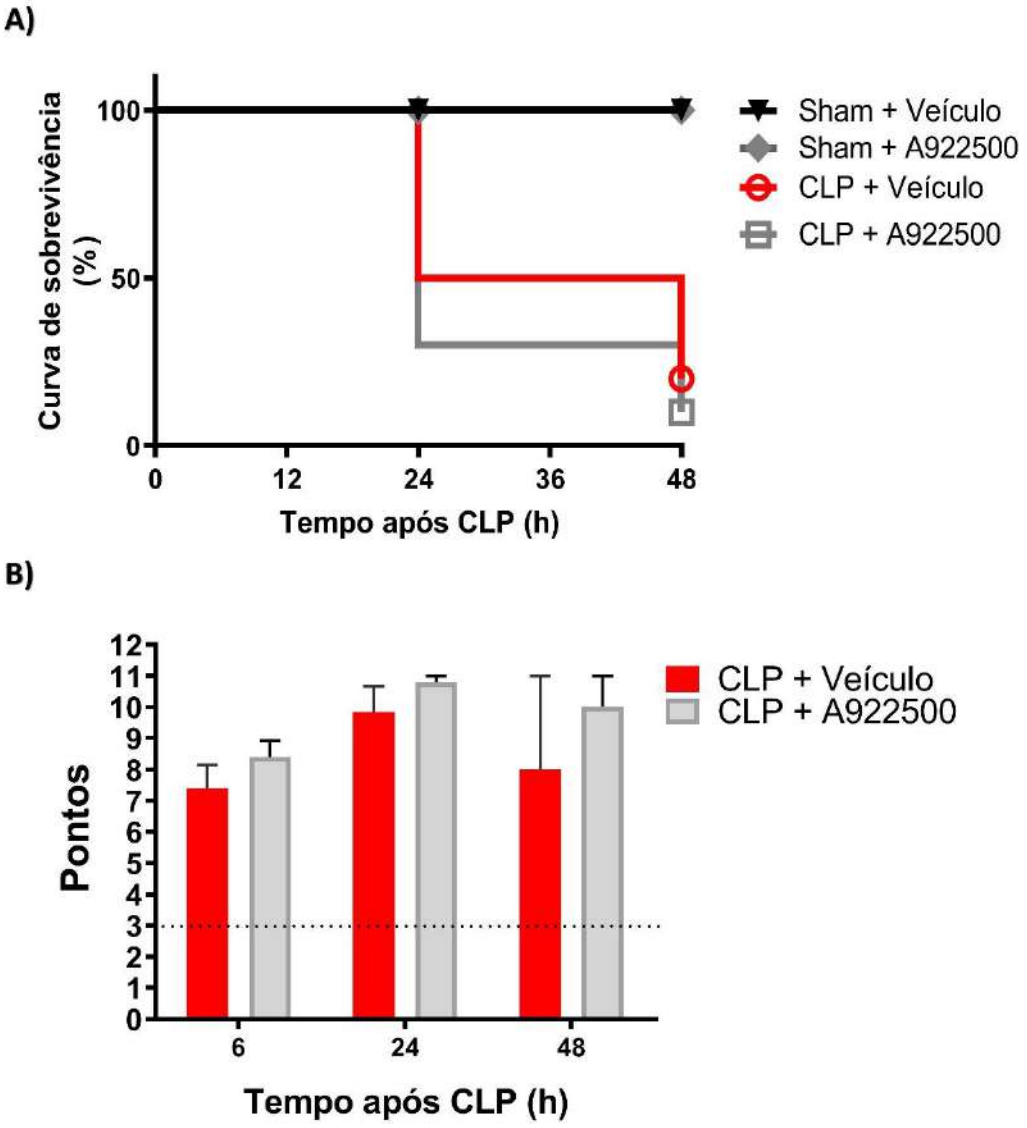

Figura 14: Tratamento do A22500 não interfere nem na sobrevivência e nem na gravidade da sepse. Camundongos C57Bl/6 foram pretratados com A922500 (3mg/kg, i.g.) ou veículo. Após 1h, os animais foram submetidos à CLP. No tempo de 6h e 24h após a cirurgia os animais receberam uma segunda e terceira dose do tratamento com A922600 ou inibidor, conjuntamente com a antibioticoterapia (Meropenen, 10mg/kg, via subcutânea). Os animais foram acompanhados por 48h. **(A)** Avaliação da curva de sobrevida dos animais submetidos à sepse, tratados e não tratados com A922500 (N=10) **(B)** Avaliação do escore de gravidade da sepse nos submetidos à sepse, tratados e não tratados com A922500. N=10.

4.10. CLs de macrofágos murinos não compartimentalizam histonas

A primeira descrição da atividade antibacteriana dos CLs foi no trabalho de ANAND e colaboradores (2012). Nesse trabalho foi visto que nos embriões de *Drosophila melanogaster*, a principal proteína responsável pela atividade antibacteriana eram as histonas. Além disso nesse mesmo trabalho foi reportada a presença de histona nos CLs hepáticos induzidos por injeção de LPS em camundongos C57BL/6 como um indício de que o mesmo mecanismo antibacteriano aconteceria em mamíferos. Como nossos dados preliminares indicavam que os CLs poderiam ter uma atividade antibacteriana, nós investigamos se havia a presença das histonas nessa organela.

Para investigar essa possibilidade, nosso primeiro desenho experimental foi avaliar se durante a biogênese de CLs também haveria o aumento da expressão das histonas H2A e H2B nos lisados totais de macrófagos estimulados com LPS e INFγ. Diferente do esperado, nós não observarmos nenhuma alteração na expressão nem da H2A **(Figura 15A)** e nem da H2B **(Figura 15B)**. Como não houve diferença na expressão das histonas, investigamos se haveria uma reorganização dessas proteínas do núcleo para os CLs. Para isso nós utilizamos dois modelos clássicos de indução de CLs, tratamento com LPS e IFNγ e com ácido oléico. E mesmo através da imunofluorescência confoncal não foi possível a identificação da histona H2A em outros compartimentos celulares, a não ser a nuclear **(Figura 15C-D).**

Como as histonas estão majoritariamente no núcleo das células passamos a nos perguntar se esta presença maciça não poderia estar mascarando a presença das histonas em outros compartimentos celulares, dificultando a identificação das histonas nos CLs. Para contornar essa limitação, nós purificamos CLs de 100 milhões de macrófagos através do fracionamento celular por gradiente de sacarose. Por western blot, também não foi possível a identificação da presença de Histonas na Fração F1, onde se localizam os CLs **(Figura 15E)**.

Por fim, nossa última abordagem experimental foi fazer a transfecção da Histona H1 fusionada a GFP em uma linhagem de macrófagos, com posterior estimulação dessas células com LPS + IFNγ. Novamente nós não identificamos a presença de histonas nos CLs dos macrófagos **(Figura 15F)**.

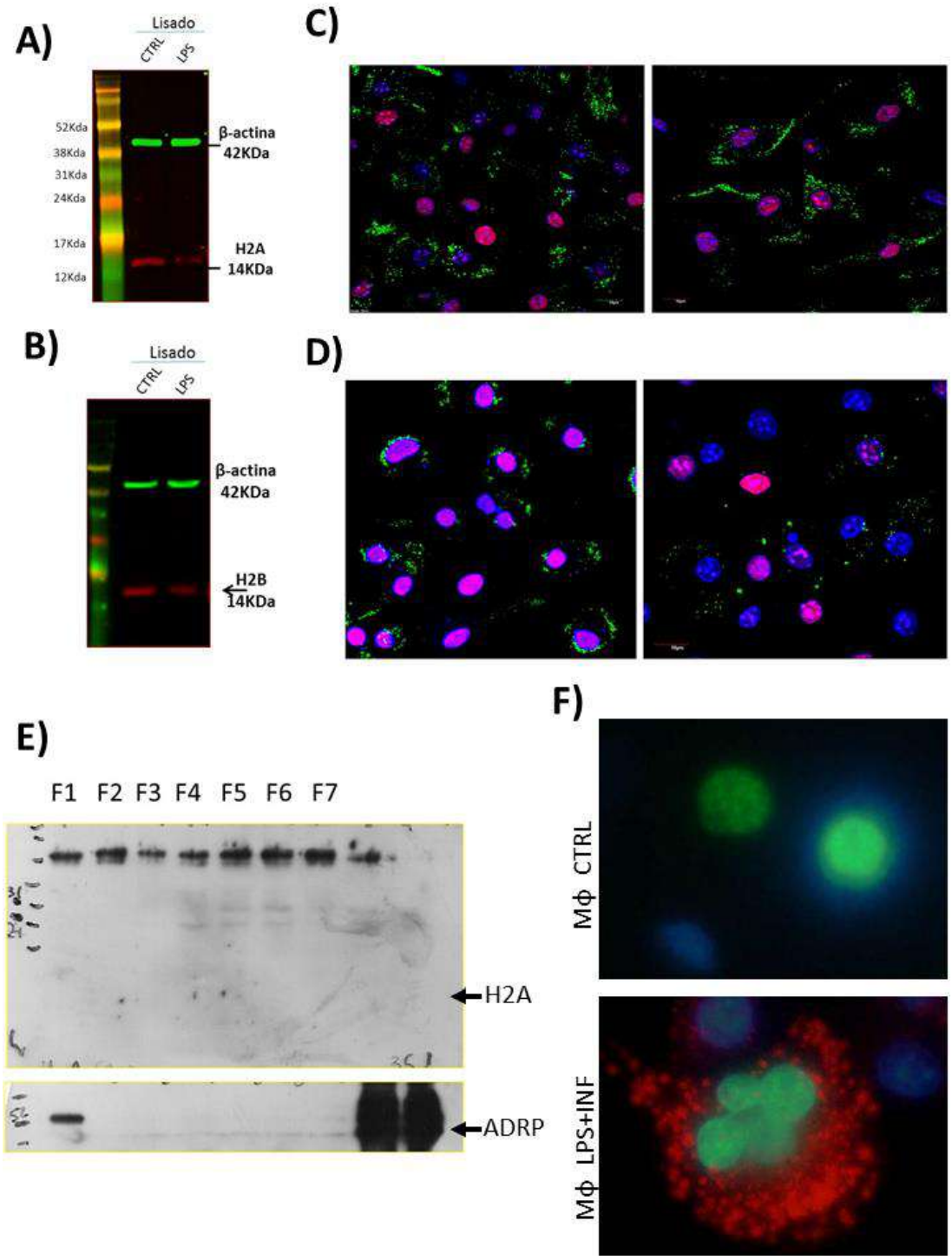

Figura 15: Histonas não se localizam no CLs de macrófagos. Expressão da histona **(A)** H2A e **(B)** H2B em macrófagos BMDM estimulados com LPS (500 ng/mL) mais IFNγ (10 ng/mL) por 24h. Imagens de microscopia confocal de macrófagos BMM estimulados com **(C)** 40 µM de ácido oleico 24h ou **(D)** com *E. coli* (MOI 1: 5) por 1 h. As células foram fixadas e coradas com Bodipy 493/503 para detectar corpos lipídicos (verde), anti-H2A (rosa) e DAPI (azul). **(E)** Expressão da histona H2A e ADRP em CLs isolados por gradiente de sacarose de macrófagos ativados. **(F)** Macrófagos iBMM transfectados com histona H1 fusionada a GFP em macrófagos controle e estimulados com LPS + IFNγ após 24h.

4.11. CLs hepáticos induzidos pela sepse apresentam atividade antibacteriana

A esteatose na sepse é um fenômeno bem documentado em diversos tipos celulares e tecidos, tanto em modelos experimentais como em amostras de pacientes (GAROFALO *et al.*, 2019; PACHECO *et al.*, 2007). Porém, a função dessa organela nesses sítios ainda é desconhecida. Como prova de conceito de que os CLs de qualquer célula ou tecido podem ter um papel protetor frente à infecção, purificamos os CLs hepáticos induzidos pela sepse após 24h da cirurgia, através de gradiente de sacarose **(Figura 16A)**. Por microscopia de fluorescência, observamos que a sepse induziu não só um aumento da quantidade de CLs, mas também alterações no tamanho dessa organela **(Figura 16B).** Esses achados iniciais foram corroborados pela quantificação dos triglicerídeos e de proteínas presentes na fração F1 do gradiente **(Figura 16C-D)**. Além disso, quando analisamos a razão triglicerídeos/proteínas observamos que os CLs induzidos pela sepse eram mais proteicos do que aqueles presentes nos animais controle **(Figura 16E)**.

Como prova de conceito de que os CLs induzidos pela sepse poderiam ter atividade antibacteriana, nós mimetizamos a interação bactéria/CLs novamente, mas agora com os CLs do fígado **(Figura 16F)**. Observamos que os CLs hepáticos induzidos pela sepse apresentaram atividade antibacteriana, evidenciado pela diminuição significativa do número de bactérias viáveis crescidas nas placas de ágar LB **(Figura 16G-H)**. Ao mesmo tempo, esse fenômeno não foi observado para os CLs purificados dos animais Sham **(Figura 16G-H)**.

Nosso próximo passo foi analisar, se assim como acontece em *Drosophila*, essa atividade antibacteriana estaria relacionada ao conteúdo protéico dessa organela. Para isso nós precipitamos as proteínas presentes na fração F1 do gradiente com acetona, e as ressuspendemos em Tris 0,1M, realizamos novamente o ensaio de morte bacteriana em placa, mas em vez de CLs intactos, nós colocamos 100 µg de proteínas derivadas do CLs **(Figura 16I)**. Assim como observado para os CLs intactos, as proteínas derivados dos CLs dos animais sépticos apresentaram atividade antibacteriana significativa em relação ao controle negativo, mas também em relação ao animais Sham **(Figura 16J-K).** Esse conjunto de resultados demonstra pela primeira vez que os CLs participam de forma direta da resposta antibacteriana.

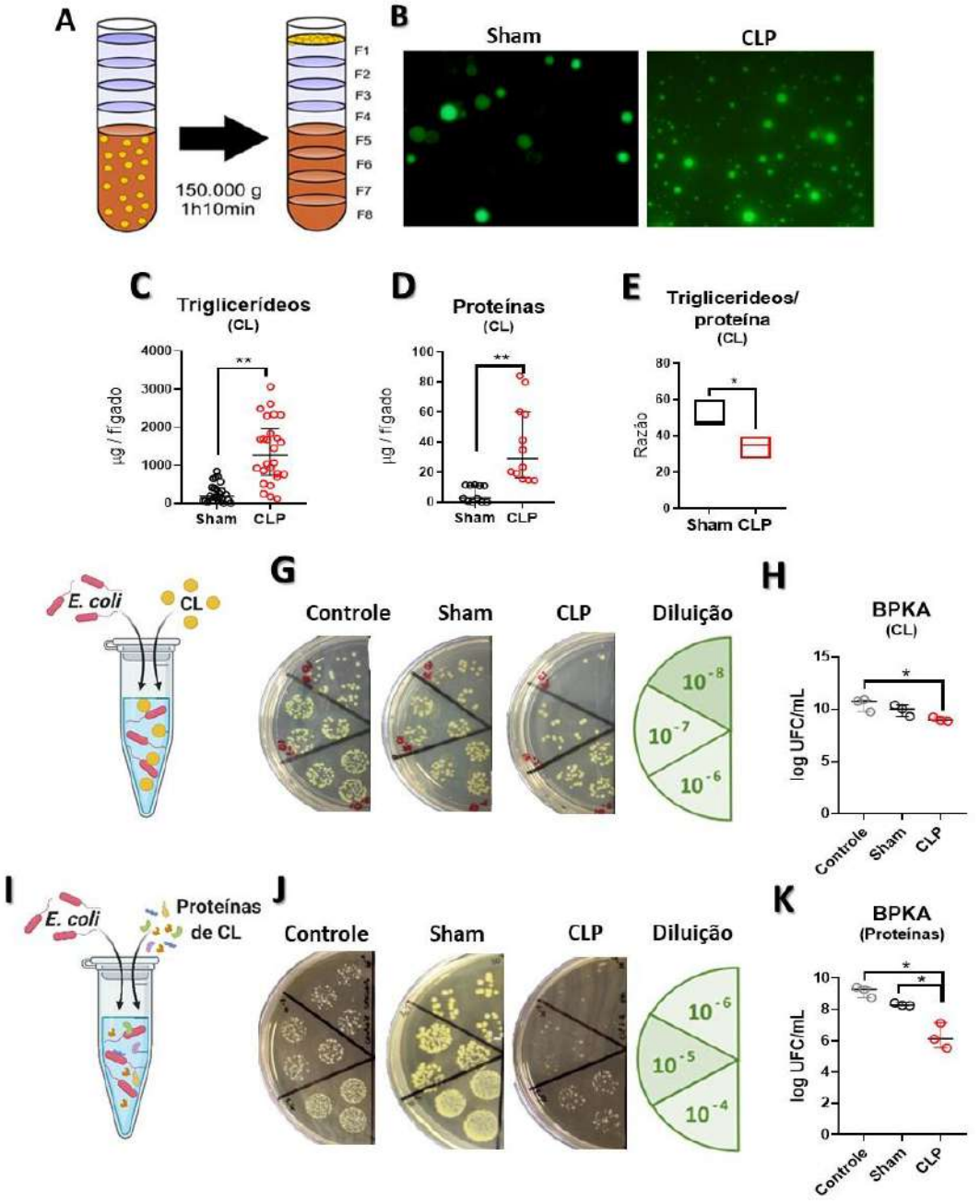

Figura 16: Corpúsculo lipídico hepático induzido pela sepse possuem atividade antibacteriana. CLs foram purificados do fígado de animais sépticos após 24h da cirurgia. **(A)** Esquema representativo do gradiente de sacarose. **(B)** Microscopia de fluorescência dos CLs purificados do fígado de animais sham e CLP. Os CLs foram marcados com bodipy. **(C)** Quantificação da quantidade de triglicerídeos (n=25/grupo) e de **(D)** proteínas (n=12/grupo) presentes na fração F1 dos gradientes. **(E)** Razão triglicerídeos/proteínas presente nas frações F1 dos gradientes (n=3). **(F)** Desenho experimental da atividade antibacteriana dos CLs intactos. Para esse ensaio foram aplicados 100 uL da fração de CLs intactos a partir da F1 do gradiente de sacarose **(G)** Fotos representativas do ensaio de morte célular em placa (BPKA). (n=3) **(H)** Quantificação do numero de UFC do ensaio BPKA (n=3). **(I)** Desenho experimental da atividade antibacteriana das proteínas de CLs. Para esse ensaio foram aplicados 100 µg de proteínas de CLs **(J)** Fotos representativas do ensaio de morte célular em placa (BPKA). (n=3) **(H)** Quantificação do numero de UFC do ensaio BPKA (n=3). *Cada ponto representa um animal analisado*. A análise estatística foi feita usando o teste ANOVA One-way seguida do pós-teste de Turkey.* significa $p < 0,05$

4.12. A atividade antibacteriana das proteínas de CLs é dependente da dose e do tempo

Para confirmar a atividade do conteúdo proteico de CLs induzidos pela sepse, nós repetimos o ensaio de morte bacteriana em placa (**Figura 17A**), mas dessa vez nós trocamos a *E. coli* por uma outra bactéria extracelular, a *K. pneumoniae*. Em frente a essa nova bactéria, a propriedade antibacteriana dos CLs foi ainda mais proeminente do que a vista nas mesmas condições frente à *E. coli* (**Figura 17B-C**).

Por fim, nós avaliamos se essa nova propriedade dos CLs seria dose e temporalmente dependente. Para responder a essa pergunta nós testamos duas concentrações das proteínas de CLs (25µg e 100µg). Observamos que na maior concentração de proteínas a atividade antibacteriana foi mais proemimente do que na menor concentração (**Figura 17D-E**), indicando que a propriedade antibacteriana das proteínas dos CLs é dose dependente. Em relação à propriedade temporalmente dependente, avaliamos se os CLs hepáticos induzidos pela sepse em 48h continuariam apresentando antividade antibacteriana, e observamos que não, os CLs de 48h não apresentaram nenhuma atividade antibacteriana (**Figura 17D-E**), e isso corrobora com resultados dos leucócitos. Em ambos os casos, a atividade antibacteriana é aguda (6h e 24h).

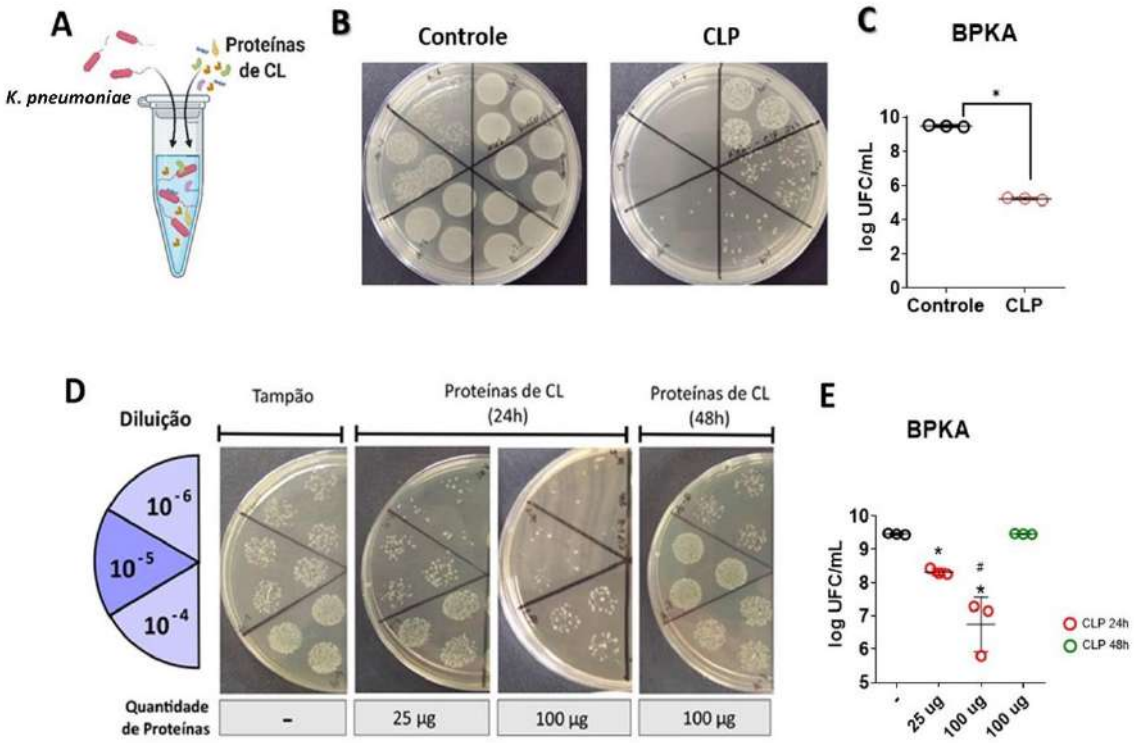

Figura 17: Proteínas de CLs possuem atividade antibacteriana e esta atividade parecer ser quantidade dependente. Proteinas de CLs foram precipitadas a partir da fração F1 do gradiente de sacarose e ressuspendidas em Tris 10 mM pH 8,0 **(A)** Desenho experimental dos experimentos. **(B)** Nesse ensaio foram utilizados 100µg proteínas de CLs induzidos pela sepse contra *K. pneumoniae*. (n=3) **(C)** Quantificação do número de UFC do ensaio BPKA contra *K. pneumoniae*. **(D)** Fotos representativas do ensaio de morte célular em placa (BPKA) com diferentes quantidades de proteínas de CLs induzidos pela sepse de 24h ou 48h contra *E. coli*. **(E)** Quantificação do número de UFC do ensaio BPKA. Cada ponto representa um experimento diferente. A análise estatística foi feita usando o teste ANOVA One-way seguida do pós-teste de Turkey.* significa $p < 0,05$ em relação com Tampão, # diferença em relação a 25µg de proteínas.

4.13. CLs compartimentalizam proteínas pró-hospedeiro

Como nossos dados e dos nossos colaboradores não confirmaram a presença de histonas nos CLs, começamos a pesquisar novos possíveis alvos que fossem responsáveis pela atividade antibacteriana dos CLs. Nesse contexto, a partir de colaboração multicêntrica cujo objetivo era caracterizar a atividade antibacteriana dos CLs, o grupo liderado pelo professor Albert Pol identificou no proteoma dos CLs hepático de camundongos estimulados com LPS a compartimentalização de importantes vias relacionadas à resposta imune inata, inclusive com a presença de proteínas com atividades antibacterianas **(Anexo 2)**. Nesse trabalho foi constatado que os CLs funcionam como um elemento central na resposta pró-hospedeiro, integrando a resposta imune inata com o metabolismo. Com base nesses novos alvos, realizamos ensaios de western blot para novas proteínas candidatas pela ação antibacteriana dos CLs (**Figura 18**). Nós identificamos na fração F1 dos animais CLP a presença das proteínas HMGB-1, uma proteína semelhante a histona, e a Catelicidina (CAMP), duas proteínas cuja atividade antibacteriana já foi demostrado, além da Viperina, uma proteína antiviral, juntamente com a Plin2, a principal proteína estrutural dos CLs (**Figura 18B**). Além disso essas proteínas não foram observadas na fração F1 dos animais Sham, o que reforça que elas podem ser as responsáveis pela atividade antibacteriana e pró-hospedeiro vista nos resultados anteriores.

A presença dessas proteínas não só indica que os CLs compartimentalizam duas proteínas comprovadamente com atividade antibacteriana, a CAMP e a HMGB-1, mas também que a resposta as diferentes respostas pró-hospedeiro são interconectadas, o que é evidenciada pela presença da Viperina nos CL induzidos pela sepse.

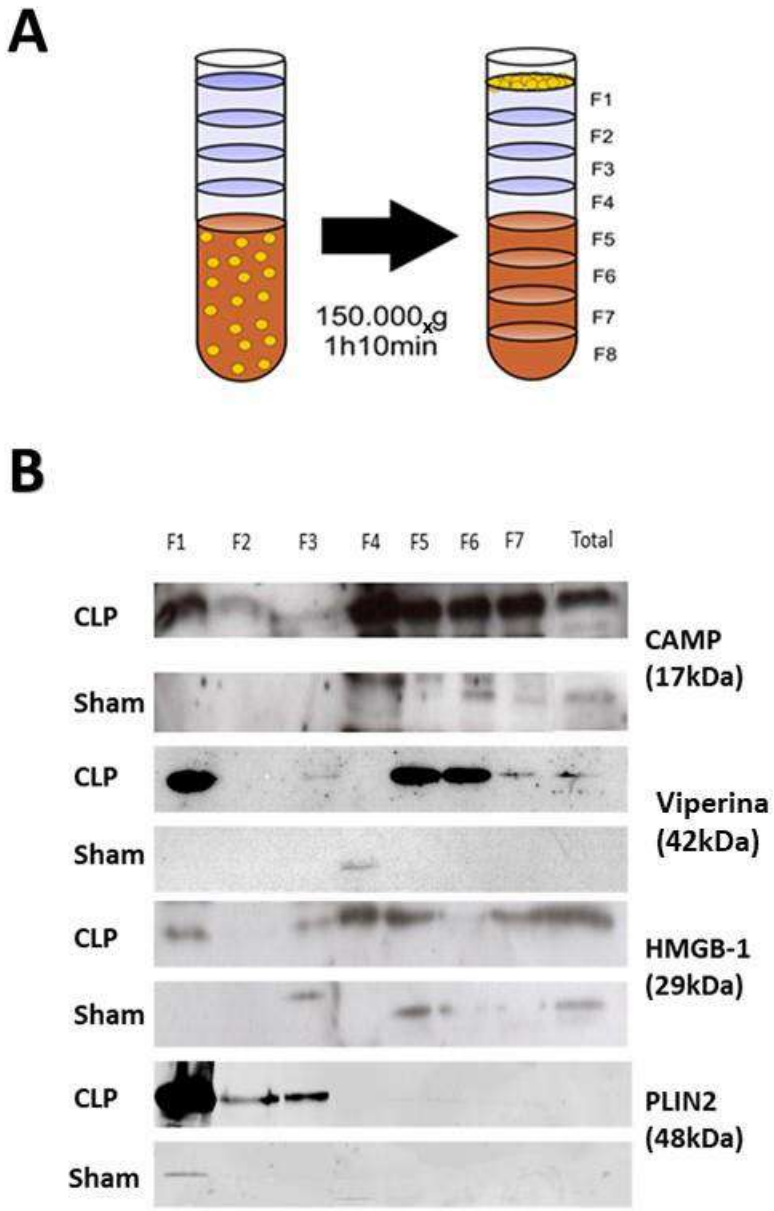

Figura 18: Proteinas pró-hospedeiro de compartimentalizam nos CLs induzidos pela sepse. (A) Esquema representativo do gradiente de sacarose. **(B)** Westhern blot dos gradientes de sacarose oriundos das amostras de fígado de animais sham e CLs evidenciado a presença de proteínas com atividade anti-patogenos nos CLs dos animais sépticos (F1), juntamente na fração com a proteína estrutural dos CLs (Plin2). CAMP: Catelicidina; HMGB-1: high-mobility group protein 1; Perilipina 2: Plin2. (n=2)

5. DISCUSSÃO

Nas últimas duas décadas diversos trabalhos reportaram a participação dos CLs na patogêneses de diferentes agentes infecciosos, incluindo vírus (CARVALHO *et al.*, 2012; MIYANARI *et al.*, 2007; SAMSA *et al.*, 2009), bactérias (D'AVILA *et al.*, 2006, 2008; KUMAR; COCCHIARO; VALDIVIA, 2006; MATTOS *et al.*, 2011b; NEYROLLES *et al.*, 2006), fungos (SORGI *et al.*, 2009) e protozoários (ARAÚJO-SANTOS *et al.*, 2014; D'AVILA *et al.*, 2011; GOMES *et al.*, 2014; MELO *et al.*, 2003; MOTA *et al.*, 2014). A partir desse conjunto de dados foi demostrado que os CLs são centrais na relação patógeno/hospedeiro, seja como uma fonte de energia para patógenos intracelulares e/ou como parte de uma estratégia de escape do sistema imunológico. Em contrapartida, descobertas recentes vêm demonstrando que há um outro lado dessa interação patógeno-hospedeiro, onde os CLs também podem agir em favor do hospedeiro e contra os patógenos intracelulares (ANAND *et al.*, 2012; HINSON; CRESSWELL, 2009). Essas novas propriedades dos CLs estavam relacionadas principalmente a mudanças na composição das proteínas associada à estas organelas (BOUGNÈRES *et al.*, 2009; HELBIG *et al.*, 2005; HINSON; CRESSWELL, 2009).

Nossos dados mostram que os CLs participam do controle da infecção bacteriana, tanto in vitro como in vivo. Nós observamos que a modulação do acúmulo dessa organela afeta a capacidade de *killing* dos macrófagos e resulta no descontrole da carga bacteriana na sepse. Além disso, demonstramos que CLs são organelas centrais no metabolismo celular e na resposta inflamatória dos macrófagos durante infecções bacterianas, tanto como local de síntese de eicosanóides como um modulador da secreção de citocinas inflamatórias. Além disso, a partir da análise dos CLs hepáticos induzidos pela sepse demonstramos que os CLs apresentam atividade antibacteriana direta, sendo uma importante plataforma de compartimentalização de proteínas pró-hospedeiro. Em conjunto, nossos dados mostram que os CLs são centrais na resposta imune inata frente a infecções bacterianas.

Apesar dos CLs estarem presentes durante a infecção de uma ampla gama de bactérias (LIBBING *et al.*, 2019), pouco se sabe sobre o papel dessa organela na infecção por bactérias extracelulares, a exemplo da *E. coli*, ou por patógenos intracelulares não obrigatórios, como a *Salmonella typhimirium*. Especificamente em infecções bacterianas, o que se sabe sobre o papel dos CLs nesse fenômeno é principalmente a partir de dados

derivados do estudo de patógenos intracelulares altamente especializados, como *M. tuberculosis, M. leprae*, *M. bovis* e *C. trachomatis,* que adquiriram a capacidade de modular o metabolismo da célula hospedeira e a síntese de eicosanoides (CAO *et al.*, 2007; D'AVILA *et al.*, 2006; DANIEL *et al.*, 2011; MATTOS *et al.*, 2011b) Nas infecções por micobactérias, os CLs atuam como local de síntese de PGE_2, associado a diminuição das citocinas do tipo Th1 e elevação de IL-10 (ALMEIDA *et al.*, 2009; D'AVILA *et al.*, 2008; MATTOS *et al.*, 2011a). Porém, a presença dessa organela em contextos pró-inflamatórios durante a infecção por diversas bactérias (NICOLAOU; GOODALL; ERRIDGE, 2012; PACHECO *et al.*, 2002; QADRI, 2004) é um forte indício de que essa organela poderia ter um outro papel nesse processo.

Embora pareça contraditório com a literatura atual, a indução dos CLs como resposta do hospedeiro não pode ser subestimada, da mesma forma que a própria produção de PGE_2 pode ser tanto pró-inflamatória como antiinflamatória dependente do agente patogênico, do local e do estágio da infecção, além da quantidade desse mediador no sítio da infecção (AGARD; ASAKRAH; MORICI, 2013; KALINSKI, 2012; NAKANISHI; ROSENBERG, 2013; PECCHI *et al.*, 2009; SHEPPE *et al.*, 2018). A participação da PGE_2 como um dos indutores da reprogramação glicolítica e da resposta pró-inflamatória em macrófagos foi observado durante a infecção por *S. typhimurium* (SHEPPE *et al.*, 2018). E, no contexto inflamatório, a própria produção de lactato já foi reportada como indutor da síntese de PGE_2 (WEI *et al.*, 2015), esta por sua vez já foi associada com a inibição da β-oxidação, levando ao acúmulo de CLs (HENKEL *et al.*, 2012). Além disso, a PGE_2 em macrófagos é um importante regulador da óxido nítrico-sintase induzida (iNOS), podendo ser tanto ativador como repressor, dependendo da dose (MILANO *et al.*, 1995). De forma interessante, nós vimos que ao bloquear a biossíntese de CLs nos macrófagos, há alteração não apenas da síntese de PGE_2 e de lactato, mas também da diminuição da produção de NO e de MCP-1/CCL2, dois mediadores essenciais para o *clearance* bacteriano na sepse (GOMES *et al.*, 2013). Em conjunto, esses dados mostram que a atividade antibacteriana dos macrófagos é modulada pela presença dos CLs, sugerindo que essa organela seja central na reprogramação imunometabólica dos macrófagos.

Esse novo papel dos CLs como uma imunoplataforma central na resposta antibacteriana também acontece in vivo, durante a sepse. A atuação dos CLs como local de síntese de LTB_4 durante a sepse já tinha sido previamente reportado pelo nosso grupo de pesquisa (PACHECO *et al.*, 2007), porém o papel dos CLs na resposta antibacteriana

ainda era desconhecido. Além de um potente quimioatraente de leucócitos, o LTB_4 induz a ativação celular, amplificação das funções antimicrobianas e da resposta inflamatória (LI *et al.*, 2015). E, assim como o esperado, o bloqueio da biossíntese de CLs resultou na diminuição da sintese de LTB_4 de forma expressiva nos leucócitos peritoneais. Além disso, quando analisada a resposta inflamatória afetada pelo bloqueio da biossíntese de CLs, observa-se uma modulação principalmente das citocinas do eixo LTB_4/IL-6. Nesse contexto, o LTB_4 induz a transcrição e a síntese da IL-6 (ROLA-PLESZCZYNSKI; STANKOVA, 1992). Por sua vez, a IL-6 reforça junto com o LTB_4 a produção de MCP-1/CCL2 (BISWAS *et al.*, 1998; HUANG *et al.*, 2004), e existe uma grande interseção entre esses mediadores inflamatórios (NIWA *et al.*, 2016; PACHECO *et al.*, 2007). Nesse processo, LTB_4 induz ainda a sintese iNOS e a produção de NO (SANTOS *et al.*, 2013; TALVANI *et al.*, 2002). Vale ressaltar que o papel protetor do LTB_4 durante infecções parasitárias é fotemente dependente da ação do NO (SANTOS *et al.*, 2013; TALVANI *et al.*, 2002). Na sepse, o papel do NO junto com MCP-1 é essencial para o *clearance* bacteriano.

Entretanto, o papel protetor dos CLs não se estente a todas as infecções bacterianas. Apesar da *Salmonella* e a *E. coli* serem enterobactérias filogeneticamente próximas (MORAN *et al.*, 2005), nós não observamos um papel protetor dos CL durante a infecção pela *Salmonella enterica* sorovar Thyphimurium (Kiarely *el al.*, unp – Anexo 3). Diferente ao observado na infecção pela *E. coli* e durante a sepse, o uso do inibidor da DGAT-1 não interferiu na resposta inflamatória dos macrófagos infectados pela *Salmonella*. E, de forma supreendente, a inibição do acúmulo de CLs durante a infecção por *Salmonella* não foi acompanhada pela redução dos níveis de PGE_2. Curiosamente, a resposta dos macrófagos foi pró-inflamatória tanto para a *E. coli* como para a *Salmonella*, diferente do que foi observado para *M. leprae* e *M. bovis*, onde os CLs como local de síntese de PGE_2 estava associado à diminuição das citocinas do tipo Th1 e elevação de IL-10 (ALMEIDA *et al.*, 2009; D'AVILA *et al.*, 2008; MATTOS *et al.*, 2011a). Esses resultados indicam que apesar de ser fenótipo comum a uma grande várias infecções bacterianas, o papel desempenhado pelos CLs é fortemente dependente do agente infeccioso.

E a ausência do papel protetor e imunoregulador dos CL durante a infecção pela *Salmonella* thyphimurium provavelmente está relacionado ao processo de indução da biogênese dessa organela. Nesse caso, nós observamos que a indução dos CL é um mecanismo dependente da viabilidade da bacteria e da atividade do sistema de secreção

do tipo 3 (T3SS), um dos principais fatores de patogenicidade da *Salmonella* (Anexo 3). E esses resultados reforçam o processo descrito por NAWABI e colaboradores (2008), no qual a proteína efetora SseJ secretada pelo T3SS é essencial para a formação dos CLs induzida pela *Salmonella* nas células HeLa e em macrofagos RAW. Além disso, a atuação de proteínas efetoras secretadas pelo T3SS na modulação do metabolismo lipídico da célula hospedeiro já foi reportada durante a infecção por *Chlamydia trachomatis* (DAI; LI, 2014; KUMAR; COCCHIARO; VALDIVIA, 2006) e *Pseudomonas aeruginosa* (FELICIANO *et al.*, 2008). A ação de fatores de patogenicidade como indutores da biogênese de CL, principalmente nas infecções por patógenos intracelulares, pode explicar o papel pró-patógenos dos CLs nesses modelos. E justamente ausência dos fatores de patogenicidade pode explicar por que durante a infecção por *Mycobacterium smegmatis*, uma bactéria não patogênica, não há a biogênese de CL (D'AVILA *et al.*, 2006).

Ainda nesse contexto patógeno-hospedeiro, a própria resposta do hospedeiro também pode estar associada com as diferentes respostas associadas aos CLs. A biogênese de CLs está fortemente associada ao reconhecimento dos PAMPs pelos TLRs em leucócitos (NICOLAOU; GOODALL; ERRIDGE, 2012; PACHECO *et al.*, 2002), porém para cada patógeno há o envolvimento de TLRs diferentes (MATTOS *et al.*, 2011b; NICOLAOU; GOODALL; ERRIDGE, 2012). Apesar dessa sinalização induzir a um mesmo fenótipo, em resposta a sinais pró-inflamatórios gerados por diferentes TLRs o lipidoma dos macrófagos é remodelado de maneira diferente, com alterações significativas nas principais classes de lipídeos (glicerolipídeo, glicerofosfolipídeo, esfingolipídeo, colesterol e ácidos graxos) (HSIEH *et al.*, 2020). Como a ativação por diferentes estímulos pró-inflamatórios é um processo específico e resulta na aquisição de lipidomas distintos nos macrófagos (HSIEH *et al.*, 2020), podemos extrapolar a alterações na função dos CLs, que pode estar intimamente relacionada com a mudança na composição dessa organela. Nesse contexto, a sinalização por interferon parece desempenhar um papel central nesse processo, pois modula tanto o metabolimo lipídico (BLANC *et al.*, 2011; YORK *et al.*, 2015), assim como a composição protéica dos CLs (BOUGNÈRES *et al.*, 2009; HELBIG *et al.*, 2005; HINSON; CRESSWELL, 2009).

Apesar do papel imunomodulador dos CLs estar fortemente associado a processos inflamatórios, o papel protetor dessa organela na resposta pró-hospedeiro começou a ser caracterizada primeiro pelo armazenamento de proteínas protetoras na superfície dessa organela, participando principalmente de um sistema autônomo de

proteção das células. A presença de viperina (HINSON; CRESSWELL, 2009) e IRGM-1(HALDAR *et al.*, 2013) em resposta a uma infecção viral e parasitária, respectivamente, foram os primeiros relatos dos CLs tendo participação direta na resposta pró-hospedeiro. Tanto a viperina (FITZGERALD, 2011) como a IRGM-1 (HALDAR *et al.*, 2013) são proteínas reguladas pelas vias de interferon em resposta à infecção. Apesar do mecanismo protetor pela qual essas proteínas atuam não ser completamente elucidado, a presença da viperina nos CLs vem sendo associada como sendo uma tática local de inibição da replicação local, provavelmente perturbando a formação do complexo de replicação viral ou montagem das partículas virais (NASR *et al.*, 2012; WANG; HINSON; CRESSWELL, 2007). Já as IRGM são pequenas GTPases induzíveis por interferon (BOUGNÈRES *et al.*, 2009; HALDAR *et al.*, 2013) e fazem parte de um complexo sistema celular de reconhecimento do hospedeiro de suas próprias estruturas. Irgm3 se acumula em organelas "próprias", incluindo CLs, mas não no vacúolo parasitófago da bactéria *C. trachomatis* ou do protozoário *Toxoplasma gondii* (HALDAR *et al.*, 2013).

Diferente a que foi reportado para viperina e para IRGM, a confirmação dos CLs como uma plaforma protetora contra a infecção bacteriana foi observada em embriões de *Drosophila*. Ensaios *in vitro* publicados por ANAND e colaboradores (2012) mostram que CLs purificados de embriões de *Drosophila melanogaster* possuem atividade antibacteriana *in vitro* contra *S. epidermidis* e *E. coli*. Neste mesmo trabalho foi constatado que esta resposta antimicrobiana era devido ao conteúdo protéico dessa organela (principalmente devido a ação das histonas) e não devido aos lipídios. Nesse mesmo trabalho foi reportado que camundongos expostos ao LPS obteve um aumento da presença da histona H1 nos CLs, sugerindo que esse aumento pode estar envolvido em algum tipo de resposta antimicrobiana (ANAND *et al.*, 2012). Além disso, nas análises proteômicas de CLs de macrófagos (WANG; GERSTEIN; SNYDER, 2009), células β produtoras de insulina (LARSSON *et al.*, 2012), e oriundos do músculo esquelético (ZHANG *et al.*, 2011) mostravam a presença de histonas. Como alvo mais provável de se caracterizar essa nova função dos CLs, nós fomos analisar a presença de histonas nessa organela. Entretanto, apesar das diferentes abordagens experimentais empregadas, não conseguimos validar a presença das histonas nos CLs.

A ausência de histonas nos CLs poderia representar que a ação antibacteriana direta dos CLs poderia não acontecer nos mamíferos, ou que ela aconteceria de outra forma. Nesse contexto, como prova de conceito de que qualquer CLs induzido pela infecção poderia ter uma resposta protetiva, escolhemos um sítio central na resposta a

infecção, mas que ao mesmo tempo nos fornecesse material biólogico suficiente para caracterizar esse fenômeno. Nesse contexto, o fígado é um órgão central tanto no metabolismo como no resposta imunológica sistêmica (KUBES; JENNE; SNYDER, 2018; YAN; LI; LI, 2014). Apesar de ser classificado como um glândula anexa do sistema digestivo, o fígado é um tecido imunológico fundamental para detectar, capturar e eliminar bactérias, vírus e macromoléculas que entram no corpo através do intestino pela veia porta e/ou que estejam circulando no sangue (KUBES; JENNE; SNYDER, 2018; YAN; LI; LI, 2014). Além disso, o fígado possui a maior quantidade e diversidade de células fagocíticas do corpo, sendo uma importante barreira contra a infecções sistêmicas (KUBES; JENNE; SNYDER, 2018). Alterações hepáticas reduzem a capacidade do organismo de lidar com infecções (ANTUNES *et al.,* 2020), e aumentam as taxas de mortalidade decorrentes da sepse (YAN; LI; LI, 2014). A esteatose hepática é um achado comum no fígado *post-mortem* de pacientes sépticos (superior a 70%), sendo que a maioria destes apresentavam uma degeneração gordurosa de moderada a grave que se localizava principalmente associada com a inflamação do sistema porta/lóbular hepático (GAROFALO *et al.*, 2019).

Se no início da sepse o acúmulo de CLs foi observado apenas nos leucócitos peritoneiais, no tempo 24h após cirurgia nós observamos que a sepse não só induziu o acúmulo de CLs no fígado, como induziu alterações na composição dessa organela, evidenciada pela alteração no tamanho dos CLs como na razão triglicerídeos/proteínas. Dentro da prova de conceito de que qualquer CLs induzido por uma infecção pode ter uma resposta protetora, nós mimetizamos a interação bacteria/CLs e observamos que de fato CLs apresentavam uma atividade antibacteriana. E assim como foi reportado para *Drosophila*, a atividade antibacteriana era mais pronunciada no conteúdo protéico dessa organela, mas não devido a presença de histonas.

Após a confirmação dessa atividade antibacteriano direta das proteínas dos CLs, começarmos a procura das proteínas responsáveis por esse fenômeno. A partir dos dados proteômicos realizados pelo grupo do professor Albert Pol (Anexo 2), observamos que os CLs possuiam em sua composição a presença de um peptídeo antibacteriano clássico, a catelicidina. E essa proteína foi confirmada nos CLs hepáticos induzidos pela sepse. Diferente da maior parte dos peptídeos antibacterianos, a catelicidina também é um importante agente imunomodulador e central na ativação dos leucócitos (VAN HARTEN *et al.*, 2018). Além disso, semelhante as histonas, a catelicidina também é uma proteína catiônica, indicando que os CLs podem carrear essas proteínas ao fagossomo da mesma

forma descrita em drosophila. Nesse contexto, já foi demostrado que a catelicina apesar de ser um peptídeo antibacteriano secretado, possui um importante papel no *killing* intracelular da *M. tuberculosis*, se acumulando no fagossomo contendo o patógeno (SONAWANE *et al.*, 2011). E justamente esse processo pode estar acontecendo durante a infecção por *E. coli*, onde foi visualizada uma frequente interação bactéria/CLs. Entrentando, vale ressaltar nessa interação CLs/fagossomo ainda pode estar relacionada com a maturação dos fagossomos, conforme foi reportado com van Manen *et al.* (VAN MANEN *et al.*, 2005). Nesse trabalho foi reportado que durante a associação transitória entre CLs e o fagossomo há a liberação do ácido araquidônico do CLs para o fagossomo, que facilitaria a maturação do fagossomo (VAN MANEN *et al.*, 2005). Ainda nesse trabalho foi sugerido que nesse processo os CLs poderiam contribuir para a eliminação dos patógenos (VAN MANEN *et al.*, 2005).

De forma surpreendente, além da presença da catelicina nos CLs nós também identificamos a presença de diversas proteínas protetoras nessa organela nas análises proteômicas, incluindo a viperina e a três GTPases induzidas pela resposta imune. Além disso, nessas análises ainda foi demostrado que havia a clusterização de diversas proteínas protetoras do hospedeiro junto com PLIN2, uma das principais proteínas estruturais dos CLs (Bosh *et al.* in press). E no nosso modelo nós validamos a presença da Viperina nos CLs, e também a presença de HMGB-1, uma proteína semelhante a histona, que alguns estudos também reportaram como tendo atividade antibacteriana (CHEN *et al.*, 2014) A presença dessa ampla rede de proteção indica que os achados iniciais da Viperina e da IRGM-1 nos CLs durante infecções virais e parasitárias, respectivamente, na verdade fazem parte de um mecanismo mais amplo de proteção autônoma das células. E essa integração dessas estratégias pode estar intimamente relacionada a diversos resultados recentes que vem mostrando que atuação dessas proteínas é mais ampla e com sobreposições. Por exemplo, a viperina foi recentemente reportada como essencial no controle da infecção intracelular pela bacteria *Shigella fexneri* (HELBIG *et al.*, 2019); as pequenas GTPases e vias induzidas por interferon são um mecanismo importante na resistência contra a bactéria *C. muridarum* e contra infecções virais (GIEBEL *et al.*, 2019; PETKOVA; VIRET; FAURE, 2012); e a própria catelicidina é essencial no *killing* intracelular do parasito *Leishmania* (CRAUWELS *et al.*, 2019). Essa sobreposição da função dessas proteínas reforça que essa estratégia pró-hospedeiro seja "pluri-patógenos" de proteção autônoma das células, o que faz sentido uma vez que o fígado é susceptível a infecção por uma ampla gama de patógenos intracelulares, como HCV, *Listeria*

monocytogenes e *Salmonella* sp (KUBES; JENNE; SNYDER, 2018). Além disso, vale ressaltar que tanto a viperina (SEO; CRESSWELL, 2013) como a catelicidina (HOANG-YEN TRAN *et al.*, 2016) já foram reportadas como tendo um importante papel modulador do metabolismo lipídico, o que reforça o interconecção dos papéis metabólicos e imunológicos dos CLs. Além disso, o mecanismo de entrega dessas proteínas parece ser através da interação direta bactéria/ CL no inico da infecção, porém esse processo não acontece durante a infecção com a *Salmonella* (Anexo 2 e 3). Corrobolando com essa hipótese, o papel protetor do CL induzidos pelo ácido oleico está fortemente associado a presença de CAMP nos CL, pois ao silenciar essa proteína essa atividade é abolida (Anexo 2).

Assim como reportado para outros mecanismos essenciais para a resistência à infecção, principalmente no caso do LTB_4 (LI *et al.*, 2015) e proteínas do sistema complemento (CHARCHAFLIEH *et al.*, 2012), a atuação dos CLs como um amplificador do processo inflamatório parece ter papéis duplos na sepse. Se por um lado o papel protetor dos CLs no início da sepse é mais proeminente, a atuação dessa organela na amplificação do dano tecidual é mais sobressalente nos tempos mais tardios (TEIXEIRA *el al*, unp - Anexo 4). E justamente esse papel *dual* dos CLs pode explicar por que não observamos diferenças nem na gravidade nem na sobrevivência nos animais sépticos tratados com A922500. E assim como há uma forte correlação entre CL e a síntese de NO, a partir do tempo de 24h após a cirurgia, nos observamos uma crescente correlação entre estressez oxidativo e o acúmulo de CL, tanto nos macrófagos como no fígado. Diferente ao observado no tempo de 6h, nos tempos de 24h e 48h após a cirurgia há grande aumento de 8-isoprostano, um marcador do estressez oxidativo. E fortes indicios do nosso grupo apontam que os CLs sejam um dos principais locais de acúmulo e/ou de síntese de lipídeos oxidados nas células. E justamente essa intersecção dos CL com o estressez oxidativo, junto ao papel de amplificador do processo inflamatório, parecem contribuir para a disfunção hepática na sepse (Anexo 4). O papel deletério dos CL tanto como amplificador do estressez oxidativo (KWON *et al.*, 2017; LEE *et al.*, 2013; LIU *et al.*, 2015) e do processo inflamatório (MARSCHALLINGER *et al.*, 2020) levando a disfunção celular e orgânica já foi observada em outros modelos, principalmente envolvendo o sistema nervoso central.

Curiosamente, no tempo mais tardio da sepse, nós não observamos o papel protetor dos CL, apesar da quantidade CL ser superior ao observado nos tempos mais iniciais, o que sugere que o papel deletério dos CL não está associado com a presença das

proteínas antibacterianas nessa organela. Além disso, o papel deletério dos CL nos tempos mais tardios pode estar relacionado com a dinâmica dessa organela com as mitocôndrias. No inicio do processo inflamatório nós observamos que há a desacoplação das mitocôndrias dos CLs, envolvendo principalmente a regulação da expressão da Plin2 e Plin5 (Anexo 2). Como resultado desse processo há a diminuição da β-oxidação e da fosfolização oxidativa. Além de central no controle do imunometabolismo, essa desaclopação dos CL das mitocôndrias parece ser importante na preservação das estruturas celulares, principalmente das mitocôndrias, pois aquelas em contato com CL apresentam uma maior presença de alterações estruturais durante a sepse. Entretanto, como o papel antibacteriano dos CL se correlaciona com disfunção mitocondrial ainda carece de mais invstigações.

Com base no que foi aqui demostrado nesse estudo, os CLs são elementos centrais na resposta imunometabólica contra infecções bacterianas. Com base nesses resultados nós propomos a atuação dos CLs em ao menos três níveis na resposta imune inata frente à infecções bacterianas, como local de acúmulo de proteínas antibacterianas, como um regulador do metabolismo das células imunes e como amplificador da resposta inflamatória, principalmente através da síntese de mediadores inflamatórios. Uma melhor caracterização desse novo mecanismo da resposta imune inata pode fornecer novas ferramentas para o desenvolvimento de estratégias anti-infecciosas e antiinflamatórias.

6. CONCLUSÕES

Nesse trabalho nós demostrarmos que os CLs participam do controle da infecção bacteriana, tanto in vitro como in vivo. Nossos dados mostram que a modulação da quantidade dos CLs em leucócitos afeta a capacidade de *killing* dos macrófagos e leva ao descontrole da infecção bacteriana na sepse. Além disso, nossos dados ainda mostram que os CLs são organelas centrais na modulação do metabolismo celular, e atuam como uma imunoplataforma importante na resposta inflamatória, principalmente como local de síntese de eicosanoides tanto in vitro como in vivo. Além disso, nós apresentamos nesse trabalho que os CLs podem ter ainda uma atividade antibacteriana, principalmente devido ao seu conteúdo protéico. Nesse sentido diferente ao observado em Drosophila, durante a infecção sistêmica há compartimentalização não só de proteínas antibacterianas, mas também de proteínas antivirais e antiparasitárias, fazendo com que essa organela seja uma importante proteção autônoma das células frente as infecções intracelulares.

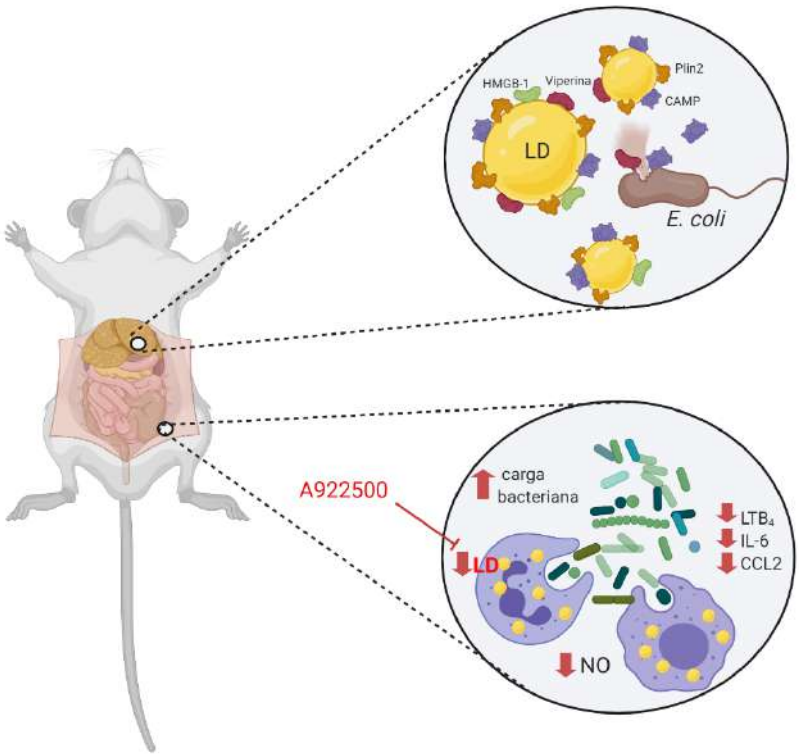

Figure 19: CLs participam da resposta antibacteriana. Nossos dados indicam que os CLs atuam na resposta imune inata em ao menos três níveis: como modulador do metabolismo celular e como amplificador do processo inflamatório nos leucócitos durante a sepse, principalmente através da modulação do eixo LTB-4/IL-6, incluindo MCP1 e óxido nítrico, sendo esseciais para o controle da carga bacteriana. Além disso, os CL atuam como uma plataforma autônoma na resistência a infecção intracelular nos hepatócitos, através da compartimentalização de importantes proteínas pró-hospedeiro, como a HMGB-1 e catelicidina, duas proteinas antibacterianas, e a viperina, uma proteína antiviral.

7. REFERÊNCIAS BIBLIOGRÁFICA

ABDELMAGEED, M. E.; EL-AWADY, M. S.; SUDDEK, G. M. Apocynin ameliorates endotoxin-induced acute lung injury in rats. **International Immunopharmacology**, *[S. l.]*, v. 30, p. 163–170, 2016. Disponível em: https://doi.org/10.1016/j.intimp.2015.12.006

AGARD, M.; ASAKRAH, S.; MORICI, L. A. PGE2 suppression of innate immunity during mucosal bacterial infection. **Frontiers in Cellular and Infection Microbiology**, *[S. l.]*, v. 4, n. AUG, p. 1–11, 2013. Disponível em: https://doi.org/10.3389/fcimb.2013.00045

AKIRA, S.; TAKEDA, K. Toll-like receptor signalling. **Nature Reviews Immunology**, *[S. l.]*, v. 4, n. 7, p. 499–511, 2004. Disponível em: https://doi.org/10.1038/nri1391

AKSENOV, M. Y.; MARKESBERY, W. R. Changes in thiol content and expression of glutathione redox system genes in the hippocampus and cerebellum in Alzheimer's disease. **Neuroscience Letters**, *[S. l.]*, v. 302, n. 2–3, p. 141–145, 2001. Disponível em: https://doi.org/10.1016/S0304-3940(01)01636-6

ALMEIDA, P. E. *et al.* Mycobacterium bovis Bacillus Calmette-Guérin Infection Induces TLR2-Dependent Peroxisome Proliferator-Activated Receptor γ Expression and Activation: Functions in Inflammation, Lipid Metabolism, and Pathogenesis. **Journal of Immunology**, *[S. l.]*, v. 183, n. 2, p. 1337–1345, 2009. Disponível em: https://doi.org/10.4049/jimmunol.0900365

ALMEIDA, P. E. *et al.* Differential TLR2 downstream signaling regulates lipid metabolism and cytokine production triggered by Mycobacterium bovis BCG infection. **Biochimica et Biophysica Acta - Molecular and Cell Biology of Lipids**, *[S. l.]*, v. 1841, n. 1, p. 97–107, 2014. Disponível em: https://doi.org/10.1016/j.bbalip.2013.10.008

ANAND, P. *et al.* A novel role for lipid droplets in the organismal antibacterial response. **eLife**, *[S. l.]*, v. 1, p. 1–18, 2012. Disponível em: https://doi.org/10.7554/eLife.00003

ANTUNES, M. M. *et al.* Chronic ingestion of Primex-Z®, compared to other common fat sources, drives worse liver injury and enhanced susceptibility to bacterial infections. **Nutrition**, *[S. l.]*, p. 110938, 2020. Disponível em: https://doi.org/10.1016/j.nut.2020.110938

ARAÚJO-SANTOS, T. *et al.* Role of Prostaglandin F2α Production in Lipid Bodies From

Leishmania infantum chagasi: Insights on Virulence. **The Journal of Infectious Diseases**, *[S. l.]*, v. 210, n. 12, p. 1951–1961, 2014. Disponível em: https://doi.org/10.1093/infdis/jiu299

ASSUNÇÃO, L. S. *et al.* Schistosomal-derived lysophosphatidylcholine triggers M2 polarization of macrophages through PPARγ dependent mechanisms. **Biochimica et Biophysica Acta (BBA) - Molecular and Cell Biology of Lipids**, *[S. l.]*, v. 1862, n. 2, p. 246–254, 2017. Disponível em: https://doi.org/10.1016/j.bbalip.2016.11.006

ATASHI, F.; MODARRESSI, A.; PEPPER, M. S. The Role of Reactive Oxygen Species in Mesenchymal Stem Cell Adipogenic and Osteogenic Differentiation: A Review. **Stem Cells and Development**, *[S. l.]*, 2015. Disponível em: https://doi.org/10.1089/scd.2014.0484

BANDEIRA-MELO, C. *et al.* **Signal Transduction Immunohistochemistry**. New York, NY: Springer New York, 2017. (Methods in Molecular Biology).v. 1554*E-book*. Disponível em: https://doi.org/10.1007/978-1-4939-6759-9

BANDEIRA-MELO, C.; PHOOFOLO, M.; WELLER, P. F. Extranuclear Lipid Bodies, Elicited by CCR3-mediated Signaling Pathways, Are the Sites of Chemokine-enhanced Leukotriene C 4 Production in Eosinophils and Basophils. **Journal of Biological Chemistry**, *[S. l.]*, v. 276, n. 25, p. 22779–22787, 2001. Disponível em: https://doi.org/10.1074/jbc.M101436200

BANNENBERG, G.; ARITA, M.; SERHAN, C. N. Endogenous Receptor Agonists: Resolving Inflammation. **The Scientific World JOURNAL**, *[S. l.]*, v. 7, p. 1440–1462, 2007. Disponível em: https://doi.org/10.1100/tsw.2007.188

BARROS, L. L. dos S.; MAIA, C. do S. F.; MONTEIRO, M. C. Fatores de risco associados ao agravamento de sepse em pacientes em Unidade de Terapia Intensiva. **Cadernos Saúde Coletiva**, *[S. l.]*, v. 24, n. 4, p. 388–396, 2016. Disponível em: https://doi.org/10.1590/1414-462x201600040091

BEISEL, W. R. Metabolic Response to Infection. **Annual Review of Medicine**, *[S. l.]*, v. 26, n. 1, p. 9–20, 1975. Disponível em: https://doi.org/10.1146/annurev.me.26.020175.000301

BISWAS, P. *et al.* Interleukin-6 induces monocyte chemotactic protein-1 in peripheral blood mononuclear cells and in the U937 cell line. **Blood**, *[S. l.]*, v. 91, n. 1, p. 258–265,

1998. Disponível em: https://doi.org/10.1182/blood.v91.1.258.258_258_265

BLANC, M. *et al.* Host defense against viral infection involves interferon mediated down-regulation of sterol biosynthesis. **PLoS Biology**, *[S. l.]*, v. 9, n. 3, 2011. Disponível em: https://doi.org/10.1371/journal.pbio.1000598

BOSCH, M.; PARTON, R. G.; POL, A. Lipid droplets, bioenergetic fluxes, and metabolic flexibility. **Seminars in Cell & Developmental Biology**, *[S. l.]*, n. February, p. 0–1, 2020. Disponível em: https://doi.org/10.1016/j.semcdb.2020.02.010

BOUGNÈRES, L. *et al.* A Role for Lipid Bodies in the Cross-presentation of Phagocytosed Antigens by MHC Class I in Dendritic Cells. **Immunity**, *[S. l.]*, v. 31, n. 2, p. 232–244, 2009. Disponível em: https://doi.org/10.1016/j.immuni.2009.06.022

BOZZA, P. T. *et al.* Eosinophil lipid bodies: specific, inducible intracellular sites for enhanced eicosanoid formation. **The Journal of experimental medicine**, *[S. l.]*, v. 186, p. 909–920, 1997. Disponível em: https://doi.org/10.1084/jem.186.6.909

BOZZA, P. T. *et al.* Pathways for eosinophil lipid body induction: differing signal transduction in cells from normal and hypereosinophilic subjects. **Journal of Leukocyte Biology**, *[S. l.]*, v. 64, n. 4, p. 563–569, 1998. Disponível em: https://doi.org/10.1002/jlb.64.4.563

BOZZA, P. T. *et al.* Lipid droplets in host–pathogen interactions. **Clinical Lipidology**, *[S. l.]*, v. 4, n. 6, p. 791–807, 2009. Disponível em: https://doi.org/10.2217/clp.09.63

BOZZA, P. T. *et al.* Lipid body function in eicosanoid synthesis: An update. **Prostaglandins Leukotrienes and Essential Fatty Acids**, *[S. l.]*, v. 85, n. 5, p. 205–213, 2011. Disponível em: https://doi.org/10.1016/j.plefa.2011.04.020

BOZZA, P. T.; MAGALHÃES, K. G.; WELLER, P. F. Leukocyte lipid bodies - Biogenesis and functions in inflammation. **Biochimica et Biophysica Acta - Molecular and Cell Biology of Lipids**, *[S. l.]*, v. 1791, n. 6, p. 540–551, 2009. Disponível em: https://doi.org/10.1016/j.bbalip.2009.01.005

BRASAEMLE, D. L. Thematic review series: Adipocyte Biology . The perilipin family of structural lipid droplet proteins: stabilization of lipid droplets and control of lipolysis. **Journal of Lipid Research**, *[S. l.]*, v. 48, n. 12, p. 2547–2559, 2007. Disponível em: https://doi.org/10.1194/jlr.R700014-JLR200

BUEGE, J. A.; AUST, S. D. [30] Microsomal lipid peroxidation. *In*: **Methods in Enzymology**. *[S. l.: s. n.]*. v. 71p. 302–310. *E-book*. Disponível em: https://doi.org/10.1016/S0076-6879(78)52032-6

CANABAL, J. M.; KRAMER, D. J. Management of sepsis in patients with liver failure. **Current Opinion in Critical Care**, *[S. l.]*, v. 14, n. 2, p. 189–197, 2008. Disponível em: https://doi.org/10.1097/MCC.0b013e3282f6a435

CAO, F. *et al.* Chlamydia pneumoniae-Induced Macrophage Foam Cell Formation Is Mediated by Toll-Like Receptor 2. **Infect. Immun.**, *[S. l.]*, v. 75, n. 2, p. 753–759, 2007. Disponível em: https://doi.org/10.1128/iai.01386-06

CARVALHO, F. A. *et al.* Dengue Virus Capsid Protein Binding to Hepatic Lipid Droplets (LD) Is Potassium Ion Dependent and Is Mediated by LD Surface Proteins. **Journal of Virology**, *[S. l.]*, v. 86, n. 4, p. 2096–2108, 2012. Disponível em: https://doi.org/10.1128/JVI.06796-11

CASTRILLO, A. *et al.* Crosstalk between LXR and Toll-like Receptor Signaling Mediates Bacterial and Viral Antagonism of Cholesterol Metabolism. *[S. l.]*, v. 12, p. 805–816, 2003.

CECCONI, M. *et al.* Sepsis and septic shock. **The Lancet**, *[S. l.]*, v. 392, n. 10141, p. 75–87, 2018. Disponível em: https://doi.org/10.1016/S0140-6736(18)30696-2

CERMELLI, S. *et al.* The Lipid-Droplet Proteome Reveals that Droplets Are a Protein-Storage Depot. **Current Biology**, *[S. l.]*, v. 16, n. 18, p. 1783–1795, 2006. Disponível em: https://doi.org/10.1016/j.cub.2006.07.062

CHARCHAFLIEH, J. *et al.* The Role of Complement System in Septic Shock. **Clinical and Developmental Immunology**, *[S. l.]*, v. 2012, p. 1–8, 2012. Disponível em: https://doi.org/10.1155/2012/407324

CHEN, R. *et al.* Release and activity of histone in diseases. **Cell Death and Disease**, *[S. l.]*, v. 5, n. 8, p. e1370, 2014. Disponível em: https://doi.org/10.1038/cddis.2014.337

CLAUSHUIS, T. A. M. *et al.* Thrombocytopenia is associated with a dysregulated host response in critically ill sepsis patients. **Blood**, *[S. l.]*, v. 127, n. 24, p. 3062–3072, 2016. Disponível em: https://doi.org/10.1182/blood-2015-11-680744

COCCHIARO, J. L. *et al.* Cytoplasmic lipid droplets are translocated into the lumen of

the Chlamydia trachomatis parasitophorous vacuole. **Proceedings of the National Academy of Sciences**, *[S. l.]*, v. 105, n. 27, p. 9379–9384, 2008. Disponível em: https://doi.org/10.1073/pnas.0712241105

COHEN, J. *et al.* Sepsis: a roadmap for future research. **The Lancet Infectious Diseases**, *[S. l.]*, v. 15, n. 5, p. 581–614, 2015. Disponível em: https://doi.org/10.1016/S1473-3099(15)70112-X

COLONNE, P. M.; WINCHELL, C. G.; VOTH, D. E. Hijacking Host Cell Highways: Manipulation of the Host Actin Cytoskeleton by Obligate Intracellular Bacterial Pathogens. **Frontiers in Cellular and Infection Microbiology**, *[S. l.]*, v. 6, n. September, p. 1–8, 2016. Disponível em: https://doi.org/10.3389/fcimb.2016.00107

COWLAND, J. B.; BORREGAARD, N. Granulopoiesis and granules of human neutrophils. **Immunological Reviews**, *[S. l.]*, v. 273, n. 1, p. 11–28, 2016. Disponível em: https://doi.org/10.1111/imr.12440

CRAUWELS, P. *et al.* Cathelicidin Contributes to the Restriction of Leishmania in Human Host Macrophages. **Frontiers in Immunology**, *[S. l.]*, v. 10, n. November, p. 1–12, 2019. Disponível em: https://doi.org/10.3389/fimmu.2019.02697

D'AVILA, H. *et al.* Mycobacterium bovis Bacillus Calmette-Guérin Induces TLR2-Mediated Formation of Lipid Bodies: Intracellular Domains for Eicosanoid Synthesis In Vivo. **The Journal of Immunology**, *[S. l.]*, v. 176, n. 5, p. 3087–3097, 2006. Disponível em: https://doi.org/10.4049/jimmunol.176.5.3087

D'AVILA, H. *et al.* Neutrophils recruited to the site of Mycobacterium bovis BCG infection undergo apoptosis and modulate lipid body biogenesis and prostaglandin E2 production by macrophages. **Cellular Microbiology**, *[S. l.]*, v. 10, n. 12, p. 2589–2604, 2008. Disponível em: https://doi.org/10.1111/j.1462-5822.2008.01233.x

D'AVILA, H. *et al.* Host Cell Lipid Bodies Triggered by Trypanosoma cruzi Infection and Enhanced by the Uptake of Apoptotic Cells Are Associated With Prostaglandin E2 Generation and Increased Parasite Growth. **The Journal of Infectious Diseases**, *[S. l.]*, v. 204, n. 6, p. 951–961, 2011. Disponível em: https://doi.org/10.1093/infdis/jir432

DAI, W.; LI, Z. Conserved type III secretion system exerts important roles in Chlamydia trachomatis. **International Journal of Clinical and Experimental Pathology**, *[S. l.]*, v. 7, n. 9, p. 5404–5414, 2014.

DANIEL, J. *et al.* Mycobacterium tuberculosis uses host triacylglycerol to accumulate lipid droplets and acquires a dormancy-like phenotype in lipid-loaded macrophages. **PLoS Pathogens**, *[S. l.]*, v. 7, n. 6, 2011. Disponível em: https://doi.org/10.1371/journal.ppat.1002093

DUCHARME, N. A.; BICKEL, P. E. Minireview: Lipid droplets in lipogenesis and lipolysis. **Endocrinology**, *[S. l.]*, v. 149, n. 3, p. 942–949, 2008. Disponível em: https://doi.org/10.1210/en.2007-1713

DUPRÉ-CROCHET, S.; ERARD, M.; NÜBE, O. ROS production in phagocytes: why, when, and where? **Journal of Leukocyte Biology**, *[S. l.]*, v. 94, n. 4, p. 657–670, 2013. Disponível em: https://doi.org/10.1189/jlb.1012544

ENGLERT, J. A.; ROGERS, A. J. Metabolism, Metabolomics, and Nutritional Support of Patients with Sepsis. **Clinics in Chest Medicine**, *[S. l.]*, v. 37, n. 2, p. 321–331, 2016. Disponível em: https://doi.org/10.1016/j.ccm.2016.01.011

FAN, B. *et al.* High glucose, insulin and free fatty acid concentrations synergistically enhance perilipin 3 expression and lipid accumulation in macrophages. **Metabolism**, *[S. l.]*, v. 62, n. 8, p. 1168–1179, 2013. Disponível em: https://doi.org/10.1016/j.metabol.2013.02.013

FARESE, R. V.; WALTHER, T. C. Lipid Droplets Finally Get a Little R-E-S-P-E-C-T. **Cell**, *[S. l.]*, v. 139, n. 5, p. 855–860, 2009. Disponível em: https://doi.org/10.1016/j.cell.2009.11.005

FEINGOLD, K. R. *et al.* ADRP/ADFP and Mal1 expression are increased in macrophages treated with TLR agonists. **Atherosclerosis**, *[S. l.]*, v. 209, n. 1, p. 81–88, 2010. Disponível em: https://doi.org/10.1016/j.atherosclerosis.2009.08.042

FEINGOLD, K. R. *et al.* Mechanisms of triglyceride accumulation in activated macrophages. **Journal of Leukocyte Biology**, *[S. l.]*, v. 92, n. 4, p. 829–839, 2012. Disponível em: https://doi.org/10.1189/jlb.1111537

FELICIANO, L.-F. P. *et al.* Lipid body mobilization in the ExoU-induced release of inflammatory mediators by airway epithelial cells. **Microbial Pathogenesis**, *[S. l.]*, v. 45, n. 1, p. 30–37, 2008. Disponível em: https://doi.org/10.1016/j.micpath.2008.01.008

FITZGERALD, K. A. The Interferon Inducible Gene: Viperin. **Journal of Interferon &**

Cytokine Research, *[S. l.]*, v. 31, n. 1, p. 131–135, 2011. Disponível em: https://doi.org/10.1089/jir.2010.0127

FLEISCHMANN, C. *et al.* Assessment of Global Incidence and Mortality of Hospital-treated Sepsis. Current Estimates and Limitations. **American Journal of Respiratory and Critical Care Medicine**, *[S. l.]*, v. 193, n. 3, p. 259–272, 2016. Disponível em: https://doi.org/10.1164/rccm.201504-0781OC

FUJIMOTO, T.; OHSAKI, Y. Proteasomal and autophagic pathways converge on lipid droplets. **Autophagy**, *[S. l.]*, v. 2, n. 4, p. 299–301, 2006. Disponível em: https://doi.org/2904 [pii]

FUJIMOTO, T.; PARTON, R. G. Not just fat: The structure and function of the lipid droplet. **Cold Spring Harbor Perspectives in Biology**, *[S. l.]*, v. 3, n. 3, p. 1–17, 2011. Disponível em: https://doi.org/10.1101/cshperspect.a004838

GAJDA, E.; BUGLA-PŁOSKOŃSKA, G. Lysozyme – occurrence in nature, biological properties and possible applications. **Postępy Higieny i Medycyny Doświadczalnej**, *[S. l.]*, v. 68, p. 1501–1515, 2014. Disponível em: https://doi.org/10.5604/17322693.1133100

GAO, J.; SERRERO, G. Adipose differentiation related protein (ADRP) expressed in transfected COS-7 cells selectively stimulates long chain fatty acid uptake. **Journal of Biological Chemistry**, *[S. l.]*, v. 274, n. 24, p. 16825–16830, 1999. Disponível em: https://doi.org/10.1074/jbc.274.24.16825

GAROFALO, A. M. *et al.* Histopathological changes of organ dysfunction in sepsis. **Intensive Care Medicine Experimental**, *[S. l.]*, v. 7, n. S1, p. 45, 2019. Disponível em: https://doi.org/10.1186/s40635-019-0236-3

GARRIDO, A. G.; FIGUEIREDO, L. F. P. De; SILVA, M. R. E. Experimental models of sepsis and septic shock : an overview. **Acta Cirúrgica Brasileira**, *[S. l.]*, v. 19, n. 2, p. 82–88, 2004. Disponível em: https://doi.org/10.1590/S0102-86502004000200001

GIEBEL, A. M. *et al.* Genetic screen in chlamydia muridarum reveals role for an interferon-induced host cell death program in antimicrobial inclusion rupture. **mBio**, *[S. l.]*, v. 10, n. 2, p. 1–16, 2019. Disponível em: https://doi.org/10.1128/mBio.00385-19

GOMES, A. F. *et al.* Toxoplasma gondii-skeletal muscle cells interaction increases lipid

droplet biogenesis and positively modulates the production of IL-12, IFN-g and PGE2. **Parasites & vectors**, *[S. l.]*, v. 7, p. 47, 2014. Disponível em: https://doi.org/10.1186/1756-3305-7-47

GOMES, R. N. *et al.* Bacterial clearance in septic mice is modulated by MCP-1/CCL2 and nitric oxide. **Shock**, *[S. l.]*, v. 39, n. 1, p. 63–69, 2013. Disponível em: https://doi.org/10.1097/SHK.0b013e31827802b5

HALDAR, A. K. *et al.* IRG and GBP Host Resistance Factors Target Aberrant, "Non-self" Vacuoles Characterized by the Missing of "Self" IRGM Proteins. **PLoS Pathogens**, *[S. l.]*, v. 9, n. 6, p. e1003414, 2013. Disponível em: https://doi.org/10.1371/journal.ppat.1003414

HAMILTON, B.; WARE, L. B.; MATTHAY, M. A. Lipid Mediators in the Pathogenesis and Resolution of Sepsis and ARDS. *[S. l.]*, p. 3–11, 2018. Disponível em: https://doi.org/10.1007/978-3-319-73670-9_1

HECKSHER, C. A.; LACERDA, H. R.; MACIEL, M. A. Characteristics and outcomes of patients treated with drotrecogin alpha and other interventions of the "Surviving Sepsis" campaign in clinical practice. **Revista Brasileira de terapia intensiva**, *[S. l.]*, v. 20, n. 2, p. 135–43, 2008. Disponível em: http://www.ncbi.nlm.nih.gov/pubmed/25307000

HEIPERTZ, E. L. *et al.* Circadian Rhythms Influence the Severity of Sepsis in Mice via a TLR2-Dependent, Leukocyte-Intrinsic Mechanism. **The Journal of Immunology**, *[S. l.]*, v. 201, n. 1, p. 193–201, 2018. Disponível em: https://doi.org/10.4049/jimmunol.1701677

HELBIG, K. J. *et al.* Analysis of ISG expression in chronic hepatitis C identifies viperin as a potential antiviral effector. **Hepatology**, *[S. l.]*, v. 42, n. 3, p. 702–710, 2005. Disponível em: https://doi.org/10.1002/hep.20844

HELBIG, K. J. *et al.* The interferon stimulated gene viperin, restricts Shigella. flexneri in vitro. **Scientific Reports**, *[S. l.]*, v. 9, n. 1, p. 15598, 2019. Disponível em: https://doi.org/10.1038/s41598-019-52130-8

HENKEL, J. *et al.* Stimulation of fat accumulation in hepatocytes by PGE2-dependent repression of hepatic lipolysis, β-oxidation and VLDL-synthesis. **Laboratory Investigation**, *[S. l.]*, v. 92, n. 11, p. 1597–1606, 2012. Disponível em:

https://doi.org/10.1038/labinvest.2012.128

HENRICH, S. F. *et al.* Sepsis and multiple organ dysfunction in burn. **Critical Care**, *[S. l.]*, v. 17, n. Suppl 4, p. P57, 2013. Disponível em: https://doi.org/10.1186/cc12957

HINSON, E. R.; CRESSWELL, P. The antiviral protein, viperin, localizes to lipid droplets via its N-terminal amphipathic ?-helix. **Proceedings of the National Academy of Sciences**, *[S. l.]*, v. 106, n. 48, p. 20452–20457, 2009. Disponível em: https://doi.org/10.1073/pnas.0911679106

HOANG-YEN TRAN, D. *et al.* Cathelicidin suppresses lipid accumulation and hepatic steatosis by inhibition of the CD36 receptor. **International Journal of Obesity**, *[S. l.]*, v. 40, n. 9, p. 1424–1434, 2016. Disponível em: https://doi.org/10.1038/ijo.2016.90

HORWITZ, J.; PERLMAN, R. L. Measurement of inositol phospholipid metabolism in PC12 pheochromocytoma cells. *In*: *[S. l.: s. n.]*. v. 141p. 169–175. *E-book*. Disponível em: https://doi.org/10.1016/0076-6879(87)41065-3

HOTCHKISS, R. S.; MONNERET, G.; PAYEN, D. **Sepsis-induced immunosuppression: From cellular dysfunctions to immunotherapy**. *[S. l.: s. n.]* Disponível em: https://doi.org/10.1038/nri3552

HSIEH, W.-Y. *et al.* Toll-Like Receptors Induce Signal-Specific Reprogramming of the Macrophage Lipidome. **Cell Metabolism**, *[S. l.]*, v. 32, n. 1, p. 128- 143.e5, 2020. Disponível em: https://doi.org/10.1016/j.cmet.2020.05.003

HU, X.; BINNS, D.; REESE, M. L. The coccidian parasites Toxoplasma and Neospora dysregulate mammalian lipid droplet biogenesis. **Journal of Biological Chemistry**, *[S. l.]*, v. 292, p. 11009–11020, 2017. Disponível em: https://doi.org/10.1074/jbc.M116.768176

HUANG, L. *et al.* Leukotriene B 4 Strongly Increases Monocyte Chemoattractant Protein-1 in Human Monocytes. **Arteriosclerosis, Thrombosis, and Vascular Biology**, *[S. l.]*, v. 24, n. 10, p. 1783–1788, 2004. Disponível em: https://doi.org/10.1161/01.ATV.0000140063.06341.09

HUANG, Y. L. *et al.* Toll-like receptor agonists promote prolonged triglyceride storage in macrophages. **Journal of Biological Chemistry**, *[S. l.]*, v. 289, n. 5, p. 3001–3012, 2014. Disponível em: https://doi.org/10.1074/jbc.M113.524587

ITABE, H. *et al.* Perilipins: a diversity of intracellular lipid droplet proteins. **Lipids in Health and Disease**, *[S. l.]*, v. 16, n. 1, p. 83, 2017. Disponível em: https://doi.org/10.1186/s12944-017-0473-y

JANEWAY, C. A.; MEDZHITOV, R. Innate immune recognition. **Annual Review of Immunology**, *[S. l.]*, v. 20, n. 1, p. 197–216, 2002. Disponível em: https://doi.org/10.1146/annurev.immunol.20.083001.084359

JANN, N. J. *et al.* TLR2 enhances NADPH oxidase activity and killing of Staphylococcus aureus by PMN. **Immunology Letters**, *[S. l.]*, v. 135, n. 1–2, p. 17–23, 2011. Disponível em: https://doi.org/10.1016/j.imlet.2010.09.007

JOSEPH, L. C. *et al.* Inhibition of NADPH oxidase 2 (NOX2) prevents sepsis-induced cardiomyopathy by improving calcium handling and mitochondrial function. **JCI Insight**, *[S. l.]*, 2017. Disponível em: https://doi.org/10.1172/JCI.INSIGHT.94248

KALINSKI, P. Regulation of Immune Responses by Prostaglandin E 2. **The Journal of Immunology**, *[S. l.]*, v. 188, n. 1, p. 21–28, 2012. Disponível em: https://doi.org/10.4049/jimmunol.1101029

KING, A. J. *et al.* Diacylglycerol Acyltransferase 1 Inhibition Lowers Serum Triglycerides in the Zucker Fatty Rat and the Hyperlipidemic Hamster. **Journal of Pharmacology and Experimental Therapeutics**, *[S. l.]*, v. 330, n. 2, p. 526–531, 2009. Disponível em: https://doi.org/10.1124/jpet.109.154047

KING, A. J. *et al.* In vivo efficacy of acyl CoA: Diacylglycerol acyltransferase (DGAT) 1 inhibition in rodent models of postprandial hyperlipidemia. **European Journal of Pharmacology**, *[S. l.]*, v. 637, n. 1–3, p. 155–161, 2010. Disponível em: https://doi.org/10.1016/j.ejphar.2010.03.056

KNIGHT, M. *et al.* Lipid droplet formation in Mycobacterium tuberculosis infected macrophages requires IFN- γ / HIF-1 α signaling and supports host defense. **PLoS Neglected Tropical Diseases**, *[S. l.]*, v. 14, n. 1, p. 1–26, 2018. Disponível em: https://doi.org/10.1371/journal.ppat.1006874

KONG, X. *et al.* NADPH Oxidase-Dependent Reactive Oxygen Species Mediate Amplified TLR4 Signaling and Sepsis-Induced Mortality in Nrf2-Deficient Mice. **The Journal of Immunology**, *[S. l.]*, 2010. Disponível em: https://doi.org/10.4049/jimmunol.0902315

KUBES, P.; JENNE, C.; SNYDER, J. Annual Review of Immunology Immune Responses in the Liver. **Annual Review of Immunology**, *[S. l.]*, v. 36, n. 9, p. 1–31, 2018. Disponível em: https://doi.org/10.1146/annurev-immunol

KUMAR, Y.; COCCHIARO, J.; VALDIVIA, R. H. Report The Obligate Intracellular Pathogen Chlamydia trachomatis Targets Host Lipid Droplets. **Current Biology**, *[S. l.]*, v. 16, p. 1646–1651, 2006. Disponível em: https://doi.org/10.1016/j.cub.2006.06.060

KWON, Y.-H. *et al.* Hypothalamic lipid-laden astrocytes induce microglia migration and activation. **FEBS Letters**, *[S. l.]*, 2017. Disponível em: https://doi.org/10.1002/1873-3468.12691

LANGLEY, R. J. *et al.* An Integrated Clinico-Metabolomic Model Improves Prediction of Death in Sepsis. **Science Translational Medicine**, *[S. l.]*, v. 5, n. 195, p. 195ra95-195ra95, 2013. Disponível em: https://doi.org/10.1126/scitranslmed.3005893

LARSSON, S. *et al.* Characterization of the Lipid Droplet Proteome of a Clonal Insulin-producing β-Cell Line (INS-1 832/13). **Journal of Proteome Research**, *[S. l.]*, v. 11, n. 2, p. 1264–1273, 2012. Disponível em: https://doi.org/10.1021/pr200957p

LEE, S.-J. *et al.* Mitochondrial dysfunction induces formation of lipid droplets as a generalized response to stress. **Oxidative medicine and cellular longevity**, *[S. l.]*, v. 2013, p. 327167, 2013. Disponível em: https://doi.org/10.1155/2013/327167

LI, X. J. *et al.* Dual role of leukotriene B4 receptor type 1 in experimental sepsis. **Journal of Surgical Research**, *[S. l.]*, v. 193, n. 2, p. 902–908, 2015. Disponível em: https://doi.org/10.1016/j.jss.2014.09.013

LI, Z. *et al.* Lipid droplets control the maternal histone supply of Drosophila embryos. **Current Biology**, *[S. l.]*, v. 22, n. 22, p. 2104–2113, 2012. Disponível em: https://doi.org/10.1016/j.cub.2012.09.018

LIBBING, C. L. *et al.* Lipid Droplets: A Significant but Understudied Contributor of Host–Bacterial Interactions. **Cells**, *[S. l.]*, v. 8, n. 4, p. 354, 2019. Disponível em: https://doi.org/10.3390/cells8040354

LISSNER, C. R.; SWANSON, R. N.; O'BRIEN, A. D. Genetic control of the innate resistance of mice to Salmonella typhimurium: Expression of the Ity gene in peritoneal and splenic macrophages isolated in vitro. **Journal of Immunology**, *[S. l.]*, v. 131, n. 6,

p. 3006–3013, 1983.

LIU, L. *et al.* Glial Lipid Droplets and ROS Induced by Mitochondrial Defects Promote Neurodegeneration. **Cell**, *[S. l.]*, v. 160, n. 1–2, p. 177–190, 2015. Disponível em: https://doi.org/10.1016/j.cell.2014.12.019

LOBO, S. M. *et al.* Mortality due to sepsis in Brazil in a real scenario: The Brazilian ICUs project. **Revista Brasileira de Terapia Intensiva**, *[S. l.]*, v. 31, n. 1, p. 1–4, 2019. Disponível em: https://doi.org/10.5935/0103-507X.20190008

LORENTE, L. *et al.* Sustained high serum malondialdehyde levels are associated with severity and mortality in septic patients. **Critical Care**, *[S. l.]*, v. 17, n. 6, p. R290, 2013. Disponível em: https://doi.org/10.1186/cc13155

LUHR, R. *et al.* Trends in sepsis mortality over time in randomised sepsis trials: a systematic literature review and meta-analysis of mortality in the control arm, 2002–2016. **Critical Care**, *[S. l.]*, v. 23, n. 1, p. 241, 2019. Disponível em: https://doi.org/10.1186/s13054-019-2528-0

LUNA-GOMES, T. *et al.* Eosinophils as a Novel Cell Source of Prostaglandin D2: Autocrine Role in Allergic Inflammation. **The Journal of Immunology**, *[S. l.]*, v. 187, n. 12, p. 6518–6526, 2011. Disponível em: https://doi.org/10.4049/jimmunol.1101806

MACHADO, F. R. *et al.* Getting a consensus: advantages and disadvantages of Sepsis 3 in the context of middle-income settings. **Revista Brasileira de Terapia Intensiva**, *[S. l.]*, v. 28, n. 4, p. 361–365, 2016. Disponível em: https://doi.org/10.5935/0103-507X.20160068

MAGALHAES, K. G. *et al.* Schistosomal lipids activate human eosinophils via Toll-like receptor 2 and PGD2 receptors: 15-LO role in cytokine secretion Kelly. **Frontiers in Immunology**, *[S. l.]*, 2018. Disponível em: https://doi.org/10.3389/fimmu.2018.03161

MARSCHALLINGER, J. *et al.* Lipid-droplet-accumulating microglia represent a dysfunctional and proinflammatory state in the aging brain. **Nature Neuroscience**, *[S. l.]*, v. 23, n. 2, p. 194–208, 2020. Disponível em: https://doi.org/10.1038/s41593-019-0566-1

MARTINS, I. C. *et al.* The disordered N-terminal region of dengue virus capsid protein contains a lipid-droplet-binding motif. **Biochemical Journal**, *[S. l.]*, v. 444, n. 3, p. 405–

415, 2012. Disponível em: https://doi.org/10.1042/BJ20112219

MATTOS, K. A. *et al.* Lipid droplet formation in leprosy: Toll-like receptor-regulated organelles involved in eicosanoid formation and Mycobacterium leprae pathogenesis. **Journal of Leukocyte Biology**, *[S. l.]*, v. 87, n. 3, p. 371–384, 2010. Disponível em: https://doi.org/10.1189/jlb.0609433

MATTOS, K. A. *et al.* Modulation of lipid droplets by Mycobacterium leprae in Schwann cells: A putative mechanism for host lipid acquisition and bacterial survival in phagosomes. **Cellular Microbiology**, *[S. l.]*, v. 13, n. 2, p. 259–273, 2011 a. Disponível em: https://doi.org/10.1111/j.1462-5822.2010.01533.x

MATTOS, K. A. *et al.* TLR6-Driven Lipid Droplets in Mycobacterium leprae-Infected Schwann Cells: Immunoinflammatory Platforms Associated with Bacterial Persistence. **The Journal of Immunology**, *[S. l.]*, v. 187, n. 5, p. 2548–2558, 2011 b. Disponível em: https://doi.org/10.4049/jimmunol.1101344

MCCARVILLE, J.; AYRES, J. Disease tolerance: concept and mechanisms. **Current Opinion in Immunology**, *[S. l.]*, v. 50, p. 88–93, 2018. Disponível em: https://doi.org/10.1016/j.coi.2017.12.003

MCRAE, S. *et al.* The hepatitis C virus-induced NLRP3 inflammasome activates the sterol regulatory element-binding protein (SREBP) and regulates lipid metabolism. **Journal of Biological Chemistry**, *[S. l.]*, v. 291, n. 7, p. 3254–3267, 2016. Disponível em: https://doi.org/10.1074/jbc.M115.694059

MEDZHITOV, R. Origin and physiological roles of inflammation. **Nature**, *[S. l.]*, v. 454, n. 7203, p. 428–435, 2008. Disponível em: https://doi.org/10.1038/nature07201

MEDZHITOV, R. Inflammation 2010: New Adventures of an Old Flame. **Cell**, *[S. l.]*, v. 140, n. 6, p. 771–776, 2010. Disponível em: https://doi.org/10.1016/j.cell.2010.03.006

MEI, C. *et al.* Chlamydia pneumoniae induces macrophage-derived foam cell formation via PPAR α and PPAR γ-dependent pathways. **Cell Biology International**, *[S. l.]*, v. 33, n. 3, p. 301–308, 2009. Disponível em: https://doi.org/10.1016/j.cellbi.2008.12.002

MELO, R. C. N. *et al.* Macrophage lipid body induction by Chagas disease in vivo: Putative intracellular domains for eicosanoid formation during infection. **Tissue and Cell**, *[S. l.]*, v. 35, n. 1, p. 59–67, 2003. Disponível em: https://doi.org/10.1016/S0040-

8166(02)00105-2

MELO, R. C. N. *et al.* Lipid bodies: Structural markers of inflammatory macrophages in innate immunity. **Inflammation Research**, *[S. l.]*, v. 55, n. 8, p. 342–348, 2006. Disponível em: https://doi.org/10.1007/s00011-006-5205-0

MELO, R. C. N. *et al.* Lipid Bodies in Inflammatory Cells. **Journal of Histochemistry & Cytochemistry**, *[S. l.]*, v. 59, n. 5, p. 540–556, 2011 a. Disponível em: https://doi.org/10.1369/0022155411404073

MELO, R. C. N. *et al.* Imaging Lipid Bodies Within Leukocytes with Different Light Microscopy Techniques. *In*: **Polymorphism: in the Pharmaceutical Industry**. *[S. l.: s. n.]*. p. 149–161. *E-book*. Disponível em: https://doi.org/10.1007/978-1-60761-950-5_9

MILANO, S. *et al.* Prostaglandin E2 regulates inducible nitric oxide synthase in the murine macrophage cell line J774. **Prostaglandins**, *[S. l.]*, v. 49, n. 2, p. 105–115, 1995. Disponível em: https://doi.org/10.1016/0090-6980(94)00004-G

MIYANARI, Y. *et al.* The lipid droplet is an important organelle for hepatitis C virus production. **Nature Cell Biology**, *[S. l.]*, v. 9, n. 9, p. 1089–1097, 2007. Disponível em: https://doi.org/10.1038/ncb1631

MONSON, E. *et al.* Intracellular Lipid Droplet Accumulation Occurs Early Following Viral Infection and Is Required for an Efficient Interferon Response. **bioRxiv**, *[S. l.]*, p. 2020.02.12.946749, 2020. Disponível em: https://doi.org/10.1101/2020.02.12.946749

MONSON, E. A. *et al.* Lipid droplet density alters the early innate immune response to viral infection. **PLoS ONE**, *[S. l.]*, v. 13, n. 1, p. 1–18, 2018. Disponível em: https://doi.org/10.1371/journal.pone.0190597

MORAN, N. A. *et al.* Evolutionary Relationships of Three New Species of Enterobacteriaceae Living as Symbionts of Aphids and Other Insects. **Applied and Environmental Microbiology**, *[S. l.]*, v. 71, n. 6, p. 3302–3310, 2005. Disponível em: https://doi.org/10.1128/AEM.71.6.3302-3310.2005

MOTA, L. A. M. *et al.* Culture of mouse peritoneal macrophages with mouse serum induces lipid bodies that associate with the parasitophorous vacuole and decrease their microbicidal capacity against Toxoplasma gondii. **Memorias do Instituto Oswaldo Cruz**, *[S. l.]*, v. 109, n. 6, p. 767–774, 2014. Disponível em: https://doi.org/10.1590/0074-

0276140119

MURRAY, P. J.; WYNN, T. A. Protective and pathogenic functions of macrophage subsets. **Nature Reviews Immunology**, *[S. l.]*, v. 11, n. 11, p. 723–737, 2011. Disponível em: https://doi.org/10.1038/nri3073

NAKANISHI, M.; ROSENBERG, D. W. Multifaceted roles of PGE2 in inflammation and cancer. **Seminars in Immunopathology**, *[S. l.]*, v. 35, n. 2, p. 123–137, 2013. Disponível em: https://doi.org/10.1007/s00281-012-0342-8

NASR, N. *et al.* HIV-1 infection of human macrophages directly induces viperin which inhibits viral production. **Blood**, *[S. l.]*, v. 120, n. 4, p. 778–788, 2012. Disponível em: https://doi.org/10.1182/blood-2012-01-407395

NAWABI, P.; CATRON, D. M.; HALDAR, K. Esterification of cholesterol by a type III secretion effector during intracellular Salmonella infection. **Molecular Microbiology**, *[S. l.]*, v. 68, n. 1, p. 173–185, 2008. Disponível em: https://doi.org/10.1111/j.1365-2958.2008.06142.x

NEYROLLES, O. *et al.* Is Adipose Tissue a Place for Mycobacterium tuberculosis Persistence? **PLoS ONE**, *[S. l.]*, v. 1, n. 1, p. e43, 2006. Disponível em: https://doi.org/10.1371/journal.pone.0000043

NICOLAOU, G.; GOODALL, A. H.; ERRIDGE, C. Diverse Bacteria Promote Macrophage Foam Cell Formation Via Toll-Like Receptor-Dependent Lipid Body Biosynthesis. **Journal of Atherosclerosis and Thrombosis**, *[S. l.]*, v. 19, n. 2, p. 137–148, 2012. Disponível em: https://doi.org/10.5551/jat.10249

NIWA, A. *et al.* Interleukin-6, MCP-1, IP-10, and MIG are sequentially expressed in cerebrospinal fluid after subarachnoid hemorrhage. **Journal of Neuroinflammation**, *[S. l.]*, v. 13, n. 1, p. 217, 2016. Disponível em: https://doi.org/10.1186/s12974-016-0675-7

NOGUEIRA, A. C. *et al.* CHANGES IN PLASMA FREE FATTY ACID LEVELS IN SEPTIC PATIENTS ARE ASSOCIATED WITH CARDIAC DAMAGE AND REDUCTION IN HEART RATE VARIABILITY. **Shock**, *[S. l.]*, p. 1, 2007. Disponível em: https://doi.org/10.1097/shk.0b013e31815abbc6

O'CALLAGHAN, E. K. *et al.* Long-Lasting Effects of Sepsis on Circadian Rhythms in the Mouse. **PLoS ONE**, *[S. l.]*, v. 7, n. 10, p. e47087, 2012. Disponível em:

https://doi.org/10.1371/journal.pone.0047087

O'NEILL, L. A. J.; KISHTON, R. J.; RATHMELL, J. A guide to immunometabolism for immunologists. **Nature Reviews Immunology**, *[S. l.]*, v. 16, n. 9, p. 553–565, 2016. Disponível em: https://doi.org/10.1038/nri.2016.70

OLZMANN, J. A.; CARVALHO, P. Dynamics and functions of lipid droplets. **Nature Reviews Molecular Cell Biology**, *[S. l.]*, v. 20, n. March, 2019. Disponível em: https://doi.org/10.1038/s41580-018-0085-z

PACHECO, P. *et al.* Lipopolysaccharide-Induced Leukocyte Lipid Body Formation In Vivo: Innate Immunity Elicited Intracellular Loci Involved in Eicosanoid Metabolism. **The Journal of Immunology**, *[S. l.]*, v. 169, n. 11, p. 6498–6506, 2002. Disponível em: https://doi.org/10.4049/jimmunol.169.11.6498

PACHECO, P. *et al.* Monocyte Chemoattractant Protein-1/CC Chemokine Ligand 2 Controls Microtubule-Driven Biogenesis and Leukotriene B4-Synthesizing Function of Macrophage Lipid Bodies Elicited by Innate Immune Response. **The Journal of Immunology**, *[S. l.]*, v. 179, n. 12, p. 8500–8508, 2007. Disponível em: https://doi.org/10.4049/jimmunol.179.12.8500

PATAT, S. A. *et al.* Antimicrobial activity of histones from hemocytes of the Pacific white shrimp. **European Journal of Biochemistry**, *[S. l.]*, v. 271, n. 23–24, p. 4825–4833, 2004. Disponível em: https://doi.org/10.1111/j.1432-1033.2004.04448.x

PAWLAK, M.; LEFEBVRE, P.; STAELS, B. Molecular mechanism of PPARα action and its impact on lipid metabolism, inflammation and fibrosis in non-alcoholic fatty liver disease. **Journal of Hepatology**, *[S. l.]*, v. 62, n. 3, p. 720–733, 2015. Disponível em: https://doi.org/10.1016/j.jhep.2014.10.039

PECCHI, E. *et al.* Prostaglandins and sickness behavior: Old story, new insights. **Physiology and Behavior**, *[S. l.]*, v. 97, n. 3–4, p. 279–292, 2009. Disponível em: https://doi.org/10.1016/j.physbeh.2009.02.040

PEREIRA-DUTRA, F. S. *et al.* Fat, fight, and beyond: The multiple roles of lipid droplets in infections and inflammation. **Journal of Leukocyte Biology**, *[S. l.]*, v. 106, n. 3, p. 563–580, 2019. Disponível em: https://doi.org/10.1002/JLB.4MR0119-035R

PETERS-GOLDEN, M. *et al.* Leukotrienes: Underappreciated Mediators of Innate

Immune Responses. **The Journal of Immunology**, *[S. l.]*, v. 174, n. 2, p. 589–594, 2005. Disponível em: https://doi.org/10.4049/jimmunol.174.2.589

PETKOVA, D. S.; VIRET, C.; FAURE, M. IRGM in autophagy and viral infections. **Frontiers in Immunology**, *[S. l.]*, v. 3, n. JAN, p. 1–7, 2012. Disponível em: https://doi.org/10.3389/fimmu.2012.00426

PEYRON, P. *et al.* Foamy Macrophages from Tuberculous Patients ' Granulomas Constitute a Nutrient-Rich Reservoir for M . tuberculosis Persistence. **PLOS Pathogens**, *[S. l.]*, v. 4, n. 11, p. 1–14, 2008. Disponível em: https://doi.org/10.1371/journal.ppat.1000204

PLOEN, D. *et al.* TIP47 plays a crucial role in the life cycle of hepatitis C virus. **Journal of Hepatology**, *[S. l.]*, v. 58, n. 6, p. 1081–1088, 2013. Disponível em: https://doi.org/10.1016/j.jhep.2013.01.022

POL, A.; GROSS, S. P.; PARTON, R. G. Biogenesis of the multifunctional lipid droplet: Lipids, proteins, and sites. **The Journal of Cell Biology**, *[S. l.]*, v. 204, n. 5, p. 635–646, 2014. Disponível em: https://doi.org/10.1083/jcb.201311051

QADRI, F. Acute dehydrating disease caused by Vibrio cholerae serogroups O1 and O139 induce increases in innate cells and inflammatory mediators at the mucosal surface of the gut. **Gut**, *[S. l.]*, v. 53, n. 1, p. 62–69, 2004. Disponível em: https://doi.org/10.1136/gut.53.1.62

QUARTIN, A. A. *et al.* Magnitude and duration of the effect of sepsis on survival. **JAMA: The Journal of the American Medical Association**, *[S. l.]*, v. 277, n. 13, p. 1058–1063, 1997. Disponível em: https://doi.org/10.1001/jama.277.13.1058

RANNIKKO, J. *et al.* Sepsis-related mortality in 497 cases with blood culture-positive sepsis in an emergency department. **International Journal of Infectious Diseases**, *[S. l.]*, v. 58, p. 52–57, 2017. Disponível em: https://doi.org/10.1016/j.ijid.2017.03.005

REINHART, K. *et al.* New Approaches to Sepsis: Molecular Diagnostics and Biomarkers. **Clinical Microbiology Reviews**, *[S. l.]*, v. 25, n. 4, p. 609–634, 2012. Disponível em: https://doi.org/10.1128/CMR.00016-12

REIS, P. A. *et al.* Statins prevent cognitive impairment after sepsis by reverting neuroinflammation, and microcirculatory/endothelial dysfunction. **Brain, Behavior, and**

Immunity, *[S. l.]*, v. 60, p. 293–303, 2017. Disponível em: https://doi.org/10.1016/j.bbi.2016.11.006

ROGERS, A. J. *et al.* Metabolomic Derangements Are Associated with Mortality in Critically Ill Adult Patients. **PLoS ONE**, *[S. l.]*, v. 9, n. 1, p. e87538, 2014. Disponível em: https://doi.org/10.1371/journal.pone.0087538

ROGERS, D. C. *et al.* Behavioral and functional analysis of mouse phenotype: SHIRPA, a proposed protocol for comprehensive phenotype assessment. **Mammalian Genome**, *[S. l.]*, v. 8, n. 10, p. 711–713, 1997. Disponível em: https://doi.org/10.1007/s003359900551

ROINGEARD, P.; MELO, R. C. N. Lipid droplet hijacking by intracellular pathogens. **Cellular Microbiology**, *[S. l.]*, n. October 2016, p. 1–8, 2017. Disponível em: https://doi.org/10.1111/cmi.12688

ROLA-PLESZCZYNSKI, M.; STANKOVA, J. Leukotriene B4 enhances interleukin-6 (IL-6) production and IL-6 messenger RNA accumulation in human monocytes in vitro: Transcriptional and posttranscriptional mechanisms. **Blood**, *[S. l.]*, v. 80, n. 4, p. 1004–1011, 1992. Disponível em: https://doi.org/10.1182/blood.v80.4.1004.bloodjournal8041004

RUDD, K. E. *et al.* Global, regional, and national sepsis incidence and mortality, 1990–2017: analysis for the Global Burden of Disease Study. **The Lancet**, *[S. l.]*, v. 395, n. 10219, p. 200–211, 2020. Disponível em: https://doi.org/10.1016/S0140-6736(19)32989-7

RUSSELL, D. G. *et al.* Foamy macrophages and the progression of the human TB granuloma. **Nat Immunol**, *[S. l.]*, v. 10, n. 9, p. 943–948, 2009. Disponível em: https://doi.org/10.1038/ni.1781.Foamy

SAKA, H. A.; VALDIVIA, R. Emerging roles for lipid droplets in immunity and host-pathogen interactions. **Annual Review of Cell and Developmental Biology**, *[S. l.]*, v. 28, n. 1, p. 411–437, 2012. Disponível em: https://doi.org/10.1146/annurev-cellbio-092910-153958

SAMANTA, D. *et al.* Manipulation of Host Cholesterol by Obligate Intracellular Bacteria. **Frontiers in Cellular and Infection Microbiology**, *[S. l.]*, v. 7, n. May, p. 1–14, 2017. Disponível em: https://doi.org/10.3389/fcimb.2017.00165

SAMRA, J. S.; SUMMERS, L. K. M. M.; FRAYN, K. N. **Sepsis and fat metabolismBritish Journal of Surgery**, set. 1996. Seção 9, p. 1186–1196. Disponível em: https://doi.org/10.1002/bjs.1800830906

SAMSA, M. M. *et al.* Dengue virus capsid protein usurps lipid droplets for viral particle formation. **PLoS Pathogens**, *[S. l.]*, v. 5, n. 10, 2009. Disponível em: https://doi.org/10.1371/journal.ppat.1000632

SANTOS, P. C. *et al.* The Pivotal Role of 5-Lipoxygenase-Derived LTB4 in Controlling Pulmonary Paracoccidioidomycosis. **PLoS Neglected Tropical Diseases**, *[S. l.]*, v. 7, n. 8, 2013. Disponível em: https://doi.org/10.1371/journal.pntd.0002390

SCHIEBER, A. M. P.; AYRES, J. S. Thermoregulation as a disease tolerance defense strategy. **Pathogens and Disease**, *[S. l.]*, v. 74, n. 9, p. 1–15, 2016. Disponível em: https://doi.org/10.1093/femspd/ftw106

SCHNEIDER, D. S.; AYRES, J. S. Two ways to survive infection: what resistance and tolerance can teach us about treating infectious diseases. **Nature Reviews Immunology**, *[S. l.]*, v. 8, n. 11, p. 889–895, 2008. Disponível em: https://doi.org/10.1038/nri2432. Acesso em: 8 mar. 2020.

SEO, J.-Y.; CRESSWELL, P. Viperin Regulates Cellular Lipid Metabolism during Human Cytomegalovirus Infection. **PLoS Pathogens**, *[S. l.]*, v. 9, n. 8, p. e1003497, 2013. Disponível em: https://doi.org/10.1371/journal.ppat.1003497

SEO, J.-Y.; YANEVA, R.; CRESSWELL, P. Viperin: A Multifunctional, Interferon-Inducible Protein that Regulates Virus Replication. **Cell Host & Microbe**, *[S. l.]*, v. 10, n. 6, p. 534–539, 2011. Disponível em: https://doi.org/10.1016/j.chom.2011.11.004

SEREZANI, C. H. *et al.* Leukotrienes Are Essential for the Control of Leishmania amazonensis Infection and Contribute to Strain Variation in Susceptibility. **The Journal of Immunology**, *[S. l.]*, v. 177, n. 5, p. 3201–3208, 2006. Disponível em: https://doi.org/10.4049/jimmunol.177.5.3201

SHARMA, N. K. *et al.* Lipid metabolism impairment in patients with sepsis secondary to hospital acquired pneumonia, a proteomic analysis. **Clinical Proteomics**, *[S. l.]*, v. 16, n. 1, p. 1–13, 2019. Disponível em: https://doi.org/10.1186/s12014-019-9252-2

SHEPPE, A. E. F. *et al.* PGE2 Augments Inflammasome Activation and M1 Polarization

in Macrophages Infected With Salmonella Typhimurium and Yersinia enterocolitica. **Frontiers in Microbiology**, *[S. l.]*, v. 9, n. October, p. 1–16, 2018. Disponível em: https://doi.org/10.3389/fmicb.2018.02447

SILK, E. *et al.* The role of extracellular histone in organ injury. **Cell Death and Disease**, *[S. l.]*, v. 8, n. 5, p. e2812, 2017. Disponível em: https://doi.org/10.1038/cddis.2017.52

SILVA, A. R. *et al.* Lipid bodies in oxidized LDL-induced foam cells are leukotriene-synthesizing organelles: a MCP-1/CCL2 regulated phenomenon. **Biochimica et Biophysica Acta - Molecular and Cell Biology of Lipids**, *[S. l.]*, v. 1791, p. 1066–1075, 2009. Disponível em: https://doi.org/10.1016/j.bbalip.2009.06.004

SINGER, M. *et al.* The Third International Consensus Definitions for Sepsis and Septic Shock (Sepsis-3). **JAMA**, *[S. l.]*, v. 315, n. 8, p. 801, 2016. Disponível em: https://doi.org/10.1001/jama.2016.0287

SOARES, M. P.; TEIXEIRA, L.; MOITA, L. F. Disease tolerance and immunity in host protection against infection. **Nature Reviews Immunology**, *[S. l.]*, v. 17, n. 2, p. 83–96, 2017. Disponível em: https://doi.org/10.1038/nri.2016.136

SOEHNLEIN, O.; LINDBOM, L. Phagocyte partnership during the onset and resolution of inflammation. **Nature Reviews Immunology**, *[S. l.]*, v. 10, n. 6, p. 427–439, 2010. Disponível em: https://doi.org/10.1038/nri2779

SONAWANE, A. *et al.* Cathelicidin is involved in the intracellular killing of mycobacteria in macrophages. **Cellular Microbiology**, *[S. l.]*, v. 13, n. 10, p. 1601–1617, 2011. Disponível em: https://doi.org/10.1111/j.1462-5822.2011.01644.x

SORGI, C. A. *et al.* Histoplasma capsulatum Cell Wall -Glucan Induces Lipid Body Formation through CD18, TLR2, and Dectin-1 Receptors: Correlation with Leukotriene B4 Generation and Role in HIV-1 Infection. **The Journal of Immunology**, *[S. l.]*, v. 182, n. 7, p. 4025–4035, 2009. Disponível em: https://doi.org/10.4049/jimmunol.0801795

STRNAD, P. *et al.* Liver — guardian , modifier and target of sepsis. **NATURE REVIEWS GASTROENTEROLOGY & HEPATOLOGY**, *[S. l.]*, v. 14, p. 55–66, 2017. Disponível em: https://doi.org/10.1038/nrgastro.2016.168

SYED, G. H.; SIDDIQUI, A. Effects of hypolipidemic agent nordihydroguaiaretic acid on lipid droplets and hepatitis C virus. **Hepatology**, *[S. l.]*, v. 54, n. 6, p. 1936–1946,

2011. Disponível em: https://doi.org/10.1002/hep.24619

SZATMARI, I. *et al.* PPARgamma regulates the function of human dendritic cells primarily by altering lipid metabolism. **Blood**, *[S. l.]*, v. 110, n. 9, p. 3271–3280, 2007. Disponível em: https://doi.org/10.1182/blood-2007-06-096222

SZELES, L.; TOROCSIK, D.; NAGY, L. PPARγ in immunity and inflammation: cell types and diseases. **Biochimica et Biophysica Acta (BBA) - Molecular and Cell Biology of Lipids**, *[S. l.]*, v. 1771, n. 8, p. 1014–1030, 2007. Disponível em: https://doi.org/10.1016/j.bbalip.2007.02.005

TALVANI, A. *et al.* Leukotriene B4 induces nitric oxide synthesis in Trypanosoma cruzi-infected murine macrophages and mediates resistance to infection. **Infection and Immunity**, *[S. l.]*, v. 70, n. 8, p. 4247–4253, 2002. Disponível em: https://doi.org/10.1128/IAI.70.8.4247-4253.2002

TAVARES, N. *et al.* Degranulating Neutrophils Promote Leukotriene B 4 Production by Infected Macrophages To Kill Leishmania amazonensis Parasites. **The Journal of Immunology**, *[S. l.]*, v. 196, n. 4, p. 1865–1873, 2016. Disponível em: https://doi.org/10.4049/jimmunol.1502224

TENG, O.; ANG, C. K. E.; GUAN, X. L. Macrophage–Bacteria Interactions—A Lipid-Centric Relationship. **Frontiers in Immunology**, *[S. l.]*, v. 8, n. December, 2017. Disponível em: https://doi.org/10.3389/fimmu.2017.01836

TOLEDO, D. A. M. *et al.* Lipid Body Organelles within the Parasite Trypanosoma cruzi: A Role for Intracellular Arachidonic Acid Metabolism. **PLOS ONE**, *[S. l.]*, v. 11, n. 8, p. e0160433, 2016. Disponível em: https://doi.org/10.1371/journal.pone.0160433

VALLOCHI, A. L. *et al.* Lipid Droplet, a Key Player in Host-Parasite Interactions. **Frontiers in Immunology**, *[S. l.]*, v. 9, n. May, 2018. Disponível em: https://doi.org/10.3389/fimmu.2018.01022

VAN HARTEN, R. M. *et al.* Cathelicidins: Immunomodulatory antimicrobials. **Vaccines**, *[S. l.]*, v. 6, n. 3, 2018. Disponível em: https://doi.org/10.3390/vaccines6030063

VAN MANEN, H.-J. *et al.* Single-cell Raman and fluorescence microscopy reveal the association of lipid bodies with phagosomes in leukocytes. **Proceedings of the National**

Academy of Sciences, *[S. l.]*, v. 102, n. 29, p. 10159–10164, 2005. Disponível em: https://doi.org/10.1073/pnas.0502746102

VAN MEER, G.; VOELKER, D. R.; FEIGENSON, G. W. Membrane lipids: where they are and how they behave. **Nature Reviews Molecular Cell Biology**, *[S. l.]*, v. 9, n. 2, p. 112–124, 2008. Disponível em: https://doi.org/10.1038/nrm2330

VAN WYNGENE, L.; VANDEWALLE, J.; LIBERT, C. Reprogramming of basic metabolic pathways in microbial sepsis: therapeutic targets at last? **EMBO Molecular Medicine**, *[S. l.]*, v. 10, n. 8, p. e8712, 2018. Disponível em: https://doi.org/10.15252/emmm.201708712

VIKTOROVA, E. G. *et al.* Phospholipid synthesis fueled by lipid droplets drives the structural development of poliovirus replication organelles. **PLOS Pathogens**, *[S. l.]*, v. 14, n. 8, p. e1007280, 2018. Disponível em: https://doi.org/10.1371/journal.ppat.1007280

VINCENT, J. L. *et al.* Assessment of the worldwide burden of critical illness: The Intensive Care Over Nations (ICON) audit. **The Lancet Respiratory Medicine**, *[S. l.]*, v. 2, p. 380–386, 2014. Disponível em: https://doi.org/10.1016/S2213-2600(14)70061-X

WALTHER, T. C.; FARESE, R. V. Lipid Droplets and Cellular Lipid Metabolism. **Annual Review of Biochemistry**, *[S. l.]*, v. 81, n. 1, p. 687–714, 2012. Disponível em: https://doi.org/10.1146/annurev-biochem-061009-102430

WANG, A. *et al.* Opposing Effects of Fasting Metabolism on Tissue Tolerance in Bacterial and Viral Inflammation. **Cell**, *[S. l.]*, v. 166, n. 6, p. 1512- 1525.e12, 2016. Disponível em: https://doi.org/10.1016/j.cell.2016.07.026

WANG, A.; LUAN, H. H.; MEDZHITOV, R. An evolutionary perspective on immunometabolism. **Science**, *[S. l.]*, v. 363, n. 6423, p. eaar3932, 2019. Disponível em: https://doi.org/10.1126/science.aar3932

WANG, X.; HINSON, E. R.; CRESSWELL, P. The Interferon-Inducible Protein Viperin Inhibits Influenza Virus Release by Perturbing Lipid Rafts. **Cell Host & Microbe**, *[S. l.]*, v. 2, n. 2, p. 96–105, 2007. Disponível em: https://doi.org/10.1016/j.chom.2007.06.009

WANG, Z.; GERSTEIN, M.; SNYDER, M. RNA-Seq: a revolutionary tool for transcriptomics. **Nature Reviews Genetics**, *[S. l.]*, v. 10, n. 1, p. 57–63, 2009. Disponível em: https://doi.org/10.1038/nrg2484

WARE, L. B. *et al.* Plasma biomarkers of oxidant stress and development of organ failure in severe sepsis. **Shock (Augusta, Ga.)**, *[S. l.]*, v. 36, p. 12–7, 2011. Disponível em: https://doi.org/10.1097/SHK.0b013e318217025a

WEI, L. *et al.* Lactate promotes PGE2 synthesis and gluconeogenesis in monocytes to benefit the growth of inflammation-associated colorectal tumor. **Oncotarget**, *[S. l.]*, v. 6, n. 18, p. 16198–16214, 2015. Disponível em: https://doi.org/10.18632/oncotarget.3838

WEIS, S. *et al.* Metabolic Adaptation Establishes Disease Tolerance to Sepsis. **Cell**, *[S. l.]*, v. 169, n. 7, p. 1263- 1275.e14, 2017. Disponível em: https://doi.org/10.1016/j.cell.2017.05.031

WELLER, P. F. Leukocyte lipid droplets - Structure and function as "Eicosasomes". **Transactions of the American Clinical and Climatological Association**, *[S. l.]*, v. 127, p. 328–340, 2016. Disponível em: http://www.ncbi.nlm.nih.gov/pubmed/28066068

WELTE, M. A. Expanding roles for lipid droplets. **Current Biology**, *[S. l.]*, v. 25, n. 11, p. R470–R481, 2015. Disponível em: https://doi.org/10.1016/j.cub.2015.04.004

WESTPHAL, G. A. *et al.* Análise da qualidade de vida após a alta hospitalar em sobreviventes de sepse grave e choque séptico. **Revista Panamericana de Salud Pública**, *[S. l.]*, v. 31, n. 6, p. 499–505, 2012. Disponível em: https://doi.org/10.1590/S1020-49892012000600008

WILFLING, F. *et al.* Triacylglycerol synthesis enzymes mediate lipid droplet growth by relocalizing from the ER to lipid droplets. **Developmental Cell**, *[S. l.]*, v. 24, n. 4, 2013. Disponível em: https://doi.org/10.1016/j.devcel.2013.01.013

WINTERS, B. D. *et al.* Long-term mortality and quality of life in sepsis: A systematic review*. **Critical Care Medicine**, *[S. l.]*, v. 38, n. 5, p. 1276–1283, 2010. Disponível em: https://doi.org/10.1097/CCM.0b013e3181d8cc1d

XU, Q. *et al.* NADPH oxidases are essential for macrophage differentiation. **Journal of Biological Chemistry**, *[S. l.]*, 2016. Disponível em: https://doi.org/10.1074/jbc.M116.731216

YAN, J.; LI, S. S.; LI, S. S. The Role of the Liver in Sepsis. **International Reviews of Immunology**, *[S. l.]*, v. 33, n. 6, p. 498–510, 2014. Disponível em: https://doi.org/10.3109/08830185.2014.889129

YORK, A. G. *et al.* Limiting Cholesterol Biosynthetic Flux Spontaneously Engages Type I IFN Signaling. **Cell**, *[S. l.]*, v. 163, n. 7, p. 1716–1729, 2015. Disponível em: https://doi.org/10.1016/j.cell.2015.11.045

YU, W. *et al.* Co-compartmentalization of MAP kinases and cytosolic phospholipase A2 at cytoplasmic arachidonate-rich lipid bodies. **The American journal of pathology**, *[S. l.]*, v. 152, n. 3, p. 759–769, 1998.

ZHANG, H. *et al.* Proteome of skeletal muscle lipid droplet reveals association with mitochondria and apolipoprotein A-I. **Journal of Proteome Research**, *[S. l.]*, v. 10, n. 10, p. 4757–4768, 2011. Disponível em: https://doi.org/10.1021/pr200553c

Anexo 1

PEREIRA-DUTRA, FILIPE S.; TEIXEIRA, LIVIA; SOUZA COSTA, MARIA FERNANDA; BOZZA, PATRÍCIA T. **Fat, fight, and beyond: The multiple roles of lipid droplets in infections and inflammation**. *JOURNAL OF LEUKOCYTE BIOLOGY*, v.106, p.563 - 580, 2019

DOI: 10.1002/JLB.4MR0119-035R

JLB JOURNAL OF LEUKOCYTE BIOLOGY

REVIEW

Fat, fight, and beyond: The multiple roles of lipid droplets in infections and inflammation

Filipe S. Pereira-Dutra | Livia Teixeira | Maria Fernanda de Souza Costa | Patrícia T. Bozza

Laboratório de Imunofarmacologia, Instituto Oswaldo Cruz, Fundação Oswaldo Cruz, Rio de Janeiro, Brazil

Correspondence
Patrícia T. Bozza, Laboratório de Imunofarmacologia, Instituto Oswaldo Cruz, Fundação Oswaldo Cruz, Avenida Brasil, 4365, Manguinhos, Rio de Janeiro, RJ, CEP 21045–900, Brazil.
Email: pbozza@ioc.fiocruz.br

Abstract

Increased accumulation of cytoplasmic lipid droplets (LDs) in host nonadipose cells is commonly observed in response to numerous infectious diseases, including bacterial, parasite, and fungal infections. LDs are lipid-enriched, dynamic organelles composed of a core of neutral lipids surrounded by a monolayer of phospholipids associated with a diverse array of proteins that are cell and stimulus regulated. Far beyond being simply a deposit of neutral lipids, LDs have come to be seen as an essential platform for various cellular processes, including metabolic regulation, cell signaling, and the immune response. LD participation in the immune response occurs as sites for compartmentalization of several immunometabolic signaling pathways, production of inflammatory lipid mediators, and regulation of antigen presentation. Infection-driven LD biogenesis is a complexly regulated process that involves innate immune receptors, transcriptional and post-transcriptional regulation, increased lipid uptake, and new lipid synthesis. Accumulating evidence demonstrates that intracellular pathogens are able to exploit LDs as an energy source, a replication site, and/or a mechanism of immune response evasion. Nevertheless, LDs can also act in favor of the host as part of the immune and inflammatory response to pathogens. Here, we review recent findings that explored the new roles of LDs in the context of host-pathogen interactions.

KEYWORDS
metabolism, lipid droplets, infection, inflammation

1 | INTRODUCTION

Lipids are a major and most diverse class of biomolecules, which play an important role in both the physiology and pathophysiology of living systems. In addition to acting as structural components of cell membranes, lipids are also energy sources as well as signaling molecules during infection and inflammation.[1–4] In the cell, the main lipid storage sites are lipid droplets (LDs) or lipid bodies, a ubiquitous organelle that can be found in virtually all types of cells from prokaryotes to multicellular eukaryotes.[5,6]

In recent decades, LDs have gone from being perceived as only a source of energy storage to being described as complex and dynamic organelles centrally involved in energy and lipid homeostasis, membrane biosynthesis, cell signaling, and handling of hydrophobic vitamin and cell protection to lipotoxicity.[7–13] Structurally, LDs are endoplasmic reticulum (ER)-derived organelles composed of a core of neutral lipids (triacylglycerol, diacylglycerol, and cholesterol ester) surrounded by a monolayer of phospholipids associated with a diverse composition of proteins.[14,15]

The size, number, function, and composition of LDs differ considerably among different cell types and even in individual cells in a population.[5,13,16] The LD proteome has been reported as dynamic and complex in several cell types and stimulatory conditions.[17–19] Accumulating data demonstrate not only the protein diversity but also the compartmentalization of signaling and metabolic pathways on LDs, mainly lipid metabolism[20] and eicosanoid synthesis.[21,22]

Furthermore, LDs are also involved in inflammatory and infectious diseases.[23] The participation of LDs in infectious disease pathogenesis has been reported for all classes of pathogens, such as viruses,[24,25] bacteria,[26,27] fungi,[28] and protozoa,[29,30] suggesting that

Abbreviations: BCG, bacillus Calmette—Guérin; DENV, dengue virus; FA, fatty acids; HCV, hepatitis C virus; Lam, lipoarabinomannan; LD, lipid droplet; NS, nonstructural; PAF, platelet-activating factor; PAMP, pathogen-associated molecular pattern; PRR, pattern recognition receptor; PV, parasitophorous vacuole; TAG, triacylglycerol.

Received: 26 January 2019 | Revised: 16 April 2019 | Accepted: 26 April 2019

LDs participate in the innate and adaptative host immune response to infection. Host LDs may also be exploit as part of the adaptation of pathogens to escape the immune system and as an energy source for intracellular pathogens.[31–33] Here, we review the complex relationship between host LDs and pathogens, highlighting the multiple roles of LDs in pathogen survival and proliferation, as well as in the host's protective response, in the context of host-pathogen interactions.

2 | LD BIOGENESIS IN CELLS OF THE IMMUNE RESPONSE

Although LDs are almost absent in resting leukocytes and other cells of the immune response, increases in the size and number of LDs in cells involved in infectious and inflammatory processes occur so often that LDs have been considered structural markers of inflammation.[6,15] LD biogenesis is a rapid and highly regulated process whose mechanisms and mobilized signaling pathways are dependent on the infectious agent and cell type involved. Of note, LD biogenesis involves multiple steps and de novo LD formation occurs mostly in the ER where the enzymes involved in neutral lipid synthesis are localized providing triacylglicerols and sterol esters for LD formation.[34] Proposed biogenesis models suggest that LDs bud from the outer leaflet of the ER. However, it is still debatable whether at least part of newly formed LDs remains associated with the ER and/or contain remnant ER-derived membranes.[34,35]

Although the molecular mechanisms that govern LD biogenesis during inflammation and infection are still incompletely understood, it occurs as a multimediated process that involves increased lipid uptake, lipolysis inhibition, and new lipid synthesis. Moreover, it has been demonstrated that this phenomenon depends not only on the direct interaction between the pathogen and host cells but also on the indirect mechanisms of a bystander amplification-induced system through bacterial components and/or host-generated cytokines and chemokines.[26,27,36–40]

Pioneer work by Pacheco et al.[36] demonstrates that LDs biogenesis in leukocytes can be triggered by the recognition of pathogen-associated molecular pattern (PAMP) by specific receptors of the innate immunity (PRRs, pattern recognition receptors).[36] Among PRRs described, the TLR family stands out as a well-established molecular pathway for LD biogenesis induction by infectious agents (Table 1).

LPS-induced LD formation in leukocytes was demonstrated to occur through a mechanism largely dependent on TLR4 in cooperation with CD14.[36] Bacterial infection with *Chlamydia pneumoniae* is also capable of inducing foam cell formation[41] in a pathway dependent on TLR2 and TLR4, but not TLR3, as well as the mobilization of the adapter molecules Myeloid differentiation primary response 88 (MyD88) and TIR-domain-containing adapter-inducing IFN-β (TRIF).[42,43] TLRs, mainly TLR2, are essential receptors involved in the recognition of distinct mycobacterial products.[44] Signaling through TLR2 proved to be essential to trigger LD formation in macrophages during purified bacterial wall component lipoarabinomannan stimuli or *Mycobacterium bovis*[45,46] and *Mycobacterium leprae* infection;[38] in this last case, the deletion of TLR6, which is reported to heterodimerize with TLR2, also impaired LD formation not only in macrophages but also in Schwann cells.[26] Although stimulation of TLR2 is essential, it is not sufficient to induce LD biogenesis because zymosan and Pam_3Cys, potent agonists of TLR2, and the nonpathogenic bacterium *Mycobacterium smegmatis* fail to induce these organelles; therefore, other cofactors must be involved.[45,46]

The participation of the TLR in the LD biogenesis is not restricted to bacteria. Fungal infection with *Histoplasma capsulatum*, the causative agent of pulmonary histoplasmosis, has been described to induce an increase in leukocyte LD numbers in a dose- and time-dependent manner, and the TLR2, CD18, and Dectin-1 pathways have been shown to be essential for this mechanism.[28] Similarly, during macrophage infection by the parasitic protozoan *T. cruzi*, the dependence on TLR2 signaling, but not TLR4, for LD biogenesis has been demonstrated.[47] However, the identification of another receptor or downstream signaling pathway involved in the biogenesis of LDs during *T. cruzi* infection remains unknown.

Furthermore, signaling through intracellular PRRs also has been shown to be involved in LD biogenesis. During infection by hepatitis C virus (HCV), activation of NLRP3, a member of the NOD-like receptor (NLR) family responsible for triggering inflammasome activation, was associated with changes in lipid homeostasis observed in infected cells.[48–50] The HCV-activated NLRP3 inflammasome causes the activation of SREBPs that up-regulate lipogenic genes, and these alterations result in the intracellular accumulation of LDs.[48] Since HCV has absolute reliance on host lipids in the various stages of the viral life cycle, LD formation proved to be crucial for liver disease pathogenesis associated with chronic HCV[51,52] (Fig. 2). On the other hand, NLRP3-deficient macrophages infected with *C. pneumoniae* present a significant increase in LD number, probably because activation of the NLRP3 inflammasome is closely associated with capture or use of LDs in chlamydial inclusions in infected BMMs, which is in agreement with the fact that NLRP3 activation favors the growth of *C. pneumonia*.[53]

Downstream pathways involved in LD biogenesis were shown to involve the activation of transcription factors including master regulators of lipid metabolism and nuclear receptors, such as peroxisome proliferator-activated receptors (PPARs), liver X receptor (LXR), SREBPs, and HIF.[42,45,48,51,54–59] Members of subfamily of PPARs, LXR, and SREBPs sense the intracellular lipid environment and modulate expression of key genes in fatty acid uptake, lipid synthesis, lipolytic enzymes, and LD biogenesis.[54,60] Of note, NFκB was shown to counter-regulate LD biogenesis because its inhibition lead to enhanced TLR2-triggered LD formation.[57] The activation of TLR signaling induce the increasing of expressions of several enzymes involved in the synthesis of triglycerides and/or cholesterol ester, such as fatty acid synthase (FASN), diacylglycerol-O-acyltransferase (DGAT-1 and DGAT-2), and acyl-CoA:cholesterol O-acyltransferases (ACAT1 and ACAT2).[61–63] When de novo lipid synthesis is blocked, the biogenesis of LD downstream of TLR activation is severely impaired.[39,47]

Also favoring lipid accumulation, TLR activation has reported the increase in the expression of several receptors involved in

TABLE 1 Receptors of innate immunity involved in inducing LD biogenesis by different pathogens

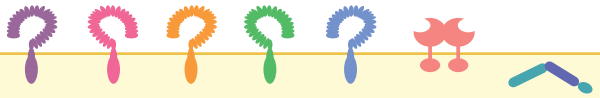

		TLR2	TRL4	TRL5	TRL6	TRL9	Dectin-1	NLR3	References
Bacterias									
	A. baumannii	●	●						63
	C. pneumoniae	●	●						41-43
	E. coli	●	●	●					63
	K. pneumoniae	●		●					63
	M. bovis BCG	●							45,46
	M. leprae	●			●				26,38
	M. tuberculosis	●							40-113
	P. aeruginosa	●							63
	P.diminuta	●	●						63
	P. vulgaris	●							63
	S. aureus	●							63
	S. epidermidis	●							63
	S. salivarisus								63
Bacterial derivates									
	CpG DNA					●			63
	Flagellin			●					63
	LPS		●						36
	LAM	●							45-46
Virus									
	HCV							●	48-50
Fungus									
	H. capsulatum	●	●				●		28
Parasites									
	T. cruzi	●							47
	S.mansoni	●							100

increased lipid uptake and transport,[57,61,62,64] as well as the decrease in expression of lipolytic enzymes, mainly adipose triglyceride lipase (ATGL).[61,62] The increase in the lipid content in the cells is accompanied by the increase in the expression of LD structural proteins, mainly adipose differentiation-related protein/Perilipin-2 (ADRP/Plin2)[62,65,66] and tail-interacting protein of 47 kD/Perilipin-3 (TIP47/Plin3).[67,68] Moreover, these structural proteins are essential to LDs assembly and biogenesis.[69]

Among these regulators, PPARs have been the most explored during the infectious process. PPAR can directly impact LD formation by modulating ADRP/Plin2 expression, a protein intrinsically associated with LD surfaces with major functions in lipid homeostasis in nonadipocyte cells.[65,70,71] The Plin2 gene has a response element for PPARs, and its expression is positively regulated by their agonists.[72] Additionally, PPARs regulate proteins involved in triggering de novo lipogenesis, including fatty acid synthase, and gene regulatory factors LXR and SREBPs[60] (Fig. 1).

PPARs are expressed by leukocytes, including T cells, B cells, dendritic cells, and macrophages[54,73] and are highly expressed in foam cells within atherosclerotic lesions.[74] Studies have demonstrated that the expression and function of the nuclear receptor are regulated by bacterial components[55,75,76] and are associated with LD biogenesis. Almeida and colleagues demonstrated that experimental infection by *M. bovis* BCG is able to up-regulate the expression and/or activation of PPARγ and induce lipid-laden macrophages, a phenotype that is abrogated when infected cells are pretreated with GW9662, a selective antagonist of PPARγ.[52] All of these mechanisms are under the control of TLR2 signaling because BCG-induced PPARγ expression, LD formation, and TNF-α generation were drastically inhibited in TLR-2-deficient mice.[52,76] However, activation of the TLR2 pathway is not sufficient to induce PPARγ expression because stimulation with the nonpathogenic bacterium *M. smegmatis* may activate TLR2-dependent TNF-α production without an increase in PPARγ expression.[52,76] This finding raises the possibility of the participation of other cofactors

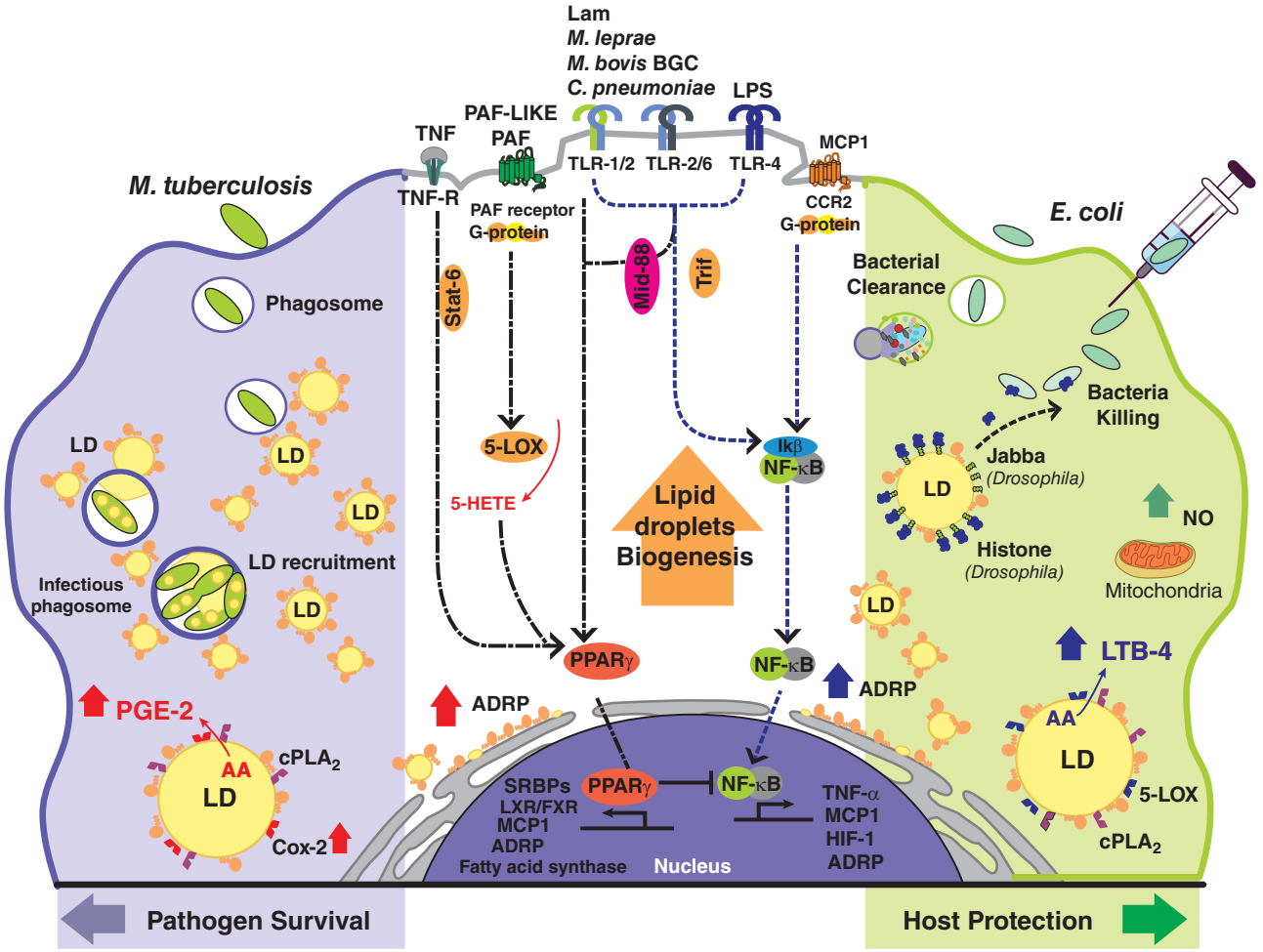

FIGURE 1 **The roles of lipid droplets (LDs) at bacterial infections.** LD biogenesis is a higher regulated process, involving several receptors of innate immunity, including TLR, which recognize bacteria or parts of bacteria. Moreover, several cytokines and lipid mediator molecules induced the LDs accumulations, such as MCP-1/CCL2, hydroxyeicosatetraenoic acid (5-HETE), platelet-activating factor (PAF), and PAF-like molecules. Activation of the receptors of these molecules started a complex signaling cascade that culminates in the activation of peroxisome proliferator-activated receptor γ (PPAR-γ) or NF-κB, which directly or indirectly induce the activation of several lipogenic genes (SRBPS, LXR/FXR, HIF-1, fatty acid synthase) and structural proteins of LDs, such as PLIN2/ADRP. After the induction, bacteria recruit the LDs to the vicinities of the bacteria-containing endosomes. The interaction of LDs with bacteria-containing phagosomes leads to the release of LDs contents, such as cholesterol and triacylglycerol, which serve as a nutritional source for pathogen bacteria survival and proliferation. In addition, LDs are also important players in innate immunity. Host-pathogen interaction leads to the biosynthesis and secretion of inflammatory mediators such as prostaglandin E_2 (PGE_2) through arachidonic acid (AA)-derived cyclooxygenase (COX-2) pathways. PGE_2 may potentially inhibit Th1 response, thus favoring pathogen proliferation. In contrast to LDs recruitment mechanisms to the pathogen benefit, innate immunity actors, such as histones in *Drosophila*, are localized at the LD surface and may act as antibacterial proteins. Besides, LDs are also a site for production of leukotriene B_4 (LTB_4), a pro-inflammatory eicosanoids AA-derivated lipoxygenase (5-LOX) pathways, associated with the pathogen's elimination

in this signaling; indeed, BCG-induced PPARγ expression and LD formation are largely dependent on CD36 activation in association with CD11b/CD18 and CD14 compartmentalized on lipid rafts.[57]

During the infectious process, the observation that LD biogenesis can be triggered in relatively short timeframes and occurs both in cells carrying the infectious agent and likewise in uninfected cells demonstrates that this phenomenon does not depend exclusively on direct interaction between pathogens and the host cell, but indirect mechanisms may amplify this response.[47] In fact, several molecules produced during the inflammatory response act in a paracrine manner, inducing LD formation, including lipid mediators, cytokines, and chemokines.

Platelet-activating factor (PAF) and PAF-like molecules are inflammatory phospholipids recognized by a single G protein-coupled PAF receptor[77] and play an important role in LD biogenesis in leukocytes such as neutrophils[78] and eosinophils.[21,79] Blocking the PAF receptor with an antagonist or inactivation of ligands recognized by the PAF receptor by administration of phospholipase PAF acetylhydrolase significantly inhibits LD formation induced by oxLDL, LPS, or sepsis.[80,81] Studies with pharmacological inhibition and genetically deficient mice show that the downstream pathway behind rapid PAF-induced LD formation in PMNs depends on 5-lipoxygenase (5-LO) activity to form 5(S)-hydroxyeicosatetraenoic acid, as well as subsequent stimulation of protein kinase C and phospholipase C;[78] PAF-induced LD biogenesis

requires new protein synthesis, may be amplified by PPARγ activation, and has an intense crosstalk with MCP-1/CCL2 signaling.[36,78,81,82]

The monocyte chemoattractant protein (MCP-1, also known as chemokine ligand 2 [CCL2]) is a central chemokine in mononuclear cell recruitment.[83] In different models such as saturated fatty acid-[84,85] or oxLDL-rich conditions,[66] leptin stimuli in tumor cells,[86] polymicrobial infection, or LPS-driven inflammatory responses,[37] the increase in MCP-1/CCL2 production occurs in parallel to LD formation. Indeed, MCP-1/CCL2 directly induces a dose-dependent increase in the numbers of cytoplasmic LDs in vitro within resident peritoneal macrophages isolated from naive mice, indicating that its effect occurs through cell migration independent pathways. During sepsis or LPS-induced inflammation, LD biogenesis in leukocytes was virtually absent in MCP-1/CCL2$^{-/-}$ mice.[37] MCP-1/CCL2 was also centrally involved in foam cell formation induced by oxLDL because pretreatment with neutralizing anti-MCP-1/CCL2 inhibited macrophage ADRP/Plin2 expression and drastically reduced the number of LDs.[66] MCP-1/CCL-2 paracrine activity has been shown to induce LD biogenesis through its cognate receptor CCR2, MAP kinase, ERK, and PI3K downstream signaling, and requires the maintenance of a well-organized microtubule network because both microtubule-disrupting and -stabilizing drugs (colchicine and taxol, respectively) have inhibitory effects on LD biogenesis.[37] Although MCP-1/CCL2 produced in the course of BCG infection has a proven role in leukocyte recruitment,[87] it is not essential for signaling of LD formation. Indeed, BCG infection triggered LD biogenesis in MCP-1/CCL2$^{-/-}$ in similar amounts in wild-type mice.[46] This finding suggests that the cell migration may modulate, but is not essential for LD accumulation in leukocytes during inflammation, and redundant LD-triggering mechanism may occur in mycobacterial infections, which is also independent of both TNF-α and IFN-γ.[46] In this context, IL-6, a STAT-activating cytokine, has been described to increase intracellular mycobacterial survival via effects on triglyceride deposition in macrophages. IL-6 treatment potentiated the increase in intracellular LDs driven by *M. bovis* BCG infection and promoted intracellular mycobacterial survival probably by enhancing bacterial access to host triglycerides. These effects were dependent on DGAT1 activation, and DGAT-1 inhibition abolished the ability of mycobacteria to drive LD accumulation and eliminated the ability of IL-6 to promote mycobacterial survival.[88]

3 | LD FUNCTIONS IN INFLAMMATION

Eicosanoids are lipids derived from enzymatic oxygenation of arachidonic acid via the cyclooxygenase (COX) and lipoxygenase (LOX) pathways. In contrast to their precursor, eicosanoids are newly formed and nonstorable molecules.[6,22] Moreover, eicosanoids are signaling lipids that have important roles in both physiological and pathological conditions, such as tissue homeostasis, host defense, and inflammation.[22,89] The compartmentalization of eicosanoid synthetic machinery is a crucial component in the regulation of eicosanoid synthesis and in delineating intracellular and extracellular functional actions of eicosanoids.[89,90] Substantial evidence has demonstrated that LDs are specialized intracellular sites for eicosanoid synthesis, often associated with the inflammatory, infectious, and neoplastic processes.[15,22,23]

In leukocytes, LDs are one of the principle storage sites of arachidonic acid, esterified in phospholipids on the LD monolayer and in triglycerides at LD core from where it can be mobilized by phospholipases or ATGL, respectively.[91–95] Furthermore, LDs compartmentalize the entire enzymatic machinery for eicosanoid synthesis, including phospholipase A2 (PLA_2),[95] activating kinases involved in the arachidonic acid mobilization pathway (ERK1/2, p85, and p38),[95] and all relevant eicosanoid-forming enzymes (COX-1, COX-2, 5-LOX, 15-LOX, 5-LO–activating protein, PGE-synthase, and LTC_4-synthase).[66,79] The presence of all these components causes LDs to be capable of rapid arachidonic acid mobilization to produce prostaglandins and leukotrienes.[21,89,90,95]

During inflammatory and/or infectious stimulation, a significant correlation has been reported between LD biogenesis and improved generation of eicosanoids in leukocytes.[6,15,47] Stimuli that induce or inhibit LD formation also coordinately enhance or inhibit eicosanoid synthesis, respectively, in activated leukocytes in a dose-dependent manner.[22,96] In this context, it has been experimentally demonstrated that LDs are main sites of production of leukotriene C_4 (LTC_4),[66,97] leukotriene B_4 (LTB_4),[37,66] prostaglandin E_2 (PGE_2),[46,47,98] prostaglandin D_2 (PGD_2),[99] and eoxin C_4 (EXC_4)[100] during inflammatory and infectious conditions. Other data further indicate that LDs could be the site of synthesis of lipoxin B_4 (LXB_4)[58] and prostaglandin F2alpha (PGF2α),[58,101] however, they still need validation. Several studies have shown that numerous pathogens stimulate the biosynthesis of PGE_2, which could act as an anti-inflammatory mediator favoring the persistence of the pathogen.[22,96] In this situation, LDs were reported as being a site for PGE_2 generation during infection by *M. bovis* BCG[46] and *T. cruzi*.[47] In both infections, PGE_2 production was reported as permissive to pathogens and probably downmodulate macrophage antimicrobial response.[46,47] Furthermore, PGE_2 not only affects infected leukocytes but may also inhibit Th1 responses, which would favor pathogen proliferation and dissemination.[102] Moreover, LDs in colon cancer cells are active organelles involved in PGE_2 synthesis and may have implications in the pathogenesis of adenocarcinoma of the colon.[98]

In contrast, the synthesis of LTB_4, a pro-inflammatory mediator, has also been reported in LDs during the inflammatory response, such as observed during sepsis or endotoxemia.[37] LTB_4 generation during infection contributes to parasite killing[103,104] through indirect effects mediated by amplification of other inflammatory molecules, mediating the recruitment and activation of effector cells.[105] The balance between the generation of PGE_2 and LTB_4 is central in the immune response.[22,105] As a platform for the synthesis of these lipid mediators, LDs probably play an important role both in the survival of pathogens and in the effective host response to infection, but it is still unclear which events mediate each type of response.

The synthesis of inflammatory lipid mediators on LDs also makes this organelle a central component of the leukocyte response in inflammation. As a site of production of LTC_4, PGD_2, and EXC_4, the LDs

are also intimately involved in autocrine and intracrine signal transduction in immune cells,[89,100] especially in eosinophils. For example, LTC_4 activates an intracrine signal-transducing pathway that mediates secretion of eosinophil granules, including cytokine IL-4.[106] In comparison, PGD_2, also synthesized on LDs, is an autocrine signal for eosinophil activation,[99] probably acting as a signal amplifier through the activation of 5-LOX[99] and 15-LOX.[100] The production of EXC_4, which occurs on eosinophil LDs, has implications in host-pathogen interactions.[100] Schistosoma-derived lipids induced EXC_4 synthesis that activated eosinophils to release TGF-β, an immunomodulatory and pro-fibrotic mediator.[100]

In addition to a site of synthesis of inflammatory lipid mediators, LDs are also involved in other functions during the host response to infection. The presence of the pro-inflammatory cytokine TNF-α and macrophage migration inhibitory factor (MIF) was reported in LDs from leukocytes.[36,107,108] However, the biological implication of the association between TNF-α and LDs remains to be understood. In addition, the association of LDs with other cytokines is still unknown. Recent studies have reported the participation of LDs in the IFN response, both in signaling pathways and in the effectiveness of the response.[11,109] Proteins key to the antiviral virus-inhibitory protein, ER-associated, IFN-inducible (viperin),[31] and antiparasitic (immunity-related GTPase M)[33] activities are observed to be loaded on LDs after IFN stimulation.

4 | LD FUNCTIONS IN BACTERIAL INFECTION

Bacterial pathogens display an efficient set of adaptations that support crucial infection events, including bacterial survival, replication, and host immune evasion.[4,110] For successful infection and replication, numerous bacterial pathogens have evolved many approaches to subvert host cellular functions and metabolism.[4,110,111] A change in host lipid homeostasis and LDs biogenesis upon bacterial infection is highly pronounced in both human and experimental infections[6,36,96,112] (Fig. 1).

The subversion of LDs by pathogenic bacteria to complete their own life cycle has been reported for several intracellular bacteria, such as *M. tuberculosis*,[40,113] *M. bovis*,[46] *M. leprae*,[26] *C. trachomatis*,[114] and *C. pneumoniae*.[42] The inhibition of lipid metabolism and/or interference with LDs homeostasis impact bacterial survival[38,115] and/or replication[116] within the host cells. The LD accumulation during bacterial infection is usually associated with a mechanism to obtain an energy resource from the host, as well as a strategy to escape the immune system through increased generation of eicosanoids.[15,22,29,96]

The presence of foam cells, LD-filled macrophages, is a recurrent feature in mycobacterial infections.[38,40,45] The formation of foam cells is a process apparently critical for bacterial persistence in the host and for the pathogenesis of mycobacteria.[39,113,117] For successful infection and persistence of *M. tuberculosis*[115] and *M. lepra*,[39] host lipid molecules are essential. In *M. tuberculosis* infection, the presence of foam cells can be found in both early infection stages[113] and granulomas.[40] In addition to the formation of foam macrophages, during *M. lepra* infection, the same phenotype has also been reported in Schwann cells.[39]

Usurpation of fatty acids released from the host triglycerides stored in LDs is a vital source of energy for mycobacteria, and the storage of fatty acids in the form of triglycerides in bacterial LDs could be linked to the dormancy and reactivation of *M. tuberculosis*.[40,113] Cholesterol is another lipid essential to mycobacterial survival.[118,119] *M. tuberculosis* has the capacity to use cholesterol as an energy source, which is important during latent-phase infection.[119,120] Despite being essential for building blocks for *M. lepra* growth and survival, cholesterol metabolism is not coupled with energy production.[118]

During the mycobacterium infections, the LDs are redistributed or recruited to vicinity of bacterium-containing phagosome.[115,121] Interfering with cytoskeletal function affects not only the impairment of recruitment of host LDs to the phagosome but also the decline of *M. leprae* survival in infected cells.[39] This process enables the capture of lipids by mycobacteria (Fig. 1), suggesting that the LDs are tightly apposed to phagosomes and that there is the physics interaction between LDs and phagosomes.[40,46] With the continuation of infection, mycobacterial-containing phagosomes engulf cellular LDs and this process, which is reminiscent of autophagy, resulted in the transfer of host LDs into bacteria.[40,115]

On the other hand, Knight et al.[58] proposed that LD formation in macrophages might not be an *M. tuberculosis*-induced process but could be a glycolytic programming event dependent on IFN-γ and HIF1-α signaling in murine macrophages. Additionally, in this same work, IFN-γ-induced LDs were an important platform for the production of a broad range of host protective eicosanoids, especially LXB_4 and PGE_2, improving the macrophage immune response.[58] However, the presence of IFN-γ is not sufficient to induce LDs accumulation, requiring a second signal via TLR2,[58] which does not exclude the *M. tuberculosis* as a possible inducer of LDs biogenesis. Interestingly, in this system, *M. tuberculosis* was able to acquire host lipids in the absence of LDs but not in the presence of IFN-γ-induced LDs.[58] Although it seems contradictory to current literature, the induction of LDs as a host response cannot be underestimated, which suggests that LD is an initial protective organelle to the host but some pathogens may have co-opted it over pathogen-host co-evolution.

LD accumulation has also been observed in *C. trachomatis* infection of epithelial mucosal cells.[114,116] Neutral lipids from host LDs appear to be crucial for bacterial propagation of *C. trachomatis*.[116] During *C. trachomatis* infection, LD accumulation inside the chlamydial inclusion[116] was reported. Impairment of lipid metabolism by triacsin C treatment and the consequent inhibition of LD biosynthesis also reduced chlamydial proliferation and the size of the chlamydial inclusion.[116] In a mouse model, incorporation of LDs into the bacterium-containing vacuole has also been observed in infection by *C. muridarum*.[122]

In contrast to other pathogens, *C. trachomatis* induces the translocation of an entire LD from the host cytoplasm into the lumen of the chlamydial inclusion in a process resembling endocytosis.[114] The full

molecular mechanism of capture and translocation of an LD into the chlamydial inclusion remains to be elucidated; however, experimental data suggested that the chlamydial protein Lda3 plays a major role in this organelle sequestration.[114] Lda3 has tropism for both LDs and the inclusion membrane, which suggests that it can mediate the formation of links between them. Moreover, the overexpression of Lda3 leads to the redistribution and replacement of ADRP/Plin2 from the surface of host LDs.[114]

Although LDs are usually seen only as a structure favoring the survival of pathogenic bacteria, several studies have demonstrated the presence of LDs in pro-inflammatory environments.[36,63,123] In sepsis, a life-threatening organ dysfunction caused by a dysregulated host response to infection,[124] changes in lipid metabolism are often observed in the form of LD accumulation in several cell types both in vivo and in vitro, including in leukocytes from septic patients.[36] The LD accumulation in the inflammatory microenvironment was also reported during natural infection of *Vibrio cholerae* serogroups O1 and O139.[123] LD accumulation induced by *V. cholerae* infection was only in mucosal mast cells and not in polymorphonuclear neutrophils.[123] Nicolaou et al.[63] reported that both Gram-negative (*Acinetobacter baumannii*, *Escherichia coli*, *Klebsiella pneumoniae*, *Pseudomonas aeruginosa*, *Pseudomonas diminuta*, and *Proteus vulgaris*) and Gram-positive bacteria (*Staphylococcus aureus*, *Staphylococcus epidermidis*, and *Streptococcus salivarius*) induced the intracellular accumulation of cholesterol ester in macrophages, probably in the LDs, which is a characteristic phenotype of the foam cells. In this work, it was shown that the cholesterol ester accumulation induced by bacteria or PAMP was a highly regulated process mainly involving TLR-2, TLR-4, and TLR-5.[63] Furthermore, these TLRs not only induced lipid storage but also promoted the secretion of the pro-inflammatory cytokine IL-6.[63] Curiously, one of *P. aeruginosa* multiple virulence factors is the type III secretion toxin ExoU, which has cytosolic PLA2 activity[125] with a strong implication in increasing prostaglandin production,[126,127] promote in macrophages infected a significantly decreased LD contents with the release of free AA and PGE_2.[127] This suggests that part of the pathogenic mechanism of toxins ExoU from *P. aeruginosa* could be the mobilization host lipids from LDs.[112] Taken together, these findings suggest that LD accumulation could participate in inflammatory amplification during bacterial infection.

Additionally, van Manen et al.[91] suggested that LDs could contribute to increased production of reactive oxygen species through the activation of NADPH oxidase. For superoxide production, NADPH oxidase seems to require arachidonic acid stimulation.[128] Through a transient LD-phagosome association, LD release of arachidonic acid near the phagosome could be used to locally activate NADPH oxidase and/or to facilitate phagosome maturation.[91] In both cases, the LDs could contribute to the elimination of pathogens.[91] Moreover, Fock et al.[129] reported that mitochondrial reactive oxygen species contribute to the LPS-induced shift of lipid metabolism and LD biogenesis in epithelial cells.[129] Together, these results suggest that there is probably a close crosstalk between LDs and oxidative stress in infection, which has not yet been fully explored, but which may have a profound impact on the pathogen-host interaction.

An important paradigm shift was the discovery of antibacterial function by the LDs reported by Anand et al.[32] In vitro assays show that LDs purified from *Drosophila melanogaster* embryos possess in vitro antibacterial activity against *S. epidermidis* and *E. coli*. In this same work, it was verified that this antimicrobial response was due to the protein content of this organelle, mainly due to the action of histones.[32] Despite being a cationic protein canonically involved in the formation and maintenance of nucleosomes,[130] histones are cytotoxic in vitro and in vivo when located in the extracellular environment, or when in excess in the cytoplasm, furthermore, they have a strong ability to kill bacteria[130–132] (Fig. 1). Compartmentalization of histones on LDs was first detected during oogenesis[18] and involved the participation of the LD protein Jabba, which interacts physically with histones to recruit them to the organelle and keeps them stored through a weak electrostatic interaction.[133] Mutant fly embryos lacking Jabba have drastically reduced histone stores, and when challenged by intraembryonic inoculation with *E. coli*, they lost the capacity to control bacterial infections and showed a low survival rate.[32] The role of histones in antibacterial activity seems not to be restricted to the embryonic period. Jabba mutant adult flies, when inoculated with the intracellular bacteria *Listeria monocytogenes*, presented higher and faster mortality than did the wild-type flies.[32]

The presence of histones in LDs seems not to be limited to insects. LDs isolated from the livers of mice challenged with LPS showed increased loading of histone H1.[32] The identification of histones in LD proteomic analyses of rat sebocytes[134] and human macrophages[135] has been reported. Localized histones as protective proteins on LDs against intracellular bacteria may indicate the existence of a new type of conserved innate immunity, but the absence of proteins homologous to *Drosophila* Jabba in mammals[133] leaves the mechanism and nature of histone-LD interactions still unknown in mammals.

The presence of LD in host immune cells during bacterial infection is a recurrent phenomenon in the literature. Although great advances were made in recent years to characterize the mechanisms of biogenesis and functions during infection, several issues remain open. Collectively, LD formed during bacterial infection involves multimediated and specific mechanisms that vary according to both the pathogen and the host cells involved. The functional outcome of the increased LD accumulation may favor the pathogen as the described subversion of this organelle by intracellular pathogenic bacteria as part of the evasion mechanism of the system or as an energy source; or may act pro-host immune response. Future studies are in need to better characterize the specificities of this complex interactions according to the different infections.

5 | LDs AND VIRUS INFECTION

Viruses are obligate intracellular pathogens that subvert host metabolism and cellular structures for viral replication and assembly.[49,136] In the cytoplasm of the cell, all positive-stranded RNA (+RNA) viruses of eukaryotes promote an extensive modification of the host membrane web, transforming them into a

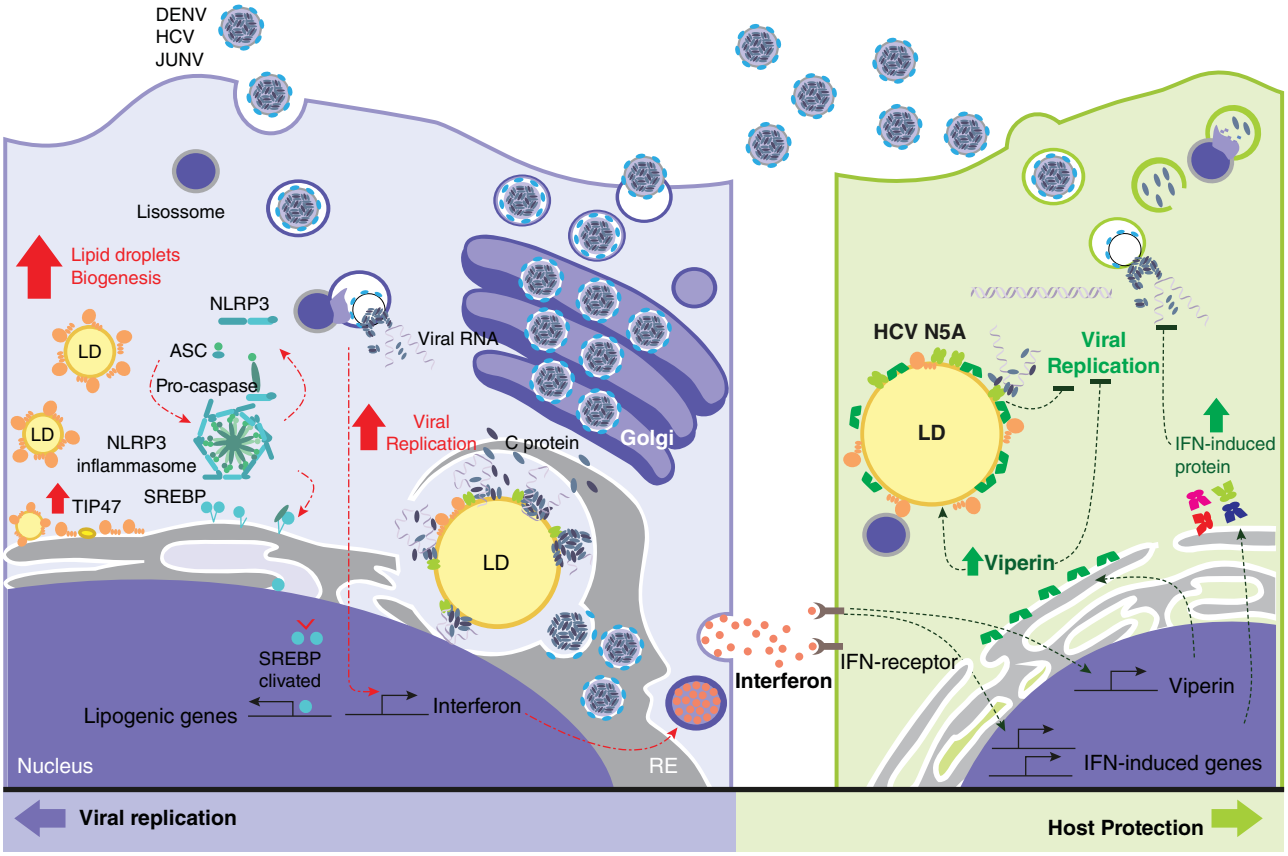

FIGURE 2 **The roles of lipid droplets (LDs) at viral infections.** Lipid metabolism and LDs are important components in the positive strand (+) RNA viral cycle, such as flavivirus members. During viral infection, there is the induction of LD in a process involving the activation of NACHT, LRR, and PYD domains-containing protein 3 (NLRP3) inflammasome, which cleaved the sterol regulatory element-binding proteins (SREBPs), activating the lipogenesis genes and the structural LDs proteins, such as PLIN3/TIP 47. After LD accumulation, it can be a platform for viral replication and/or assembly of several viruses, such as hepatitis C virus (HCV) and dengue virus (DENV). On LDs, the presence of HCV core (C) protein and NS5A complexes has been reported, together with the LD-associated proteins PLIN3/TIP47, which facilitate the interaction of LDs with specialized areas of the ER-containing NS5A. After assembly, the pro-virus goes to the lumen of the endoplasmic reticulum (ER) and the complex Golgi until they are released to the extracellular environment. In contrast, the presence of LDs could be required for an effective early innate response to viral infection, which is mainly related to IFN response. IFN signaling activates hundreds of genes (IFN induced), vital in the host response mechanism to viral infection, including viperin. Viperin is a potent antiviral protein that accumulates in ER and LDs, inhibiting the virus replication

specialized microenvironment that is thought to support viral RNA synthesis.[136–138] In this process, strong evidence has demonstrated that lipid metabolism and LDs are important components in the +RNA viral life cycle, either as one of the sites for viral replication and/or assembly or as a source of energy through autophagy[96,139] (Fig. 2).

Several (+)RNA viruses use host LDs at different steps of their life cycle, such as reovirus,[140] rotavirus,[141] norovirus,[142] Junín virus,[143] and poliovirus,[10] as well as various members of the Flaviviridae.[24,25,144] These viruses manipulate lipid metabolism for efficient viral morphogenesis, and inhibition of lipid metabolism and/or interference with LD homeostasis decreases viral replication and/or assembly.[25,52,143]

Although the replication of flaviviruses is associated with the endoplasmic reticulum, LDs are also an important component of viral morphogenesis.[24,25,52,145] In this context, several viral proteins have been reported on LDs, including nonstructural proteins (NS) linked to replication, such NS4B,[146] NS5A, and NS3 protein[144,145] of HCV, as well as the capsid core proteins of HCV,[147,148] GB virus-B,[149] and dengue virus (DENV).[24,25,150] In addition to the presence of viral proteins on LDs, the presence of HCV viral RNA was reported in this organelle.[52] Furthermore, proteomic research reported the presence of ribosomes and chaperones on LDs,[151] which suggest that the LDs may hypothetically be capable of supporting viral replication and assembly independent of the ER, but this has not been proven experimentally yet.

The anchoring of the viral proteins in LDs involves the presence of an amphipathic α-helix.[25,52,152] For the DENV core protein, 2 leucine residues (L50 or L54) in the α2 helix are essential for LD association.[25] In comparison, for HCV and GB virus-B core proteins, the motif essential for LD anchoring contained proline residues in the α-helix. In addition to the intrinsic structure of the viral proteins, it has also been proposed that several host proteins could mediate the anchoring of viral proteins onto LDs. In this context, LD-associated protein PLIN3/TIP47 is an important mediator of anchorage of HCV NS5A and core protein[68,145] and the DENV core protein[24] on LDs. HCV core and

NS5A proteins interact with DGAT1 and depend on DGAT1 activity for access to LDs.[153,154] The physical association of cell factor Rab18 with HCV NS5A promotes the interaction between LDs and sites of viral replication.[155] The use of a noncanonical function of the host trafficking system GBF1-Arf1/Arf4-COPI pathway for capsid accumulation on LD was also reported for DENV.[156]

The localization of the viral core protein and NS proteins onto LDs seems to be required for successful production of infectious viral progeny. The presence of HCV viral protein to LDs is a higher coordinated process, each step being essential for the next step in order to form the replication complexes around the NS5B RNA-dependent RNA polymerase that copies the viral genome.[52,157] The first HCV protein translocated from the ER to the LD surface is the core protein, which in turn assists in recruitment of the NS5A and this in turn recruit other viral NS proteins to the LD surface.[52,157] Mutations of HCV core and NS5A proteins, which failed to associate with LDs, reduced the production of infectious viruses, probably because of the impaired replication complexes.[52] The same phenomenon was observed for DENV, where mutations in the core protein that prevented anchoring onto LDs resulted in impaired viral replication and assembly.[25] In addition, HCV core protein induced the accumulation of LDs,[52] and steatosis is a phenotype frequently observed in HCV-infected patients.[49,50,139] These data support the role of LDs as an important platform for viral morphogenesis. However, the mechanism by which LDs gain or lose viral proteins is still an open question, as well as the possibility of some viral proteins arriving from LDs during the formation of this organelle in ER.

In addition to flaviviruses, rotaviruses also co-opt LDs for their replication. In rotavirus infection, LDs are associated with components that physically resemble viroplasms, the structure described as "factories" of virus production.[141] The LD structural proteins (PLIN1 and PLIN2/ADRP) colocalize with the rotavirus nonstructural proteins NSP2 and NSP5 and with the structural proteins VP1, VP2, and VP6.[141] The NS3 protein of human norovirus (huNoV) was tightly associated with LDs and induced convoluted membranes, structures responsible for viral replication.[142] Moreover, the μ1 outer capsid protein of reoviruses was also reported on LDs.[140]

Notwithstanding being an important viral replication site, LDs can also be an important energy and building block source for viral replication and assembly. DENV induced proviral, autophagy-dependent processing of LDs (lipophagy) in infected cells.[158,159] The induction of autophagy is another mechanism by which viruses can alter cellular lipid metabolism, by increasing cellular β-oxidation, which generates ATP and can be used in viral replication and assembly.[160–162] On the other hand, during poliovirus replication, the LDs are used as building blocks for the formation of structural development of poliovirus replication organelles. The LD's neutral lipids hydrolysis and re-route from triglyceride to phosphatidylcholine synthesis, and these are used in the formation of a viral replicative organelle-like structure to replication.[10] Despite of this remodeling membranous not be essential for viral RNA replication, this process seems be important for protection of virus replication from the host antiviral response, mainly during multicycle replication of poliovirus.[10]

Despite the participation of LDs in (+)RNA virus replication and assembly, the importance of this organelle for the other viral classes is still unknown. The only exception is polyomavirus BK, a DNA virus whose agnoprotein was reported on LDs.[163] The biological relevance of these associations remains to be determined, but these findings suggest the possibility that other virus classes may use LDs as a platform for viral particle assembly.

LDs are not always unfavorable to the host during viral infections. The presence of LDs could be required for an effective early innate response to viral infection, mainly related to type I and III IFN responses.[164] In response to viral infection by HCV, viperin was the first protective protein reported to be loaded onto LDs.[31] The antiviral protein viperin is one of the hundreds of genes regulated by the cell-signaling proteins and master regulators IFNs in response to viral infection.[165–167] The IFN-induced genes are vital in the host response mechanism to viral infection.[168,169]

Viperin has a broad and potent antiviral activity,[168,169] however the exact mechanism of viperin antiviral action remains unknown, but several indications suggest that viperin can inhibit different viruses by different pathways.[109,166] Structurally, viperin's amino-terminal amphipathic α-helix seems to be important for full antiviral activity because it is involved in protein subcellular localization[31] and physical interaction with proteins essential to viral replication.[31,143,170] Tagged proteins inhibited by viperin have been reported, including HCV NS5A,[31] DENV NS3,[170] Junín mammarenavirus N protein,[143] and probably chikungunya nsP2,[171] which are important proteins in viral RNA transcription and replication.[172–174] Furthermore, viperin seems to induce lipid raft disturbance and, as a consequence, impairment of membrane localization of viral proteins and inhibition of virus release.[175,176]

The mechanism for subcellular targeting of viperin via its α-helix to the LDs is similar to that described for the HCV NS5A viral protein, indicating that part of viperin's antiviral activity may be mediated by the subcellular localization of the protein,[31] probably acting as part of localized antiviral tactics to limit viral propagation. The viperin antiviral pathway at the LD level was also proposed for JUNG virus[143] and probably for other flaviviruses.[31] However, viperin anchorage onto LDs is dispensable for DENV inhibition.[170]

Notwithstanding, the interaction of LDs and viperin can be associated with another side of viperin's antiviral activity in addition to direct viral suppression. Saitoh et al.[177] showed strong evidence that viperin acts as a regulator for pattern recognition receptor-mediated innate immune responses, facilitating TLR7- and TLR9-mediated production of type I IFN in plasmacytoid dendritic cells. In this system, the LDs act as scaffold for TLR7 and TLR9 signaling pathways, suggesting that viperin recruits IRAK1 and TNF receptor-associated factor 6 (TRAF6) in a stimulation-dependent manner.[177] The compartmentalization IRAK1 and TRAF6 on LD facilitates the ubiquitination of IRAK1 by TRAF6, which results in the IFN regulatory factor 7 mediated induction of type I IFN.[177] In this context, the localization of viperin on the LD appears to play a key role in the regulation of host defense responses to viruses.[177]

The antiviral activity of viperin against infection by herpesvirus, flavivirus, alphavirus, orthomyxovirus, paramyxovirus, rhabdovirus,

retrovirus, and picornavirus has been confirmed.[109,168,169,171,178] For most of these viruses, the mechanism by which viperin restricts replication is not fully clear. In at least some cases, enrichment and compartmentalization of viperin on the LD surface may participate in the inhibition of viral replication.[13,166]

6 | LDs AND PROTOZOAN INTERACTIONS

Parasite protozoans have complex molecular machinery to interact with their host cell in order to evade and manipulate the immune response.[179–181] Upon entering the host target cell, the parasites are internalized within the parasitophorous vacuole (PV), a plasma membrane–derived vacuole where the parasite survives and multiplies[179,182] (Fig. 3). Overall, LD biogenesis during protozoan infection occurs in parallel with PV formation and progression in the host cell cytoplasm.[15,180] The accumulation of LDs in infected cells has been reported for several parasites, such as *Trypanosoma cruzi*,[135,183] *Leishmania amazonensis*,[184] *Leishmania major*,[185] *Leishmania infantum*,[186] *Plasmodium chabaudi*,[187] *Neospora caninum*,[61] and *Toxoplasma gondii*.[29] During parasite infection, LDs are usually associated with sustaining successful parasite replication within the PV[102,182] (Fig. 3).

The mechanisms involved in LD accumulation during parasite infection are not yet fully understood. Like other pathogens, some studies reported the participation of TLR in parasite-induced LDs, as the case of TLR-2 in the *T. cruzi* infection, which is amplified by the uptake of apoptotic cells in a mechanism dependent on integrins and TGF-β synthesis.[47] Moreover, the activation of TLR-1 and TLR-2 by *Leishmania infantum* lipophosphoglycan induced LDs accumulation in association with PPAR-γ expression.[188] On the other hand, LDs biogenesis was related to dysregulate host metabolism by the subversion of host mTOR and JNK signaling in the *T. gondii* and *N. caninum* infection.[61] Furthermore, *T. gondii* promotes the expression of some triglyceride synthesis genes and lipid transporters, and inhibits the expression of lipolytic genes, especially ATGL, favoring the LD accumulation in the host cell.[61] Several parasites lost the ability to synthesize all lipids essential for their survival, requiring the supply of lipids from the host cell, mainly cholesterol.[182] For several protozoan parasites, they rely on host LDs and their lipolytic enzymatic activities to survive and proliferate.[47,61] LDs are frequently observed around and within the PV.[180,189] The *T. gondii* PV is able to access host lipids by intercepting and engulfing LDs.[190] However, the mechanism of how protozoans acquire the host's lipids is not yet fully understood.

Parasite cells have their own LDs,[61,101,102] as well as those of the host cells, and parasite LDs are dynamic structures able to respond to host interaction and inflammatory events.[102] Moreover, parasite LDs were also reported as being a platform of compartmentalization of the eicosanoid pathway.[101,102] In Leishmania, the presence of PLA_2 and prostaglandin $F_{2\alpha}$ synthase on parasite LDs has been identified.[101] In addition to the presence of PGE synthase on LDs, the accumulation of arachidonic acid and PGE_2 formation on LDs was also reported in *T. cruzi*.[102] The production of inflammatory mediators by parasite LDs suggests that this organelle participates in an elaborate form of evasion of the immune system,[101,102] and it is even suggested that parasite LDs could be classified as a mechanism of pathogenicity.[101]

A recent result connects the antiparasitic response in the presence of LDs. Immunity-related GTPase M proteins are small IFN-inducible GTPases[33,191] and part of a complex cellular system for recognition of its own structures. Irgm3 accumulates in "self" organelles, including LDs, but not in the PV of the bacterial pathogen C. *trachomatis* or the protozoan pathogen *T. gondii*.[33] Although Irgm3 is required for resistance to *T. gondii*[192] and *L. donovani*[193] infections in mice, the roles of the interaction between Irgm3 and LDs in the elimination of the pathogen remain uncertain. It has been suggested that this interaction may be related to blockade of recruitment of LDs by the parasite or even participation of this system in antigen (Ag) presentation.[11,182] Furthermore, it remains uncertain whether LD recruitment favors parasite survival or a host cell defense mechanism (Fig. 3).

7 | LDs AND ANTIGEN PRESENTATION

The first observation of LDs in dendritic cells was reported by Steinman and Cohn,[194] which describes the morphology of dendritic cells from peripheral lymphoid organs. More recently, an increase in the number of LDs in dendritic cells has been described during infection by *Leishmania amazonensis* or *Nocardia brasiliensis* and cancer.[185,195–197] LDs have been described to interact with several organelles and structures within cells, including phagosomes,[91] autophagosomes, and the proteasome.[12] These results suggested that these lipid-rich organelles could be involved in cellular processes related to Ag presentation and immunity.

Dendritic cells are a highly specialized subset of APCs that have an important role in the initiation and maintenance of the adaptive immune response and are capable of stimulating immunologically naïve T cells. Dendritic cell activation involves capturing and processing Ags for the stable presentation of Ag-derived peptides in the context of MHC class I and II proteins, leading to the induction of the expression of chemokine receptors, cytokines, and co-stimulatory molecules.

Under conditions of stimulation of dendritic cell, TLR-ligands IFN-γ, and saponin-based adjuvants are also able to increase lipid content.[191,198,199] Bougnères et al.[191] have shown that LDs are involved in phagosome maturation and cross-presentation via MHC-I in IFN-γ-stimulated dendritic cells. In that work, it was observed that LDs co-localized with the Irgm3 GTPase, which interacts with PLIN2/ADRP and is essential for LD biogenesis. They observed that dendritic cells from Irgm3-knockout mice are impaired for accumulation of LDs and are defective in cross-presentation efficiently, similar to what was observed in PLIN2/ADRP-deficient dendritic cells. This event seems to be direct effect of absence of LDs because neither PLIN2/ADRP-deficient nor Irgm-3-deficient dendritic cells had no dysfunctionality on cell-surface phenotype, on phagocytic ability, on

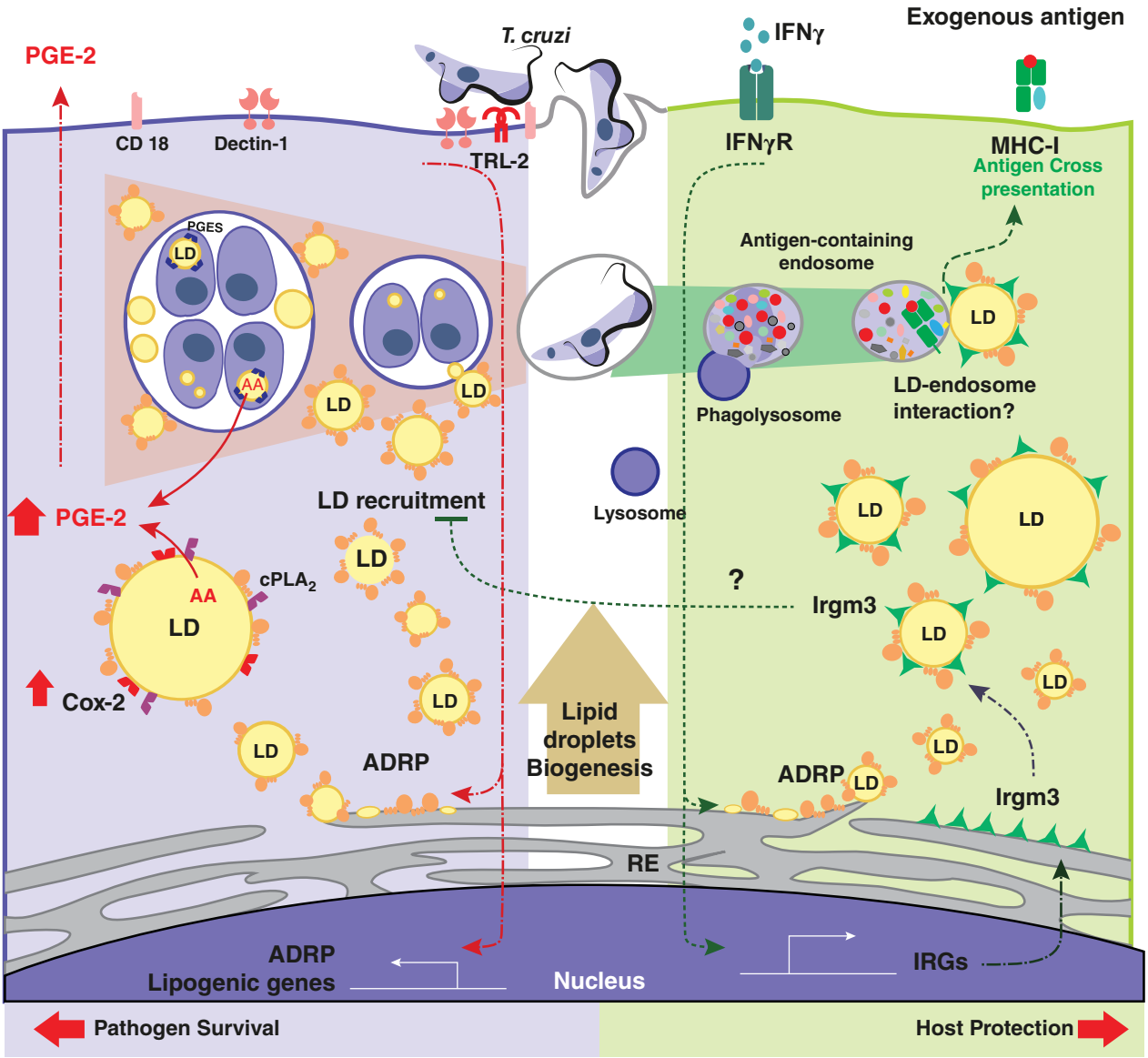

FIGURE 3 **The roles of lipid droplets (LDs) at parasite infections**. In protozoan parasite infections, innate receptor, mainly TLR and co-stimulatory receptors (CD18 and Dectin-1), induced the expression of several genes involved in liponeogenesis, including LDs structural proteins, such as adipose differentiation-related protein (ADRP). LDs are formed in the ER and accumulate in the cytoplasm. The interaction of LDs with phagosomes containing parasites leads to the discharge of LD contents, such as cholesterol and triacylglycerol, which serve as a source of lipids for parasite growth. LDs are also important players in innate immunity. Host-pathogen interaction leads to the biosynthesis and secretion of inflammatory mediators such as prostaglandin E_2 (PGE_2) through arachidonic acid (AA)-derived cyclooxygenase (COX-2) pathways. PGE_2 might favor pathogen proliferation. In addition, parasite LDs are also able to produce PGE_2 through a parasite PGE synthase (PGES). On the other hand, the activating INF-γ pathway induced the expression of Irgm3 (an immunity-related GTPase [IRG]). The IRGM3 accumulated on LD surface and might act as antiparasitic protein. It has been suggested that this interaction may be related to the blockade of recruitment of LDs by the parasite or even the participation of Ag cross-presentation via major histocompatibility complex I (MHC-I)

the ability to present peptide to CD8+ T cells, or on dendritic cell maturation[191] (Fig. 3). Moreover, dendritic cells with an increased lipid content were more competent for Ag cross-presentation.[191] In line with that, stimulation with immune stimulatory complexes containing saponin-based adjuvants, cholesterol, and phospholipids induces the biogenesis of LDs in dendritic cells in parallel to cross-presentation of Ags. Furthermore, genetic and pharmacological blockade of LD biogenesis inhibit Ag cross-presentation induction by saponin-based adjuvants, in vitro and in vivo in a tumor ablation model.[199]

Other studies have correlated lipid content with Ag presentation by dendritic cells. Ibrahim et al.[202] demonstrated that two different dendritic cell populations can be distinguished by lipid content in mouse and human livers, one with high and another with low lipid content. Moreover, the proportion of these 2 populations of dendritic cells in the liver was dependent on states associated with the lipid content of hepatic microenvironment.[200] They showed that dendritic cells with high lipid content presented an activated and immunogenic phenotype and were more effective in activating CD4 and CD8

T cells both in vitro and in vivo when compared to dendritic cells with low lipid content of same tissue.[200] Adoptive transfer of high-lipid dendritic cells delayed tumor progression by activation of cytotoxic T cells. Moreover, the pharmacological inhibition of fatty acid synthase inhibited the cross-presentation and activation of CTL CD8 T cells in vivo.[200] This effect was probably because high-lipid dendritic cells expressed elevated levels of TLRs and co-stimulatory proteins, presented a higher capacity to capture Ags, and produced higher levels of inflammatory cytokines (IL-1β, IL-6, IL-8, and IL-17α) and chemokines (IP-10, KC, MIP-1α, MIP-1β, MCP-1, and RANTES) when compared to low-lipid dendritic cells.[200] These cells also activated NK and NK T cells, suggesting that LDs could also be involved in nonclassical MHC Ag presentation.[200] Likewise, the pharmacological inhibition of LDs formation in LPS-stimulated dendritic cells inhibited cell activation, expression of costimulatory proteins, and pro-inflammatory cytokine production.[198]

In addition to its positive role in the induction of cross-presentation, other data indicate that this process is not only dependent on the presence of LDs but also on other factors that have the capacity of cross-presentation of dendritic cells. Some authors demonstrate in cancer models an opposite correlation between LD induction and Ag presentation. It was observed in murine lymphoma that lipid-enriched dendritic cells are not able to induce CD4 T cell proliferation by the reduction in the expression of co-stimulatory molecules and in cytokine production (IL-12, IL-1, and IFN-γ).[197] Accordingly, it was also demonstrated that lipid-enriched dendritic cells from tumor-bearing mice have a reduced capacity to process and present Ags to T cells, displaying a tolerogenic phenotype. Moreover, the pharmacological inhibition of lipid metabolism reduced dendritic cells containing lipids in tumor-bearing mice and restored their capacity to stimulate T cells.[196]

Dendritic cells incubated with tumor explant supernatants accumulate oxidized lipids, which correlate with the down-regulation of cross-presentation. Lipid peroxidation significantly reduced the ability of dendritic cells to stimulate CD8 T cells due to a reduction in MHC-I loaded with exogenous peptides. It is important to note that lipid peroxidation did not alter the expression of MHC-I molecules or endogenous Ag presentation.[201] This work suggests that not only the presence of LDs in dendritic cells but also their composition may be involved in LD function in the modulation of immune responses. In support of this finding, Veglia et al.[202] reported that oxidized lipids stored in LDs can inhibit cross-presentation in dendritic cells in cancer, indicating that not only the type of lipids but also the oxidative state of these in LDs has implications in antigenic presentation.

Ibrahim et al.[200] demonstrated that high lipid-content dendritic cells presented elevations in phospholipids and triglyceride levels; conversely, cholesterol and cholesteryl esters were not elevated. Accordingly, it was observed that increased levels of saturated fatty acids, such as palmitic acid, reduce MHC-I surface expression and the rate of APC-T lymphocyte conjugation.[203] Thus, LD accumulation of TAG enriched in saturated and or oxidized fatty acids may also play an indirect role in regulating MHC-I expression.[196]

Published data suggest that lipid accumulation in dendritic cells is due to an increase in the capture of lipids from the microenvironment, mainly mediated by the scavenger receptor Msr-1. It has been demonstrated that IL-17 stimulation increases the expression of Msr-1 and other genes related to lipid metabolism, increasing the number of LDs. However, IL-17 stimulation did change the expression of MHC proteins.[204] Similarly, the accumulation of TAG in dendritic cells stimulated with tumor explant supernatants was dependent on its uptake mediated by Msr-1, which was increased in dendritic cells from tumor-bearing mice. In this work, the authors showed that dendritic cells generated from Msr-1$^{-/-}$ mice failed to accumulate lipids after transfer to tumor-bearing recipients and were more effective in T-cell activation.[196] In addition, Msr-1-deficient dendritic cells showed a more mature phenotype.[205] In the absence of Msr-1, tumor-derived factors failed to inhibit Ag cross-presentation by dendritic cells, supporting the possible role of lipid uptake in the negative modulation of dendritic cell function during cancer.[201]

Several pathogens are able to down-regulate Ag presentation to escape the host immune response. It would be important to further elucidate whether these differences in lipid composition and function are directly related to disease mechanisms and could be modulated to favor the host immune response. In addition, defects in the ability to present Ags or modifications in the function of dendritic cells can lead to susceptibility to infections and cancer, and therefore especially in this context, the role of LDs needs to be further investigated, as well as the participation of the microenvironment in this process.

8 | FINAL REMARKS AND PERSPECTIVES

Innumerous intracellular pathogens co-opt host LDs to complete their own lifecycle, using LDs as an energy resource, a platform of assembly or part of their mechanisms to escape the immune response. In addition, LDs participate in several central events in the innate and adaptive immune response, both as a platform for the production of inflammatory lipid mediators and in the response to IFN. In recent years, the presence of LDs during the infectious process has ceased to be seen only as a lipid source organelle for pathogen proliferation and has started to be reported as an important organelle involved in different aspects of the host-pathogen interaction. However, critical questions remain about the formation and the multiple functions that LDs play in infectious diseases. Further investigations should help us to decipher the full range of LD functions in host protective immune response as well as to better understand pathogen-specific mechanisms evolved to take advantage of LDs for their survival and the persistence of infections. In addition, LDs are emerging as attractive target candidates for therapeutic intervention in infectious diseases that progress with increased LD accumulation. Future studies will need to include the development of selective LD inhibitors. Moreover, the safety characterization of LD inhibition is required, as lipid accumulation within LDs may act as a protective mechanism in lipid homeostasis against cellular lipotoxicity.

Take home message

Lipid droplet biogenesis and function

- Increased LDs numbers in leukocytes and other cells are observed in bacterial, viral, fungal, and parasitic infections.
- Pathogen-triggered LD biogenesis is a multimediated process that involves increased lipid uptake, lipolysis inhibition, and new lipid synthesis.
- Innate immune receptors and nuclear receptors play important roles in infection-driven LD biogenesis.
- LDs compartmentalize the eicosanoid enzymatic machinery and are sites of eicosanoid production.
- LDs are a central immunomodulator organelle, both for the pro-inflammatory and anti-inflammatory response.

Lipid droplets in pathogen survival

- Virus may use LDs as viral replication and assembly platforms.
- Intracellular bacteria and protozoa use LDs as a nutritional source for survival and replication.
- Intracellular bacteria and protozoa can induce production of PGE_2 on LDs as part of their mechanism of immune response evasion.

Lipid droplets in the host protection response

- Proteins key in antiviral (viperin) and antiparasitic (IRGM) activities are loaded onto LDs after IFN stimulation.
- LDs can store histones, exhibiting an antibacterial activity.
- LDs interact with phagosomes and appear to be involved in Ag cross-presentation.

ACKNOWLEDGMENTS

We would like to recognize present and past members of the Laboratory of Immunopharmacology for their valuable contributions. We apologize to investigators whose relevant work has not been cited because of space constraints.

The work of the authors is supported by Fundação de Amparo à Pesquisa do Rio de Janeiro (FAPERJ, Brasil); Conselho Nacional de Desenvolvimento Científico e Tecnológico (CNPq, Brasil); Coordenação de Aperfeiçoamento de Pessoal de Nível Superior (Capes).

DISCLOSURE

The authors have no other affiliations or financial involvement with any organization or entity with a financial interest in or financial conflict with the subject discussed in the manuscript.

ORCID

Patrícia T. Bozza https://orcid.org/0000-0001-8349-9529

REFERENCES

1. Subramaniam S, Fahy E, Gupta S, et al. Bioinformatics and systems biology of the lipidome. *Chem Rev*. 2011;111:6452-6490.
2. Fahy E, Subramaniam S, Murphy RC, et al. Update of the LIPID MAPS comprehensive classification system for lipids. *J Lipid Res*. 2009;50:S9-S14.
3. van Meer G, Voelker DR, Feigenson GW. Membrane lipids: where they are and how they behave. *Nat Rev Mol Cell Biol*. 2008;9:112-124.
4. Teng O, Ke C, Ang E, et al. Macrophage–bacteria interactions—a lipid-centric relationship. *Front Immunol*. 2017;8:1836.
5. Pol A, Gross SP, Parton RG. Biogenesis of the multifunctional lipid droplet: lipids, proteins, and sites. *J Cell Biol*. 2014;204:635-646.
6. Bozza PT, Magalhães KG, Weller PF. Leukocyte lipid bodies—biogenesis and functions in inflammation. *Biochim Biophys Acta Mol Cell Biol Lipids*. 2009;1791:540-551.
7. Olzmann JA, Carvalho P. Dynamics and functions of lipid droplets. *Nat Rev Mol Cell Biol*. 2019;20:137-155.
8. Fujimoto T, Parton RG. Not just fat: the structure and function of the lipid droplet. *Cold Spring Harb Perspect Biol*. 2011;3:1-17.
9. Wilfling F, Wang H, Haas JT, et al. Triacylglycerol synthesis enzymes mediate lipid droplet growth by relocalizing from the ER to lipid droplets. *Dev Cell* 2013;24:384-399.
10. Viktorova EG, Nchoutmboube JA, Ford-Siltz LA, et al. Phospholipid synthesis fueled by lipid droplets drives the structural development of poliovirus replication organelles. *PLOS Pathog*. 2018;14:e1007280.
11. Saka HA, Valdivia R. Emerging roles for lipid droplets in immunity and host-pathogen interactions. *Annu Rev Cell Dev Biol*. 2012;28:411-437.
12. Fujimoto T, Ohsaki Y. Proteasomal and autophagic pathways converge on lipid droplets. *Autophagy*. 2006;2:299-301.
13. Welte MA. Expanding roles for lipid droplets. *Curr Biol*. 2015;25:R470-R481.
14. Farese RV, Walther TC. Lipid droplets finally get a little R-E-S-P-E-C-T. *Cell*. 2009;139:855-860.
15. Melo RCN, D'Avila H, Wan H-C, et al. Lipid bodies in inflammatory cells. *J Histochem Cytochem*. 2011;59:540-556.
16. Walther TC, Farese RV. Lipid droplets and cellular lipid metabolism. *Annu Rev Biochem*. 2012;81:687-714.
17. Larsson S, Resjö S, Gomez MF, et al. Characterization of the lipid droplet proteome of a clonal insulin-producing β-cell line (INS-1 832/13). *J Proteome Res*. 2012;11:1264-1273.
18. Cermelli S, Guo Y, Gross SP, et al. The lipid-droplet proteome reveals that droplets are a protein-storage depot. *Curr Biol*. 2006;16:1783-1795.
19. Zhang H, Wang Y, Li J, et al. Proteome of skeletal muscle lipid droplet reveals association with mitochondria and apolipoprotein A-I. *J Proteome Res*. 2011;10:4757-4768.
20. Ducharme NA, Bickel PE. Minireview: lipid droplets in lipogenesis and lipolysis. *Endocrinology*. 2008;149:942-949.
21. Bozza PT, Yu W, Cassara J, et al. Pathways for eosinophil lipid body induction: differing signal transduction in cells from normal and hypereosinophilic subjects. *J Leukoc Biol*. 1998;64:563-569.
22. Bozza PT, Bakker-Abreu I, Navarro-Xavier RA, et al. Lipid body function in eicosanoid synthesis: an update. *Prostaglandins Leukot Essent Fat Acids*. 2011;85:205-213.
23. Bozza PT, Viola JPB. Lipid droplets in inflammation and cancer. *Prostaglandins, Leukot Essent Fat Acids*. 2010;82:243-250.
24. Carvalho FA, Carneiro FA, Martins IC, et al. Dengue virus capsid protein binding to hepatic lipid droplets (LD) is potassium ion dependent and is mediated by LD surface proteins. *J Virol*. 2012;86:2096-2108.

25. Samsa MM, Mondotte JA, Iglesias NG, et al. Dengue virus capsid protein usurps lipid droplets for viral particle formation. *PLoS Pathog*. 2009;5:e1000632.
26. Mattos KA, Oliveira VGC, D'Avila H, et al. TLR6-driven lipid droplets in *Mycobacterium leprae*-infected Schwann cells: immunoinflammatory platforms associated with bacterial persistence. *J Immunol*. 2011;187:2548-2558.
27. D'Avila H, Roque NR, Cardoso RM, et al. Neutrophils recruited to the site of *Mycobacterium bovis* BCG infection undergo apoptosis and modulate lipid body biogenesis and prostaglandin E2 production by macrophages. *Cell Microbiol*. 2008;10:2589-2604.
28. Sorgi CA, Secatto A, Fontanari C, et al. Histoplasma capsulatum cell wall -glucan induces lipid body formation through CD18, TLR2, and Dectin-1 receptors: correlation with leukotriene B4 generation and role in HIV-1 infection. *J Immunol*. 2009;182:4025-4035.
29. Gomes AF, Magalhães KG, Rodrigues RM, et al. *Toxoplasma gondii*-skeletal muscle cells interaction increases lipid droplet biogenesis and positively modulates the production of IL-12, IFN-g and PGE2. *Parasit Vectors*. 2014;7:47.
30. Mota LAM, Roberto-Neto J, Monteiro VG, et al. Culture of mouse peritoneal macrophages with mouse serum induces lipid bodies that associate with the parasitophorous vacuole and decrease their microbicidal capacity against *Toxoplasma gondii*. *Mem Inst Oswaldo Cruz*. 2014;109:767-774.
31. Hinson ER, Cresswell P. The antiviral protein, viperin, localizes to lipid droplets via its N-terminal amphipathic alpha-helix. *Proc Natl Acad Sci USA*. 2009;106:20452-20457.
32. Anand P, Cermelli S, Li Z, et al. A novel role for lipid droplets in the organismal antibacterial response. *Elife*. 2012;1:1-18.
33. Haldar AK, Saka HA, Piro AS, et al. IRG and GBP host resistance factors target aberrant, "non-self" vacuoles characterized by the missing of "self" IRGM proteins. *PLoS Pathog*. 2013;9:e1003414.
34. Walther TC, Chung J, Farese RV. Lipid droplet biogenesis. *Annu Rev Cell Dev Biol*. 2017;33:491-510.
35. Melo RCN, Paganoti GF, Dvorak AM, et al. The internal architecture of leukocyte lipid body organelles captured by three-dimensional electron microscopy tomography. *PLoS One*. 2013;8:e59578.
36. Pacheco P, Bozza FA, Gomes RN, et al. Lipopolysaccharide-induced leukocyte lipid body formation in vivo: innate immunity elicited intracellular loci involved in eicosanoid metabolism. *J Immunol*. 2002;169:6498-6506.
37. Pacheco P, Vieira-de-Abreu A, Gomes RN, et al. Monocyte chemoattractant protein-1/CC chemokine ligand 2 controls microtubule-driven biogenesis and leukotriene B4-synthesizing function of macrophage lipid bodies elicited by innate immune response. *J Immunol*. 2007;179:8500-8508.
38. Mattos KA, D'Avila H, Rodrigues LS, et al. Lipid droplet formation in leprosy: Toll-like receptor-regulated organelles involved in eicosanoid formation and *Mycobacterium leprae* pathogenesis. *J Leukoc Biol*. 2010;87:371-384.
39. Mattos KA, Lara FA, Oliveira VGC, et al. Modulation of lipid droplets by *Mycobacterium leprae* in Schwann cells: a putative mechanism for host lipid acquisition and bacterial survival in phagosomes. *Cell Microbiol*. 2011;13:259-273.
40. Peyron P, Vaubourgeix J, Poquet Y, et al. Foamy macrophages from tuberculous patients' granulomas constitute a nutrient-rich reservoir for *M. tuberculosis* persistence. *PLOS Pathog*. 2008;4:1-14.
41. Joshi R, Khandelwal B, Joshi D, et al. *Chlamydophila pneumoniae* infection and cardiovascular disease. *N Am J Med Sci*. 2013;5:169-81.
42. Cao F, Castrillo A, Tontonoz P, et al. *Chlamydia pneumoniae*-induced macrophage foam cell formation is mediated by Toll-like receptor 2. *Infect Immun*. 2007;75:753-759.
43. Chen S, Sorrentino R, Shimada K, et al. Chlamydia pneumoniae-induced foam cell formation requires MyD88-dependent and -independent signaling and is reciprocally modulated by liver X receptor activation. *J Immunol*. 2008;181:7186-7193.
44. Heldwein KA, Fenton MJ. The role of Toll-like receptors in immunity against mycobacterial infection. *Microbes Infect*. 2002;4:937-944.
45. Almeida PE, Silva AR, Maya-Monteiro CM, et al. *Mycobacterium bovis* bacillus Calmette-Guérin infection induces TLR2-dependent peroxisome proliferator-activated receptor γ expression and activation: functions in inflammation, lipid metabolism, and pathogenesis. *J Immunol*. 2009;183:1337-1345.
46. D'Avila H, Melo RCN, Parreira GG, et al. *Mycobacterium bovis* bacillus Calmette-Guerin induces TLR2-mediated formation of lipid bodies: intracellular domains for eicosanoid synthesis in vivo. *J Immunol*. 2006;176:3087-3097.
47. D'Avila H, Freire-de-Lima CG, Roque NR, et al. Host cell lipid bodies triggered by *Trypanosoma cruzi* infection and enhanced by the uptake of apoptotic cells are associated with prostaglandin E2 generation and increased parasite growth. *J Infect Dis*. 2011;204:951-961.
48. McRae S, Iqbal J, Sarkar-Dutta M, et al. The hepatitis C virus-induced NLRP3 inflammasome activates the sterol regulatory element-binding protein (SREBP) and regulates lipid metabolism. *J Biol Chem*. 2016;291:3254-3267.
49. Syed GH, Amako Y, Siddiqui A. Hepatitis C virus hijacks host lipid metabolism. *Trends Endocrinol Metab*. 2010;21:33-40.
50. Negro F, Sanyal AJ. Hepatitis C virus, steatosis and lipid abnormalities: clinical and pathogenic data. *Liver Int*. 2009;29:26-37.
51. Syed GH, Siddiqui A. Effects of hypolipidemic agent nordihydroguaiaretic acid on lipid droplets and hepatitis C virus. *Hepatology*. 2011;54:1936-1946.
52. Miyanari Y, Atsuzawa K, Usuda N, et al. The lipid droplet is an important organelle for hepatitis C virus production. *Nat Cell Biol*. 2007;9:1089-1097.
53. Itoh R, Murakami I, Chou B, et al. *Chlamydia pneumoniae* harness host NLRP3 inflammasome-mediated caspase-1 activation for optimal intracellular growth in murine macrophages. *Biochem Biophys Res Commun*. 2014;452:689-694.
54. Szatmari I, Töröcsik D, Agostini M, et al. PPARgamma regulates the function of human dendritic cells primarily by altering lipid metabolism. *Blood*. 2007;110:3271-3280.
55. Széles L, Töröcsik D, Nagy L. PPAR gamma in immunity and inflammation: cell types and diseases. *Biochim Biophys Acta Mol Cell Biol Lipids*. 2007;1771:1014-1030.
56. Castrillo A, Joseph SB, Vaidya SA, et al. Crosstalk between LXR and Toll-like receptor signaling mediates bacterial and viral antagonism of cholesterol metabolism. *Mol Cell*. 2003;12:805-816.
57. Almeida PE, Roque NR, Magalhães KG, et al. Differential TLR2 downstream signaling regulates lipid metabolism and cytokine production triggered by *Mycobacterium bovis* BCG infection. *Biochim Biophys Acta Mol Cell Biol Lipids*. 2014;1841:97-107.
58. Knight M, Braverman J, Asfaha K, et al. Lipid droplet formation in *Mycobacterium tuberculosis* infected macrophages requires IFN-γ/HIF-1 α signaling and supports host defense. *PLoS Negl Trop Dis*. 2018;14:1-26.
59. Mei C, He P, Cheng B, et al. *Chlamydia pneumoniae* induces macrophage-derived foam cell formation via PPAR α and PPAR γ-dependent pathways. *Cell Biol Int*. 2009;33:301-308.
60. Pawlak M, Lefebvre P, Staels B. Molecular mechanism of PPARα action and its impact on lipid metabolism, inflammation and fibrosis in non-alcoholic fatty liver disease. *J Hepatol*. 2015;62:720-733.
61. Hu X, Binns D, Reese ML. The coccidian parasites toxoplasma and neospora dysregulate mammalian lipid droplet biogenesis. *J Biol Chem*. 2017;292:11009-11020.
62. Huang YL, Morales-Rosado J, Ray J, et al. Toll-like receptor agonists promote prolonged triglyceride storage in macrophages. *J Biol Chem*. 2014;289:3001-3012.

63. Nicolaou G, Goodall AH, Erridge C. Diverse bacteria promote macrophage foam cell formation via Toll-like receptor-dependent lipid body biosynthesis. *J Atheroscler Thromb*. 2012;19:137-148.
64. Mattos KA, Oliveira VCG, Berrêdo-Pinho M, et al. *Mycobacterium leprae* intracellular survival relies on cholesterol accumulation in infected macrophages: a potential target for new drugs for leprosy treatment. *Cell Microbiol*. 2014;16:797-815.
65. Gao J, Serrero G. Adipose differentiation related protein (ADRP) expressed in transfected COS-7 cells selectively stimulates long chain fatty acid uptake. *J Biol Chem*. 1999;274:16825-16830.
66. Silva AR, Pacheco P, Vieira-de-Abreu A, et al. Lipid bodies in oxidized LDL-induced foam cells are leukotriene-synthesizing organelles: a MCP-1/CCL2 regulated phenomenon. *Biochim Biophys Acta Mol Cell Biol Lipids*. 2009;1791:1066-1075.
67. Fan B, Gu J-Q, Yan R, et al. High glucose, insulin and free fatty acid concentrations synergistically enhance perilipin 3 expression and lipid accumulation in macrophages. *Metabolism*. 2013;62:1168-1179.
68. Ploen D, Hafirassou ML, Himmelsbach K, et al. TIP47 plays a crucial role in the life cycle of hepatitis C virus. *J Hepatol*. 2013;58:1081-1088.
69. Brasaemle DL. Thematic review series: adipocyte biology. The perilipin family of structural lipid droplet proteins: stabilization of lipid droplets and control of lipolysis. *J Lipid Res*. 2007;48:2547-2559.
70. Larigauderie G, Furman C, Jaye M, et al. Adipophilin enhances lipid accumulation and prevents lipid efflux from THP-1 macrophages: potential role in atherogenesis. *Arterioscler Thromb Vasc Biol*. 2004;24:504-10.
71. Imamura M, Inoguchi T, Ikuyama S, et al. ADRP stimulates lipid accumulation and lipid droplet formation in murine fibroblasts. *Am J Physiol Endocrinol Metab*. 2002;283:E775-83.
72. Targett-Adams P, McElwee MJ, Ehrenborg E, et al. A PPAR response element regulates transcription of the gene for human adipose differentiation-related protein. *Biochim Biophys Acta - Gene Struct Expr*. 2005;1728:95-104.
73. Szanto A, Nagy L. Retinoids potentiate peroxisome proliferator-activated receptor gamma action in differentiation, gene expression, and lipid metabolic processes in developing myeloid cells. *Mol Pharmacol*. 2005;67:1935-1943.
74. Tontonoz P, Nagy L, Alvarez JG, et al. PPARγ promotes monocyte/macrophage differentiation and uptake of oxidized LDL. *Cell*. 1998;93:241-252.
75. Rajaram MVS, Brooks MN, Morris JD, et al. *Mycobacterium tuberculosis* activates human macrophage peroxisome proliferator-activated receptor gamma linking mannose receptor recognition to regulation of immune responses. *J Immunol*. 2010;185:929-942.
76. Mahajan S, Dkhar HK, Chandra V, et al. *Mycobacterium tuberculosis* modulates macrophage lipid-sensing nuclear receptors PPAR and TR4 for survival. *J Immunol*. 2012;188:5593-5603.
77. Prescott SM, Zimmerman GA, Stafforini DM, et al. Platelet-activating factor and related lipid mediators. *Annu Rev Biochem*. 2000;69:419-445.
78. Bozza PT, Payne JL, Goulet JL, et al. Mechanisms of platelet-activating factor-induced lipid body formation: requisite roles for 5-lipoxygenase and de novo protein synthesis in the compartmentalization of neutrophil lipids. *J Exp Med*. 1996;183:1515-1525.
79. Bozza PT, Yu W, Penrose JF, et al. Eosinophil lipid bodies: specific, inducible intracellular sites for enhanced eicosanoid formation. *J Exp Med*. 1997;186:909-920.
80. Gomes RN, Bozza FA, Amâncio RT, et al. Exogenous platelet-activating factor acetylhydrolase reduces mortality in mice with systemic inflammatory response syndrome and sepsis. *Shock*. 2006;26:41-9.
81. de Assis EF, Silva AR, Caiado LF, et al. Synergism between platelet-activating factor-like phospholipids and peroxisome proliferator-activated receptor gamma agonists generated during low density lipoprotein oxidation that induces lipid body formation in leukocytes. *J Immunol*. 2003;171:2090-2098.
82. Silva AR, de Assis EF, Caiado LFC, et al. Monocyte chemoattractant protein-1 and 5-lipoxygenase products recruit leukocytes in response to platelet-activating factor-like lipids in oxidized low-density lipoprotein. *J Immunol*. 2002;168:4112-4120.
83. Gerard C, Rollins BJ. Chemokines and disease. *Nat Immunol*. 2001;2:108-115.
84. Ozawa S, Ueda S, Li Y, et al. Fatty acid binding protein 3 as a potential mediator for diabetic nephropathy in eNOS deficient mouse. *Biochem Biophys Res Commun*. 2014;454:531-536.
85. Kwon Y-H, Kim J, Kim C-S, et al. Hypothalamic lipid-laden astrocytes induce microglia migration and activation. *FEBS Lett*. 2017:591:1742-1751.
86. Fazolini NPB, Cruz ALS, Werneck MBF, et al. Leptin activation of mTOR pathway in intestinal epithelial cell triggers lipid droplet formation, cytokine production and increased cell proliferation. *Cell Cycle*. 2015;14:2667-2676.
87. Penido C, Vieira-de-Abreu A, Bozza MT, et al. Role of monocyte chemotactic protein-1/CC chemokine ligand 2 on gamma delta T lymphocyte trafficking during inflammation induced by lipopolysaccharide or *Mycobacterium bovis* bacille Calmette-Guerin. *J Immunol*. 2003;171:6788-6794.
88. Péan CB, Schiebler M, Tan SWS, et al. Regulation of phagocyte triglyceride by a STAT-ATG2 pathway controls mycobacterial infection. *Nat Commun*. 2017;8:14642.
89. Weller PF. Leukocyte lipid bodies—structure and function as "EICOSASOMES." *Trans Am Clin Climatol Assoc*. 2016;127:328-340.
90. Bandeira-melo C, Paiva LA, Amorim NRT, et al. EicosaCell: an imaging-based assay to identify spatiotemporal eicosanoid synthesis. *Methods Mol Biol*. 2017;1554:127-141.
91. van Manen H-J, Kraan YM, Roos D, et al. Single-cell Raman and fluorescence microscopy reveal the association of lipid bodies with phagosomes in leukocytes. *Proc Natl Acad Sci USA*. 2005;102:10159-10164.
92. Weller PF, Monahan-earley RA, Dvorak HF, et al. Cytoplasmic lipid bodies of human eosinophils subcellular isolation and analysis of arachidonate incorporation. *Am J Pathol*. 1991;138:141-148.
93. Dichlberger A, Schlager S, Maaninka K, et al. Adipose triglyceride lipase regulates eicosanoid production in activated human mast cells. *J Lipid Res*. 2014;55:2471-2478.
94. Schlager S, Goeritzer M, Jandl K, et al. Adipose triglyceride lipase acts on neutrophil lipid droplets to regulate substrate availability for lipid mediator synthesis. *J Leukoc Biol*. 2015;98:837-850.
95. Yu W, Bozza PT, Tzizik DM, et al. Co-compartmentalization of MAP kinases and cytosolic phospholipase A2 at cytoplasmic arachidonate-rich lipid bodies. *Am J Pathol*. 1998;152:759-769.
96. Roingeard P, Melo RCN. Lipid droplet hijacking by intracellular pathogens. *Cell Microbiol*. 2017;1-8.
97. Bandeira-Melo C, Phoofolo M, Weller PF. Extranuclear lipid bodies, elicited by ccr3-mediated signaling pathways, are the sites of chemokine-enhanced leukotriene C 4 production in eosinophils and basophils. *J Biol Chem*. 2001;276:22779-22787.
98. Accioly MT, Pacheco P, Maya-Monteiro CM, et al. Lipid bodies are reservoirs of cyclooxygenase-2 and sites of prostaglandin-E2 synthesis in colon cancer cells. *Cancer Res*. 2008;68:1732-1740.
99. Luna-Gomes T, Magalhaes KG, Mesquita-Santos FP, et al. Eosinophils as a novel cell source of prostaglandin D2: autocrine role in allergic inflammation. *J Immunol*. 2011;187:6518-6526.
100. Magalhaes KG, Gomes TL, Santos FM, et al. Schistosomal lipids activate human eosinophils via Toll-like receptor 2 and PGD2 receptors: 15-LO role in cytokine secretion Kelly. *Front Immunol*. Epub ahead of print 2018. https://doi.org/10.3389/fimmu.2018.03161.

101. Araújo-santos T, Rodríguez NE, Moura-pontes S, et al. Role of prostaglandin F 2 α production in lipid bodies from *Leishmania infantum* chagasi: insights on virulence. *J Infect Dis*. 2014;210:1951-1961.
102. Toledo DAM, Roque NR, Teixeira L, et al. Lipid body organelles within the parasite *Trypanosoma cruzi*: a role for intracellular arachidonic acid metabolism. *PLoS One*. 2016;11:e0160433.
103. Tavares N, Afonso L, Suarez M, et al. Degranulating neutrophils promote leukotriene B 4 production by infected macrophages to kill *Leishmania amazonensis* parasites. *J Immunol*. 2016;196:1865-1873.
104. Serezani CH, Perrela JH, Russo M, et al. Leukotrienes are essential for the control of *Leishmania amazonensis* infection and contribute to strain variation in susceptibility. *J Immunol*. 2006;177:3201-3208.
105. Peters-Golden M, Canetti C, Mancuso P, et al. Leukotrienes: underappreciated mediators of innate immune responses. *J Immunol*. 2005;174:589-594.
106. Neves JS, Radke AL, Weller PF. Cysteinyl leukotrienes acting via granule membrane-expressed receptors elicit secretion from within cell-free human eosinophil granules. *J Allergy Clin Immunol*. 2010;125:477-482.
107. Beil WJ, Weller PF, Peppercorn MA, et al. Ultrastructural immunogold localization of subcellular sites of TNF-α in colonic Crohn's disease. *J Leukoc Biol*. 1995;58:284-298.
108. Assunção-Miranda I, Amaral FA, Bozza FA, et al. Contribution of macrophage migration inhibitory factor to the pathogenesis of dengue virus infection. *FASEB J*. 2010;24:218-228.
109. Seo J-Y, Yaneva R, Cresswell P. Viperin: a multifunctional, interferon-inducible protein that regulates virus replication. *Cell Host Microbe*. 2011;10:534-539.
110. Colonne PM, Winchell CG, Voth DE. Hijacking host cell highways: manipulation of the host actin cytoskeleton by obligate intracellular bacterial pathogens. *Front Cell Infect Microbiol*. 2016;6:1-8.
111. Samanta D, Mulye M, Clemente TM, et al. Manipulation of host cholesterol by obligate intracellular bacteria. *Front Cell Infect Microbiol*. 2017;7:1-14.
112. Bozza PT, D'Avila H, Almeida PE, et al. Lipid droplets in host–pathogen interactions. *Clin Lipidol*. 2009;4:791-807.
113. Russell DG, Cardona P, Kim M, et al. Foamy macrophages and the progression of the human TB granuloma. *Nat Immunol*. 2009;10:943-948.
114. Cocchiaro JL, Kumar Y, Fischer ER, et al. Cytoplasmic lipid droplets are translocated into the lumen of the *Chlamydia trachomatis* parasitophorous vacuole. *Proc Natl Acad Sci USA*. 2008;105:9379-9384.
115. Daniel J, Maamar H, Deb C, et al. Mycobacterium tuberculosis uses host triacylglycerol to accumulate lipid droplets and acquires a dormancy-like phenotype in lipid-loaded macrophages. *PLoS Pathog*. 2011;7:e1002093.
116. Kumar Y, Cocchiaro J, Valdivia RH. Report the obligate intracellular pathogen *Chlamydia trachomatis* targets host lipid droplets. *Curr Biol*. 2006;16:1646-1651.
117. Xu B, You LL, Wu Y, et al. Transmission electron microscopy (TEM) observations of female oocytes from *Nilaparvata lugens* (Hemiptera: Delphacidae): antibiotic jinggangmycin (JGM)-induced stimulation of reproduction and associated changes in hormone levels. *J Econ Entomol*. 2016;109:1677-1682.
118. Marques MAM, Berrêdo-pinho M, Rosa TLSA, et al. The essential role of cholesterol metabolism in the intracellular survival of *Mycobacterium leprae* is not coupled to central carbon. *J Bacteriol*. 2015;197:3698-3707.
119. Pandey AK, Sassetti CM. Mycobacterial persistence requires the utilization of host cholesterol. *Proc Natl Acad Sci USA*. 2008;105:4376-4380.
120. Brzostek A, Pawelczyk J, Rumijowska-Galewicz A, et al. Mycobacterium tuberculosis is able to accumulate and utilize cholesterol. *J Bacteriol*. 2009;191:6584-6591.
121. Barisch C, Paschke P, Hagedorn M, et al. Lipid droplet dynamics at early stages of *Mycobacterium marinum* infection in Dictyostelium. *Cell Microbiol*. 2015;17:1332-1349.
122. Rank RG, Whittimore J, Bowlin AK, et al. In vivo ultrastructural analysis of the intimate relationship between polymorphonuclear leukocytes and the chlamydial developmental cycle. *Infect Immun*. 2011;79:3291-3301.
123. Qadri F, Bhuiyan TR, Dutta KK, et al. Acute dehydrating disease caused by *Vibrio cholerae* serogroups O1 and O139 induce increases in innate cells and inflammatory mediators at the mucosal surface of the gut. *Gut*. 2004;53:62-69.
124. Singer M, Deutschman CS, Seymour CW, et al. The third international consensus definitions for sepsis and septic shock (Sepsis-3). *JAMA*. 2016;315:801.
125. Phillips RM, Six DA, Dennis EA, et al. In vivo phospholipase activity of the *Pseudomonas aeruginosa* cytotoxin ExoU and protection of mammalian cells with phospholipase A2 inhibitors. *J Biol Chem*. 2003;278:41326-41332.
126. Saliba AM, Nascimento DO, Silva MCA, et al. Eicosanoid-mediated proinflammatory activity of *Pseudomonas aeruginosa* ExoU. *Cell Microbiol*. 2005;7:1811-1822.
127. Feliciano L-FP, Plotkowski M-C, Bozza PT, et al. Lipid body mobilization in the ExoU-induced release of inflammatory mediators by airway epithelial cells. *Microb Pathog*. 2008;45:30-37.
128. Curnutte JT, Badwey JA, Robinson JM, et al. Studies on the mechanism of superoxide release from human neutrophils stimulated with arachidonate. *J Biol Chem*. 1984;259:11851-11857.
129. Fock E, Bachteeva V, Lavrova E, et al. Mitochondrial-targeted antioxidant MitoQ prevents *E. coli* lipopolysaccharide-induced accumulation of triacylglycerol and lipid droplets biogenesis in epithelial cells. *J Lipids*. 2018;2018:1-11.
130. Silk E, Zhao H, Weng H, et al. The role of extracellular histone in organ injury. *Cell Death Dis*. 2017;8:e2812.
131. Patat SA, Carnegie RB, Kingsbury C, et al. Antimicrobial activity of histones from hemocytes of the Pacific white shrimp. *Eur J Biochem*. 2004;271:4825-4833.
132. Chen R, Kang R, Fan X-G, et al. Release and activity of histone in diseases. *Cell Death Dis*. 2014;5:e1370.
133. Li Z, Thiel K, Thul PJ, et al. Lipid droplets control the maternal histone supply of Drosophila embryos. *Curr Biol*. 2012;22:2104-2113.
134. Nagai A, Sato T, Akimoto N, et al. Isolation and identification of histone H3 protein enriched in microvesicles secreted from cultured sebocytes. *Endocrinology*. 2005;146:2593-2601.
135. Wan H-C, Melo RCN, Jin Z, et al. Roles and origins of leukocyte lipid bodies: proteomic and ultrastructural studies. *FASEB J*. 2006;21:167-178.
136. Romero-Brey I, Bartenschlager R. Membranous replication factories induced by plus-strand RNA viruses. *Viruses*. 2014;6:2826-2857.
137. Strating JR, van Kuppeveld FJ. Viral rewiring of cellular lipid metabolism to create membranous replication compartments. *Curr Opin Cell Biol*. 2017;47:24-33.
138. Van Der Hoeven B, Oudshoorn D, Koster AJ, et al. Biogenesis and architecture of arterivirus replication organelles. *Virus Res*. 2016;220:70-90.
139. Herker E, Ott M. Emerging role of lipid droplets in host/pathogen interactions * lipid droplets: more than just fat storage. *J Biol Chem*. 2012;287:2280-2287.
140. Coffey CM, Sheh A, Kim IS, et al. Reovirus outer capsid protein 1 induces apoptosis and associates with lipid droplets, endoplasmic reticulum, and mitochondria. *J Virol*. 2006;80:8422-8438.
141. Cheung W, Gill M, Esposito A, et al. Rotaviruses associate with cellular lipid droplet components to replicate in viroplasms, and compounds disrupting or blocking lipid droplets inhibit viroplasm formation and viral replication. *J Virol*. 2010;84:6782-6798.

142. Doerflinger SY, Cortese M, Romero-Brey I, et al. Membrane alterations induced by nonstructural proteins of human norovirus. *PLOS Pathog*. 2017;13:e1006705.
143. Peña Cárcamo JR, Morell ML, Vázquez CA, et al. The interplay between viperin antiviral activity, lipid droplets and Junín mammarenavirus multiplication. *Virology*. 2018;514:216-229.
144. He Y, Staschke KA, Tan SL. HCV NS5A: a multifunctional regulator of cellular pathways and virus replication. In: Tan SL, ed. *Hepatitis C Viruses: Genomes and Molecular Biology*. Poole, UK: Horizon Scientific Press; 2006: Chapter 9. Available from: http://www.ncbi.nlm.nih.gov/pubmed/21250384.
145. Vogt DA, Camus G, Herker E, et al. Lipid droplet-binding protein TIP47 regulates hepatitis C virus RNA replication through interaction with the viral NS5A protein. *PLoS Pathog*. 2013;9:1-14.
146. Tanaka T, Kuroda K, Ikeda M, et al. Hepatitis C virus NS4B targets lipid droplets through hydrophobic residues in the amphipathic helices. *J Lipid Res*. 2013;54:881-892.
147. Boulant S, Montserret R, Hope RG, et al. Structural determinants that target the hepatitis C virus core protein to lipid droplets. *J Biol Chem*. 2006;281:22236-22247.
148. Boulant S, Targett-adams P, Mclauchlan J. Disrupting the association of hepatitis C virus core protein with lipid droplets correlates with a loss in production of infectious virus. *J Gen Virol*. 2018;2204-2213.
149. Hourioux C, Ait-goughoulte M, Patient R, et al. Core protein domains involved in hepatitis C virus-like particle assembly and budding at the endoplasmic reticulum membrane. *Cell Microbiol*. 2007;9:1014-1027.
150. Shah PS, Link N, Jang GM, et al. Comparative flavivirus-host protein interaction mapping reveals mechanisms of dengue and Zika virus pathogenesis resource comparative flavivirus-host protein interaction mapping reveals mechanisms of dengue and Zika virus pathogenesis. *Cell*. 2018;175:1931-1945.
151. Wan H-CH-C, Melo RCN, Weller PF, et al. Roles and origins of leukocyte lipid bodies: proteomic and ultrastructural studies. *FASEB J*. 2006;21:167-178.
152. Hope RG, Murphy DJ, McLauchlan J. The domains required to direct core proteins of hepatitis C virus and GB virus-B to lipid droplets share common features with plant oleosin proteins. *J Biol Chem*. 2002;277:4261-4270.
153. Herker E, Harris C, Hernandez C, et al. Efficient hepatitis C virus particle formation requires diacylglycerol acyltransferase-1. *Nat Med*. 2010;16:1295-1298.
154. Camus G, Herker E, Modi AA, et al. Diacylglycerol acyltransferase-1 localizes hepatitis C virus NS5A protein to lipid droplets and enhances NS5A interaction with the viral capsid core. *J Biol Chem*. 2013;288:9915-9923.
155. Salloum S, Wang H, Ferguson C, et al. Rab18 binds to hepatitis C virus NS5A and promotes interaction between sites of viral replication and lipid droplets. *PLoS Pathog*. 2013;9:e1003513.
156. Iglesias NG, Mondotte JA, Byk LA, et al. Dengue virus uses a non-canonical function of the host GBF1-Arf-COPI system for capsid protein accumulation on lipid droplets. *Traffic*. 2015;16:962-977.
157. Rouille Y, Delgrange D, Roingeard P, et al. Subcellular localization of hepatitis C virus structural proteins in a cell culture system that efficiently replicates the virus. *J Virol*. 2006;80:2832-2841.
158. Jordan TX, Randall G. Dengue virus activates the AMP kinase-mTOR axis to stimulate a proviral lipophagy. *J Virol*. 2017;91:1-13.
159. Host C, Zhang JS, Lan Y, et al. Flaviviruses exploit the lipid droplet protein AUP1 to trigger lipophagy and drive virus production. *Cell Host Microbe*. 2018;23:819-831.e5.
160. Heaton NS, Randall G. Dengue virus-induced autophagy regulates lipid metabolism. *Cell Host Microbe*. 2010;8:422-432.
161. Ahmad L, Mostowy S, Sancho-Shimizu V. Autophagy-virus interplay: from cell biology to human disease. *Front Cell Dev Biol*. 2018;6:1-8.
162. Chan ST, Ou JJ. Hepatitis C virus-induced autophagy and host innate immune response. *Viruses*. 2017;5:1-10.
163. Unterstab G, Gosert R, Leuenberger D, et al. The polyomavirus BK agnoprotein co-localizes with lipid droplets. *Virology*. 2010;399:322-331.
164. Monson EA, Crosse KM, Das M, et al. Lipid droplet density alters the early innate immune response to viral infection. *PLoS One*. 2018;13:1-18.
165. Helbig KJ, Lau DTY, Semendric L, et al. Analysis of ISG expression in chronic hepatitis C identifies viperin as a potential antiviral effector. *Hepatology*. 2005;42:702-710.
166. Fitzgerald KA. The interferon inducible gene: viperin. *J Interf Cytokine Res*. 2011;31:131-135.
167. Rabbani MAG, Ribaudo M, Guo J-T, et al. Identification of interferon-stimulated gene proteins that inhibit human parainfluenza virus type 3. *J Virol*. 2016;90:11145-11156.
168. Duschene KS, Broderick JB. Viperin: a radical response to viral infection. *Biomol Concepts*. 2012;3:255-266.
169. Helbig KJ, Beard MR. The role of viperin in the innate antiviral response. *J Mol Biol*. 2014;426:1210-1219.
170. Helbig KJ, Carr JM, Calvert JK, et al. Viperin is induced following dengue virus type-2 (DENV-2) infection and has anti-viral actions requiring the C-terminal end of viperin. *PLoS Negl Trop Dis*. 2013;7:e2178.
171. Teng TS, Foo SS, Simamarta D, et al. Viperin restricts chikungunya virus replication and pathology. *J Clin Invest*. 2012;122:4447-4460.
172. Fros JJ, van der Maten E, Vlak JM, et al. The C-Terminal domain of chikungunya virus nsP2 independently governs viral RNA replication, cytopathicity, and inhibition of interferon signaling. *J Virol*. 2013;87:10394-10400.
173. Chiang P-Y, Wu H-N. The role of surface basic amino acids of dengue virus NS3 helicase in viral RNA replication and enzyme activities. *FEBS Lett*. 2016;590:2307-2320.
174. Zhang Y, Li L, Liu X, et al. Crystal structure of Junin virus nucleoprotein. *J Gen Virol*. 2013;94:2175-2183.
175. Wang X, Hinson ER, Cresswell P. The interferon-inducible protein viperin inhibits influenza virus release by perturbing lipid rafts. *Cell Host Microbe*. 2007;2:96-105.
176. Nasr N, Maddocks S, Turville SG, et al. HIV-1 infection of human macrophages directly induces viperin which inhibits viral production. *Blood*. 2012;120:778-788.
177. Saitoh T, Satoh T, Yamamoto N, et al. Antiviral protein viperin promotes toll-like receptor 7- and toll-like receptor 9-mediated type i interferon production in plasmacytoid dendritic cells. *Immunity*. 2011;34:352-363.
178. Lindqvist R, Mundt F, Gilthorpe JD, et al. Fast type I interferon response protects astrocytes from flavivirus infection and virus-induced cytopathic effects. *J Neuroinflammation*. 2016;13:277.
179. Sibley DL. Invasion and intracellular survival by protozoan parasites. *Immunol Rev*. 2011;240:72-91.
180. Toledo DAM, Avila HD, Melo RCN. Host lipid bodies as platforms for intracellular survival of protozoan parasites. *Front Immunol*. 2016;7:1-6.
181. Filardy AA, Guimarães-Pinto K, Nunes MP, et al. Human kinetoplastid protozoan infections: where are we going next? *Front Immunol*. 2018;9:1-7.
182. Vallochi AL, Teixeira L, Oliveira KDS, et al. Lipid droplet, a key player in host-parasite interactions. *Front Immunol*. 2018;9:1022.
183. Melo RCN, Ávila HD, Fabrino DL, et al. Macrophage lipid body induction by Chagas disease in vivo: putative intracellular domains for eicosanoid formation during infection. *Tissue Cell*. 2003;35:59-67.
184. Rabhi I, Rabhi S, Ben-Othman R, et al. Transcriptomic signature of Leishmania infected mice macrophages: a metabolic point of view. *PLoS Negl Trop Dis*. 2012;6:e1763.
185. Lecoeur H, Giraud E, Prévost M-CC, et al. Reprogramming neutral lipid metabolism in mouse dendritic leucocytes hosting live *Leishmania amazonensis* Amastigotes. *PLoS Negl Trop Dis*. 2013;7:e2276.

186. Rodríguez NE, Lockard RD, Turcotte EA, et al.. Lipid bodies accumulation in *Leishmania infantum*- infected C57BL/6 macrophages. *Parasite Immunol*. 2017;39:1-5.
187. Dumont ME, Dei-Cas E, Maurois P, et al. Histopathologie du foie et du rein au cours du paludisme: rapports avec la dyslipoprotéinémie palustre. *Ann Parasitol Hum Comparée*. 1988;63: 171-183.
188. Lima JB, Araújo-santos T, Lázaro-souza M, et al. Leishmania infantum lipophosphoglycan induced-prostaglandin E2 production in association with PPAR-γ expression via activation of Toll like receptors-1 and 2. *Sci Rep*. 2017;7:1-11.
189. Melo RCN, Fabrino DL, Dias FF, et al. Lipid bodies: structural markers of inflammatory macrophages in innate immunity. *Inflamm Res*. 2006;55:342-348.
190. Nolan SJ, Romano JD, Coppens I. Host lipid droplets: an important source of lipids salvaged by the intracellular parasite *Toxoplasma gondii*. *PLOS Pathog*. 2017;1-38.
191. Bougnères L, Helft J, Tiwari S, et al. A role for lipid bodies in the cross-presentation of phagocytosed antigens by MHC class I in dendritic cells. *Immunity*. 2009;31:232-244.
192. Hunn JP, Feng CG, Sher A, et al. The immunity-related GTPases in mammals: a fast-evolving cell- autonomous resistance system against intracellular pathogens. *Mamm Genome*. 2011;22:43-54.
193. Murray HW, Mitchell-Flack M, Taylor GA, et al. IFN-γ-induced macrophage antileishmanial mechanisms in mice: a role for immunity-related GTPases, Irgm1 and Irgm3, in *Leishmania donovani* infection in the liver. *Exp Parasitol*. 2015;157:103-109.
194. Steinman RM, Cohn ZA. Identification of a novel cell type in peripheral lymphoid organs of mice. *J Exp Med*. 1973;137: 1142-1162.
195. Meester I, Rosas-Taraco AG, Salinas-Carmona MC. *Nocardia brasiliensis* induces formation of foamy macrophages and dendritic cells in vitro and in vivo. *PLoS One*. 2014;9:e100064.
196. Herber DL, Cao W, Nefedova Y, et al. Lipid accumulation and dendritic cell dysfunction in cancer. *Nat Med*. 2010;16:880-886.
197. Gao F, Liu C, Guo J, et al. Radiation-driven lipid accumulation and dendritic cell dysfunction in cancer. *Sci Rep*. 2015;5:9613.
198. Everts B, Amiel E, Huang SC-C, et al. TLR-driven early glycolytic reprogramming via the kinases TBK1-IKKε supports the anabolic demands of dendritic cell activation. *Nat Immunol*. 2014;15:323-332.
199. den Brok MH, Büll C, Wassink M, et al. Saponin-based adjuvants induce cross-presentation in dendritic cells by intracellular lipid body formation. *Nat Commun*. 2016;7:13324.
200. Ibrahim J, Nguyen AH, Rehman A, et al. Dendritic cell populations with different concentrations of lipid regulate tolerance and immunity in mouse and human liver. *Gastroenterology*. 2012;143: 1061-1072.
201. Cao W, Ramakrishnan R, Tuyrin VA, et al. Oxidized lipids block antigen cross-presentation by dendritic cells in cancer. *J Immunol*. 2014;192:2920-2931.
202. Veglia F, Tyurin VA, Mohammadyani D, et al. Lipid bodies containing oxidatively truncated lipids block antigen cross-presentation by dendritic cells in cancer. *Nat Commun*. 2017;8:2122.
203. Shaikh SR, Mitchell D, Carroll E, et al. Differential effects of a saturated and a monounsaturated fatty acid on MHC class I antigen presentation. *Scand J Immunol*. 2008;68:30-42.
204. Salvatore G, Bernoud-Hubac N, Bissay N, et al. Human monocyte-derived dendritic cells turn into foamy dendritic cells with IL-17A. *J Lipid Res*. 2015;56:1110-22.
205. Wang XY, Facciponte J, Chen X, et al. Scavenger receptor-A negatively regulates antitumor immunity. *Cancer Res*. 2007;67: 4996-5002.

How to cite this article: Pereira-Dutra FS, Teixeira L, de Souza Costa MF, Bozza PT. Fat, fight, and beyond: The multiple roles of lipid droplets in infections and inflammation. *J Leukoc Biol*. 2019;1-18. https://doi.org/10.1002/JLB.4MR0119-035R

Anexo 2

BOSCH, M.; SANCHEZ-ALVAREZ, M.; FAJARDO, A.; KAPETANOVIC, R.; STEINER, B.; **DUTRA, Filipe**; MOREIRA, L.; LOPEZ, J. A.; CAMPO, R.; MARI, M.; MORALES-PAYTUVI, F.; TORT, O.; GUBERN, A.; TEMPLIN, R. M.; CURSON, J. E. B.; MARTEL, N.; CATALA, C.; LOZANO, F.; TEBAR, F.; ENRICH, C.; VAZQUEZ, J.; POZO, M. A.; SWEET, M. J.; **BOZZA, P. T**.; GROSS, S. P.; PARTON, R. G.; POL, A. **Mammalian lipid droplets are innate immune hubs integrating cell metabolism and host defense.** *SCIENCE*, Vol. 370, Issue 6514, eaay8085.

RESEARCH ARTICLE SUMMARY

INNATE IMMUNITY

Mammalian lipid droplets are innate immune hubs integrating cell metabolism and host defense

Marta Bosch*†, Miguel Sánchez-Álvarez†, Alba Fajardo, Ronan Kapetanovic, Bernhard Steiner, Filipe Dutra, Luciana Moreira, Juan Antonio López, Rocío Campo, Montserrat Marí, Frederic Morales-Paytuví, Olivia Tort, Albert Gubern, Rachel M. Templin, James E. B. Curson, Nick Martel, Cristina Català, Francisco Lozano, Francesc Tebar, Carlos Enrich, Jesús Vázquez, Miguel A. Del Pozo, Matthew J. Sweet, Patricia T. Bozza, Steven P. Gross, Robert G. Parton*, Albert Pol*

INTRODUCTION: In all eukaryotic cells, lipid droplets (LDs) store and supply essential lipids to produce signaling molecules, membrane building blocks, and metabolic energy. The LD monolayer also accommodates proteins not obviously related to lipids, such as transcription factors, chromatin components, and toxic proteins.

Common parasites (such as trypanosomes and *Plasmodium falciparum*), bacteria (such as mycobacteria and *Chlamydia*), and viruses (such as hepatitis C and dengue) induce and target LDs during their life cycles. The current view is that LDs support infection, providing microorganisms with substrates for effective growth.

RATIONALE: Successful innate defense is critical for survival, and host species have efficiently coevolved with pathogens to develop a plethora of immune responses. Multiple cues, including cellular stress and danger-associated molecular patterns such as lipopolysaccharide (LPS), induce LD formation. Thus, LD localization and dynamics may potentially be advantageous for organizing an intracellular host defense. We have investigated the possibility that mammalian LDs have a direct and regulated role in innate immunity.

RESULTS: We show that mammalian LDs are endowed with a protein-mediated antimicrobial capacity, which is up-regulated during polymicrobial sepsis and by LPS. Light and electron microscopy demonstrated specific association of LDs and bacteria in human macrophages, suggesting the existence of docking mechanisms that facilitate the engagement of antibacterial LD proteins with bacteria.

A comparative mass spectrometry profiling of proteins differentially associated with LDs in response to LPS (LPS-LDs) revealed the profound remodeling of the organelle proteome. A stringent evaluation identified 689 proteins differentially regulated on LPS-LDs (317 enriched and 372 reduced). Ingenuity Pathway Analysis revealed an enrichment of innate immune system–related components and reduction of metabolism-related LD-resident proteins. Additional analyses suggested that LDs serve as innate immune hubs, integrating major intra- and extracellular immune responses.

Among the five members of the perilipin family of LD surface proteins (PLINs), PLIN5 was the only one down-regulated on LPS-LDs. PLIN5 reduction promoted physical and functional disconnection of LPS-LDs and mitochondria, with a concomitant reduction of oxidative metabolism and ketogenesis. Forced PLIN5 reexpression increased the number of LD-mitochondria contacts, reducing LD-bacteria interactions and compromising the antimicrobial capacity of cells.

By contrast, PLIN2 was the most up-regulated PLIN on LPS-LDs. Gene interaction analysis revealed that multiple immune proteins nucleated around PLIN2 in response to LPS. LPS-LDs accrued several interferon-inducible proteins such as viperin, IGTP, IIGP1, TGTP1, and IFI47. Furthermore, LPS-LDs also accumulated cathelicidin (CAMP), a broad-spectrum antimicrobial peptide with chemotactic properties. Cells overexpressing a LD-associated CAMP were more resistant to different bacterial species, including *Escherichia coli*, methicillin-resistant *Staphylococcus aureus*, and *Listeria monocytogenes*.

CONCLUSION: These results demonstrate that LDs form a first-line intracellular defense. They act as a molecular switch in innate immunity, responding to danger signals by both reprogramming cell metabolism and eliciting protein-mediated antimicrobial mechanisms. Mechanisms of LD trafficking and docking with phagocytic and parasitophorous membranes, observed here and described for several pathogens, may facilitate the delivery of immune proteins located on the LD surface. Intracellular LDs can provide infected cells with several biological benefits, serving as a location to attract pathogens as well as coordinating different immune systems that operate simultaneously against different classes of pathogens. LDs may also sequester cytotoxic compounds (such as antimicrobial peptides), reducing damage to other cellular organelles. In view of the widespread resistance to current antibiotics, this study helps decipher molecular mechanisms involved in antimicrobial defense that could be exploited for development of new anti-infective agents. ■

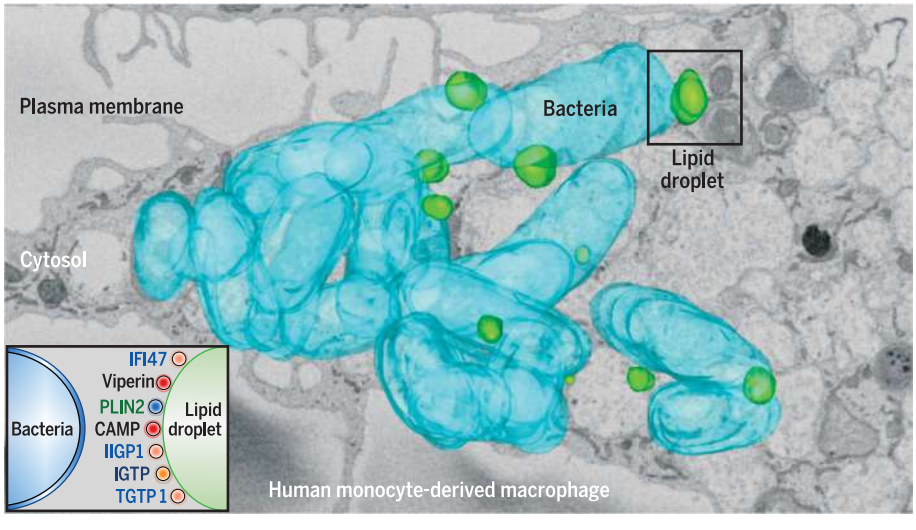

LDs mediate innate immune defense. Serial blockface scanning electron microscopy data reconstruction showing an infected macrophage. Bacteria (blue) and LDs (green) in the three-dimensional dataset have been colored and projected onto a single image. LDs associate with the bacteria surface (black square). This interaction is proposed to bring a specific set of antipathogenic proteins in contact with the membrane-enclosing bacteria (inset).

The list of author affiliations is available in the full article online.
*Corresponding author. Email: martabosch@ub.edu (M.B.); r.parton@imb.uq.edu.au (R.G.P.); apols@ub.edu (A.P.)
†These authors contributed equally to this work.
Cite this article as M. Bosch *et al.*, *Science* **370**, eaay8085 (2020). DOI: 10.1126/science.aay8085

READ THE FULL ARTICLE AT
https://doi.org/10.1126/science.aay8085

RESEARCH ARTICLE

INNATE IMMUNITY

Mammalian lipid droplets are innate immune hubs integrating cell metabolism and host defense

Marta Bosch[1,2]*†, Miguel Sánchez-Álvarez[3]†, Alba Fajardo[1], Ronan Kapetanovic[4,5,6], Bernhard Steiner[4], Filipe Dutra[7], Luciana Moreira[7], Juan Antonio López[8,9], Rocío Campo[8], Montserrat Marí[10,11], Frederic Morales-Paytuví[1], Olivia Tort[1], Albert Gubern[1], Rachel M. Templin[4,12], James E. B. Curson[4,5,6], Nick Martel[4], Cristina Català[13], Francisco Lozano[13], Francesc Tebar[1,2], Carlos Enrich[1,2], Jesús Vázquez[8,9], Miguel A. Del Pozo[3], Matthew J. Sweet[4,5,6], Patricia T. Bozza[7], Steven P. Gross[14], Robert G. Parton[4,12]*, Albert Pol[1,2,15]*

Lipid droplets (LDs) are the major lipid storage organelles of eukaryotic cells and a source of nutrients for intracellular pathogens. We demonstrate that mammalian LDs are endowed with a protein-mediated antimicrobial capacity, which is up-regulated by danger signals. In response to lipopolysaccharide (LPS), multiple host defense proteins, including interferon-inducible guanosine triphosphatases and the antimicrobial cathelicidin, assemble into complex clusters on LDs. LPS additionally promotes the physical and functional uncoupling of LDs from mitochondria, reducing fatty acid metabolism while increasing LD-bacterial contacts. Thus, LDs actively participate in mammalian innate immunity at two levels: They are both cell-autonomous organelles that organize and use immune proteins to kill intracellular pathogens as well as central players in the local and systemic metabolic adaptation to infection.

Lipid droplets (LDs) are the major lipid storage organelles of eukaryotic cells (*1*). Common parasites (such as trypanosomes and *Plasmodium falciparum*), bacteria (such as mycobacteria and *Chlamydia*), and viruses [such as hepatitis C (HCV) and dengue (DENV)] induce and target LDs during their life cycles (*2*). The current view is that LDs support infection, providing invaders with substrates for survival and/or growth (*3*). However, successful innate defense is critical for survival, and host immune responses have coevolved with pathogens, developing a plethora of defense mechanisms. There is some limited evidence that LDs actively participate in innate defense (*4*, *5*). For example, three innate immune system–related proteins localize to the LDs of infected cells: (i) viperin, which is active against two viruses assembled on LDs (HCV and DENV) (*6*); (ii) interferon-γ (IFN-γ)–inducible guanosine triphosphatase (GTPase) (IGTP), which is required for resistance to *Toxoplasma gondii* (*7*); and (iii) histones on LDs, which increase the survival of bacterially challenged *Drosophila* embryos (*8*). We analyzed whether mammalian LDs have a direct or regulated role in immune defense. Because all eukaryotic cells accumulate LDs, this innate defense mechanism may be ubiquitous and therefore serve as a suitable target for therapeutic intervention.

Results

Mammalian LDs display regulated protein-mediated antibacterial activity

We selected hepatic LDs as a proof of concept that mammalian LDs participate in innate immunity. The liver modulates the systemic immune response, and hepatic LDs are targeted by LD-related pathogens (*9*). We tested the antibacterial capacity of hepatic LD proteins in a bacterial killing assay of *Escherichia coli*, an abundant component of the intestinal microbiota and cause of serious clinical infections. First, we injected mice with lipopolysaccharide (LPS), an activator of innate immunity (*10*). Because LPS-treated animals (LPS-mice) reduce food intake, LPS-mice were additionally fasted and compared with mice injected with saline buffer and identically fasted (CTL-mice). Both treatments promoted similar hepatic triglyceride levels (Fig. 1, A, B, and C), although morphological differences between LDs were evident from transmission electron microscopy (TEM). The number of LDs in LPS-treated livers (LPS-LDs) was higher than in those of fasted animals (CTL-LDs), although LPS-LDs were smaller (Fig. 1, D and E). CTL- and LPS-LDs were purified (Fig. 1F and fig. S1A), and LD proteins were incubated with *E. coli*. Bacterial viability was estimated from the resulting colony-forming units (CFUs). LD proteins reduced bacterial growth, and LPS-LD proteins demonstrated enhanced antibacterial capacity (Fig. 1G). This enhancement was confirmed in suspension cultures (fig. S1C) and by use of LD proteins from fed mice (fig. S1, D and E). To determine LD antibacterial activity during an actual infection, mouse liver LDs were obtained after cecal ligation and puncture (CLP), a model of polymicrobial sepsis. CLP-LD proteins exhibited enhanced antibacterial capacity when compared with CTL-LDs (fig. S1, B and F). LPS- and CLP-LD proteins reduced bacterial growth even after a shorter incubation time (fig. S1, G and H). Bacterial growth was unaffected by oleic acid (OA), the major fatty acid component of hepatic LDs, or by cytosolic proteins from CTL- and LPS-livers (fig. S1, I and J). Thus, mammalian LDs have a protein-mediated antibacterial capacity, which is regulated by infection.

Next, we analyzed whether LDs reduce bacterial growth in human monocyte-derived macrophages (HMDMs) from healthy donors. In HMDMs, LD accumulation was promoted by incubation with OA, a fatty acid efficiently esterified into LDs (*11*). Untreated and LD-loaded HMDMs were infected with either nonpathogenic *E. coli* or the professional intramacrophage pathogen *Salmonella enterica* serovar Typhimurium (*Salm*). HMDMs responded to infection by increasing LD numbers (Fig. 1H). *E. coli* survival (Fig. 1I), but not phagocytic capacity (Fig. 1K), was reduced in LD-loaded HMDMs. By contrast, LDs did not reduce *Salm* survival (Fig. 1J), which is in keeping with this pathogen's ability to avoid antimicrobial responses (*12*). In *E. coli*–infected macrophages, LDs were often in the proximity of bacteria (Fig. 1, M to Q). Comparative analyses demonstrated that LDs were closer to and more frequently established longer contacts with *E. coli* than with *Salm* (Fig. 1L and fig. S2, A and B). These LD–*E. coli* contact sites increased in loaded HMDMs (fig. S2, C and D). TEM analysis revealed that in LD–*E. coli* contact sites, the LD monolayer (containing LD proteins) produced an apparent discontinuity in

[1]Cell Compartments and Signaling Group, Institut d'Investigacions Biomèdiques August Pi i Sunyer (IDIBAPS), 08036, Barcelona, Spain. [2]Department of Biomedical Sciences, Faculty of Medicine, Universitat de Barcelona, 08036, Barcelona, Spain. [3]Mechanoadaptation and Caveolae Biology Laboratory, Cell and Developmental Biology Area, Centro Nacional de Investigaciones Cardiovasculares (CNIC). 28029, Madrid, Spain. [4]Institute for Molecular Bioscience (IMB), University of Queensland, Brisbane, Queensland 4072, Australia. [5]IMB Centre for Inflammation and Disease Research, University of Queensland, Brisbane, Queensland 4072, Australia. [6]Australian Infectious Diseases Research Centre, University of Queensland, Brisbane, Queensland 4072, Australia. [7]Laboratório de Imunofarmacologia, Instituto Oswaldo Cruz, FIOCRUZ, Rio de Janeiro, RJ, CEP 21.040-900, Brazil. [8]Cardiovascular Proteomics Laboratory, Vascular Pathophysiology Area, CNIC, Instituto de Salud Carlos III 28029, Madrid, Spain. [9]Centro de Investigación Biomédica en Red, Enfermedades Cardiovasculares (CIBER-CV), Instituto de Salud Carlos III 28029, Madrid, Spain. [10]Department of Cell Death and Proliferation, Institut d'Investigacions Biomèdiques de Barcelona (IIBB)–CSIC, Barcelona, Spain. [11]Hepatocellular Signaling and Cancer Team, IDIBAPS, 08036, Barcelona, Spain. [12]Centre for Microscopy and Microanalysis, University of Queensland, Brisbane, Queensland 4072, Australia. [13]Immunoreceptors of the Innate and Adaptive System Team, IDIBAPS, 08036, Barcelona, Spain. [14]Department of Developmental and Cell Biology, University of California, Irvine, Irvine, CA 92697, USA. [15]Institució Catalana de Recerca i Estudis Avançats (ICREA), 08010, Barcelona.
*Corresponding author. Email: martabosch@ub.edu (M.B.); r.parton@imb.uq.edu.au (R.G.P.); apols@ub.edu (A.P.) †These authors contributed equally to this work.

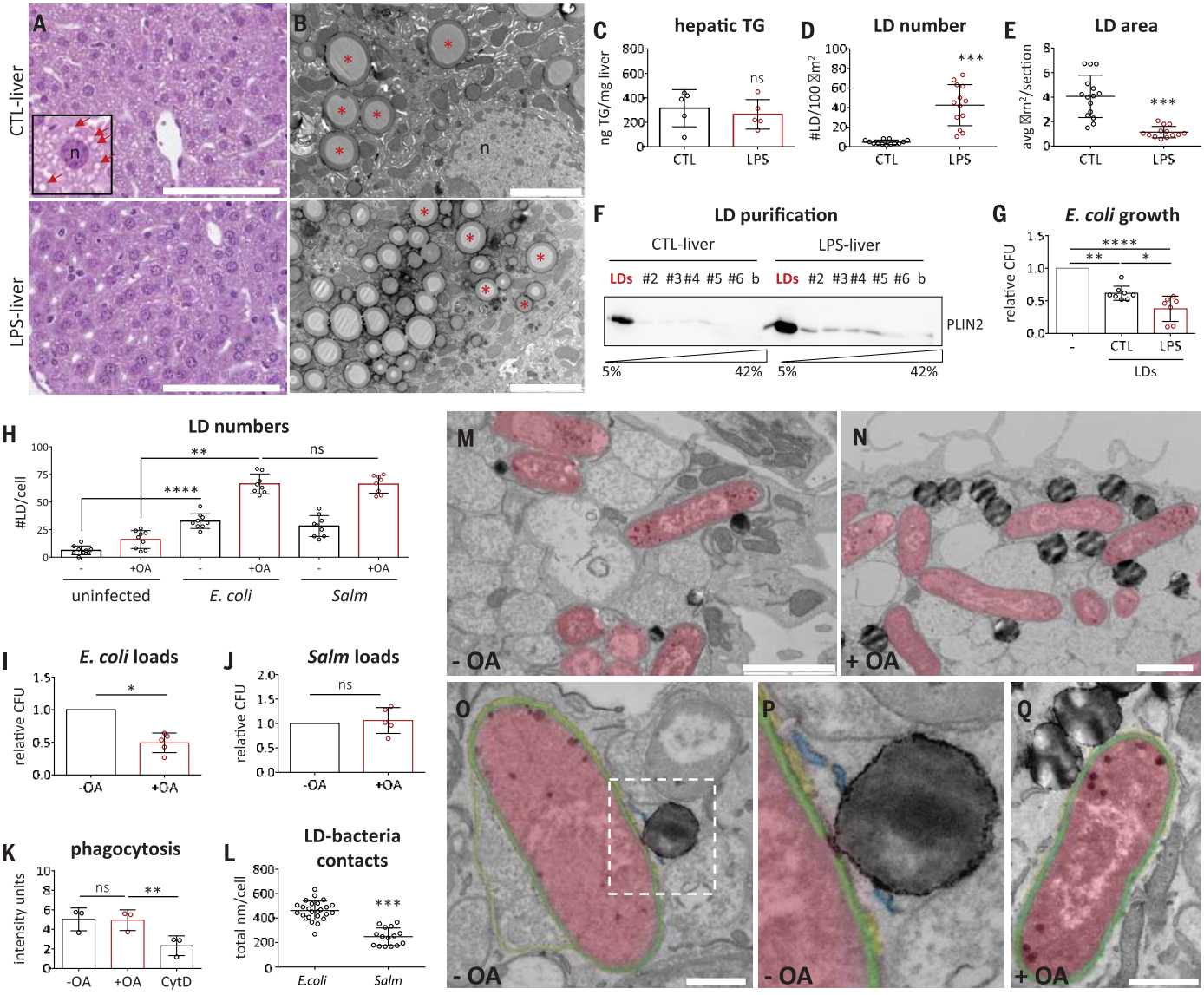

Fig. 1. Mammalian LDs display regulated protein-mediated antibacterial activity. (**A**) H&E-stained sections and (**B**) TEM images of (top) CTL- or (bottom) LPS-livers. Red arrows [(A), inset] and asterisks (B) indicate LDs, and "n" indicates the selected hepatocyte nucleus. Images are representative of (A) five or (B) two mice per condition. Scale bars, 100 μm (A) and 5 μm (B). (**C**) Hepatic triacylglycerol levels (TG) in CTL- and LPS-mice (five mice per condition). (**D**) Hepatic LD number and (**E**) mean LD area measured in TEM images of CTL- or LPS-livers. For each condition, at least 13 random liver sections, obtained from two mice per condition, were quantified (fig. S6). (**F**) CTL- and LPS-livers were fractionated in sucrose density gradients, and LDs floated onto the top fraction ("LDs"), as assessed with anti-PLIN2 immunoblotting (fig. S1A) (representative of five mice per condition). (**G**) *E. coli* were incubated for 16 hours in (gray) standard medium or medium supplemented with proteins from (black) CTL- or (red bar) LPS-LDs. CFU measurements were normalized to the standard medium condition ($n \geq 7$ independent experiments) (fig. S1). (**H**) Unloaded (black) and OA-loaded HMDMs (red bars) were infected with *E. coli* or *Salm* for 4 hours. LD number per cell was quantified in TEM images. At least eight macrophages per group, obtained in three independent experiments, were analyzed. (**I** and **J**) Control (black) and OA-loaded HMDMs (red bars) were infected with (I) *E. coli* or (J) *Salm* and bacterial loads (CFU) determined 24 hours later ($n = 5$ independent experiments). (**K**) Control (black) and OA-loaded HMDMs (red bars) were incubated with pHrodo *E. coli* and bacterial loads measured (fluorescence units) ($n = 3$ independent experiments). Cyt D was used to inhibit phagocytosis. (**L**) Length of LD-bacteria contacts per cell was measured in TEM images of OA-loaded HMDMs infected with *E. coli* or *Salm* for 4 hours. At least 15 macrophages per group, obtained in three independent experiments, were analyzed (fig. S2, A to D). (**M**, **O**, and **P**) Control and (**N** and **Q**) OA-loaded HMDMs were infected with *E. coli* for 4 hours and analyzed in TEM images. Representative images have been pseudocolored blue (ER), red (*E. coli* interior), green (periplasm), and yellow (vacuolar membrane) (fig. S2, E and F) (representative of three independent experiments). Scale bars, 2 μm [(M) and (N)] and 0.5 μm [(O) and (Q)]. All graphs show means ± SD; ns, not significant; $*P < 0.05$, $**P < 0.01$, $***P < 0.001$, $****P < 0.0001$ in a paired *t* test [(C) to (E), (H) to (J), and (L)], and one-way ANOVA test [(G) and (K)].

the bacterial vacuolar membrane and probably interacted with the bacterial periplasm (Fig. 1, O to Q, and fig. S2, E and F). Thus, LD-loaded macrophages display enhanced antibacterial capacity, which suggests the existence of docking mechanisms that enable or facilitate the engagement of antibacterial LD proteins with bacteria.

Quantitative mass spectrometry analysis of LPS-LDs

To characterize the enhanced LPS-LD antibacterial capacity, we performed comparative mass spectrometry profiling of proteins differentially associated with LPS- or CTL-LDs (*13*). CTL- and LPS-livers were analyzed in parallel. Stringent analysis [false discovery rate (FDR) < 1] of LPS-livers identified 8563 proteins, of which 1136 (cut-off $|\Delta Zq| \geq 1.8$, where ΔZq reflects the differential Zq score for a protein in LPS-livers when compared with CTL-livers.) were differentially expressed (553 enriched and 583 reduced) (Fig. 2A and tables S1 and S2). In LPS-LDs, 3392 proteins were identified (table S3), of which 689 were differentially distributed (317 enriched and 372 reduced) (tables S4 and S5). Only 8% of the enriched and 0.8% of the down-regulated proteins in LPS-LDs followed an equivalent profile in LPS-livers (Fig. 2, A and B, and fig. S3A), indicating autonomous changes in LPS-LDs. Functional annotation enrichment analysis revealed the up-regulation of proteins related to the acute phase and inflammatory responses and reduction of mitochondrial proteins cofractionating with LDs (Fig. 2B and fig. S2A).

Published proteomic analyses show that ~7 to 10% of proteins in LD fractions are bona fide LD-resident proteins (*14*, *15*), reflecting the tight interaction of LDs with other organelles. Of 3392 identified proteins in LPS-LDs, 238 (7%) were annotated as LD-resident proteins with the Ingenuity Pathway Analysis (IPA) platform or with at least one of the above proteomic analyses (Fig. 2C and table S6). Of these LD proteins, 72 were LPS-regulated (59 enriched and 13 reduced) (table S7). Thus, 30% of the identified LD proteome, including the five perilipins (PLINs), was LPS-sensitive. PLIN2 (ΔZq = 6.47) and RAB18 (ΔZq = 7.10) were highly enriched, and PLIN5 was the only down-regulated PLIN (ΔZq = −4.13) (table S7). Two immune proteins previously described on LDs, viperin (RSAD2, ΔZq = 8.12) and IGTP (IRGM3, ΔZq = 6.7), were identified on LPS-LDs, validating our proteomic strategy (table S4). IPA analysis of these LD-resident proteins demonstrated enrichment of innate immunity–related components and reduction of metabolism-related LD-resident proteins (fig. S3B).

To identify relevant candidates on LPS-LDs, we initially performed hierarchical clustering of proteins with similar variation profiles across each individual replicate, likely reflecting coregulation (Fig. 2D). Gene interaction analysis of correlated proteins revealed the existence of several functionally connected protein networks, such as clusters of RAB GTPases, a cluster containing PLIN1 and histones, and a network of metabolism regulators, including PLIN3, PNPLA2 (ATGL), and ACSL4 (fig. S4A). The cluster containing proteins ranking highest for enrichment (ΔZq > 3.14) nucleated around PLIN2 and included viperin, IGTP, and several immune GTPases (GVIN, IFGGA1, IFGGB55, IFI47, and IFI35) (Fig. 2D). These functionally related proteins may also physically interact. We confirmed that PLIN2 interacts with IGTP (*7*) and detected a weak interaction with cathelicidin (fig. S4B). Last, we performed a gene interaction analysis across the whole LPS-sensitive LD proteome (ΔZq > 1.8). This analysis retrieved complex protein networks (Fig. 2E), suggesting that LDs are innate immune hubs integrating major intra- and extracellular responses.

We validated the proteomic data with immunoblotting and confirmed enrichment of PLIN2 and PLIN3 on LPS-LDs in contrast with the unregulated lipase HSL (ΔZq = 0.04) (Fig. 3A). PLIN2 expression was further confirmed in mouse liver sections (fig. S5A). PLIN2 in LPS- and CLP-livers was predominantly expressed in hepatocytes around periportal regions where cells receive blood and regulatory inflammatory mediators. Direct transcriptional regulation of LD proteins by inflammatory stimuli (fig. S5B) was assessed in human hepatic HuH7 cells treated with LPS, tumor necrosis factor (TNF), or IFN-γ. *PLIN2* and *PLIN5* expression was differentially regulated by individual cytokines (fig. S5C). Thus, LPS likely regulates LD protein composition directly and in conjunction with paracrine signaling networks.

Physical and functional uncoupling of LPS-LDs and mitochondria

Mitochondria are key organelles for innate immunity (*16*). During nutrient starvation, LDs contact mitochondria to supply fatty acids, fueling oxidative phosphorylation (OXPHOS) (*17*). By contrast, challenged innate immune cells increase aerobic glycolysis and reduce OXPHOS (*16*). Therefore, uncoupling LPS-LDs and mitochondria (Fig. 2B) may contribute to a reduction of OXPHOS in infected cells. Reduced interaction between LPS-LDs and mitochondria was confirmed through decreased cofractionation of ATP5D [a subunit of adenosine 5′-triphosphate (ATP) synthase, an OXPHOS enzyme] when compared with CTL-LDs (Fig. 3, A and B). Functional annotation of reduced mitochondrial proteins cofractionating with LPS-LDs matched with the whole mitochondrial proteome (MitoCarta 2.0) (Fig. 3C). This does not reflect a reduced mitochondrial content of LPS-livers as determined by hepatic citrate synthase activity and liver cytochrome oxidase (*COI*) gene copy number (Fig. 3, D and E). The reduced number of contacts between LPS-LDs and mitochondria was then confirmed with TEM (Fig. 3F and fig. S6). In these images, endoplasmic reticulum (ER) membranes often separated LPS-LDs and mitochondria (fig. S6C). Last, we confirmed two functional consequences of uncoupling: (i) reduced mitochondrial β-oxidation of lipids supplied by LDs in LPS-primary hepatocytes (Fig. 3, G and H) and (ii) lower levels of circulating ketones in LPS-mice serum (Fig. 3I). These results extend and mechanistically explain early observations showing reduced β-oxidation and ketogenesis in rats infected with *Streptococcus pneumoniae*, *Francisella tularensis*, and *S.* Typhimurium (*18*).

PLIN5 tethers LDs and mitochondria (*17*). PLIN5 is the only PLIN down-regulated in LPS-LDs (fig. S3B and tables S5 and S7). During fasting, to facilitate LD-mitochondria contacts, PLIN5 levels increase on hepatic LDs (Fig. 3J). However, PLIN5 levels on LDs were reduced when fasted mice were treated with LPS (Fig. 3, A and J). Further, human *PLIN5* expression promoted coclustering of LDs and mitochondria in HuH7 cells (Fig. 3K). To explore the role of PLIN5 during infection, *PLIN5* was transfected in LPS-responsive human embryonic kidney (HEK) 293-TLR4$^+$ cells (fig. S7, A to C), and the LD-mitochondria contacts were quantified. *PLIN5* expression increased the number and length of these contacts (Fig. 3L and fig. S7, D to F). In LPS-treated HEK293-TLR4$^+$ cells, the overall length of the contacts was reduced in CTL- but not in *PLIN5*-expressing cells (Fig. 3L). In *PLIN5*-expressing cells, LPS only modestly reduced the total number of contacts (fig. S7E) and increased the average length of remaining contacts (fig. S7F). Thus, LPS directly regulates dynamics of LD-mitochondria contacts. Furthermore, PLIN5 down-regulation appears to be involved in the LPS-induced metabolic reprogramming.

We next evaluated the role of PLIN5 in other aspects of immune defense. *PLIN5*-overexpressing HEK293 cells exhibited a significantly reduced capacity to clear *E. coli* by comparison with that of *PLIN3*-overexpressing control cells (Fig. 3, M and N). Furthermore, THP-1 cells lentivirally transduced with *PLIN5* and subsequently infected with *E. coli* exhibited increased numbers of LD-mitochondria contacts (fig. S7, G to I), reduced LD-bacteria interactions (fig. S7J), and impaired antimicrobial capacity (Fig. 3, O and P). Thus, LPS-mediated PLIN5 down-regulation reduces LD-mitochondria tethering, enabling an effective antimicrobial response.

LDs accumulate and use innate immune proteins

Our proteomic analyses predicted complex immune protein networks on LDs (Fig. 2, D and E,

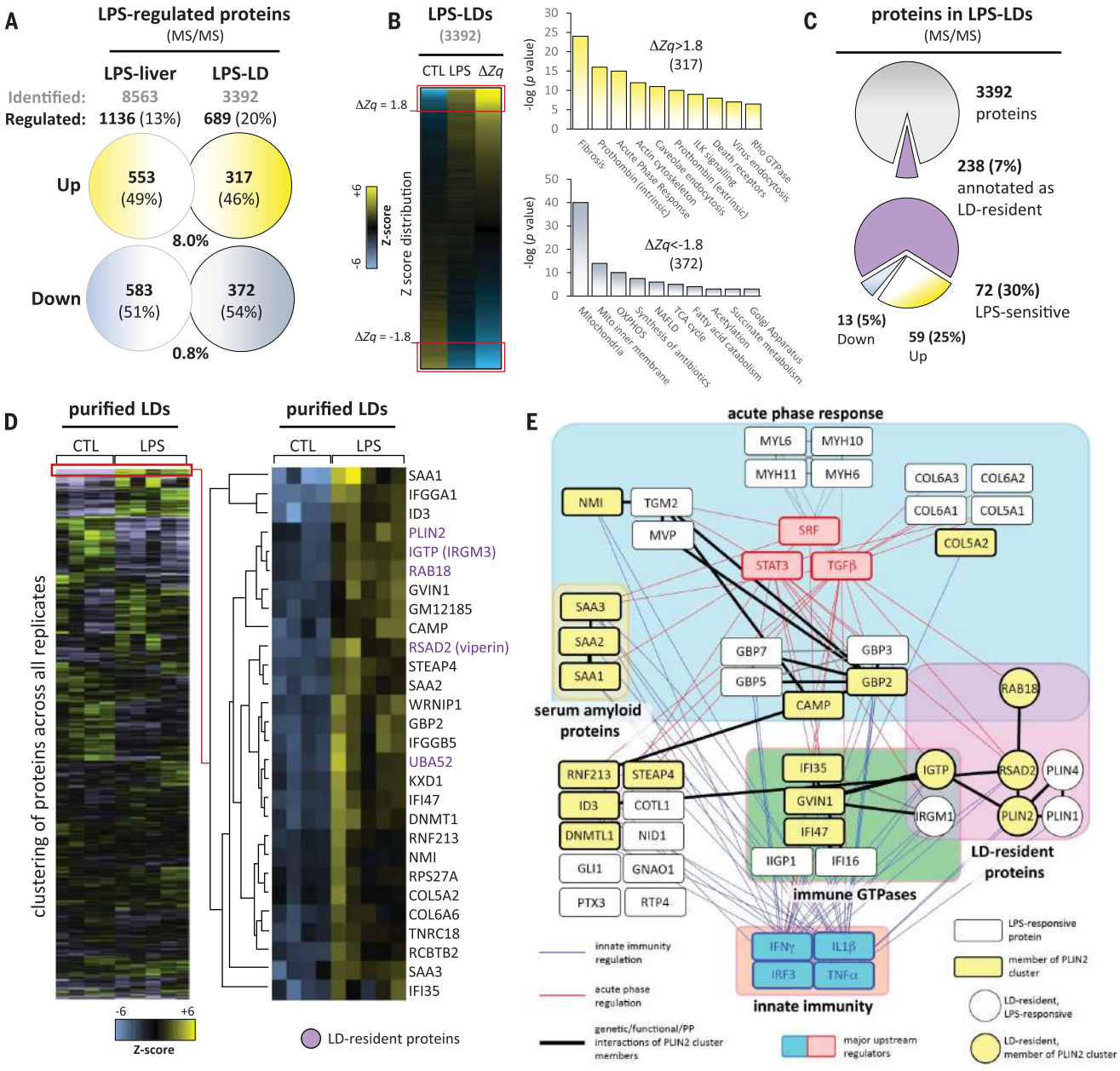

Fig. 2. Quantitative mass spectrometry analysis of LPS-LDs. (**A**) Summary of changes in the proteome of LPS-livers (n = 3 independent mice) and LPS-LDs (n = 5 independent LD fractions) when compared with those in CTL-livers (n = 3 independent mice) or CTL-LDs (n = 4 independent LD fractions), respectively. "Identified" (gray letters) indicates identified proteins, and "Regulated" (black letters) indicates proteins significantly cut-off $|\Delta Zq| \geq 1.8$ modified by LPS. Among modified proteins, yellow and blue circles indicate up- and down-regulated proteins, respectively (tables S1 to S5). (**B**) Functional annotation enrichment analysis of proteins increasing ($|\Delta Zq| > 1.8$; yellow graphs) or decreasing ($|\Delta Zq| < -1.8$; blue graphs) on LPS-LDs when compared with CTL-LDs. Enrichment as compared with the mouse genome for each category is expressed as −log (P value). Analyses for CTL- and LPS-livers are shown in fig. S3A. (**C**) Pie charts summarizing LPS-induced changes in bona fide LD proteins. Protein details are in tables S6 and S7, and annotated interactions are provided in fig. S3B. (**D**) Hierarchical clustering of Zq values across replicates identifies functionally coherent protein subsets similarly regulated by LPS [threshold for cluster analysis, correlation coefficient (r) > 0.78]. The cluster nucleated around PLIN2 is included. Five additional clusters are detailed in fig. S4A. (**E**) Gene subnetwork from IPA analysis of all identified proteins up-regulated in LPS-LDs.

and fig. S4A). Given that many known antipathogenic proteins were associated with the PLIN2 cluster (Fig. 2D), we next assessed components of this cluster for LD association. The antiparasitic protein IGTP and the antiviral protein viperin as well as three GTPases (IIGP1, TGTP1, and IFI47) all associated with LDs (Fig. 4, A to C, and figs. S8 and S9). Thus, multiple proteins associated with responses to different classes of pathogens localize to LDs.

The PLIN2 cluster also includes cathelicidin (CAMP; ΔZq = 7.25), a broad-spectrum antimicrobial peptide with chemotactic and immunomodulatory properties (*19*). Cathelicidins are synthesized as proproteins which, after cleaving an N-terminal signal peptide, follow the exocytic pathway (fig. S10A). We confirmed the accumulation of CAMP on LPS-LDs (Fig. 4A) and the distribution of a human-tagged CAMP between the ER and LDs of HuH7 cells (Fig. 4B and fig. S10, B to E). CAMP on LDs had a

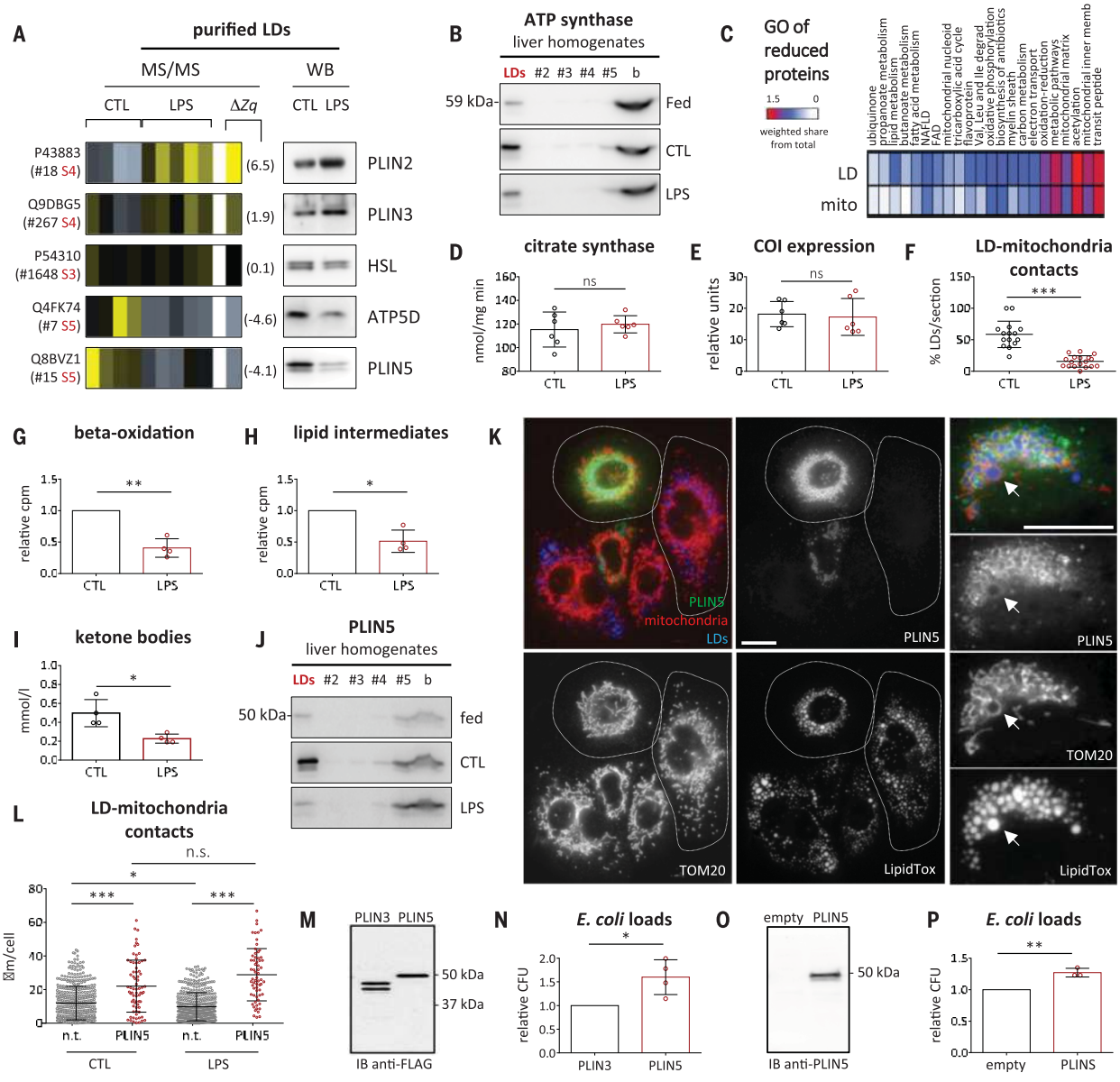

Fig. 3. Physical and functional uncoupling of LPS-LDs and mitochondria.
(**A**) Relative enrichment of selected proteins. Protein enrichment in LPS-LDs illustrated by a heatmap code (blue, depletion; yellow, enrichment). The Δ*Zq*, UniProt ID, ranking (tables S3 to S5), and a representative immunoblot (representative of three mice per condition) are indicated. (**B**) Fed-, CTL-, and LPS-livers were fractionated in sucrose gradients, and LD–mitochondria cofractionation was determined through immunoblotting of ATP5D (a subunit of ATP synthase) (representative of three mice per condition). (**C**) Functional categories of down-regulated mitochondrial proteins cofractionating with LPS-LDs are compared with the whole mitochondrial proteome (MitoCarta 2.0). (**D** and **E**) The mitochondrial content of CTL- (black) and LPS-livers (red bars) was determined from (D) citrate synthase activity and (E) DNA copy number of COI (relative to GAPDH) (n = 6 independent livers). (**F**) Percentage of LDs interacting with mitochondria in CTL- (black) and LPS-livers (red bars) was quantified in TEM images. At least 15 random sections, obtained from two mice per condition, were analyzed (fig. S6). (**G**) Mitochondrial beta-oxidation and (**H**) formation of soluble intermediates (ketone bodies) of lipids stored in LDs were quantified for 16 hours in primary hepatocytes left untreated (black) or treated with LPS (red bars) (four mice per condition). (**I**) Ketones in sera of CTL- (black) and LPS-mice (red bars) (four mice per condition). (**J**) Fed-, CTL-, and LPS-livers were fractionated in density gradients and PLIN5 distribution analyzed by immunoblotting (representative of five mice per condition). (**K**) HuH7 cells were transfected with a tagged *PLIN5* and labeled with anti-FLAG antibodies (PLIN5), anti-TOM20 antibodies (mitochondria), and LipidTox (LDs). Contours of a representative transfected and nontransfected cell are indicated. (Right) An additional transfected cell. The arrows indicate a mitochondrion completely enwrapping a LD (representative of three independent experiments). Scale bar, 20 μm. (**L**) LPS-sensitive HEK293-TLR4$^+$ cells transfected with a tagged *PLIN5* were loaded with OA (black) or with OA+LPS (red dots). The length of LD-mitochondria contacts per cell was measured in confocal microscopy images (an example is available in fig. S7, D to F). Sixty-six transfected cells and 470 nontransfected cells, obtained from three independent experiments, were analyzed. (**M** and **N**) HEK293 cells were transfected with FLAG-tagged *PLIN3* or *PLIN5* and loaded with OA, and (M) protein expression was determined by means of immunoblotting. (N) Cells were infected with *E. coli*, and bacterial loads quantified after 4 hours (n = 4 independent experiments). (**O** and **P**) THP-1 cells were transduced with *PLIN5*-encoding or empty lentiviral vectors. (O) PLIN5 expression was confirmed through immunoblotting. (P) Transduced cells were infected with *E. coli*, and bacterial loads were evaluated after 8 hours (n = 3 independent experiments) (fig. S7, G to J). All graphs show means ± SD; ns, not significant; $^*P < 0.05$, $^{**}P < 0.01$, $^{***}P < 0.001$, in a paired t test [(D), (E), (G) to (I), (M), and (N)], one-way ANOVA test (L), and two-sided Student's z test on proportions (F).

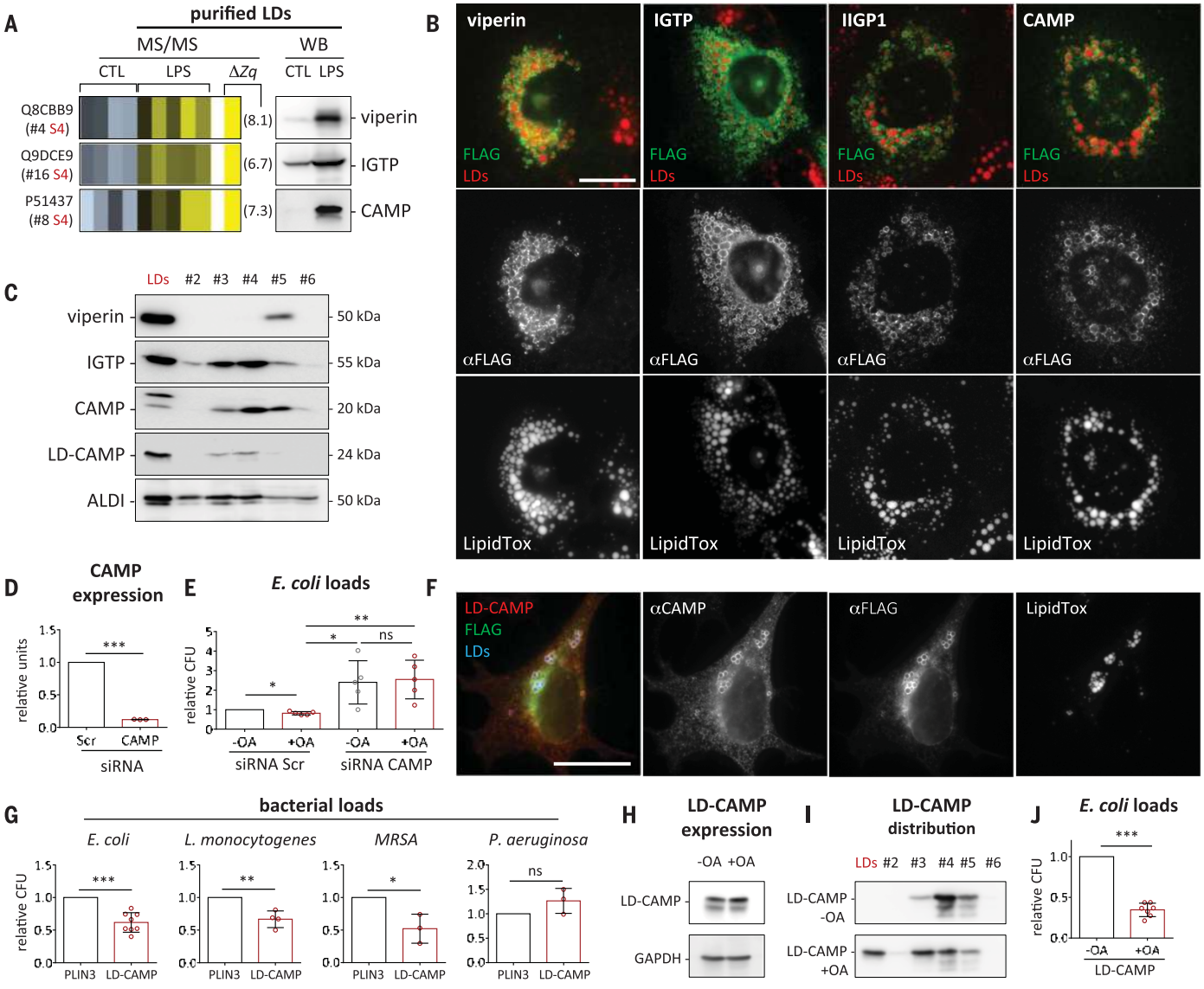

Fig. 4. LDs accumulate and use innate immune proteins. (**A** to **C**) Relative enrichment of selected proteins. Protein enrichment in LPS-LDs was evaluated as in Fig. 3. Accumulation of transfected proteins on LDs was confirmed in HuH7 cells by means of (B) immunofluorescence and (C) fractionation in density gradients (figs. S8 to S10 and S12). Scale bar, 20 μm. (**D** and **E**) HMDMs were transfected with a scrambled (Scr) or with a CAMP siRNA, and (D) CAMP expression was determined by means of quantitative RT-PCR. Then, unloaded and OA-loaded HMDMs were infected with *E. coli* for 8 hours, and bacterial loads (CFU) were quantified (n = 5 independent experiments). (**F**) HEK293 cells were transfected with a tagged LD-*CAMP* (fig. S12) and loaded with OA. LD-CAMP was detected on LDs (LipidTox) with antibodies to FLAG and to CAMP. The image is representative of three independent experiments. Scale bar, 20 μm. (**G**) HEK293 cells were transfected with LD-*CAMP* (red) or *PLIN3* (black bars), loaded with OA, and infected with the indicated bacteria for 4 hours. Bacterial loads were quantified, and CFU values were normalized to *PLIN3*-cells ($n \geq 3$ independent experiments). (**H** to **J**) LD-*CAMP*–transfected HEK293 cells were incubated in control (black) or OA containing medium (red). (H) Cellular LD-CAMP levels and (I) LD accumulation were assessed through immunoblotting with anti-CAMP antibodies. (J) These cells were then infected with *E. coli* for 4 hours, and bacterial loads were quantified (n = 7). All graphs show means ± SD; ns, not significant; $^*P < 0.05$, $^{**}P < 0.01$, $^{***}P < 0.001$ in a paired t test.

higher molecular weight than that of CAMP in the ER (Fig. 4C and fig. S10E), suggesting that the CAMP hydrophobic domain functions as both a signal peptide cleaved for secretion via the ER as well as an uncleaved LD-targeting signal. An equivalent dual distribution occurs for other LD proteins that contain signal peptides, such as apolipoproteins (*20*). The low–molecular weight (20 kDa) CAMP species corresponded to the protein with a cleaved signal peptide following the secretory pathway (fig. S10, F to H). Distribution of overexpressed CAMP, as well as other immune LD proteins, was not directly affected by LPS-TLR4 signaling (fig. S11). Thus, LPS does not directly regulate the intracellular trafficking of these proteins.

We next investigated the role of CAMP in HMDMs. Silencing of *CAMP* (Fig. 4D) impaired the antibacterial response of the macrophages against *E. coli* (Fig. 4E). Furthermore, although LD loading significantly reduced bacterial survival, this treatment regime was unable to do so in CAMP-silenced HMDMs. Thus, the antibacterial activity of LDs in HMDMs appears to require CAMP. To further explore this possibility, a LD-resident CAMP was engineered through substitution of the CAMP signal peptide with

the ALDI LD-targeting motif (fig. S12, A and B) (*21*). Modified CAMP (LD-CAMP) accumulated on LDs of HuH7 cells (fig. S12, C to F) and showed a single electrophoretic mobility pattern, matching the higher–molecular weight CAMP that localized to LDs (Fig. 4C and fig. S12C). Next, HEK293 cells were transfected with LD-*CAMP*, and protein distribution on LDs was confirmed with antibodies to CAMP (Fig. 4F), demonstrating a native conformation. The antimicrobial capacity of LD-CAMP was then assessed. Bacterial loads of *E. coli*, *Listeria monocytogenes*, and methicillin-resistant *Staphylococcus aureus* (MRSA) were significantly reduced in LD-*CAMP*–expressing cells when compared with those expressing the *PLIN3* control (Fig. 4G). By contrast, *Pseudomonas aeruginosa* loads were not affected by LD-*CAMP*, suggesting that this pathogen subverts this innate defense response. The impact of LD-*CAMP* overexpression on bacterial survival was dependent on LD formation (Fig. 4, H to J). The tagged LD-*CAMP* demonstrated a similar antibacterial activity to that of wild-type *CAMP* and a slightly augmented stability when compared with an untagged LD-*CAMP* (fig. S12, G to J). Thus, LDs act as a molecular switch in innate immunity, responding to danger signals by both reprogramming cell metabolism and eliciting protein-mediated antimicrobial defense.

Discussion

Pathogens require host-derived lipids to support their life cycles, with LDs providing a source of these lipids (*22*). As a result, LDs also have the potential to deliver effective host defenses against intracellular pathogens. We show that at least 30% of the LD proteome is LPS-sensitive, suggesting that innate immunity has developed a host defense program that includes extensive LD remodeling. Our analyses demonstrate that complex clusters of immunity-related proteins organize on LDs of infected cells. In addition to previously described LD-resident immune proteins, such as viperin and IGTP, we have identified IIGP1, TGTP1, and IFI47. Our analysis also identified CAMP as a professional antibacterial protein efficiently functioning on LDs. These proteins may act individually, in a coordinated manner, and/or synergistically to kill pathogens.

Mechanisms of LD trafficking and docking with phagocytic and parasitophorous membranes, observed here and described for several pathogens (*23*–*26*), may facilitate the delivery of immune proteins located on the LD surface. Accumulation on LDs may provide stability to these proteins and may restrict these potentially cytotoxic peptides to LDs, preventing indiscriminate cellular damage (*27*). In this respect, we have shown that LPS triggers physical separation of LDs and mitochondria, at least partly because of reduced PLIN5 levels on LPS-LDs (*28*). Uncoupling likely reflects both a self-protection program (to avoid mitochondrial damage, in view of their prokaryotic evolutionary origin) and a means to maximize or increase the number of LDs available to interact with bacteria. Simultaneously, the reduced LD-mitochondria interaction may lead to distinctive immunometabolic features: (i) the accumulation of host LDs, resulting from reduced mitochondria-mediated LD consumption; (ii) reduced OXPHOS displayed by infected cells, owing to decreased fatty acid oxidation; and (iii) the low rates of ketogenesis displayed by infected animals.

These studies highlight that mammalian LDs constitute an intracellular first line of defense. LDs actively participate in at least two levels of the innate immune response, accumulating and using antibacterial proteins as well as regulating immune cell metabolism. Because widespread resistance to current antibiotics is common among pathogens, understanding the cellular mechanisms that elicit LD-mediated defense may inform future strategies for the development of anti-infective therapies (*29*, *30*).

Materials and methods

Plasmids

pCMV6-*IGTP*-myc-FLAG (MR224617), pCMV6-*CAMP*-myc-FLAG (RC208872), pCMV6-*IIGP1*-myc-FLAG (MR206520), pCMV6-*TGTP1*-myc-FLAG (MR206553), and pCMV6-*IFI47*-myc-FLAG (MR206684) were purchased from OriGene Technologies (Rockville, Maryland). pcDNA3.1-*VIPERIN*-FLAG (OHu13432) was from Genscript (Piscataway, New Jersey). pcDNA3.1- *PLIN5*-FLAG (OHu04126) from GenScript was subcloned into pCMV6-myc-FLAG vector using primers containing EcoRI and XmaI sites. The LD-*CAMP* construct was derived from the plasmid pCMV6-*CAMP*-myc-FLAG: an equivalent EcoRI/BspEI sequence of pCMV6-*CAMP*-myc-FLAG was designed replacing the *CAMP* signal peptide (MKTQRDGHSLGRWSLVLLLLGLVMPLAII) with the hydrophobic domain of *ALDI* (MDALVLFLQLLVLLLTLPLHLLALLGC) acquired from GeneScript, cloned in a PUC57 plasmid. Both fragments were swapped after an EcoRI/BspEI digestion. *CAMP* ΔN mutant, results from deletion of the amino acids 1-32. The cDNAs were acquired from GenScript and subcloned into pCMV6-myc-FLAG vector following the same strategy. pCMV6-*CAMP*-untagged was generated by polymerase chain reaction (PCR) using primers containing EcoRI and XmaI sites. The plasmid pCMV6-*PLIN2*-myc-FLAG tagged was derived from the plasmid pGFP-*PLIN2*, provided by Dr John McLauchlan (Institute of Virology, Glasgow) and subcloned into pCMV6 by PCR using primers containing EcoRI and XhoI sites. The plasmid pCMV6- *PLIN3*-myc-FLAG tagged was derived from the plasmid pCDNA 3×myc-tagged *PLIN3* provided by S. Pfeffer (Stanford University School of Medicine, Stanford, California), and subcloned into pCMV6 by PCR using primers containing EcoRI and XhoI sites. The lentiviral system utilizing pFTRE3G-PGK-puro (kindly provided by James Murphy, Walter and Elizabeth Hall Institute of Medical Research) for doxycycline-inducible gene expression has previously been described (*31*, *32*). The plasmid pFTRE3G-*PLIN5* was obtained by subcloning *PLIN5* into pFTRE3G by PCR using primers containing BamHI sites.

Mouse studies

Animals and models of infection

C57BL/6J male mice (8 to 10 weeks old) were purchased from Charles River Laboratories (Wilmington, Massachussetts). Animals were kept under a controlled humidity and lighting schedule with a 12 hours dark period. Food and water were available ad libitum. All animals received humane care in compliance with institutional guidelines regulated by the European Community. The experimental protocols were approved by the Animal Care Committee of the University of Barcelona. The day before the experiment, animals were fasted overnight (16 hours) and in some cases intraperitoneally injected with 200 μl of saline buffer (CTL) or 6 mg/kg LPS (final dose) (L2639, Sigma-Aldrich, St Louis, Missouri). In some experiments (fed condition) food was available ad libitum. To induce sepsis by cecal ligation and puncture (CLP), mice were anesthetized with an intraperitoneal injection of 100 mg/kg ketamine (Richter Pharma AG, Wels) and 10 mg/kg xylazine (Rompun, Bayer, Leverkusen, Germany) and a 1-cm incision was made on the abdomen. The cecum was exposed and ligated below the ileocecal junction. A double puncture was made using a 22G needle, to induce severe sepsis. Sham-operated animals (CTL) underwent an identical laparotomy but without CLP. All mice received 1 ml of sterile saline subcutaneously as fluid resuscitation and antibiotic therapy by subcutaneous injection of 10 mg/kg meropenen (Merck Research Laboratory, Whitehouse Station, New Jersey) 6 hours after surgery.

Histological analysis

Liver sections were prepared and processed for hematoxylin and eosin (H&E) staining as previously described (*33*). For immunohistochemistry, liver sections were prepared and processed as described previously (*34*). The slides were blocked by incubation in 5% normal goat serum in PBS for 1 hour at room temperature followed by incubation with anti-PLIN2 antibody (1:200; ab78920, Abcam, Cambridge, UK) overnight at 4°C. Sections were then washed three times in PBS and incubated with secondary goat anti-rabbit immunoglobulin G (IgG) Alexa Fluor 647 (1:250; A21244, ThermoFisher Scientific, Waltham, Massachussetts)

for 45 min at RT. After washing three times in PBS, slides were mounted with Dako Fluorescence Mounting Medium (Agilent Dako, #S3023).

Liver fractionation and hepatic LD purification

After liver perfusion with 0.9% NaCl and 0.1% EDTA solution, the liver was placed on a Petri dish, chopped with a scalpel for two min and transferred into a Dounce tissue grinder at a ratio of 1 g of tissue to 3 ml of homogenization buffer (25 mM Tris-HCl, pH 7.5, 100 mM KCl, 1 mM EDTA, and 5 mM EGTA). After three up-and-down strokes of each loose- and tight-pestle, the liver homogenate was centrifuged at 500*g* for 10 min at 4°C. 2.5 ml of the resulting post-nuclei supernatant (PNS) were mixed with an equal volume of 2.5 M sucrose and placed at the bottom of a sucrose step gradient of 25%, 15%, 10%, and 5% (w/v) sucrose in homogenization buffer, with an additional top layer of 25 mM Tris-HCl, pH 7.5, 1 mM EDTA and 5 mM EGTA, and centrifuged at 12,000*g* for 1 hour at 4°C (SW-41Ti rotor, Beckman Coulter, Pasadena, California). Six or seven fractions were collected from the top. Equal volumes of each fraction were used for immunoblotting. To purify LDs, the LD fraction on the top of the gradient was recovered and concentrated by re-floating LDs at 16,000*g* for 10 min at 4°C. The lower phase containing the excess buffer was removed by aspiration with a syringe and four volumes of ice-cold acetone were added to precipitate proteins and kept 48 hours at -20°C. The samples were centrifuged at 16,000*g* for 10 min at 4°C, the pellet washed with cold acetone 3 times, air-dried and reconstituted with 10 mM Tris-HCl, pH 7.5. After sonication, protein concentration was quantified by CBQCA protein quantitation kit (ThermoFisher Scientific). To purify cytosol extracts, 200 µl of PNS plus 600 µl of homogenization buffer were centrifuged at maximal speed for 1 hour ($1 \times 10^6 g$ in S140-AT Fixed Angle Rotor, ThermoFisher Scientific). A syringe (23G needle) was inserted below the floating LDs to remove 200 µl of cytoplasm and proteins were precipitated as described previously.

Bacterial killing assay (BKA)

E. coli (ATCC 25922) were grown to an O.D. at 600 nm of 1 and diluted 1:100 (1.5×10^5 colony-forming units (CFU/ml)). One hundred microliters of bacterial culture were mixed with 15 or 25 µg of LD-proteins. Incubation buffer (33 mM KH_2PO_4, 60 mM K_2HPO_4, 10 mM Na_2SO_4, 1.7 mM sodium citrate, 10 mM $MgSO_4$) was then added up to 200 µl. Cultures were incubated for the indicated times at 37°C in a shaking incubator. Serial dilutions were plated in triplicate on LB-agar plates and surviving bacteria were quantitated as CFU/ml after overnight incubation at 37°C. Alternatively, overnight incubations were centrifuged at 11,000*g* for 30 s and the bacterial pellet was resuspended in PBS and measured the absorbance by optical density at 600 nm with a Modulus Microplate Multimode Reader (Promega, Madison, Wisconsin). For monitoring bacterial growth in the presence or absence of OA (175 µg/ml) or gentamicin (200 µg/ml), *E. coli* cultures were diluted to an O.D. at 600 nm of 0.1 in 96-well flat-bottom plates and incubated at 37°C shaking. O.D. at 600 nm readings were taken every 20 min and monitored using a POLARstar Omega reader (BMG Labtech, Germany).

Serum parameters, hepatic triacylglycerol quantification, and mitochondrial content

Blood was extracted by cardiac puncture and sera obtained after centrifugation of blood samples at 6,000*g* for 15 min at 4°C in serum heparin separator tubes (Becton Dickinson, Franklin Lakes, New Jersey). Ketone bodies in serum were measured using a Ketone Body Assay Kit (MAK134; Sigma-Aldrich) according to the manufacturer's instructions. Triacylglycerol content of the liver was determined using the Triglyceride Detection Kit following manufacturer's instructions (BioSystems, Barcelona, Spain). Citrate synthase activity was measured as a reliable marker of mitochondrial content as previously described (*35*).

Fatty acid beta-oxidation

Primary hepatocytes were isolated as previously (*36*). To accumulate radiolabeled fatty acids in LDs, cells were treated for 4 hours with 1 µCi/ml of [^{14}C]-OA 175 µg/ml (NEC317050C, PerkinElmer, Waltham, Massachussetts). The media was then replaced with fresh media at 175 µg/ml of OA for an additional 4 hours followed by an overnight incubation with DMEM 0% FCS, low glucose (0.75 g per liter) with or without LPS (100 µg/ml) and sealed. Oxidation measurements were performed by trapping the released [^{14}C] carbon dioxide in a parafilm-sealed system on filter paper soaked in 1 M potassium hydroxide and measured using a Wallac 1409 Liquid Scintillation Counter. The rate of beta-oxidation was calculated as the amount of trapped [^{14}C] carbon dioxide in relative units produced per 0.5×10^6 cells. Results are expressed as the beta-oxidation rate relative to the untreated condition. Lipid soluble intermediates include those incompletely oxidized acid-soluble metabolites containing ^{14}C and were obtained after precipitation with perchloric acid and measured using a liquid scintillation counter.

Human macrophages studies

Cell culture

Human monocyte-derived macrophages (HMDMs) were obtained by differentiating CD14$^+$ monocytes as previously described (*37*). The human monocytic THP-1 cell line was obtained from the American Type Culture Collection (Rockville, Maryland). Cells were cultured in Roswell Park Memorial Institute 1640 Medium (RPMI, Gibco, ThermoFisher Scientific) containing 10% heat inactivated FBS (Bovogen Biologicals, Melbourne, VI, Australia), 5mM sodium pyruvate (Gibco), 10 mM HEPES (Gibco), 50 U/ml penicillin (Invitrogen, Carlsbad, California) and 50 µg/ml streptomycin (Invitrogen). Infection media are similar to complete media but without penicillin–streptomycin.

Bacterial strains and infection assays

For HMDMs infection, the following bacterial strains were used: *S.* Typhimurium SL1344 and *E. coli* K-12 MG1655. THP-1 cells were infected with *E. coli* K-12 MG1655. To induce LD formation, cells were treated with OA (178 µg/ml final) 18 hours prior infection. Bacterial infections were performed as previously described (*37*), with a multiplicity of infection (MOI) of 10 for *S.* Typhimurium and 100 for *E. coli*.

Flow cytometry

HMDMs were seeded at 0.5×10^6 cells/ml and treated with or without OA (178 ng/ml) for 16 hours. The next day, heat-killed pHrodoTM Green *E. coli* BioParticlesTM Conjugate (#P35366, ThermoFisher Scientific) were added to the well (50 µg/well) for 90 min. Cytochalasin D (10 µM, 30 min pre-treatment) was used as positive control to block phagocytosis (ThermoFisher Scientific). Cells were then harvested in ice-cold PBS containing 0.1% sodium azide and 25 mM EDTA. Flow cytometric analysis was performed using a GALLIOS Flow Cytometer (Beckman Coulter) and data were analyzed using Kaluza Analysis 1.3. software.

Fluorescence and quantitation of LD-bacteria proximity

HMDMs, plated on coverslips, were treated with OA (175 µg/ml) for 16 hours, then infected with *E. coli* strain MG1655 (MOI 10) or *Salmonella* SL1344 strain (MOI 10), both expressing mCherry constitutively. At 4 hours post-infection, cells were stained with BODIPY 647 (10 µg/ml; Molecular Probes Eugene, Oregon) for 30 min, before being washed with PBS and fixed with 4% paraformaldehyde (Electron Microscopy Science, Hatfield, Pennsylvania) for 10 min. Cells were then stained with 4′,6-diamidino-2-phenylindole (DAPI) (20 ng/ml) and mounted on slides.

HMDM siRNA experiments

Day 6 HMDMs were harvested and resuspended in IMDM complete media containing 10 mM HEPES buffer (pH 7.2 to 7.5, Gibco). Combined sets of CAMP small interfering RNA (siRNA) (GGAAGCUGUGCUUCGUGCUAUAGAU, AUCUAUAGCACGAAG CACAGCUUCC, GACAUCAGUUGUGAUAAGGAUAACA,

UGUUAUCCUUAUCAC AACUGAUGUC, GCUUCACAGUGAAAGAGACAGUGUG, and CACACUGUCUCCUUC ACUGUGAAGC) or scramble siRNA were used as previously described (*38*). After 24 hours recovery, cells were treated with OA (37.5 μg/ml) for another 18 hours. HMDMs were then infected with *E. coli*.

Gene overexpression in THP-1 by lentiviral transduction

Lentiviral transduction was used for gene overexpression of *PLIN5* in THP-1 cells as previously described (*38*).

Cell culture studies

Cell culture and treatments

HuH7 and HEK293 cells were cultured in Dulbecco's modified Eagle's medium (DMEM, Biological Industries, Cromwell, Connecticut) 10% v/v fetal bovine serum (Biological Industries) supplemented with 4 mM L-glutamine, 1 mM pyruvate (Sigma-Aldrich), 50 U/ml penicillin, 50 μg/ml streptomycin, and non-essential amino acids (Biological Industries). HEK293 cells stably expressing human Toll-like receptor 4 (HEK293-TLR4$^+$) have been characterized previously (*39*). OA treatments were performed using OA (O1008, Sigma-Aldrich) conjugated to fatty acid-free BSA (A8806, Sigma-Aldrich) at a molar ration of 6:1. Cells were treated with recombinant human TNFα (20 ng/ml; 300-01A, Preprotech, Rocky Hill, New Jersey), and IFNγ (10ng/ml; 300-02, Preprotech) and LPS (500 ng/ml) for 16 hours. Cells expressing CAMP-ΔN mutant were treated with MG132 (5 μM; 474790, Merck) for 24 hours.

Transfection

Six-well plates were seeded with 3×10^5 HuH7 cells or 4×10^5 HEK293 or HEK293-TLR4$^+$ cells. Twenty-four hours after plating, cells were transfected using GENEJET PLUS (SignaGen, Rockville, Maryland), following the manufacturer's instructions. Six hours after transfection, cells were treated with OA (175 μg/ml) for 16 hours.

Bacterial strains and infection assays

The bacterial strains used were: *E. coli* (ATCC 25922), MRSA (strain 162057-900), *P. aeruginosa* (ATCC 27853), and *L. monocytogenes* (strain 10403S). HEK293 or HEK293-TLR4$^+$ cells were seeded at 4×10^5 cells/plate in 6-well plates and transfected the next day. Six hours after transfection, culture media was replaced for antibiotic-free cell culture medium in presence of OA (175 μg/ml) and left overnight. Bacteria were grown overnight to stationary phase. The following day, bacteria were diluted 1:10 and grown to an O.D. at 600 nm of 0.54 to 0.56. They were then washed twice and resuspended in antibiotic-free cell culture medium and used at MOI of 0.5. Each infection was performed in triplicate wells. After 1 hour, extracellular bacteria were removed by incubation with 200 μg/ml gentamycin-containing medium (G1914, Sigma-Aldrich) for 1 hour, followed by incubation with 20 μg/ml gentamycin-containing medium for 4 hours. To determine intracellular bacterial loads, cells were lysed with 0.1% Triton X-100 (T8787, Sigma-Aldrich) for 5 min and plated onto LB medium supplemented with 1.5% (w/v) agar.

Cell fractionation

HuH7 cells were seeded at 1.5×10^6 cells/plate, transfected the next day and loaded with 175 μg/ml OA overnight. Three 100-mm culture plates were used per each condition. A sucrose density gradient was performed as previously described (*40*).

Protein purification and coimmunoprecipitation

For purification of myc-tagged proteins, HuH7 cells were plated in 100-mm culture plates at 10×10^6 cells/plate, transfected the next day and loaded with 175 μg /ml OA overnight. Myc-tagged proteins from the cellular extract and secreted into the media were purified using a c-myc protein purification kit (MBL, Nagoya, Japan) according to the manufacturer's instructions. Samples were processed by SDS–PAGE and analyzed by immunoblotting. For immunoprecipitation, transfected HuH7 cells (five 100-mm culture plates per condition) were collected and lysed in buffer containing 50 mM Tris-HCl at pH 7.5, 150 mM NaCl, 5 mM EDTA, and 1% Triton X-100 supplemented with proteases and phosphatases inhibitors. Cell lysates were homogenized with a 23G needle syringe 10 times and centrifuged for 20 min at 16,000*g* at 4°C. The supernatant was then incubated with 1 μg of anti- FLAG antibody for 2 hours at 4°C, followed by addition of protein G Sepharose beads (P3296, Sigma-Aldrich) for 1 hour at 4°C. Immunoprecipitated proteins were washed three times with lysis buffer, suspended in 2X Laemmli buffer and analyzed by immunoblotting.

Gene expression by quantitative PCR (qPCR)

For quantitative RT-PCR, total RNA was isolated from liver homogenates, HuH7 or HEK293-TLR4$^+$ cells using the RNeasy Lipid Tissue Mini Kit (QIAGEN, Hilden, Germany) according to the manufacturer's instructions. One microgram of total RNA was used for cDNA synthesis using the High Capacity cDNA Reverse Transcription Kit (Applied Bioscience, ThermoFisher Scientific) according to the manufacturer's instructions. qRT-PCR was performed using the Brilliant SYBR Green qPCR Master Mix (# 600548, Agilent Technologies, Santa Clara, California) and detected by the Mx3000P QPCR System (Agilent Technologies).

The following are the primers used for real-time PCR:

GAPDH: forward, 5′-CGACTTCAACAGCAACTCCCACTCTTCC-3′ and reverse 5′-TGGGTGGTCCAGGGTTTCTTACTCCTT-3′. Cytochrome C oxidase subunit I (*COI*): forward, 5′-GCCCCAGATATAGCATTCCC-3′ and reverse 5′-GTTCATCCTGTTCCTGCTCC-3′. *PLIN2*: forward 5′-ACACCCTCCTGTCCAACATC-3′ and reverse 5′-AAGGGACCTACCAGCCAGTT-3′. *PLIN5*: forward 5′-GCGGTCTGCGATGTTTACAG-3′ and reverse 5′-CTCCGAAGGTTGCTGGAGAA-3′. *RAB18*: forward 5′-GACGTGCTAACCACCCTGAA-3′ and reverse 5′-AACACCCTGTGCACCTCTAT-3′. *HSL*: forward 5′-CACCAGCCAACACTCAGCTA-3′ and reverse 5′-GTGTGAGGAGGGTCATCGTT-3′. *HPRT*: forward 5′-GCAGTACAGCCCCAAAATGG-3′ and reverse 5′-AACAAAGTCTGGCCTGTATCCAA-3′. *CAMP*: forward 5′-CTGTCCCCATACACCGCTTC-3′ and reverse 5′-GACACAGTGTGCCCCAGGAC-3′. *TNFα*: forward 5′-CCATGTTGTAGCAAACCCTCAA-3′ and reverse 5′-GCTGGTTATCTCTCAGCTCCA-3′. *IL8*: forward 5′-AGACAGCAGAGCACACAAGC-3′ and reverse 5′-ATGGTTCCTTCCGGTGGT-3′. *18 S:* forward 5′-CGGCTACCACATCCAAGGAA-3′ and reverse 5′-GCTGGAATTACCGCGGCT-3′. The relative expression of each mRNA was normalized to the internal reference *GAPDH* (liver), *18S* (cultured cells), or hypoxanthine phosphoribosyl transferase (*HPRT*; macrophages).

TLR4-mediated IL-8 release assay

HEK293-TLR4$^+$ cells were seeded at 4×10^5 cells/plate in 48-well plates in the presence or absence of LPS (250 ng/ml) for 18 hours. One hundred microliters of culture supernatant was used to measure interleukin-8 (IL-8) levels using the Human enzyme-linked immunosorbent assay (ELISA) IL-8 Set assay (555244; BD OptEIA, BD Biosciences) according to the manufacturer's protocol and detected by Epoch Multiplate Spectrophotometer (BioTek, Winooski, Vermont).

Immunofluorescence

HuH7 cells were grown in 10-mm glass coverslips. For HEK293 and HEK293-TLR4$^+$ cells, glass coverslips were coated with 50 μg/ml of fibronectin (Sigma-Aldrich) for 30 min at room temperature and rinsed twice with PBS before seeding cells. Cells were fixed for 60 min in 4% paraformaldehyde, permeabilized in 0.15% Triton X-100 for 10 min, followed by blocking with 1% BSA (A7906, Sigma-Aldrich), 0.1% Tween in PBS for 15 min. Labeling was achieved by incubating cells for 1 hour at room temperature with primary antibodies diluted in blocking solution: rabbit polyclonal anti-PLIN2 (1:500; ab108323, Abcam), rabbit polyclonal anti-CAMP (1:200; ab 180760, Abcam), rabbit polyclonal anti-TOM20 (1:500; ab186734, Abcam), mouse monoclonal anti-FLAG (1:500; F1804; Sigma). Primary antibodies were detected

with donkey anti-mouse IgG Alexa Fluor 488 (A21202), donkey anti-mouse IgG Alexa Fluor 555 (A31570), donkey anti-rabbit IgG Alexa Fluor 555 (A321094), and chicken anti-mouse IgG Alexa Fluor 647 (A21463) from ThermoFisher Scientific, diluted 1:250 in blocking solution. Finally, cells were labeled with DAPI (1:4000; ThermoFisher) and LDs were stained with BODIPY 493/503 (1:1000; Molecular Probes) for 10 min at room temperature, washed twice with PBS and coverslips were mounted with Mowiol (475904; Calbiochem, Merck). Alternatively, LDs were labeled with LipidTOX Deep Red (H34477; Molecular Probes) at 1:100 dilution in mounting media.

Microscopy

Optical and fluorescence microscopy

Imaging of H&E staining was performed with a Leica DMRB optical microscope (Leica, Wetzlar, Germany) equipped with a Leica DFC450 digital camera, using the 63X oil immersion objective lens. For immunohistochemistry and immunofluorescence, images were collected using a Leica AF600 motorized microscopy system (Leica Microsystems, Manheim, Germany) equipped with a DMI6000 microscope, a Leica PL APO 63X numerical aperture 1.4 oil immersion, a high-resolution monochrome ORCA-spark CMOS Digital Camera, and a mercury metal halide bulb Leica EL6000 as light source. DAPI was acquired with a band pass excitation filter 340-380 nm, dichromatic mirror (400 nm) and a long pass emission filter (425 nm). A488 was acquired with a band excitation filter 480/40 nm, dichromatic mirror 505 nm and a band pass emission filter (527/30 nm). A555 was acquired with a band pass excitation filter 531/40 nm, dichromatic mirror reflection 499-555 and transmission 659-730 nm and a band pass emission filter (593/40 nm). A647 was acquired with excitation band pass filter 628/40 nm, dichromatic mirror reflection 549-651 nm and transmission 699-726 nm and a band pass emission filter (692/40 nm). Images were collected using the LAS X Navigator software. High-resolution images of liver areas were captured using the Tile Scan acquisition mode. For quantitation of LD-bacteria proximity, images were taken with 63X objective lens using a Zeiss Axiovert 200 Upright Microscope Stand with LSM 710 Meta Confocal Scanner, with spectral detection and Airyscan super resolution detector. Two-photon imaging with a fully tunable Mai Tai eHP DeepSee 760-1040nm laser (Zeiss, Oberkochen, Germany). Images were analyzed using the Adobe Photoshop CS3 software (Adobe Systems Inc. San Jose, California) and ImageJ (NIH).

Electron microscopy and morphological measurements

Liver samples, HMDMs, or THP-1 cells in 3-cm dishes were processed for TEM as described previously (*41*). For TEM, ultrathin sections (60 nm) were cut using an ultramicrotome (EM U26, Leica, Germany) and collected on copper mesh grids. Imaging was conducted on a Hitachi 7700 (Tokyo, Japan) at 80 kV. For serial block-face scanning electron microscopy (SBF-SEM), the stub was transferred to a Zeiss Sigma scanning electron microscope fitted with a Gatan 3view. Sectioning and imaging were conducted at 50-nm intervals with a voxel size of 11.5 by 11.5 nm, allowing for a field of view of 46 by 46 μm. Data obtained from SBF-SEM were analyzed using Imod software (*42*). Image stacks were aligned manually using the Midas command. Structures of interest were then segmented using the manual drawing tool aided by an automated interpolator tool. A mesh was placed on the objects allowing then to be viewed in three dimensions.

Image analysis

Image analysis was performed using FIJI-Image J (Wayne Rasband, NIH) (*43*, *44*). Custom-made macros were programmed with instructions for the automated image analysis pipelines.

LD-mitochondria contacts

Confocal images from fluorescently labeled HEK293 cells, Mitochondria (TOM20), LD (BODIPY), PLIN5 and nuclei (DAPI), were acquired to analyze contacts between mitochondria and LD under LPS and PLIN5 expression (fig. S7). Briefly, cells were segmented, individualized, and stored as Regions of Interest (ROI). LD segmentation was achieved through a Trainable Weka Segmentation classifier (*45*) on LD (BODIPY) channel image and mitochondria were segmented by intensity thresholding (autothreshold method "Otsu"). Contact regions between mitochondria and LD were first obtained by using the Colocalization Highlighter plugin (Pierre Bourdoncle, Institut Jacques Monod, Service Imagerie, Paris) and converted to a contour line section by skeletonization. Contact length and contact counts were quantified from each cell and stored in the results table. Mean PLIN5 intensity was quantified from each cell to differentiate expressing PLIN5 cells. The computer code is available at https://zenodo.org/badge/latestdoi/280189667.

Distribution of selected tagged human LD-proteins

To analyze distribution of selected tagged human LD-proteins in HuH7 cells, confocal *z*-sections from cells labeled with DAPI, anti-FLAG antibodies, anti-PLIN2 antibodies, and LipidTox were acquired. Briefly, cells were defined manually and LD-intensity thresholded. They were then converted to binary images stored in ROI Manager. The sum of intensities from anti-FLAG or anti-PLIN2 from LD ROIs was divided by the sum of intensities of anti-FLAG or anti-PLIN2 from each cell, multiplied by 100 and expressed as percentage of anti-FLAG or anti-PLIN2 protein on LDs respectively. LDs that contained at least one pixel of anti-FLAG or anti-PLIN2 labeling were counted as positive LDs for that labeling. The total counts of positive LDs for anti-FLAG or anti-PLIN2 was divided by the total amount of LDs and expressed as a percentage. The computer code is available at https://zenodo.org/badge/latestdoi/280200243.

Immunoblotting

Cells were washed twice with cold PBS before being scraped into ice-cold 10 mM Tris, pH 7.5, 150 mM NaCl, 5 mM EDTA 0.1% Triton X-100 and a mixture of protease and phosphatase inhibitors. Cells were homogenized by sonication at 4°C. Protein was quantified with the Bio-Rad Protein Assay kit (Bio-Rad, Hercules, California). Immunoblotting of cells was performed as described previously (*46*). The blots were incubated with primary antibodies for 1 hour at room temperature. The primary antibodies used were: rabbit polyclonal anti-GFP (1:5000; ab290, Abcam), rabbit polyclonal anti-PLIN2 (1:5000; ab78920, Abcam), rabbit polyclonal anti- PLIN5 (1:1000; ab222811, Abcam), rabbit polyclonal anti-EEA1 (1:200; ab2900, Abcam), rabbit polyclonal anti-VAP-A (1:5000; ab181067, Abcam), mouse monoclonal anti-viperin (1:1000; ab107359, Abcam), rabbit polyclonal anti-CAMP (1:1000; ab180760, Abcam), guinea pig polyclonal anti-PLIN 3 (1:500; GP32, Progen, Heidelberg, Germany), guinea pig polyclonal PLIN5 (1:1000; GP31, Progen), guinea pig polyclonal PLIN2 (1:2000; GP41, Progen), mouse monoclonal anti-GM130 (1:2000; Labs 810822,BD-Biosciences San Jose, California), mouse monoclonal anti-Na/K ATPase (1:1000; 05-369 Upstate-Millipore, Darmstadt, Germany) rabbit polyclonal anti-HSL (1:1000; 4107, Cell Signaling, Leiden, the Netherlands), mouse monoclonal anti- IGTP (1:200; sc-136317, Santa Cruz Biotechnology, Dallas, Texas), rabbit polyclonal anti-CAMP (1:500; TA306515, OriGene), mouse monoclonal anti-FLAG (1:1000; F1804, Sigma-Aldrich), mouse monoclonal anti-ATP synthase (1:500; 7H10BD4F9, ThermoFisher Scientific), and goat polyclonal anti-GAPDH (1:5000; A00191, GenScript). After incubation with primary antibodies, membranes were washed and incubated with the following peroxidase-conjugated secondary antibodies (1:3000): goat anti-rabbit IgG (H+L)–HRP conjugate (1706515, BioRad), goat anti-mouse IgG (H+L)-HRP conjugate (1706516, BioRad), and peroxidase AffiniPure donkey anti-goat IgG (H+L) (705-035-147, Jackson ImmunoResearch, Ely, UK). HRP-conjugated secondary antibodies were detected with ECL (Biological Industries) and visualized using ImageQuant LAS4000 (GE Healthcare, Chicago, Illinois). Immunoblots were quantified using the Fiji-ImageJ software (NIH).

Quantitative proteomics and functional annotation analyses

Proteins were precipitated from either isolated lipid droplets (four and five independent replicates for CTL- and LPS-treated, respectively) or liver homogenates (three independent replicates per condition) with ice-cold acetone and solubilized in lysis buffer (50 mM Tris-HCl, pH 7.5, 2% SDS and 10 mM TCEP [Tris-(2-carboxyethyl)-phosphine hydrochloride]. Protein concentration in spun supernatants was determined by infrared spectrometry. Approximately 100 μg of total protein per sample were digested using standard FASP procedures. After alkylation, proteins were digested overnight at 37°C with modified trypsin (Promega) in 50 mM ammonium bicarbonate at a 30:1 protein:trypsin (w/w) ratio. Resulting peptides were eluted in 50 mM ammonium bicarbonate and 0.5 M sodium chloride. Trifluoroacetic acid (TFA) was added to a final concentration of 1%. Eluates were desalted through C18 Oasis-HLB cartridges (Waters corporation, Milford, Massachussetts), dried, and resuspended in 100 mM triethylammonium bicarbonate (TEAB) buffer. Equal amounts of each peptide sample were labeled using the 10-plex TMT Reagents (ThermoFisher Scientific) according to manufacturer's protocol. For increased proteome coverage, TMT-labeled samples were fractionated by high-pH reverse-phase chromatography (Pierce High pH Reversed-Phase Peptide Fractionation Kit, # 84868; ThermoFisher Scientific). Labeled peptides were chromatographed through a C-18 reversed phase nano-column (75 μm I.D. × 50 cm, 2-μm particle size, Acclaim PepMap RSLC, 100 C18; ThermoFisher Scientific) in a continuous acetonitrile gradient consisting of 0 to 30% B in 360 min, 50 to 90% B in 3 min (A = 0.1% formic acid; B = 90% acetonitrile, 0.1% formic acid; flow rate of 200 nl/min) for analysis in an Orbitrap Fusion mass spectrometer (ThermoFisher Scientific). Tandem mass spectrometry (MS/MS) spectra from the Nth-most intense parent ions were analyzed along the chromatographic run. For peptide identification, all spectra were analyzed with Proteome Discoverer (v. 2.1.0.81) using SEQUEST-HT (ThermoFisher Scientific) and queried onto the Uniprot database with the following search parameters: 2 maximum missed tryptic sites; precursor and fragment mass tolerances of 2 Da and 0.02 Da, respectively; carbamidomethyl cysteine and TMT modifications at N-terminal and Lys residues as fixed modifications, and methionine oxidation as dynamic modification. Peptide identification was performed using the probability ratio method (*47*), and FDR was calculated using inverted databases. The relative abundance of each protein was estimated from ion intensities of peptides with an FDR ≤ 1% and expressed in units of standard deviation according to their estimated variances (Zq values), as previously described (*13*). Hierarchical clustering was computed across all individual replicates (averaged distance) and a 0.78 correlation cut-off was established for subsequent analysis. Functional protein analysis was performed using the system biology triangle (SBT) algorithm and Ingenuity Pathway Analysis (IPA, QIAGEN) (*48*). Upstream pathway analysis and network modeling of interested protein clusters were run using the IPA platform (QIAGEN), and network representation was layered out using Cytoscape 2.0. Analysis shown in Fig. 3C shows the relative proportion of proteins identified for each indicated functional annotation term (retrieved from DAVID resource 6.7, including all KEGG and GO terms), from either mitochondrial protein identified among LPS-LD down-regulated proteins, or the MitoCarta 2.0 reference proteome. Mass spectrometry data have been deposited in Peptide Atlas (ID: PASS01610).

Statistical analysis

All data shown in graphs are the mean ± SD. Statistical significance was determined using paired t test, one-way analysis of variance (ANOVA) multiple comparisons test, or two-sided students z test on proportions, as specified in figure legends [not significant (ns), $^{*}P < 0.05$, $^{**}P < 0.01$, $^{***}P < 0.001$, and $^{****}P < 0.0001$].

Figure preparation

Figures were created using Microsoft PowerPoint (Microsoft 365 MSO). Images were edited with Adobe Photoshop CS3 software (Adobe Systems). GraphPad Prism 7 (GraphPad Software) was used to create graphs and calculate statistical significances.

REFERENCES AND NOTES

1. A. Pol, S. P. Gross, R. G. Parton, Review: Biogenesis of the multifunctional lipid droplet: lipids, proteins, and sites. *J. Cell Biol.* **204**, 635–646 (2014). doi: 10.1083/jcb.201311051; pmid: 24590170
2. A. L. Vallochi, L. Teixeira, K. D. S. Oliveira, C. M. Maya-Monteiro, P. T. Bozza, Lipid Droplet, a key player in host-parasite interactions. *Front. Immunol.* **9**, 1022 (2018). doi: 10.3389/fimmu.2018.01022; pmid: 29875768
3. P. Roingeard, R. C. Melo, *Cell. Microbiol.* 10.1111/cmi.12688 (2017).
4. M. Knight, J. Braverman, K. Asfaha, K. Gronert, S. Stanley, Lipid droplet formation in Mycobacterium tuberculosis infected macrophages requires IFN-γ/HIF-1α signaling and supports host defense. *PLOS Pathog.* **14**, e1006874 (2018). doi: 10.1371/journal.ppat.1006874; pmid: 29370315
5. R. C. Melo, A. M. Dvorak, Lipid body-phagosome interaction in macrophages during infectious diseases: Host defense or pathogen survival strategy? *PLOS Pathog.* **8**, e1002729 (2012). doi: 10.1371/journal.ppat.1002729; pmid: 22792061
6. E. R. Hinson, P. Cresswell, The antiviral protein, viperin, localizes to lipid droplets via its N-terminal amphipathic alpha-helix. *Proc. Natl. Acad. Sci. U.S.A.* **106**, 20452–20457 (2009). doi: 10.1073/pnas.0911679106; pmid: 19920176
7. L. Bougnères *et al.*, A role for lipid bodies in the cross-presentation of phagocytosed antigens by MHC class I in dendritic cells. *Immunity* **31**, 232–244 (2009). doi: 10.1016/j.immuni.2009.06.022; pmid: 19699172
8. P. Anand *et al.*, A novel role for lipid droplets in the organismal antibacterial response. *eLife* **1**, e00003 (2012). doi: 10.7554/eLife.00003; pmid: 23150794
9. U. Protzer, M. K. Maini, P. A. Knolle, Living in the liver: Hepatic infections. *Nat. Rev. Immunol.* **12**, 201–213 (2012). doi: 10.1038/nri3169; pmid: 22362353
10. J. C. Kagan, Lipopolysaccharide Detection across the Kingdoms of Life. *Trends Immunol.* **38**, 696–704 (2017). doi: 10.1016/j.it.2017.05.001; pmid: 28551077
11. A. Herms *et al.*, AMPK activation promotes lipid droplet dispersion on detyrosinated microtubules to increase mitochondrial fatty acid oxidation. *Nat. Commun.* **6**, 7176 (2015). doi: 10.1038/ncomms8176; pmid: 26013497
12. J. Behnsen, A. Perez-Lopez, S. P. Nuccio, M. Raffatellu, Exploiting host immunity: The Salmonella paradigm. *Trends Immunol.* **36**, 112–120 (2015). doi: 10.1016/j.it.2014.12.003; pmid: 25582038
13. P. Navarro *et al.*, General statistical framework for quantitative proteomics by stable isotope labeling. *J. Proteome Res.* **13**, 1234–1247 (2014). doi: 10.1021/pr4006958; pmid: 24512137
14. N. Krahmer *et al.*, Protein correlation profiles identify lipid droplet proteins with high confidence. *Mol. Cell. Proteomics* **12**, 1115–1126 (2013). doi: 10.1074/mcp.M112.020230; pmid: 23319140
15. K. Bersuker *et al.*, A proximity labeling strategy provides insights into the composition and dynamics of lipid droplet proteomes. *Dev. Cell* **44**, 97–112.e7 (2018). doi: 10.1016/j.devcel.2017.11.020; pmid: 29275994
16. E. L. Mills, B. Kelly, L. A. J. O'Neill, Mitochondria are the powerhouses of immunity. *Nat. Immunol.* **18**, 488–498 (2017). doi: 10.1038/ni.3704; pmid: 28418387
17. M. Bosch, R. G. Parton, A. Pol, *Semin. Cell Dev. Biol.* 10.1016/j.semcdb.2020.02.010 (2020).
18. H. A. Neufeld, J. A. Pace, F. E. White, The effect of bacterial infections on ketone concentrations in rat liver and blood and on free fatty acid concentrations in rat blood. *Metabolism* **25**, 877–884 (1976). doi: 10.1016/0026-0495(76)90120-7; pmid: 181658
19. A. Fabisiak, N. Murawska, J. Fichna, LL-37: Cathelicidin-related antimicrobial peptide with pleiotropic activity. *Pharmacol. Rep.* **68**, 802–808 (2016). doi: 10.1016/j.pharep.2016.03.015; pmid: 27117377
20. X. Shu, L. Nelbach, R. O. Ryan, T. M. Forte, Apolipoprotein A-V associates with intrahepatic lipid droplets and influences triglyceride accumulation. *Biochim. Biophys. Acta* **1801**, 605–608 (2010). doi: 10.1016/j.bbalip.2010.02.004; pmid: 20153840
21. S. Turró *et al.*, Identification and characterization of associated with lipid droplet protein 1: A novel membrane-associated protein that resides on hepatic lipid droplets. *Traffic* **7**, 1254–1269 (2006). doi: 10.1111/j.1600-0854.2006.00465.x; pmid: 17004324
22. C. L. Libbing, A. R. McDevitt, R. P. Azcueta, A. Ahila, M. Mulye, Lipid droplets: A significant but understudied contributor of host bacterial interactions. *Cells* **8**, 354 (2019). doi: 10.3390/cells8040354; pmid: 30991653
23. J. L. Cocchiaro, Y. Kumar, E. R. Fischer, T. Hackstadt, R. H. Valdivia, Cytoplasmic lipid droplets are translocated into the lumen of the *Chlamydia trachomatis* parasitophorous vacuole. *Proc. Natl. Acad. Sci. U.S.A.* **105**, 9379–9384 (2008). doi: 10.1073/pnas.0712241105; pmid: 18591669
24. P. Peyron *et al.*, Foamy macrophages from tuberculous patients' granulomas constitute a nutrient-rich reservoir for M. tuberculosis persistence. *PLOS Pathog.* **4**, e1000204 (2008). doi: 10.1371/journal.ppat.1000204; pmid: 19002241
25. K. A. Mattos *et al.*, Modulation of lipid droplets by Mycobacterium leprae in Schwann cells: A putative mechanism for host lipid acquisition and bacterial survival in phagosomes. *Cell. Microbiol.* **13**, 259–273 (2011). doi: 10.1111/j.1462-5822.2010.01533.x; pmid: 20955239
26. S. J. Nolan, J. D. Romano, I. Coppens, Host lipid droplets: An important source of lipids salvaged by the intracellular parasite *Toxoplasma gondii*. *PLOS Pathog.* **13**, e1006362 (2017). doi: 10.1371/journal.ppat.1006362; pmid: 28570716
27. J. S. Mader, N. Mookherjee, R. E. Hancock, R. C. Bleackley, The human host defense peptide LL-37 induces apoptosis in a calpain- and apoptosis-inducing factor-dependent manner involving Bax activity. *Mol. Cancer Res.* **7**, 689–702 (2009). doi: 10.1158/1541-7786.MCR-08-0274; pmid: 19435812
28. S. N. Keenan *et al.*, Perilipin 5 deletion in hepatocytes remodels lipid metabolism and causes hepatic insulin resistance in mice. *Diabetes* **68**, 543–555 (2019). doi: 10.2337/db18-0670; pmid: 30617219
29. D. J. Greenwood *et al.*, Subcellular antibiotic visualization reveals a dynamic drug reservoir in infected macrophages. *Science* **364**, 1279–1282 (2019). doi: 10.1126/science.aat9689; pmid: 31249058
30. R. Dubey *et al.*, Lipid droplets can promote drug accumulation and activation. *Nat. Chem. Biol.* **16**, 206–213 (2020). doi: 10.1038/s41589-019-0447-7; pmid: 31932720

31. D. M. Moujalled *et al*., TNF can activate RIPK3 and cause programmed necrosis in the absence of RIPK1. *Cell Death Dis.* **4**, e465 (2013). doi: 10.1038/cddis.2012.201; pmid: 23328672
32. J. M. Murphy *et al*., The pseudokinase MLKL mediates necroptosis via a molecular switch mechanism. *Immunity* **39**, 443–453 (2013). doi: 10.1016/j.immuni.2013.06.018; pmid: 24012422
33. M. Bosch *et al*., Hepatic primary and secondary cholesterol deposition and damage in niemann-pick disease. *Am. J. Pathol.* **186**, 517–523 (2016). doi: 10.1016/j.ajpath.2015.12.002; pmid: 26784526
34. A. Tutusaus *et al*., A functional role of GAS6/TAM in nonalcoholic steatohepatitis progression implicates AXL as therapeutic target. *Cell. Mol. Gastroenterol. Hepatol.* **9**, 349–368 (2020). doi: 10.1016/j.jcmgh.2019.10.010; pmid: 31689560
35. A. Barrientos, In vivo and in organello assessment of OXPHOS activities. *Methods* **26**, 307–316 (2002). doi: 10.1016/S1046-2023(02)00036-1; pmid: 12054921
36. M. Bosch *et al*., Caveolin-1 deficiency causes cholesterol-dependent mitochondrial dysfunction and apoptotic susceptibility. *Curr. Biol.* **21**, 681–686 (2011). doi: 10.1016/j.cub.2011.03.030; pmid: 21497090
37. R. Kapetanovic *et al*., *Salmonella* employs multiple mechanisms to subvert the TLR-inducible zinc-mediated antimicrobial response of human macrophages. *FASEB J.* **30**, 1901–1912 (2016). doi: 10.1096/fj.201500061; pmid: 26839376
38. C. J. Stocks *et al*., *J. Leukoc. Biol.* **2020**, 1–11 (2020).
39. S. Lauer, Y. A. Kunde, T. A. Apodaca, B. Goldstein, E. Hong-Geller, Soluble MD2 increases TLR4 levels on the epithelial cell surface. *Cell. Immunol.* **255**, 8–16 (2009). doi: 10.1016/j.cellimm.2008.08.009; pmid: 18845299
40. A. Kassan *et al*., Acyl-CoA synthetase 3 promotes lipid droplet biogenesis in ER microdomains. *J. Cell Biol.* **203**, 985–1001 (2013). doi: 10.1083/jcb.201305142; pmid: 24368806
41. A. Herms *et al*., Cell-to-cell heterogeneity in lipid droplets suggests a mechanism to reduce lipotoxicity. *Curr. Biol.* **23**, 1489–1496 (2013). doi: 10.1016/j.cub.2013.06.032; pmid: 23871243
42. J. R. Kremer, D. N. Mastronarde, J. R. McIntosh, Computer visualization of three-dimensional image data using IMOD. *J. Struct. Biol.* **116**, 71–76 (1996). doi: 10.1006/jsbi.1996.0013; pmid: 8742726
43. J. Schindelin *et al*., Fiji: An open-source platform for biological-image analysis. *Nat. Methods* **9**, 676–682 (2012). doi: 10.1038/nmeth.2019; pmid: 22743772
44. C. A. Schneider, W. S. Rasband, K. W. Eliceiri, NIH Image to ImageJ: 25 years of image analysis. *Nat. Methods* **9**, 671–675 (2012). doi: 10.1038/nmeth.2089; pmid: 22930834
45. I. Arganda-Carreras *et al*., Trainable Weka Segmentation: A machine learning tool for microscopy pixel classification. *Bioinformatics* **33**, 2424–2426 (2017). doi: 10.1093/bioinformatics/btx180; pmid: 28369169
46. A. Pol, D. Ortega, C. Enrich, Identification and distribution of proteins in isolated endosomal fractions of rat liver: Involvement in endocytosis, recycling and transcytosis. *Biochem. J.* **323**, 435–443 (1997). doi: 10.1042/bj3230435; pmid: 9163335
47. S. Martínez-Bartolomé *et al*., Properties of average score distributions of SEQUEST: The probability ratio method. *Mol. Cell. Proteomics* **7**, 1135–1145 (2008). doi: 10.1074/mcp.M700239-MCP200; pmid: 18303013
48. F. García-Marqués *et al*., A novel systems-biology algorithm for the analysis of coordinated protein responses using quantitative proteomics. *Mol. Cell. Proteomics* **15**, 1740–1760 (2016). doi: 10.1074/mcp.M115.055905; pmid: 26893027

ACKNOWLEDGMENTS

We thank M. Calvo and G. Martín and acknowledge the use of the Advanced Optical Microscopy Facility of the University of Barcelona. We are indebted to C. Ferguson and J. Rae and acknowledge the use of the Australian Microscopy and Microanalysis Research Facility at the Center for Microscopy and Microanalysis at The University of Queensland. We thank J. Murphy (Walter and Elizabeth Hall Institute of Medical Research, Melbourne, Australia) for providing the pF_TRE3G_PGK_puro construct. We are indebted to the Protein Expression Facility (University of Queensland) for valuable assistance. We thank the Australian Red Cross Blood Service for providing buffy coats for the isolation of human monocytes. Last, we are indebted to the Citomics unit of IDIBAPS for their technical help. **Funding:** M.B. acknowledges support from 31/U/2016 from Fundació Marató de TV3. R.K. acknowledges support from an Australian Research Council Discovery Early Career Research Award (DE130100470). B.S. is supported by an Early Postdoc Mobility fellowship from the Swiss National Science Foundation (P2ZHP3_184024). M.J.S. is supported by a National Health and Medical Research Council (NHMRC) Senior Research Fellowship (APP1107914). M.S.-A. was recipient of a CNIC IPP fellowship (COFUND 2014). M.M. is supported by the Instituto de Salud Carlos III (FIS PI19/01410). O.T. is founded by Amgen 2018 Competitive Grant Program. A.P., R.G.P., S.P.G., and P.T.B. have been supported by RGP0020/2015 from the Human Frontier Science Program (HFSP). A.P. is supported by the Ministerio de Ciencia e Innovación (MICINN, RTI2018-098593-B-I00), Fundació Marató de TV3 (31/U/2016), and the CERCA Programme/Generalitat de Catalunya. R.G.P. was supported by the NHMRC of Australia (program grant APP1037320 and Senior Principal Research Fellowship 569452), and the Australian Research Council Centre of Excellence in Convergent Bio-Nanoscience and Technology (CE140100036). P.T.B. is supported by Conselho Nacional de Desenvolvimento Científico e Tecnológico (CNPq) of Brazil and Fundaçao de Amparo a Pesquisa do Estado do Rio de Janeiro (FAPERJ). M.A.D.P. was funded by MICINN (project grants SAF2014-51876-R and SAF2017-83130-R; and IGP-SO grant MINSEV1512-07-2016) and was a Worldwide Cancer Research Foundation grantee (#15-0404). J.V. is supported by MICINN (BIO2015-67580-P) and from the Carlos III Institute of Health-Fondo de Investigación Sanitaria (PRB2, IPT13/0001—ISCIII-SGEFI/FEDER, ProteoRed). The CNIC is supported by the MICINN and the Pro-CNIC Foundation and is a Severo Ochoa Center of Excellence (MICINN award SEV-2015-0505). **Author contributions:** M.B. and M.S.-A. contributed equally. Conceptualization: M.B., P.T.B., S.P.G., R.G.P., and A.P. Methodology: M.B., M.S.-A., and A.F. Formal analysis: M.B., R.G.P., and A.P. Investigation: M.B., M.S.-A., A.F., R.K., B.S., F.D., L.M., M.M., F.M.-P., O.T., A.G., R.M.T., J.E.B.C., C.C., N.M., J.A.L., R.C., and F.T. Resources and supervision: F.L., C.E., M.A.D.P., M.J.S., J.V., P.T.B., S.P.G., R.G.P., and A.P. Data curation: M.B., M.S.-A., F.T., R.G.P., and A.P. Writing (original draft): R.G.P. and A.P. Writing (review and editing): M.B., M.S.-A., M.S., P.T.B., S.P.G., R.G.P., and A.P. Visualization: R.G.P. and A.P. Project administration: P.T.B., S.P.G., R.G.P., and A.P. Funding acquisition: P.T.B., S.P.G., R.G.P., and A.P. **Competing interests:** None declared. **Data and materials availability:** Mass spectrometry data have been deposited in Peptide Atlas (ID: PASS01610). Computer code#1 to measure LD–mitochondria contacts can be found at https://zenodo.org/badge/latestdoi/280189667. Computer code#2 to quantify distribution of LD proteins can be found in: https://zenodo.org/badge/latestdoi/280200243. All other data are available in the main text or the supplementary materials.

SUPPLEMENTARY MATERIALS

science.sciencemag.org/content/370/6514/eaay8085/suppl/DC1
Materials and Methods
Figs. S1 to S12
Tables S1 to S7

View/request a protocol for this paper from *Bio-protocol*.

19 July 2019; resubmitted 29 April 2020
Accepted 21 August 2020
10.1126/science.aay8085

Mammalian lipid droplets are innate immune hubs integrating cell metabolism and host defense

Marta Bosch, Miguel Sánchez-Álvarez, Alba Fajardo, Ronan Kapetanovic, Bernhard Steiner, Filipe Dutra, Luciana Moreira, Juan Antonio López, Rocío Campo, Montserrat Marí, Frederic Morales-Paytuví, Olivia Tort, Albert Gubern, Rachel M. Templin, James E. B. Curson, Nick Martel, Cristina Català, Francisco Lozano, Francesc Tebar, Carlos Enrich, Jesús Vázquez, Miguel A. Del Pozo, Matthew J. Sweet, Patricia T. Bozza, Steven P. Gross, Robert G. Parton and Albert Pol

Science **370** (6514), eaay8085.
DOI: 10.1126/science.aay8085

Cells drop a bomb on pathogens

Lipid droplets (LDs) accumulate in cells to serve as lipid storage organelles. They are also an attractive source of nutrients for many pathogens. Bosch *et al.* show that various proteins involved in innate immunity form complexes on LDs in response to bacterial lipopolysaccharide (see the Perspective by Green). Upon activation, LDs became physically uncoupled from mitochondria, driving a shift in cells from oxidative phosphorylation to aerobic glycolysis. This work highlights the ability of LDs both to kill pathogens directly and to establish a metabolic environment conducive to host defense. This may inform future antimicrobial strategies in the age of antibiotic resistance.

Science, this issue p. eaay8085; see also p. 294

Supplementary Material for

Mammalian lipid droplets are innate immune hubs integrating cell metabolism and host defense

Marta Bosch*, Miguel Sánchez-Álvarez, Alba Fajardo, Ronan Kapetanovic, Bernhard Steiner, Filipe Dutra, Luciana Moreira, Juan Antonio López, Rocío Campo, Montserrat Marí, Frederic Morales-Paytuví, Olivia Tort, Albert Gubern, Rachel M. Templin, James E. B. Curson, Nick Martel, Cristina Català, Francisco Lozano, Francesc Tebar, Carlos Enrich, Jesús Vázquez, Miguel A. Del Pozo, Matthew J. Sweet, Patricia T. Bozza, Steven P. Gross, Robert G. Parton*, Albert Pol*

*Corresponding author. Email: martabosch@ub.edu (M.B.); r.parton@imb.uq.edu.au (R.G.P.); apols@ub.edu (A.P.)

Published 16 October 2020, *Science* **370**, eaay8085 (2020)
DOI: 10.1126/science.aay8085

This PDF file includes:

Materials and Methods
Figs. S1 to S12
Tables S1 to S7

Other Supplementary Material for this manuscript includes the following:
(available at science.sciencemag.org/content/370/6514/eaay8085/suppl/DC1)

MDAR Reproducibility Checklist

Supplementary Figures

Fig. S1. LDs have a protein-mediated antibacterial capacity.

(**A**) LDs were isolated from mouse livers by sucrose density gradient fractionation. The LD-resident proteins PLIN2, PLIN3, and PLIN5 fractionated into the top fraction, determined by immunoblotting ("b" indicates the bottom of the gradient). Based on the indicated organelle-specific markers, the top fraction was free of Golgi, endoplasmic reticulum, endosomes, and plasma membrane components (representative of three independent CTL-mice). (**B**) For the bacterial killing assays (BKA), *E. coli* were cultured in standard growth media, or additionally treated with LD proteins (from CTL- or CLP-LDs). After 16 hours, serial dilutions of the culture were plated in soft agar (black numbers). The number of growing colonies (colony forming units, CFU) was counted and referred to the control condition (representative of six mice per condition). (**C**) *E. coli* were cultured in growth media containing 25 μg of proteins from hepatic CTL- (black) or LPS-LDs (red bars), optical density (O.D.) was measured after 16 hours and normalized to average O.D. of the cultures treated with CTL-LDs (n = 8). (**D**) *E. coli* were incubated for 4 hours in growth media (gray) or with 15 μg of LD proteins purified from the liver of mice fed overnight ad libitum (black bars) (n = 4). (**E**) *E. coli* were incubated for 4 hours with hepatic LD proteins purified from mice fed overnight ad libitum (black) or from mice additionally treated with LPS (red bars) (n = 3). (**F**) *E. coli* were incubated for 4 hours in growth media containing 15 μg of proteins from CTL- (black) or CLP-LDs (red bars). Bacterial growth was determined as relative CFU to the CTL condition (n = 6). (**G** and **H**) *E. coli* were cultured for indicated times in either growth media (green) or in media containing 15 μg of proteins from CTL- (black), LPS-LDs (red circles; G), or CLP-LDs (red circles; H). At indicated times, bacterial growth was quantified relative to the CFU of the control condition ($n \geq 5$). (**I**) *E. coli* were cultured in growth media with or without OA or in growth media containing gentamicin. The O.D. of bacterial cultures was assessed every 20 minutes (combined from two independent experiments). (**J**) *E. coli* were cultured in growth media (green circles) or in the presence of 25 μg of proteins from the cytosol of CTL- (black) or LPS-livers (red circles). Relative CFU were assessed 4 hours post-incubation and compared to the buffer condition (n = 4). All graphs show mean ± SD; not significant (ns), * $P<0.05$, ** $P<0.01$, *** $P<0.001$ in a paired *t*-test. Red asterisks indicate statistically significant differences between different types of LDs. The number of independent experiments is indicated by "n".

Bosch et al., Figure S1

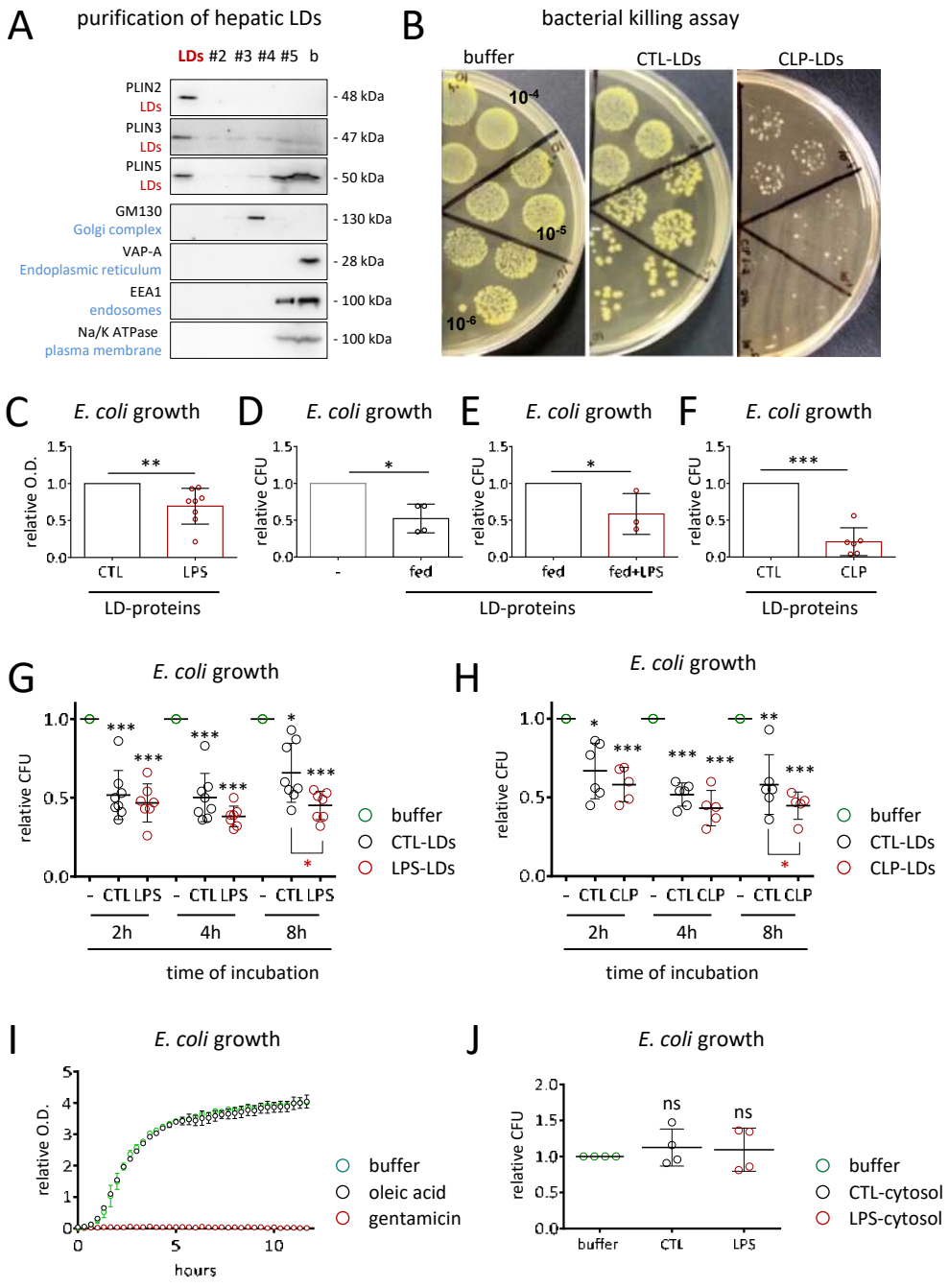

Fig. S2. LDs interact with bacteria in human macrophages.

(**A** and **B**) HMDMs were cultured for 24 hours with OA and subsequently infected for 4 hours with *E. coli* or *Salm* constitutively expressing mCherry. LDs were stained with BODIPY 647 and the distance of bacteria to the nearest LD was quantified in random confocal microscopy images (A). At least 90 bacteria per condition, obtained from 3 independent experiments, were analyzed. The percentage of bacteria in contact with LDs was quantified from random confocal microscopy images (B). At least 30 bacteria per condition, obtained from three independent experiments, were analyzed. (**C** and **D**) Control (black) and OA-loaded HMDMs (red dots) were infected with *E. coli* or *Salm* for 4 hours. Cells were fixed, processed for TEM, and the number of LD-bacteria contact counted. At least 15 cells per condition, obtained from 3 independent experiments, were analyzed. (**E** and **F**) Control (E) and OA-loaded HMDMs (F) were infected with *E. coli* for 4 hours, fixed, and processed for TEM analysis (representative of 3 independent experiments). The bacteria and the ER have been pseudocolored (blue: putative ER; red: *E. coli* interior (excluding periplasm); green: periplasm with bounding membranes; yellow: vacuolar membrane). The phospholipid monolayer of LDs (red asterisks) caused a discontinuity in the bacterial vacuolar membrane (yellow). Scale bars: 500 nm (E); and 1 μm (F). All graphs show mean ± SD; not significant (ns), * $P<0.05$, ** $P<0.01$, *** $P<0.001$ in a paired *t*-test.

Bosch et al., Figure S2

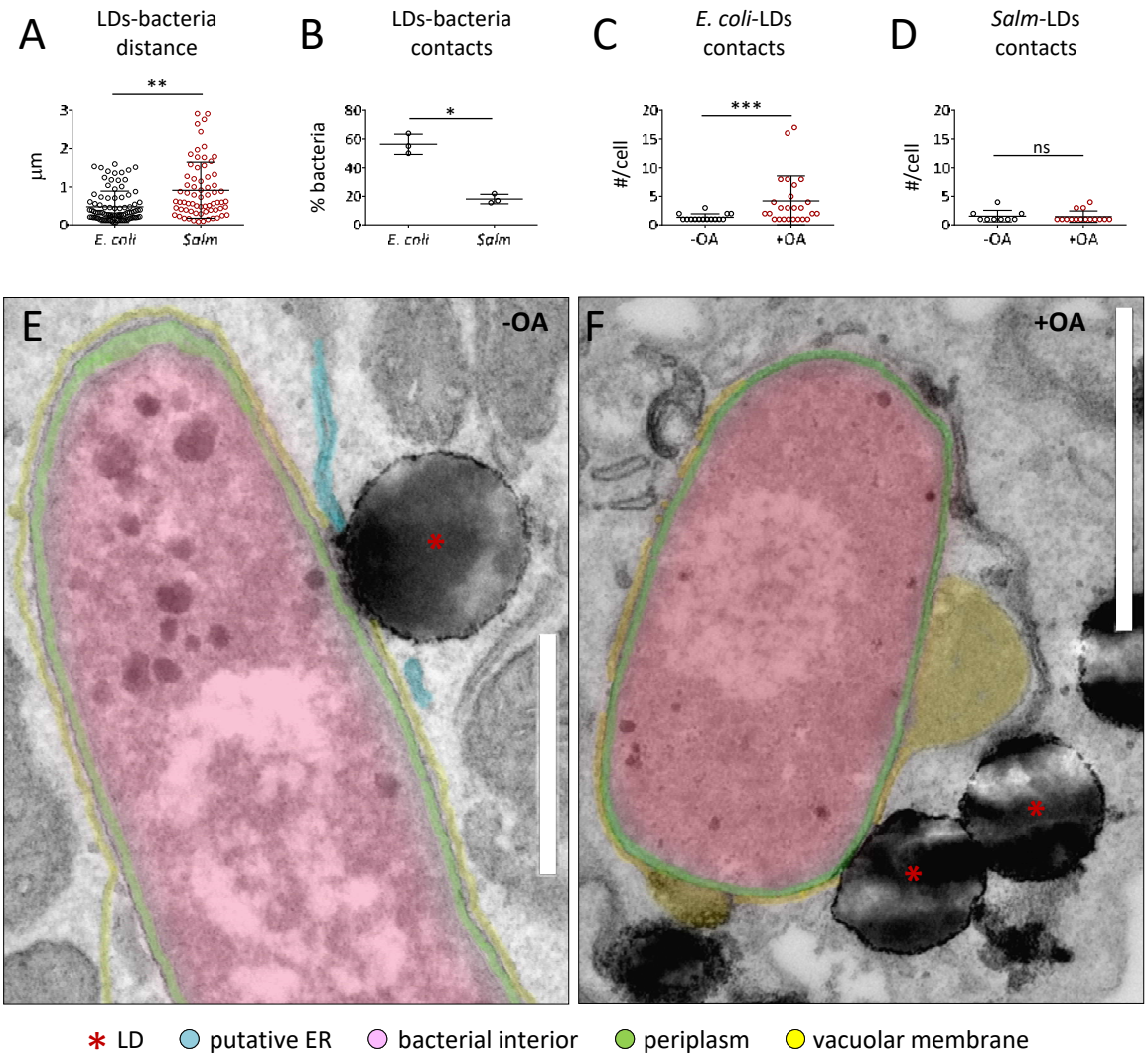

Fig. S3. The LD proteome is specifically regulated by LPS.

(**A**) Functional annotation enrichment analysis of proteins increasing (ΔZq>1.8; yellow hue) or decreasing (ΔZq<minus 1.8; blue hue), in LPS-livers when compared to CTL-livers (table S1; and table S2). Relative enrichment for each category against the mouse genome is expressed as minus log (*p* value). In contrast to LPS-LDs (Fig. 2B), functional annotation categories related to mitochondria were not significantly modified in LPS-liver. (**B**) Gene interaction network and functional annotation grouping of bona fide LD proteins significantly regulated in LPS-LDs versus CTL-LDs (see table S7). Immunity-related proteins, histones, and most PLINs are upregulated (yellow). In contrast, phospholipid and fatty acid metabolism-related LD proteins are down regulated (blue). PLIN5 is the only downregulated member of the PLIN family. Mass spectrometry data have been deposited in Peptide Atlas (ID: PASS01610).

Bosch et al., Figure S3

A gene ontology (GO) analysis LPS-liver

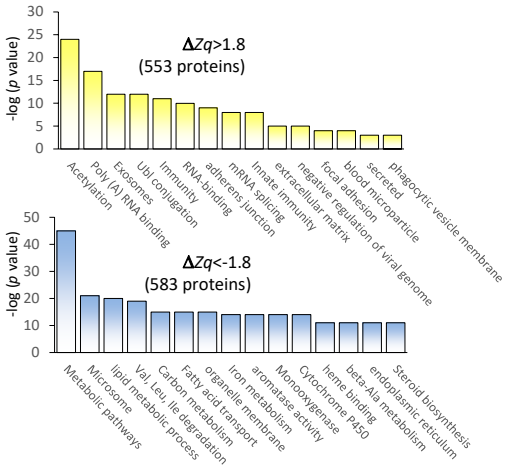

B gene interaction analysis bona fide LD proteins

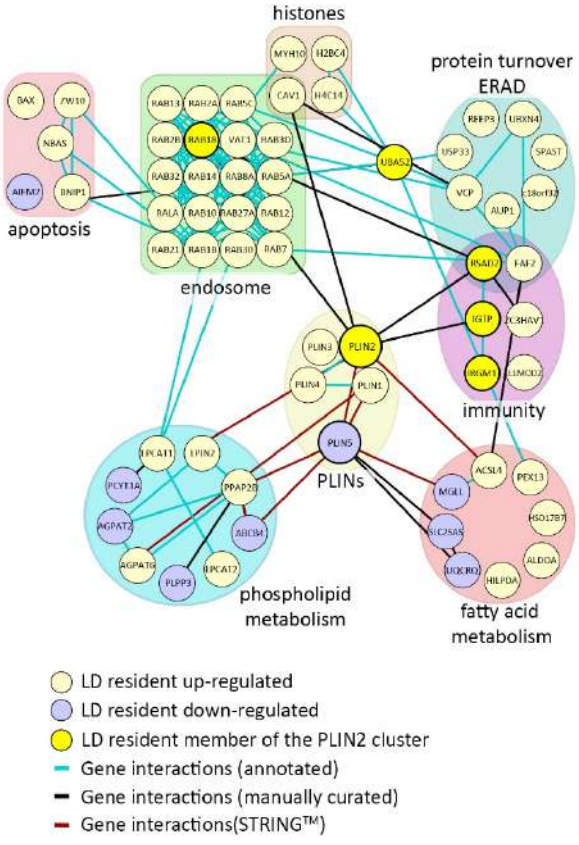

Fig. S4. Complex functional clusters of immune proteins organize on LPS-LDs.

(**A**) High-correlation protein clusters identified on LPS-LDs. Hierarchical clustering of *Zq* values across biological replicates (four CTL-LDs and five LPS-LDs) identified functionally related protein subsets with similar LPS response profiles. Five protein clusters are detailed. (**B**) Physical interaction within components of the PLIN2 cluster was assessed by co-immunoprecipitation experiments. myc-FLAG-tagged *IGTP* (*IRGM3*) was transfected for 24 hours in HuH7 cells. IGTP was immunoprecipitated using anti-FLAG antibodies (left panel) and interaction with endogenous PLIN2 evaluated by immunoblotting (right panel). Weak co-immunoprecipitation of myc-FLAG-tagged CAMP with PLIN2 was also detected (see fig. S10) (representative of two independent experiments).

Bosch et al., Figure S4

A

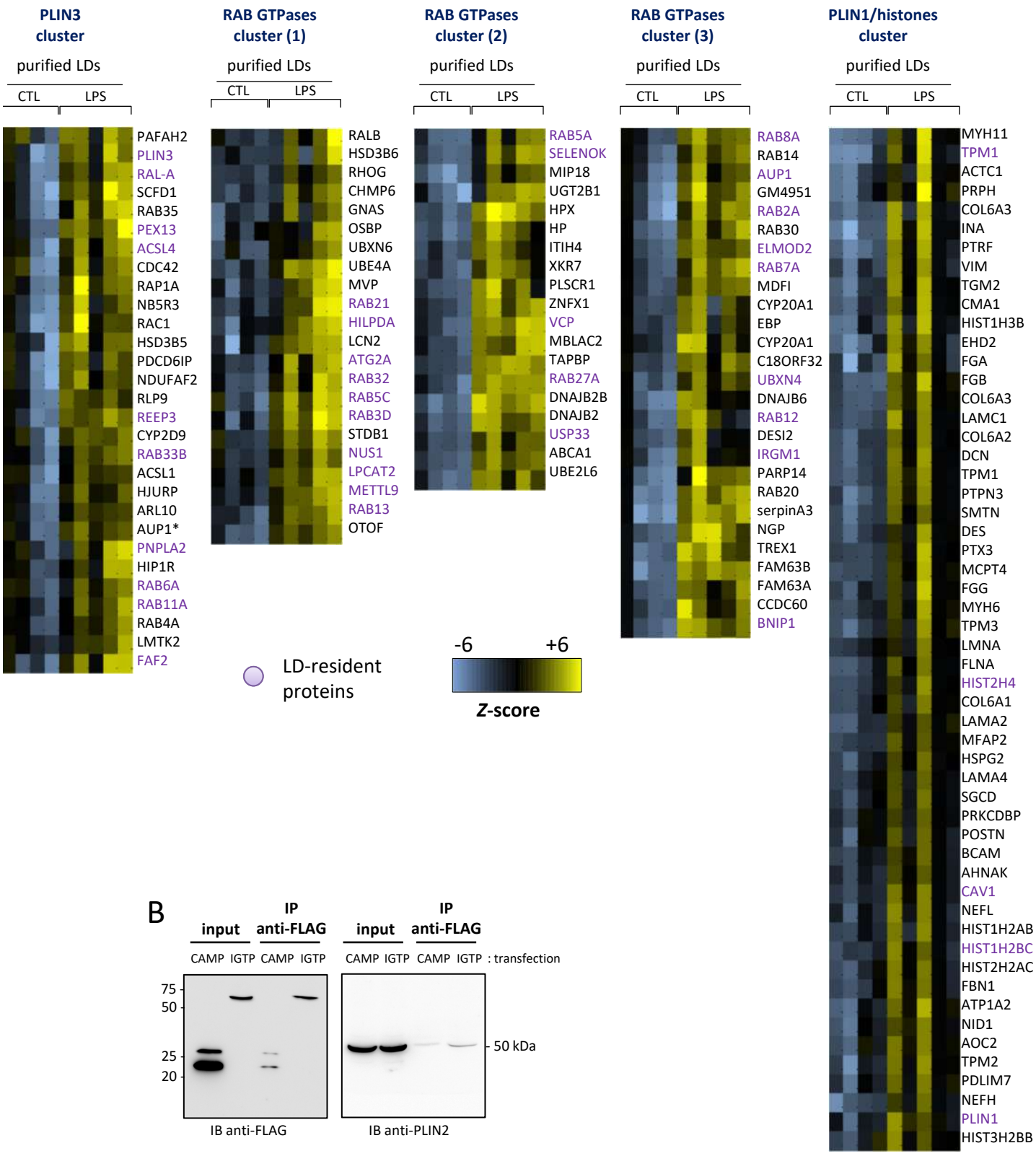

B

Fig. S5. Hepatic LDs and LD proteins are regulated by cytokines.

(**A**) Sections of CLP- (left), LPS- (top right), and CTL-liver (bottom right) were fixed and stained with anti-PLIN2 antibodies (LDs, red) and DAPI (nuclei, blue). In CLP and LPS-livers, PLIN2 was strongly expressed in hepatocytes at the peri-portal region (PP), when compared to hepatocytes located in peri-vein regions (PV). In CTL-livers, PLIN2 was observed being homogenously distributed (representative of two mice per condition). Periportal hepatocytes receive both nutrient-rich blood from the portal vein, and oxygen-rich blood via the hepatic artery, which contains circulating hormones and cytokines. This expression profile suggests that during inflammation and infection, LPS-LDs accumulate in specialized hepatocytes. Scale bars: 50 μm. (**B**) In-silico IPA analysis of potential upstream regulators of LPS-LDs proteins was performed. The network was modeled restricting LPS-TLR4 signaling to myeloid cells and mapping downstream events to hepatocytes. Indicated phospho-signaling target sites in selected LPS-LDs proteins were retrieved from Group-based Prediction System database. (**C**) Human hepatic HuH7 cells were treated for 16 hours with LPS, TNF, or IFNγ. Relative expression of the indicated genes encoding LD proteins was quantified by qRT-PCR (n = 3). Graphs show mean ± SD; not significant (ns), **P*<0.05, ***P*<0.01 in one-way ANOVA multiple comparisons test.

Bosch et al., Figure S5

A PLIN2 in mice liver

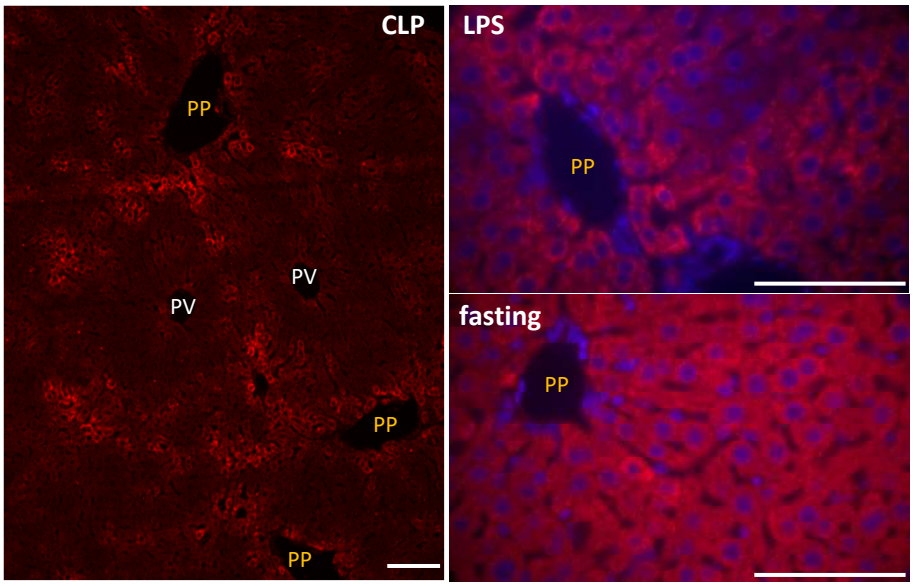

B Signaling on LDs

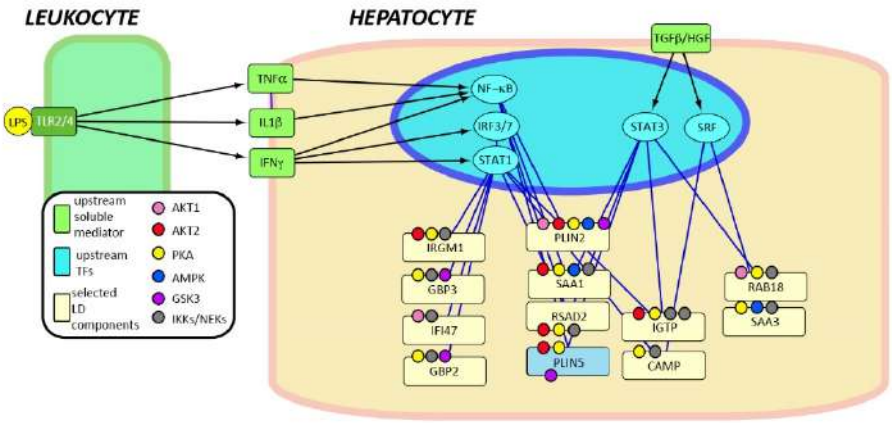

C LD proteins expression

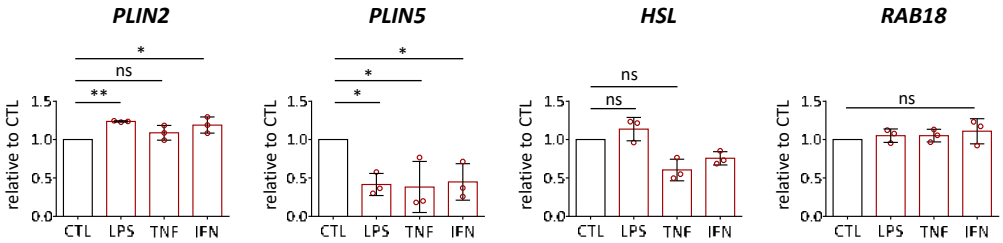

Fig. S6. LPS reduces LD-mitochondrial contacts.

(**A** to **C**) Liver sections of CTL- (A) and LPS-mice (B and C) were prepared for TEM analysis. Examples of LD-mitochondrial contacts are indicated with arrows (A, B). The white square in (B) marks a high magnification micrograph shown in (C). Arrowheads indicate membranes of the ER apparently separating LDs and mitochondria (C). Images are representative of two mice per condition. Scale bars: 5 μm (A); 2 μm (B); and 1 μm (C).

Bosch et al., Figure S6

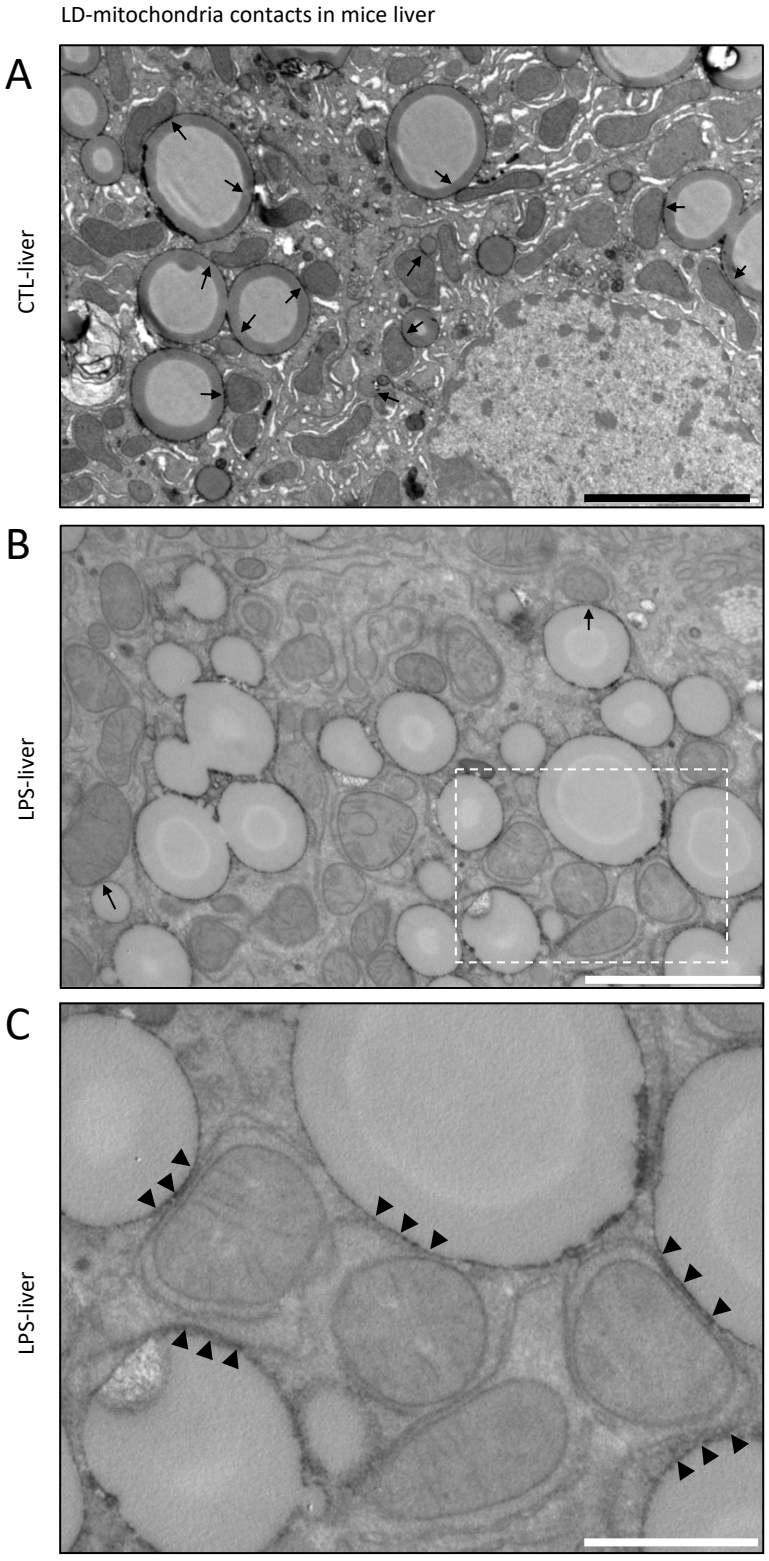

Fig. S7. PLIN5 regulates metabolism and immune defense.

(**A** and **B**) Responsiveness of HEK293-TLR4^{+} cells was measured by quantifying the LPS-induced mRNA expression of tumor necrosis factor (*TNF*) and interleukin 8 (*CXCL8*) after an overnight treatment with LPS (n = 3). (**C**) In addition, interleukin 8 (IL8) secretion in response to LPS was determined by ELISA (n = 3). (**D** to **F**) HEK293-TLR4^{+} cells were transfected with human *PLIN5* (myc-FLAG tagged) and treated for 16 hours with either OA or with OA+LPS. Cells were fixed and stained with an anti-FLAG antibody (PLIN5, purple), anti-TOM20 antibody (mitochondria, red), BODIPY (LDs, green), and DAPI (nuclei, blue). D shows a representative cell. Scale bar: 20 nm. Random confocal microscopy images of individual cells were analyzed using the computer code 1 (https://zenodo.org/badge/latestdoi/280189667) to quantify the number of LDs-mitochondria contacts (E) and the average length of each individual contact (F). 66 transfected cells and 470 non-transfected cells, obtained from three independent experiments, were analyzed. Graphs show mean ± SD; **P*<0.05, ***P*<0.01, ****P*<0.01, *****P*<0.0001; not significant (ns) in one-way ANOVA multiple comparisons test. (**G** to **J**) THP-1 cells were lentivirally transduced with constructs for doxycycline-inducible expression of *PLIN5*, or an empty vector control. Upon doxycycline induction, THP-1 cells were infected with *E. coli* for 8 hours and subsequently processed for TEM analysis. Representative TEM micrographs of cells expressing the empty vector (G, left), or *PLIN5* (H, left) are depicted. The white rectangles in G and H (left) indicate the area for a high magnification image (G, H; right) and asterisks indicate LDs in contact with mitochondria. Scale bars: 5 μm (G and H, left); 500 nm (G, right); and 1 μm (H, right). The length of the LD-mitochondria (I) and LD-bacteria (J) contacts were measured in TEM images. At least 67 cells (I) or 41 cells (J) were analyzed. Graphs show mean ± SD; ****P*<0.01 in paired *t*-test.

Bosch et al., Figure S7

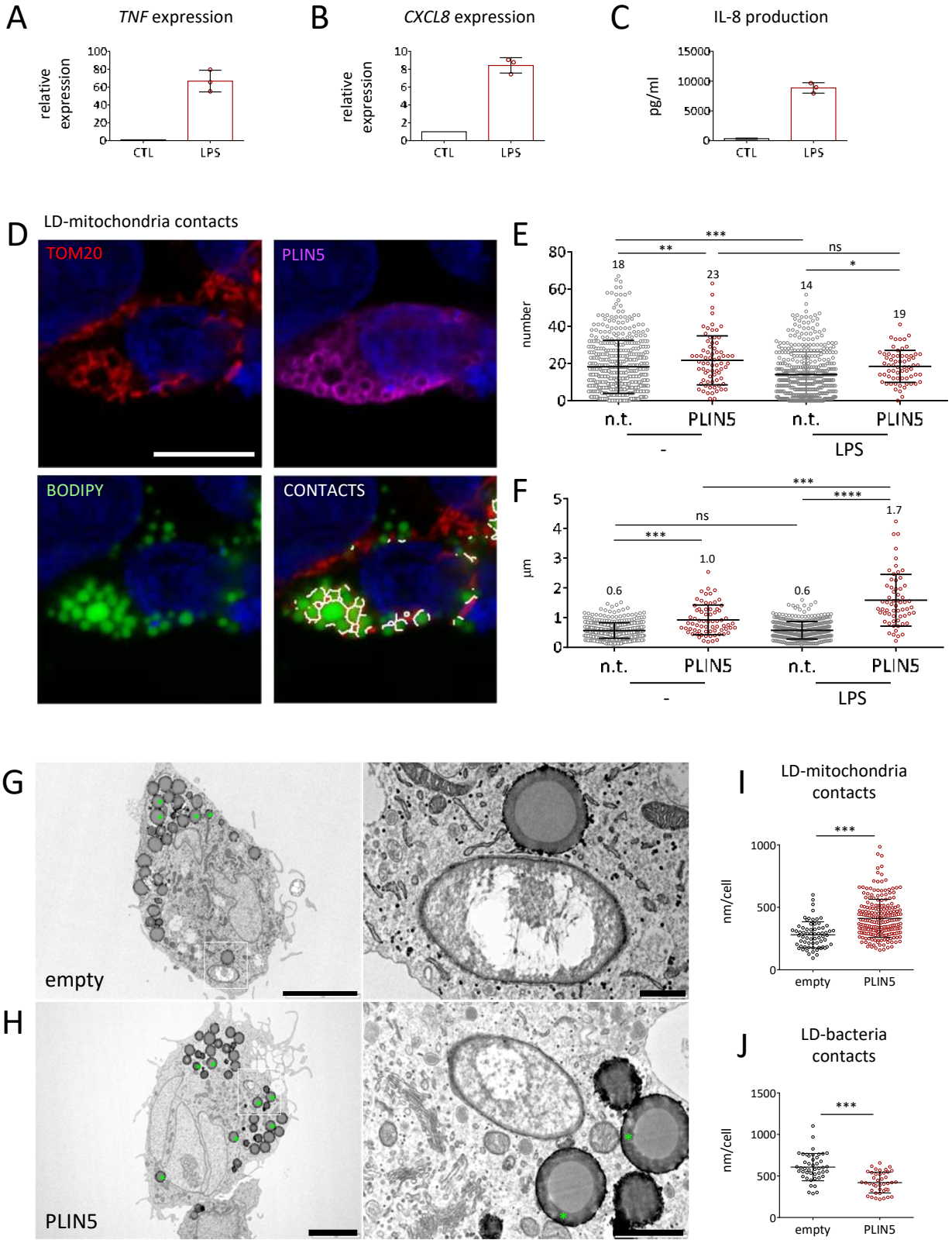

Fig. S8. Antiparasitic and antiviral proteins accumulate on LDs in HuH7 cells.

(**A** to **E**) Tagged human forms of *IGTP* (A and B) and *viperin* (D and E) were transfected in human hepatic HuH7 cells. Cells were treated with OA to induce LD formation. The distribution of indicated proteins was analyzed by confocal microscopy after 16 hours. Cells were fixed and stained with anti-FLAG antibodies (protein-of-interest; green), LipidTox (LD, blue), and anti-PLIN2 antibodies (end PLIN2, red). Representative cells are shown in A and D. High magnification of a selected region (white square) are shown in B and E. A fluorescence profile of one selected LD (white dotted line) is also included. The accumulation of proteins on LDs was quantified with a computer code as the percentage of green pixels in contact with blue pixels with the computer code 2 (https://zenodo.org/badge/latestdoi/280200243). An identically tagged PLIN2 was used as a control to quantify distribution of a bona fide LD-resident protein (C). At least 25 cells, from two independent experiments were quantified. Scale bar: 20 μm.

Bosch et al., Figure S8

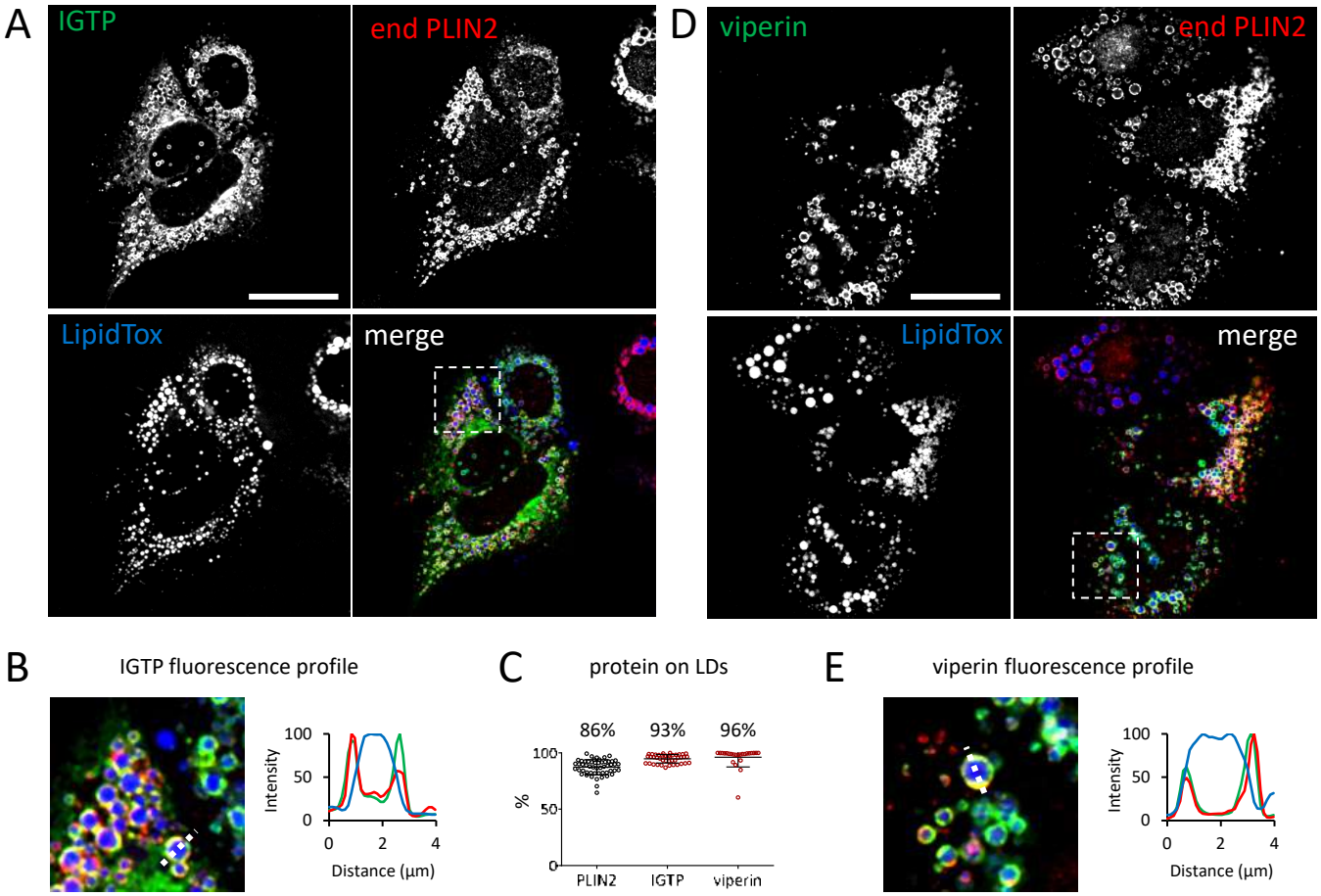

Fig. S9: Interferon-inducible immune GTPases accumulate on LPS-LDs in HuH7 cells.
(**A** to **D**) HuH7 cells were transfected with human IFI47 (A), IIGP1(B), or TGTP1 (C). Cells were treated with OA for 16 hours and protein distribution was analyzed by confocal microscopy. The distribution of the proteins was analyzed by confocal microscopy after 16 hours. Cells were fixed and stained with anti-FLAG antibodies (protein-of-interest; green), LipidTox (LD, blue), and anti-PLIN2 antibodies (end PLIN2, red). Representative cells are shown. High magnification of a selected region (white square) are included. A fluorescence profile of one selected LD (white dotted line) is also analyzed. The accumulation of proteins on LDs was quantified with a computer code as the percentage of green pixels in contact with blue pixels with the computer code 2 (https://zenodo.org/badge/latestdoi/280200243). An identically tagged PLIN2 was used as a control to quantify distribution of a bona fide LD-resident protein (D). At least 25 cells, from two independent experiments were quantified. Scale bar: 20 μm.

Bosch et al., Figure S9

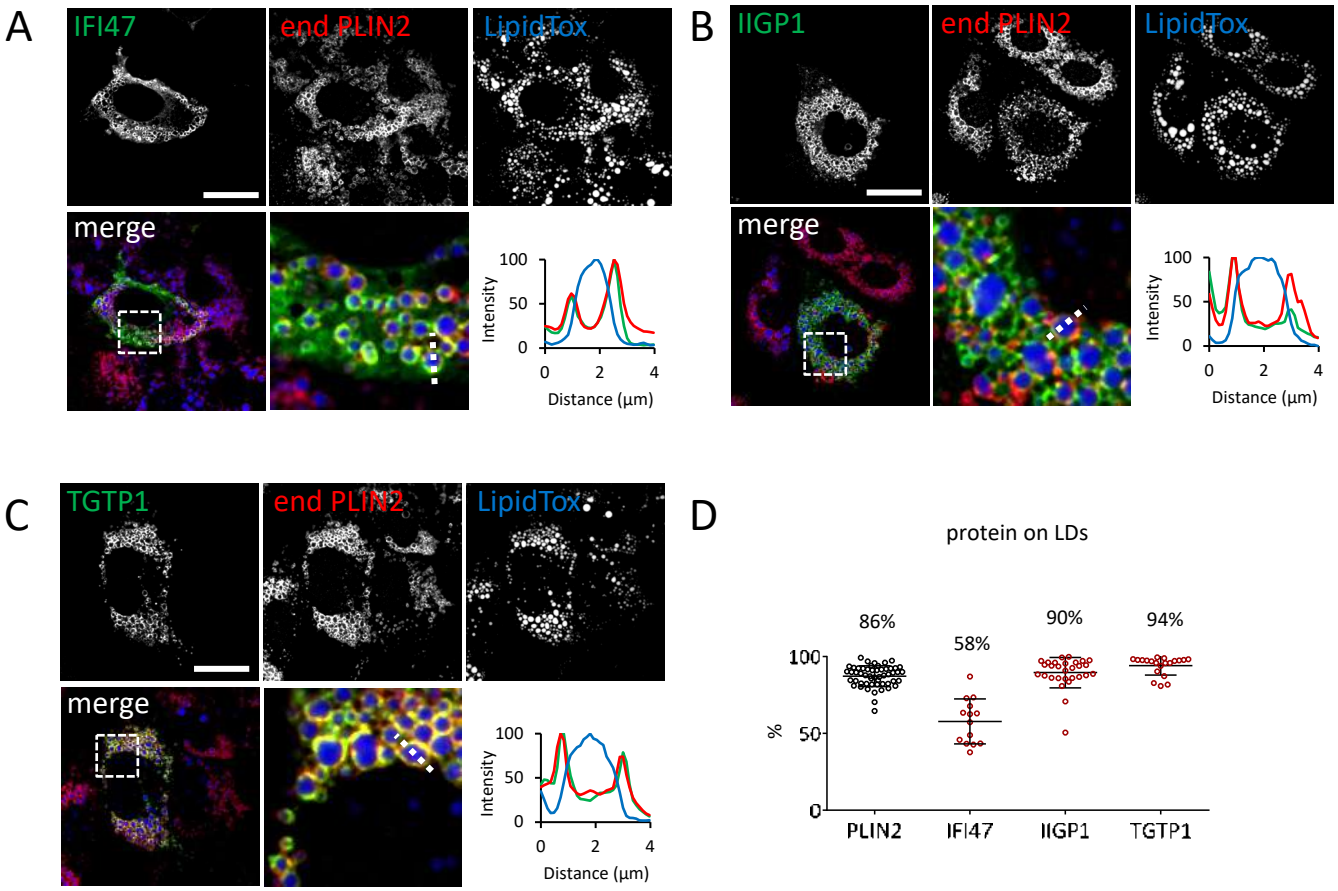

Fig. S10. The antimicrobial protein cathelicidin (CAMP) accumulates on LPS-LDs.
(**A**) Amino acid sequence of human cathelicidin pro-protein (CAMP, NCBI RefSeq protein ID NP_004336.4). Different domains of the protein are highlighted by a color code: active peptide (LL-37) in red, the hydrophobic region containing the signal peptide is indicated in yellow, and the central region in green. (**B** to **D**) HuH7 cells were transfected with a C-terminally tagged human *CAMP*. Cells were treated with OA for 16 hours and protein distribution was analyzed by confocal microscopy. The distribution of CAMP was analyzed by confocal microscopy after 16 hours. Cells were fixed and stained with anti-FLAG antibodies (CAMP; green), LipidTox (LD, blue), and anti-PLIN2 antibodies (end PLIN2, red). A representative transfected cell is shown in B. High magnification of a selected region (white square) and the fluorescence profile of one LD (white dotted line) are analyzed in C. The distribution of CAMP on LDs was quantified with a computer code as the percentage of green pixels in contact with blue pixels with the computer code 2 (https://zenodo.org/badge/latestdoi/280200243). An identically tagged PLIN2 was used as a control to quantify distribution of a bona fide LD-resident protein (D). At least 25 cells, from two independent experiments were quantified. Scale bar, 20 μm. **(E)** Human *CAMP* was transfected in HuH7 cells and subsequently cells were fractionated in sucrose density gradients. CAMP was detected with an anti-CAMP antibody (representative of 3 independent experiments). The immunoblot shows that CAMP has two different electrophoretic mobilities of ~24 (red arrow) and ~20 kDa (black arrow). The 24 kDa form of CAMP was mostly enriched on LDs. (**F**) A truncated form of CAMP lacking the signal peptide contained in the first 32 amino acids of the N-terminus was designed (ΔN). (**G**) HuH7 cells were transfected with the full-length *CAMP* (FL) or with ΔN. The ΔN mutant could only be detected by immunoblotting at comparable levels to the FL protein when cells were treated with the proteasome inhibitor MG-132, suggesting a rapid degradation of the ΔN mutant (representative of 3 independent experiments). In MG-132-treated cells, ΔN showed a single electrophoretic mobility identical to that of the 20 kDa form of CAMP, suggesting that the 24 kDa LD-form of CAMP contains an uncleaved signal peptide. (**H**) To confirm the secretion of the 20 kDa CAMP (form with a cleaved signal peptide) but not the 24 kDa CAMP, intracellular and extracellular FL and ΔN-mutant CAMP proteins were purified via their anti-myc-tags with a commercially available kit. Extra- (media) and intracellular (cells) protein distribution was evaluated by immunoblotting using an anti-CAMP antibody (representative of 3 independent experiments). Scale bar: 20 μm.

Bosch et al., Figure S10

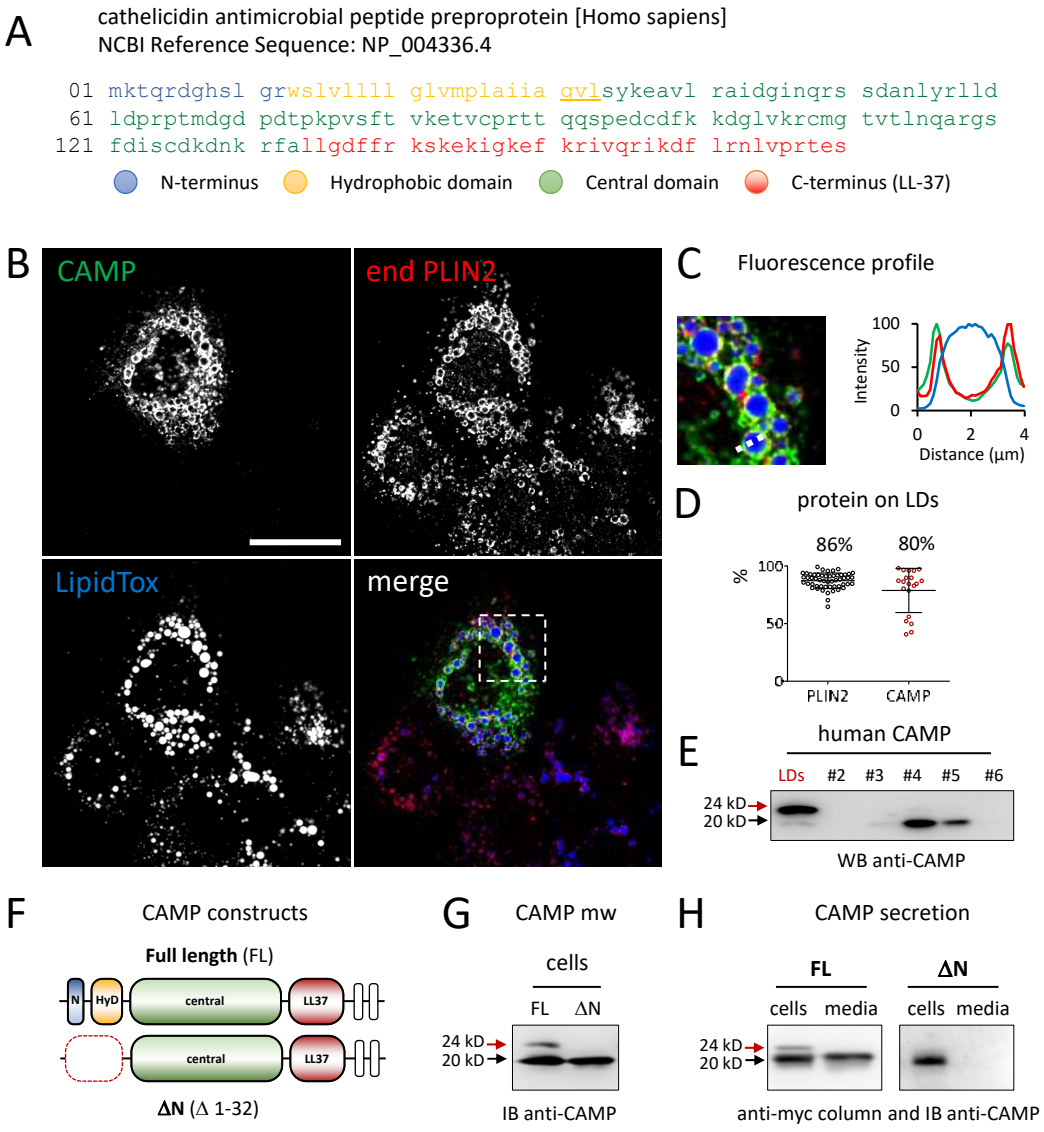

Fig. S11. The distribution of LD proteins is not directly regulated by LPS in HEK293-TLR4+ cells.

HEK293-TLR4^{+} cells were transfected with expression plasmids for the indicated tagged human LD proteins and treated for 16 hours with OA (top) or with OA + LPS (bottom). Cells were fixed and stained with anti-FLAG antibodies (POIs, red), LipidTox (LDs, green) and DAPI (nuclei, blue). White arrows indicate regions that were selected for a higher magnification insert (top right). Distribution of POIs was examined by confocal microscopy. No differences in protein distribution were observed (images are representative of two independent experiments). Scale bar: 20 μm.

Bosch et al., Figure S11

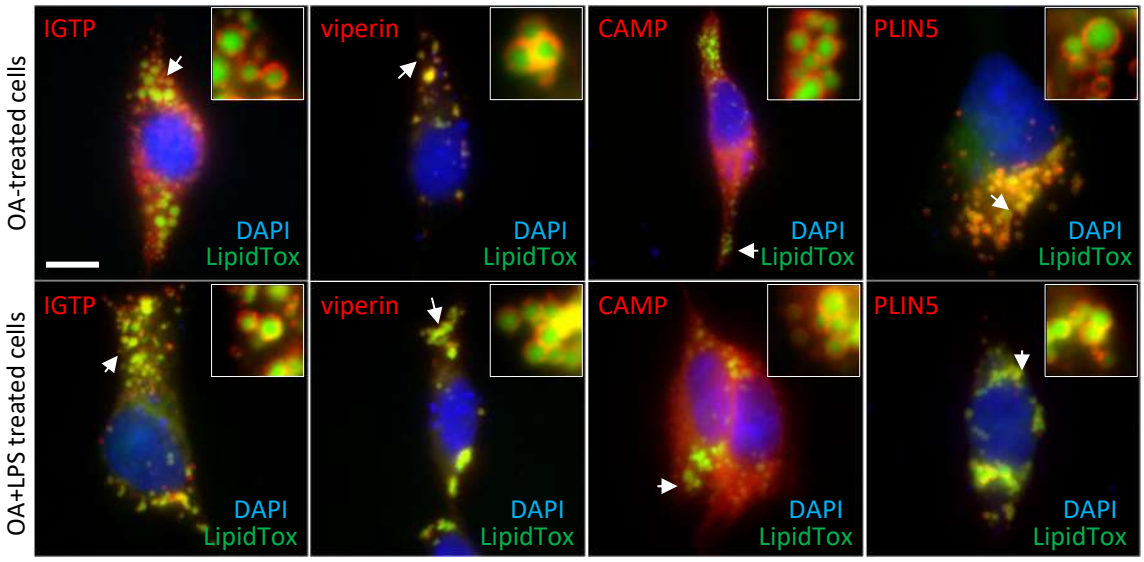

Fig. S12. Design and characterization of a LD-resident form of CAMP.

(**A** to **C**) The design of a LD-resident CAMP protein (LD-CAMP) is shown in A. The 30 amino acids corresponding to the CAMP signal peptide (blue and yellow letters in fig. S10) were substituted by the first 28 amino acids of the hydrophobic domain of ALDI (purple letters in A, TMpred in ExPASy); ALDI is a bona fide LD-resident protein. (**C**) Location of LD-CAMP on LDs was confirmed by fractionating transfected OA-treated HuH7 cells in sucrose density gradients (representative from N = 4). (**D** to **F**) HuH7 cells were transfected with LD-*CAMP*. Cells were treated with OA for 16 hours and protein distribution was analyzed by confocal microscopy. The distribution of LD-CAMP was analyzed by confocal microscopy after 16 hours. Cells were fixed and stained with anti-FLAG antibodies (LD-CAMP; green), LipidTox (LD, blue), and anti-PLIN2 antibodies (end PLIN2, red). Representative transfected cells are shown in D. High magnification of a selected region (white square) and the fluorescence profile of one LD (white dotted line) are analyzed in E. The distribution of CAMP on LDs was quantified with a computer code as the percentage of green pixels in contact with blue pixels (computer code 2 https://zenodo.org/badge/latestdoi/280200243). An identically tagged PLIN2 was used as a control to quantify distribution of a bona fide LD-resident protein (F). At least 45 cells, from two independent experiments were quantified. Scale bar: 20 μm. (**G** and **H**) HEK293-TLR4^{+} cells were transfected with *PLIN3*, LD-*CAMP*, or *CAMP* and treated with OA for 24 hours. The protein expression levels of LD-CAMP and CAMP were evaluated by immunoblotting with an anti-CAMP antibody (G). Cells were infected with *E. coli* for 4 hours and bacterial growth was quantified as relative CFU (H) (n = 5). Graphs show mean ± SD; ***P<0.001; not significant (ns) in a paired t-test. (**I** and **J**) HEK293-TLR4^{+} cells were transfected with LD-*CAMP* tagged with myc-FLAG, or with untagged LD-*CAMP*. (**I**) Cells were treated with OA for 24 hours and the protein expression levels were determined by immunoblotting with anti-FLAG antibodies and quantified by densitometry (ImageJ, n = 2). (J) Cells were infected with *E. coli* for 4 hours and bacterial growth was quantified as relative CFU (n = 5). Graphs show mean ± SD; **P<0.01 in a paired t-test. Scale bar: 20 μm.

Bosch et al., Figure S12

A

RecName: Full=Methyltransferase-like protein 7B; AltName: Full=Associated with lipid droplet protein 1; Short=ALDI; Flags: Precursor. UniProtKB/Swiss-Prot: Q562C4.1

```
  1 mdvlvpllql lvllltlplh llallgcwqp icktyfpylm atltarsykk meskkrelfs
 61 qikdlkgtsn evtllelgcg tganfqfypp gckvtcvdpn pnfekfltks maenrhlqye
121 rfivaygenm kqladssmdv vvctlvlcsv qsprkvlqev qrvlkpggll ffwehvsepq
181 gsqallwqrv leptwkhigd gchltretwk diekaqfsev qlewqpppfk wlpvgphimg
241 kavk
```

B

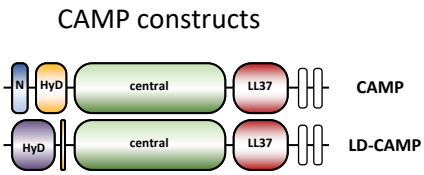

C

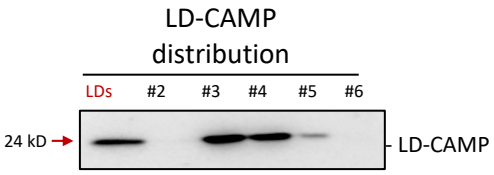

D

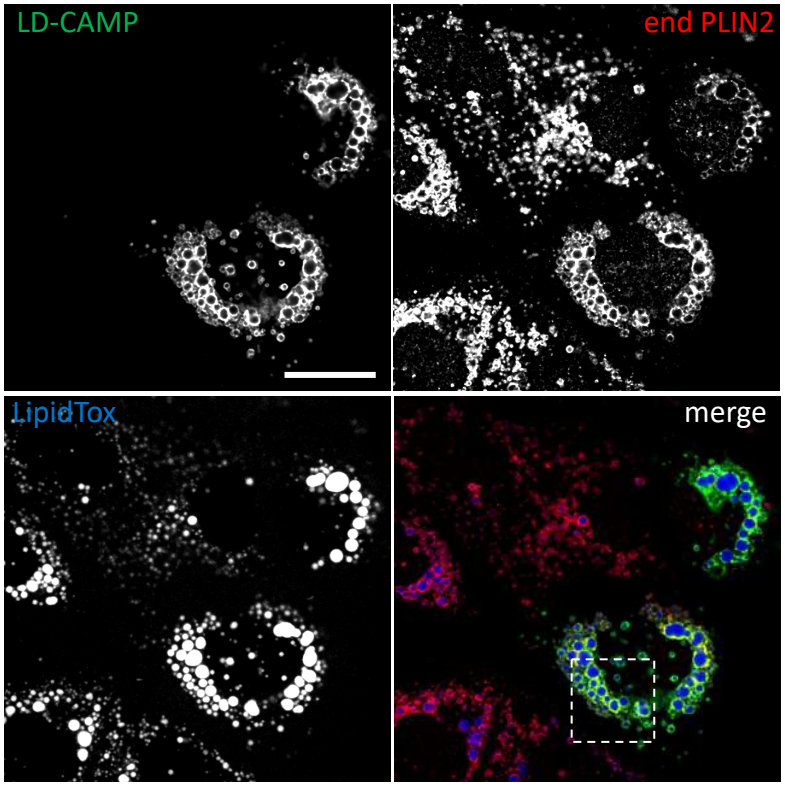

E

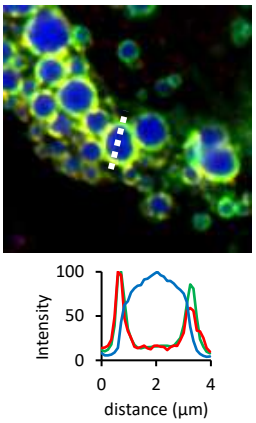

F

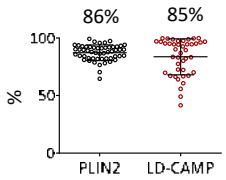

G

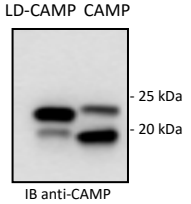

H

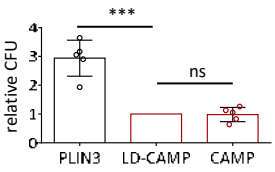

I

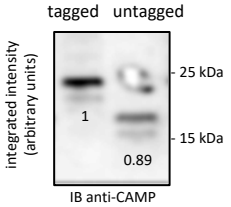

J

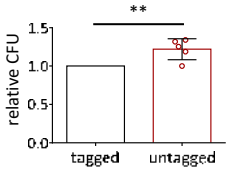

Legends to Supplementary Tables

(Mass spectrometry data have been deposited in Peptide Atlas (ID: PASS01610)).

Table S1. Proteins upregulated in LPS-livers.
The table includes proteins significantly upregulated in liver homogenates of animals treated with LPS as compared to control animals. Average differential enrichment score in LPS-treated samples versus untreated samples is indicated (ΔZq).

Table S2. Proteins downregulated in LPS-livers.
The table includes proteins significantly downregulated in liver homogenates of animals treated with LPS as compared to control animals. Average differential enrichment score in LPS-treated samples versus untreated samples is indicated (ΔZq).

Table S3. Proteins identified in LD fractions.
Proteins are ranked by differential enrichment in LPS-LDs as compared to CTL-LDs (ΔZq). Proteins found in different resources as LD core-resident proteins are highlighted in purple hue, indicating the specific sources where they were found (see table S4). Reference#1 corresponds to Krahmer et al. (*14*), #2 to Bersuker et al. (*15*), and #3 to the automated annotation by IPA platform (Qiagen bioinformatics).

Table S4. Proteins upregulated in LPS-LDs.
The table includes proteins significantly upregulated in LD fractions purified from animals treated with LPS as compared to LD fractions from livers of control animals.
Average differential enrichment score in LPS-LD samples versus CTL-LD samples is indicated (ΔZq). Proteins found in different resources as LD core- proteins are highlighted in purple hue, indicating the specific sources where they were found. Reference#1 corresponds to Krahmer et al. (*14*), #2 to Bersuker et al. (*15*), and #3 to the automated annotation by IPA platform (Qiagen bioinformatics).

Table S5. Proteins downregulated in LPS-LDs.
The table includes proteins significantly downregulated in LD fractions purified from animals treated with LPS as compared to LD fractions from livers of control animals.

Average differential enrichment score in LPS-LD samples versus CTL-LD samples is indicated (ΔZq). Proteins found in different resources as LD core- proteins are highlighted in purple hue, indicating the specific sources where they were found. Reference#1 corresponds to Krahmer et al. (*14*), #2 to Bersuker et al. (*15*), and #3 to the automated annotation by IPA platform (Qiagen bioinformatics).

Table S6. Identified LD-resident proteome.

Subset of the full proteome identified in LD fractions (see table S3) that is annotated in different resources as bona fide LD-resident proteins, preferentially localizing to this compartment. Legend for the different resources referenced is indicated. m.c. means manually curated from the reference indicated in the text. Reference#1 corresponds to Krahmer et al. (*14*), #2 to Bersuker et al. (*15*), and #3 to the automated annotation by IPA platform (Qiagen bioinformatics).

Table S7. LD-resident proteins responding to LPS.

LD-resident proteins (see Table S6) significantly unregulated (upper section) or down regulated (lower section) in LPS-LD fractions as compared to CTL-LD fractions. Differential enrichment observed in the LD dataset (table S3; table S4; and table S5) and the liver homogenate dataset (table S1; and table S2) is indicated, together with their mapping to specific protein clusters (see Fig. 2D; and fig. S4).

Anexo 3

KIARELY, E.S.; **PEREIRA-DUTRA, F.S.**; FERRARO-MOREIRA, F.; GOLTARA, T.C.; RAJÃO, M. A.; PRESTES, E.; BOZZA, M.T. BOZZA, PT. **Lipid droplet accumulation occurs early following *Salmonella* infection and contributes for intracellular bacterial replication.** Manuscrito submetido.

Lipid droplet accumulation occurs early following *Salmonella* infection and contributes for intracellular bacterial replication.

Ellen Kiarely de Souza[1]*, Filipe Santos Pereira-Dutra[1]*, Felipe Ferraro Moreira[1], Taynná da Costa Goltara Gomes[1], Matheus Andrade Rajão[3], Elisa Prestes[2], Marcelo Torres Bozza[2], Patrícia Torres Bozza[1].

1 Laboratory of Immunopharmacology, Instituto Oswaldo Cruz, Fundação Oswaldo Cruz, Fiocruz, Rio de Janeiro, Brazil.

2 Laboratory of Inflammation and Immunity, Department of Immunity, Instituto de Microbiologia Paulo de Góes, Universidade Federal do Rio de Janeiro, UFRJ, Rio de Janeiro, Brazil.

3 Program of Immunology and Tumor Biology, Instituto Nacional do Câncer, INCA, Rio de Janeiro, Brazil

Corresponding author: pbozza@ioc.fiocruz.br

Address: Laboratório de Imunofarmacologia, Fundação Oswaldo Cruz, 4365, CEP 21045-900, Phone: +5551 21-25621763, Rio de Janeiro, RJ, Brazil.

*These authors contributed equally to this work

Abstract

Salmonellosis is a public health problem caused by *Salmonella* sp., a highly adapted facultative intracellular pathogen. After internalization, *Salmonella* sp. manipulates several host process, mainly through the activation of the type III secretion system (T3SS) which are used to translocate bacterial effector into the host cytoplasm. Modification of host lipid metabolism and lipid droplet (LD) accumulation in leukocytes are common phenotypes in inflammatory and infectious processes. LDs are dynamic and complex lipid-rich organelles involved in several cellular processes, including the immune response. The present study investigated the mechanism involved in LD biogenesis in *Salmonella*-infected macrophages and its role in bacterial pathogenicity. Here, we reported that *S.* Typhimurium induced a rapid time-dependent increase of LD formation in macrophages. The LD biogenesis is a phenomenon dependent on *Salmonella*'s viability and T3SS activity, with the usurpation of Toll-Like Receptor (TLR) signaling. We also observed that *S.* Typhimurium-induced LD biogenesis is a phenomenon dependent of TLR2 signaling and counter-regulated by TLR4. Moreover, the inhibition of LD formation by A922500 significantly reduced the number of intracellular viable bacteria in 24-hours post-infection, but did not impair PGE_2, IL-1β, IL-6 and MCP-1 production. Collectively, our data demonstrate the role of LD biogenesis, via TLR2/T3SS pathway, on *S.* Typhimurium intracellular replication in macrophages, without interference in the inflammatory response, suggesting that LDs may contribute as a source of energy or nutrients.

Keywords: Lipid bodies, Lipid metabolism, *Salmonella* Typhimurium, TLRs, PGE_2

Importance

Salmonellosis is a public health problem caused by *Salmonella* sp., a highly adapted facultative intracellular pathogen, with a great capacity to modulate several processes of the host cell. Lipid droplets (LD) cell accumulation is a frequent phenotype during the infection of a myriad of pathogens, however, the mechanisms underlying the role of this organelle in several bacterial infections, such as in *S.* Typhimurium, are not fully understood. Herein, we describe that the LD biogenesis is dependent on the participation of both *Salmonella* pathogenicity factor and host signaling in macrophages. Moreover, we report that LD biogenesis triggered by *S.* Typhimurium is an early phenomenon, dependent bacterial viability and pathogenicity, and host immune receptors. Furthermore, LD accumulation contributes to optimal *S.* Typhimurium intracellular replication in macrophages, which is dissociated from immunomodulatory role of LDs. Taken together our results demonstrate that the roles for LDs as an energy source and as immunomodulatory platformer are not a conjoined phenomenon. These data set provides new perspectives for future investigations about host-pathogens interaction, and targets for future therapeutic interventions.

1. INTRODUCTION

Salmonellosis is a global public health problem caused by *Salmonella* spp., a facultative and highly adapted intracellular pathogen belonging to the family Enterobacteriaceae (1). *Salmonella* infection is one of the most common foodborne illnesses whose severity ranges from self-limiting gastroenteritis to systemic infection, including enteric fever (2–4). The severity of *Salmonella* infections varies according to serotype, animal species infected, age and health status of the host (5, 6).

A remarkable aspect of *Salmonella* infection is its ability to invade, to survive, and often to multiply within non-phagocytic cell as well as professional phagocytes (7, 8). When internalized, *Salmonella* interferes with phagosome maturation, resulting in the formation of a specialized *Salmonella*-containing vacuole (SCV), where Salmonella usually persist and replicate within the host cells (9, 10). Invasion and SCV biogenesis are dependent on the type III secretion systems (T3SS) which are used to translocate bacterial effector into the cell cytoplasm to manipulate host process (11, 12). The lipid remodeling of the host cell and consequent cholesterol accumulation and its esterification at the SCV by SseJ effector has been found to have an important role in regulating SCV dynamics and probably in intracellular bacterial survival (13).

Bacterial pathogens display a highly specialized mechanism to support crucial infection events, including subversion of host metabolism and evasion of the immune response (14, 15). In the context of host-pathogen interactions, the participation of lipid droplets in infectious disease has been reported for all classes of pathogens (16, 17). Lipid droplets (LD) or lipid bodies are complex and dynamic lipid-rich organelles virtually present in all cell types, being the mainly neutral lipid storage (17, 18). Moreover LDs are essential for various cellular processes and for the immune response (19, 20). During infection, LD biogenesis is a highly regulated process whose

mechanisms are dependent on the infectious agent and cell type involved (21, 22). Several intracellular bacteria exploit the LD to obtain an energy resource from the host, as well as a strategy to escape the immune system through increased generation of eicosanoids (23–27).

Despite the evidence of the LD participation in *Salmonella* infection (13, 28–30), the role of LDs in *Salmonella* pathogenicity not yet known. The present study investigated the mechanism involved in LD biogenesis in *Salmonella*-infected macrophages and the role of this organelle in the bacterial pathogenicity. Our findings point that *S. typhimurium* induce early LD biogenesis with the subversion of host signaling pathways, and it contributes for intracellular bacterial replication.

2. MATERIALS AND METHODS

Reagents

T3SS inhibitor cytosporone B (Cat# C2997), iDGAT-1 inhibitor A922500 (Cat# A1737), Saponin from Quillaja bark (Cat# S7900), and Oil Red O (Cat# O0625) were purchased from Sigma-Aldrich (Saint Louis, MO, USA). Luria-Bertani broth (Cat# K25-1551) and Tryptic Soy Agar (Cat# K25-610052) was obtained from Kasvi (São José do Pinhais, PR, Brazil). RPMI-1640 (cat# 22400-089), penicillin-streptomycin (Cat# 15140148), gentamicin (Cat# 15750060) and L-glutamine (Cat# 25030081) were obtained from Gibco (Grand Island, NY, USA). From DAPI (Cat# D1306) and Fluoromount-G Mounting Medium (Cat# 00-4958-02) were purchased from ThermoFisher Scientific (Waltham, MA, USA).

Mice

C57BL/6 (B6) mice were supplied by the Institute of Science and Technology in Biomodels from Oswaldo Cruz Foundation, and used at 8–12 weeks of age. All animal experiments were approved by the Institutional animal welfare committee in agreement with the Brazilian National guidelines supported by CONCEA (Conselho Nacional de Controle em Experimentação Animal) under license number L025/15 (CEUA/FIOCRUZ). Mice were maintained with rodent diet and water available *ad libitum* with 12h light–dark cycle under controlled temperature (23 ± 1 °C).

Macrophages cell culture

To obtain bone marrow-derived macrophages (BMDM), cells isolated from femur and tibia of B6 mices were cultured for 7 days in RPMI-1640 medium supplemented with 30% (vol/vol) L929 supernatant, 20% (vol/vol) heat-inactivated fetal bovine serum, 1% L-glutamine (vol/vol), and 1% penicillin-streptomycin (vol/vol) as previously described by Assunção et al., (2017). Differentiated macrophages were cultured in RPMI-1640 supplemented with 10% heat-inactivated fetal bovine serum (vol/vol), 1% L-glutamine (vol/vol), and 1% penicillin/streptomycin (vol/vol). BMDM cells were maintained at a density of $0.1x10^6$ – $5x10^5$ cells/ml. iBMM cell lineages were cultured in RPMI 1640 supplemented with 10% heat-inactivated fetal bovine serum, 1% L-glutamine (vol/vol) and 1 % penicillin/streptomycin with 5% CO_2 at 37°C. iBMM cells were maintained at a density of $0.1x10^6$ – $5x10^5$ cells/ml. Cell lines were tested for mycoplasma at regular intervals.

Bacterial strains and growth conditions

Salmonella enterica serovar Typhimurium (ATCC 14028) e *Escherichia coli* (ATCC 25922) used in this study were obtained from Enterobacteria Collection (CENT) of the Oswaldo

Cruz Foundation. The bacteria were cultured in Luria-Bertani broth (LB) for 16–18 h at 37°C to obtain stationary growth phase cultures and were then centrifuged (1,000 × g) for 10 min at 4°C. The pellets were resuspended in PBS to an OD of 0.1 at 660 nm, corresponding to 10^8 CFU/mL.

Salmonella killed by irradiation received 10^4 Gy from a cobalt source as described by Lahiri et al. (2005). The anti-virulence activities of cytosporone B (Cns-B) as a *Salmonella* T3SS inhibitor were used in this study as described by Li et al. (2013). Briefily, the Cns-B were dissolved in dimethyl sulfoxide (DMSO, Sigma) to concentrations of 100 mM as stock solution. *S. typhimurium* cells were cultured overnight a 37°C in agitation. The overnight culture was diluted 10-fold in LB in the in the absence or presence of Cns-B at a final concentration of 100 µM and cultured for 1h at 37°C.

Salmonella infection of macrophages and treatments

An *in vitro* gentamicin protection assay was used to measure invasion and intracellular proliferation of *S. typhimurium* based on the method described by Lissner et al. (1983), with some modifications. The macrophages were seeded at 1 x 10^5 and 5 x 10^5 cells per well in 24- and 12-well places (flat-bottom, tissue-culture-treated plates; Costar), respectively, and were incubated for 12 h at 37°C and 5% CO_2. Meanwhile, *S. enterica* serovar Typhimurium cells were cultured overnight at 37°C with agitation. Macrophages were infected with *S. typhimurium* at a multiplicity of infection (MOI) of 10. One hour after infection at 37°C and 5% CO_2, the culture medium was discarded and the cells were washed with PBS with 100 µg/mL gentamicin three times. RPMI supplemented with 100 µg/mL gentamicin was added to each well to kill noninvasive bacteria cells, and incubation was continued for another 1 h. After incubation, media were removed again, and a fresh media without gentamicin was added for the remainder for all the experiment time. A similar protocol was used to *E. coli* infection, using a MOI of 100. To impair the LD biogenesis,

5 μM of iDGAT1 inhibitor (A922500) was added to the cell culture and incubated for 30 min before *S. typhimurium* infection and remained for all the stimulus time, at 37°C in 5% CO2. The inhibitors were dissolved in dimethyl sulfoxide (DMSO, Sigma). For bacterial counting, at the indicated time points, cells were washed three times with PBS and lysed with 5% saponins solution. The CFU of bacteria were counted by plating the appropriate dilution in TSA plates. All experiments were done in triplicate.

Lipid droplets staining and quantification

BMDM and iBMM cells were fixed with 3.7% formaldehyde for 10 min and LDs were stained with 0.3% Oil Red O (diluted in isopropanol 60%) as previously described (35). Preparations were analyzed using a FluoView FV10i Olympus confocal microscope (Tokyo, Japan). Images were acquired, colored, and merged using Olympus FV10-ASW and Image J software. Pictures were taken with a 60× objective using FV10-ASW image software. The morphology of fixed cells was observed, and Oil red O-stained LDs were measured using the open source ImageJ software (https://imagej.nih.gov/ij/).

Cytokine analysis

Levels of interleukin 1β (IL-1β), interleukin 6 (IL-6), interleukin 10 (IL-10), monocyte chemoattractant protein-1 (MCP-1/CCL2), and Tumor Necrosis Factor-α (TNF-α) in macrophages supernatant were measured using mouse Duoset ELISA kit (R&D Systems; Minneapolis, MN, USA) according to manufacturer's instructions.

PGE_2 level measurements

Levels of Prostaglandin E_2 (PGE_2) in macrophages supernatant were measured using EIA kits (Cayman Chemical) according to manufacturer's instructions.

Lactate level determination

Lactate levels in the macrophages supernatant were measured using enzymatic lactate kit (cat# 138-1/50, Labtest diagnóstica; Lagoa Santa, MG, Brazil) performed as manufacturer's instruction.

Statistical analysis

Data obtained in this study were presented as mean ± SEM of three to six independent experiments. The normal distribution was performed using the Shapiro-Wilk test. The paired two-tailed t-test was used to evaluate the significance of the two groups. Multiple comparisons among three or more groups were performed by one-way ANOVA followed by Tukey's multiple comparison test. For all analyzes was adopted $p \leq 0.05$ as considered statistically significant.

3. RESULTS

S. typhimurium induced a rapid and expressive LD biogenesis in murine macrophages.

In several studies involving the pathogen-leukocyte interaction, a strong intercession has been reported between the with LD exploration with the success of the infection (18, 20). Although LD accumulation had been reported during *Salmonella*-infection (13), the role of this organelle in *Salmonella* pathogenesis is unknown. To determine the role LDs by *S. typhimurium* infection, we initially analyzed the dynamics of LDs accumulation with dynamics bacterial survival and

proliferation within macrophages. Interestingly, we observed that LD biogenesis induced by *S. typhimurium* is a rapid and expressive phenomenon **(Figure 1A)**. *Salmonella*-triggered LD biogenesis occurs as early as 1-hour post bacterial infection**, (Figure 1A-B)**, stayed significantly upregulated for 48-hours post-stimulation. Whereas the *Salmonella*-infected macrophages reached maximum LD induction occurred at 24 hours **(Figure 1B)**.

In this context, we also evaluated the *S. typhimurium* load within macrophages. After internalization, the number of viable intracellular bacteria decreased significantly between 1-hour and 6-hours post-infection **(Figure 1C)**. However, the bacterial load increases substantially between 6-hours and 24-hours post-infection, even exceeding amount of 1-hour **(Figure 1C)**. We also investigated the apposition to LDs between *S. typhimurium* during the infection within macrophages. Using confocal microscopy, we did not observe a frequent interaction between LD and bacteria neither in 1-hour **(Figure 1D and 1F)** nor in 6-hours post-infection **(Figure 1F)**. Whereas in 24-hours post-infection, we observed macrophages infected a close apposition to LDs and *Salmonella* **(Figure 1E-F)**.

The Salmonella-triggered early LD biogenesis is dependent of bacterial viability and T3SS activity

Although LD accumulation upon bacterial infection is highly pronounced in both human and experimental models (36, 37), the presence of LD biogenesis in early stages of infection remains relatively unexplored. To analyze if the rapid LD biogenesis is a specific event of *Salmonella* infection, we performed a comparative analysis between the *S.* Typhimurium and *E. coli*, two phylogenetically closely-related Gram-negative bacteria (38). Unlike *S.* Typhimurium**,** we observed that *E. coli* was not able to induce the early LD biogenesis in macrophages within 1-hour post-infection **(Figure 2A**), despite the greatest amount of internalized bacteria per cell

(Figure 2B). In 24-hours post-infection, both bacteria were able to induce the LD accumulation and no difference was detected in the amount of LDs in *E. coli* and *Salmonella*-stimulated macrophages **(Figure 2A)**. Interestingly, at this last time we observed a large increase in the amount of *Salmonella* per cell, and a decrease in the amount of *E. coli* **(Figure 2B)**.

As early LD biogenesis seems to be a particularity of *Salmonella* infection, our next step was to analyze the participation of the *S.* Typhimurium viability in the LD biogenesis. Macrophages were incubated with bacteria from an overnight culture (live), or with radiation-killed bacteria (dead). We observed that only live bacteria were able to induce the early LD biogenesis within 1-hour post-stimulation **(Figure 2C),** and this phenomenon was not just triggered by bacteria internalization **(Figure 2D)**. Moreover, LD amount in killed bacteria-stimulated macrophages was significantly less than those exposed to live bacteria within 24h post-stimulation **(Figure 2C)**. Since our results indicated that *Salmonella*-triggered LD biogenesis and accumulation is a process predominantly dependent on the viability of the bacteria **(Figure 2C-D)**, we also evaluated if this process would be associated with virulence mechanisms of bacteria. We checked if *Salmonella* T3SS activity would also involve the early LD biogenesis. *S.* Typhimurium were pretreated with cytosporone B (Cns-B), an anti-pathogenicity factor that inhibits T3SS **(Figure 2E)**. We observed that the use of Cns-B in *S.* Typhimurium not only reversed the early LD biogenesis within 1-hour post-stimulation, but also had a profound impact on the LD accumulation within 24-hour post-infection **(Figure 2F).** Similar to the other experiments, the rapid LD biogenesis was not related only to the internalization of bacteria, and as expected, T3SS inhibition had a profound impact on *Salmonella* intracellular replication **(Figure 2G).**

TLR signaling are required to early LD biogenesis induced by *Salmonella*

Since the activation of *S.* Typhimurium virulence genes necessary for intracellular survival, growth, and systemic infection has been associated with the subversion of Toll-like receptor (TLR) signaling (39), we investigated the functional role of TLR signaling on LD formation in *Salmonella* infection. We observed that iBMM double deletion of Myd88 and TRIF abolished the LD biogenesis induced by *Salmonella* both in 1-hour **(Figure 3A-B)** and 24-hours post-infection **(Figure 3C)**. Curiously, TRIF/MyD88 double-knockout macrophages show a significant increase in the number of viable intracellular bacteria in comparison to WT iBMM at both times analyzed **(Figure 3D-E).**

Since the recognition of *Salmonella* is largely mediated by TLR2 and TLR4, being assigned to these receptors an effective innate immune response to *Salmonella* (40–42), our next step was to analyze the participation of these key TLR in LD biogenesis. We observed that in $TLR2^{-/-}$ macrophages there was no increase of LD biogenesis induzed by *Salmonella* infection, while TLR4 deficiency lead to overproduction of LDs both in 1-hour **(Figure 3A-B)** and 24-hours post-infection **(Figure 3C)**. Neither $TLR4^{-/-}$ nor $TLR2^{-/-}$ macrophages showed a impairment of *Salmonella* internalization compared to WT iBMM **(Figure 3E)**. In 24-hours post-infection, $TLR4^{-/-}$ iBMM showed a significant increase in the bacterial load in comparison to WT iBMM. This phenomenon was not observed in $TLR2^{-/-}$ macrophages **(Figure 3F)**.

LD biogenesis contributes to intracellular bacterial replication, but not to inflammatory response

The LD biogenesis is dependent on activity of enzymes involved in the synthesis of triglycerides and/or cholesterol ester, such as diacylglycerol O-acyltransferase (DGAT-1 and DGAT-2) (43, 44). When lipid synthesis is blocked, the biogenesis of LD biogenesis is severely impaired (18). To understand the role played by LD accumulation in *Salmonella* infection, we

pretreated macrophages with a DGAT1 inhibitor (A922500) **(Figure 4A)**. The *Salmonella*-triggered LDs biogenesis was impaired in macrophages pretreated with A922500 both in 1-hour and 24-hours post-infection **(Figure 4B-C)**. Interestingly, in parallel to LD inhibition, A922500 pretreatment impaired the dynamics of bacterial load. Different from the observed in control, macrophages treated with A922500 did not show an increase of bacterial load between 1-hour and 24-hours post-infection **(Figure 4D).** Moreover, the A922500-treated macrophages showed a significant decrease in the number of viable intracellular bacteria in comparison to control in 24-hours post-infection **(Figure 4D),** despite of treatment not affecting bacteria internalization. These data suggest that LD accumulation favors the bacteria intracellular replication.

Lipid droplets are stores of the eicosanoid precursor arachidonic acid in different leukocyte subsets, and compartmentalize the entire enzymatic machinery for eicosanoid synthesis (45). We then investigated whether regulation of LD numbers by *Salmonella* also correlated with PGE_2 production. Unlike expected, the early LD biogenesis was not followed by the increase of PGE_2 level in 1-hour post-infection **(Figure 4E)**. Despite of elevated levels of PGE2 be coinciding with the time-point of the highest LD formation induced by *S.* Typhimurium in 24h-hour post-infection, the reduction of *Salmonella*-induced LD accumulation by A922500 treatment was not able to abrogate the PGE_2 production **(Figure 4E)**. Surprisingly, within the context of *Salmonella* infection, these results indicate no correlation between LD formation and PGE_2 production.

To determine whether the induction of LDs by *S.* Typhimurium would be associated to the inflammatory response of host cells, our next step was to investigate wheter LD biogenesis could be influencing the cytokine production. We observed that *S.* Typhimurium infection was able to induce an increase in IL-1β **(Figure 4E)**, IL-6 **(Figure 4F)**, and MCP-1/CCL2 production **(Figure 4G)**, and no change in the levels of IL-10 **(Figure S1A)** and TNF-α **(Figure S1B)** after 24-hours post-infection. Strikingly, the A922500 treatment did not affect the level of any of the analyzed

cytokines **(Figure 4E-G)**, suggesting an unprecedented dissociation between LD biogenesis and the inflammatory response during a bacterial infection.

Lastly, we analyzed the impact of LD biogenesis inhibition on the lactate levels, associated with glycolytic metabolism of pro-inflammatory macrophages. During *Salmonella* infection, we observed an increase in lactate level **(Figure 4I)**, andlactate production was partial impaired by A922500 treatment, suggesting that the modulation of lipid metabolism also affects the central metabolism of macrophages.

4. DISCUSSION

The present work investigated the role of LD biology during *Salmonella* Typhimurium infection in murine macrophages. The data presented herein show *S.* Typhimurium was capable of inducing a rapid and time-dependent increase in LD formation in macrophages. In addition to reinforce LD biogenesis as a phenomenon dependent on *Salmonella* T3SS activity, our data reveal the participation of the host cellular machinery in this process, as the usurpation of TLR signaling, especially TLR2, and lipid metabolic pathways. Our study further highlights the participation of LDs in bacterial pathogenesis. While the manipulating LD biogenesis significantly reduced the *S.* Typhimurium's growth within 24-hours post-infection, the inhibition of LD formation did not impair the inflammatory response induced by infection. Collectively, our data suggest LDs play an important role during *S.* Typhimurium intracellular growth, but not in the inflammatory response induced by the infection.

Despite of LD biogenesis being rapidly detected after a short time of some stimulations, including LPS stimulation (25, 46, 47), our data show that early LD biogenesis is an active process of *S.* Typhimurium infection, mainly T3SS-dependent mechanism. These results reinforced

previously data previourly published by Nawabi *et al.*, (2008), which showed that absence of *Salmonella* T3SS efector SseJ in mutant bacteria reduced cholesterol esterification and LD formation in HeLa cells and RAW macrophages (13). The participation of T3SS effector proteins in the modulation of host lipid metabolism and LD accumulation was also reported for *Chlamydia trachomatis* (48, 49), and *Pseudomonas aeruginosa* (50).

During bacterial infection, LD accumulation often initiates with activation of TLR signaling in leukocytes (44, 51–53). We demonstrated that *Salmonell*a-induced LD biogenesis also requires TLR signaling, via a TLR2-dependent mechanism and counter-regulated by TLR4 in murine macrophages. TLR activation and downstream signaling through the adapter proteins MyD88 and TRIF leads to rapid acidification of the SCV, and consequent activation of *Salmonella* virulence genes (39). Moreover, the acidification of the SCV is essential for the activation of T3SS and translocation of effector proteins into host cell cytosol (54, 55).

The contrasting role of TLR2 and TLR4 in *Salmonella*-triggered LD biogenesis may reflect the difference of these receptors in the host response to *S.* Typhimurium infection. TLR2 activation was reported as a negative regulator of immunity against *S.* Typhimurium, favoring bacterial survival (56). Furthermore, LD biogenesis by TLR2-dependent mechanism has been reported for a wide range of pathogens infections (44, 51–53). On the other hand, TLR4 is essential to the early killing of *S.* Typhimurium by murine macrophages (57), and to the controlling of *Salmonella*-infection *in vivo* (42, 58), the counter-regulatory role of TLR4 in *Salmonella*-trigger LD biogenesis might be associated with control of the bacterial killing.

The subversion of host cell LDs by pathogenic bacteria to obtain energy to promote their own survival and replication has been reported for several intracellular bacteria, such as *Chlamydia. spp* (27, 52), *Coxiella burnetti* (59), *Mycobacterium spp* (23, 25, 26). And *S. typhimurium* was not an exception. Similar to reported for *C. trachomatis* (48), LD formation

seems required for optimal *S.* Typhimurium proliferation, but not essential for intracellular survival and proliferation, as evidenced in TRIF/MyD88 double-knockout macrophages. These results are in agreement with recent data reported by Reens *et al*., (2019), which showed that lipid metabolism pathways are essential to *Salmonella* replication in proinflammatory but not anti-inflammatory macrophages.

Despite the role of LD as immunomodulatory platform mainly through the production of PGE_2, being a well-documented phenomenon for several pathogens infection (20, 36, 61), the same was not observed in *S.* Typhimurium infection in murine macrophages. Although it seems contradictory to the current literature, the dissociation of LD formation with lipid inflammatory mediator synthesis may be associated with pro-inflammatory response induced by *S.* Typhimurium. In general, the participation of LDs as a site of PGE_2 synthesis has been associated with an anti-inflammatory phenotype in macrophages, favoring the inhibition of killing activity, the downregulation of Th1-type cytokines and raising the IL-10 generation (51, 53, 62). However the PGE2 appears to have the opposite effect in *Salmonella* infected-macrophages, inducing a specific pro-inflammatory profile and amplifying the pro-inflammatory response (63). Moreover, intestinal pro-inflammatory monocytes was reported as important niche to *Salmonella* proliferation (64).

On the other hand, the decoupling of LD formation and lipid inflammatory mediator synthesis during *Salmonella* infection could also be an immune evasion strategy. Recent studies have reported the existence of another side of this host-pathogen interaction, where LDs also act in the protective response to the host, including in the antibacterial response (17, 21). Recently, we described that in response to LPS, LDs act as immunometabolic hubs integrating local and systemic metabolic adaptation to infection and assembling host defense pathways including the antimicrobial cathelicidin (65). Interestingly, as reported in this work, at the beginning of the

infection there was no interaction between *Salmonella* and LD at the beginning of the infection (65). Further investigations should help us to better understand *Salmonella*-specific mechanisms evolved to take advantage of LDs for their persistence and proliferation.

In summary, a model can be proposed in which LD biogenesis observed in *Salmonella*-infected macrophages plays a key role in bacterial pathogenesis, as a lipid source to promote optimal bacterial proliferation in proinflammatory macrophages **(Figure 5)**. Our data suggested a critical role for TLR2 in *Salmonella*–macrophages interactions, favoring the activation of *Salmonella* T3SS, and subsequent signaling for induction of LD biogenesis. On the other hand, TLR4 performs a counter-regulatory action LD biogenesis through the control of the bacterial load. Based on the above, a better understanding of the LD biology could be key to the development of novel strategies for control *Salmonella* infection.

Acknowledgments

The authors are grateful to the Microscopy Facility of the Brazilian National Cancer Institute for the acquisition of Confocal images; and to Fiocruz Luminex Platform (Subunidade Luminex-RPT03C Rede de Plataformas PDTIS, FIOCRUZ/RJ) and the assistance of MSc Edson Fernandes de Assis for use of its Luminex facilities.

Declaration of competing interest

The authors declare no competing interests.

Funding

This study was financed in part by the Coordenação de Aperfeiçoamento de Pessoal de Nível Superior– Brasil (CAPES - Finance Code 001), by the Fundação de Amparo à Pesquisa do Estado

do Rio de Janeiro (FAPERJ) and by the Conselho Nacional de Desenvolvimento Científico e Tecnológico (CNPq). The funders had no role in study design, data collection and analysis, decision to publish, or preparation of the manuscript.

Author Contributions:

ESK and FSPD: Conceived, design and performed the majority of the experiments, data analyses, co-wrote and edit the manuscript. FFM, TCGG, MAR and EP performed part of experiments and data analyses. MTB and PTB performed the experimental design, manuscript reviewing and directed all aspects of the study. All authors read and approved the final manuscript.

References

1. Finiay BB, Falkow S. 1989. Salmonella as an intracellular parasite. Mol Microbiol 3:1833–1841.
2. Bintsis T. 2017. Foodborne pathogens. AIMS Microbiol 3:529–563.
3. Gal-Mor O, Boyle EC, Grassl GA. 2014. Same species, different diseases: how and why typhoidal and non-typhoidal Salmonella enterica serovars differ. Front Microbiol 5:1–10.
4. Hoffmann S, Batz MB, Morris JG. 2012. Annual Cost of Illness and Quality-Adjusted Life Year Losses in the United States Due to 14 Foodborne Pathogens†. J Food Prot 75:1292–1302.
5. Jajere SM. 2019. A review of Salmonella enterica with particular focus on the pathogenicity and virulence factors, host specificity and adaptation and antimicrobial resistance including multidrug resistance. Vet World 12:504–521.
6. Stanaway JD, Reiner RC, Blacker BF, Goldberg EM, Khalil IA, Troeger CE, Andrews JR, Bhutta ZA, Crump JA, Im J, Marks F, Mintz E, Park SE, Zaidi AKM, Abebe Z, Abejie AN, Adedeji IA, Ali BA, Amare AT, Atalay HT, Avokpaho EFGA, Bacha U, Barac A, Bedi N, Berhane A, Browne AJ, Chirinos JL, Chitheer A, Dolecek C, El Sayed Zaki M, Eshrati B, Foreman KJ, Gemechu A, Gupta R, Hailu GB, Henok A, Hibstu DT, Hoang CL, Ilesanmi OS, Iyer VJ, Kahsay A, Kasaeian A, Kassa TD, Khan EA, Khang Y-H, Magdy Abd El Razek H, Melku M, Mengistu DT, Mohammad KA, Mohammed S, Mokdad AH, Nachega JB, Naheed A, Nguyen CT, Nguyen HLT, Nguyen LH, Nguyen NB, Nguyen TH, Nirayo YL, Pangestu T, Patton GC, Qorbani M, Rai RK, Rana SM, Ranabhat CL, Roba KT, Roberts NLS, Rubino S, Safiri S, Sartorius B, Sawhney M, Shiferaw MS, Smith DL, Sykes BL, Tran BX, Tran TT, Ukwaja KN, Vu GT, Vu LG, Weldegebreal F, Yenit MK, Murray CJL, Hay SI. 2019. The global burden of typhoid and paratyphoid fevers: a systematic analysis for the Global Burden of Disease Study 2017. Lancet Infect Dis 19:369–381.
7. Wang M, Qazi IH, Wang L, Zhou G, Han H. 2020. Salmonella Virulence and Immune

Escape. Microorganisms 8:407.
8. Eng S-K, Pusparajah P, Ab Mutalib N-S, Ser H-L, Chan K-G, Lee L-H. 2015. Salmonella : A review on pathogenesis, epidemiology and antibiotic resistance. Front Life Sci 8:284–293.
9. Monack DM, Mueller A, Falkow S. 2004. Persistent bacterial infections: The interface of the pathogen and the host immune system. Nat Rev Microbiol 2:747–765.
10. Malik-Kale P, Jolly CE, Lathrop S, Winfree S, Luterbach C, Steele-Mortimer O. 2011. Salmonella – At Home in the Host Cell. Front Microbiol 2:1–9.
11. Duncan MC, Linington RG, Auerbuch V. 2012. Chemical Inhibitors of the Type Three Secretion System: Disarming Bacterial Pathogens. Antimicrob Agents Chemother 56:5433–5441.
12. Lathrop SK, Binder KA, Starr T, Cooper KG, Chong A, Carmody AB, Steele-Mortimer O. 2015. Replication of Salmonella enterica serovar Typhimurium in human monocyte-derived macrophages. Infect Immun 83:2661–2671.
13. Nawabi P, Catron DM, Haldar K. 2008. Esterification of cholesterol by a type III secretion effector during intracellular Salmonella infection. Mol Microbiol 68:173–185.
14. Colonne PM, Winchell CG, Voth DE. 2016. Hijacking Host Cell Highways: Manipulation of the Host Actin Cytoskeleton by Obligate Intracellular Bacterial Pathogens. Front Cell Infect Microbiol 6:1–8.
15. Teng O, Ang CKE, Guan XL. 2017. Macrophage–Bacteria Interactions—A Lipid-Centric Relationship. Front Immunol 8.
16. Vallochi AL, Teixeira L, Oliveira K da S, Maya-Monteiro CM, Bozza PT. 2018. Lipid Droplet, a Key Player in Host-Parasite Interactions. Front Immunol 9.
17. Farese R V., Walther TC. 2009. Lipid Droplets Finally Get a Little R-E-S-P-E-C-T. Cell 139:855–860.
18. Bozza PT, D'Avila H, Almeida PE, Magalhães KG, Molinaro R, Almeida CJ, Maya-Monteiro CM. 2009. Lipid droplets in host–pathogen interactions. Clin Lipidol 4:791–807.
19. Saka HA, Valdivia R. 2012. Emerging roles for lipid droplets in immunity and host-pathogen interactions. Annu Rev Cell Dev Biol 28:411–437.
20. Melo RCN, D'Avila H, Wan H-C, Bozza PT, Dvorak AM, Weller PF. 2011. Lipid Bodies in Inflammatory Cells. J Histochem Cytochem 59:540–556.
21. Pereira-Dutra FS, Teixeira L, Souza Costa MF, Bozza PT. 2019. Fat, fight, and beyond: The multiple roles of lipid droplets in infections and inflammation. J Leukoc Biol 106:563–580.
22. Pol A, Gross SP, Parton RG. 2014. Biogenesis of the multifunctional lipid droplet: Lipids, proteins, and sites. J Cell Biol 204:635–646.
23. Russell DG, Cardona P, Kim M, Allain S, Altare F. 2009. Foamy macrophages and the progression of the human TB granuloma. Nat Immunol 10:943–948.
24. Peyron P, Vaubourgeix J, Poquet Y, Levillain F, Marchou B, Bardou F, Daffe M, Cardona P, Chastellier C De. 2008. Foamy Macrophages from Tuberculous Patients ' Granulomas Constitute a Nutrient-Rich Reservoir for M . tuberculosis Persistence. PLOS Pathog 4:1–14.
25. D'Avila H, Melo RCN, Parreira GG, Werneck-Barroso E, Castro-Faria-Neto HC, Bozza PT, D'Avila H, Melo RCN, Parreira GG, Werneck-Barroso E, Castro-Faria-Neto HC, Bozza PT. 2006. Mycobacterium bovis Bacillus Calmette-Guérin Induces TLR2-Mediated Formation of Lipid Bodies: Intracellular Domains for Eicosanoid Synthesis In Vivo. J Immunol 176:3087–3097.
26. Mattos KA, Oliveira VGC, D'Avila H, Rodrigues LS, Pinheiro RO, Sarno EN, Pessolani

MC V, Bozza PT. 2011. TLR6-Driven Lipid Droplets in Mycobacterium leprae-Infected Schwann Cells: Immunoinflammatory Platforms Associated with Bacterial Persistence. J Immunol 187:2548–2558.
27. Cocchiaro JL, Kumar Y, Fischer ER, Hackstadt T, Valdivia RH. 2008. Cytoplasmic lipid droplets are translocated into the lumen of the Chlamydia trachomatis parasitophorous vacuole. Proc Natl Acad Sci 105:9379–9384.
28. Guo Y-N, Hsu HS, Mumaw VR, Nakoneczna I. 1986. Electronmicroscopy studies on the bactericidal action of inflammatory leukocytes in murine salmonellosis. J Med Microbiol 21:151–159.
29. Arena ET, Auweter SD, Antunes LCM, Vogl AW, Han J, Guttman JA, Croxen MA, Menendez A, Covey SD, Borchers CH, Finlay BB. 2011. The Deubiquitinase Activity of the Salmonella Pathogenicity Island 2 Effector, SseL, Prevents Accumulation of Cellular Lipid Droplets. Infect Immun 79:4392–4400.
30. Wang C-L, Fan Y-C, Wang C, Tsai H-J, Chou C-H. 2016. The impact of Salmonella Enteritidis on lipid accumulation in chicken hepatocytes. Avian Pathol 45:450–457.
31. Assunção LS, Magalhães KG, Carneiro AB, Molinaro R, Almeida PE, Atella GC, Castro-Faria-Neto HC, Bozza PT. 2017. Schistosomal-derived lysophosphatidylcholine triggers M2 polarization of macrophages through PPARγ dependent mechanisms. Biochim Biophys Acta - Mol Cell Biol Lipids 1862:246–254.
32. Lahiri R, Randhawa B, Krahenbuhl J. 2005. Application of a viability-staining method for Mycobacterium leprae derived from the athymic (nu/nu) mouse foot pad. J Med Microbiol 54:235–242.
33. Li J, Lv C, Sun W, Li Z, Han X, Li Y, Shen Y. 2013. Cytosporone B, an Inhibitor of the Type III Secretion System of Salmonella enterica Serovar Typhimurium. Antimicrob Agents Chemother 57:2191–2198.
34. Lissner CR, Swanson RN, O'Brien AD. 1983. Genetic control of the innate resistance of mice to Salmonella typhimurium: Expression of the Ity gene in peritoneal and splenic macrophages isolated in vitro. J Immunol 131:3006–3013.
35. Melo RCN, D'Ávila H, Bozza PT, Weller PF. 2011. Imaging Lipid Bodies Within Leukocytes with Different Light Microscopy Techniques, p. 149–161. *In* Polymorphism: in the Pharmaceutical Industry.
36. Bozza PT, Magalhães KG, Weller PF. 2009. Leukocyte lipid bodies - Biogenesis and functions in inflammation. Biochim Biophys Acta - Mol Cell Biol Lipids 1791:540–551.
37. Libbing CL, McDevitt AR, Azcueta R-MP, Ahila A, Mulye M. 2019. Lipid Droplets: A Significant but Understudied Contributor of Host–Bacterial Interactions. Cells 8:354.
38. Moran NA, Russell JA, Koga R, Fukatsu T. 2005. Evolutionary Relationships of Three New Species of Enterobacteriaceae Living as Symbionts of Aphids and Other Insects. Appl Environ Microbiol 71:3302–3310.
39. Arpaia N, Godec J, Lau L, Sivick KE, McLaughlin LM, Jones MB, Dracheva T, Peterson SN, Monack DM, Barton GM. 2011. TLR Signaling Is Required for Salmonella typhimurium Virulence. Cell 144:675–688.
40. Royle MCJ, Tötemeyer S, Alldridge LC, Maskell DJ, Bryant CE. 2003. Stimulation of Toll-Like Receptor 4 by Lipopolysaccharide During Cellular Invasion by Live Salmonella typhimurium Is a Critical But Not Exclusive Event Leading to Macrophage Responses. J Immunol 170:5445–5454.
41. Lembo A, Kalis C, Kirschning CJ, Mitolo V, Jirillo E, Wagner H, Galanos C, Freudenberg MA. 2003. Differential Contribution of Toll-Like Receptors 4 and 2 to the Cytokine Response to Salmonella enterica Serovar Typhimurium and Staphylococcus aureus in Mice.

Infect Immun 71:6058–6062.
42. Talbot S, Tötemeyer S, Yamamoto M, Akira S, Hughes K, Gray D, Barr T, Mastroeni P, Maskell DJ, Bryant CE. 2009. Toll-like receptor 4 signalling through MyD88 is essential to control Salmonella enterica serovar Typhimurium infection, but not for the initiation of bacterial clearance. Immunology 128:472–483.
43. Walther TC, Farese R V. 2012. Lipid Droplets and Cellular Lipid Metabolism. Annu Rev Biochem 81:687–714.
44. Nicolaou G, Goodall AH, Erridge C. 2012. Diverse Bacteria Promote Macrophage Foam Cell Formation Via Toll-Like Receptor-Dependent Lipid Body Biosynthesis. J Atheroscler Thromb 19:137–148.
45. Bozza PT, Bakker-Abreu I, Navarro-Xavier RA, Bandeira-Melo C. 2011. Lipid body function in eicosanoid synthesis: An update. Prostaglandins Leukot Essent Fat Acids 85:205–213.
46. Pacheco P, Bozza FA, Gomes RN, Bozza M, Weller PF, Castro-Faria-Neto HC, Bozza PT. 2002. Lipopolysaccharide-Induced Leukocyte Lipid Body Formation In Vivo: Innate Immunity Elicited Intracellular Loci Involved in Eicosanoid Metabolism. J Immunol 169:6498–6506.
47. Heid H, Rickelt S, Zimbelmann R, Winter S, Schumacher H, Dörflinger Y, Kuhn C, Franke WW. 2014. On the Formation of Lipid Droplets in Human Adipocytes: The Organization of the Perilipin–Vimentin Cortex. PLoS One 9:e90386.
48. Kumar Y, Cocchiaro J, Valdivia RH. 2006. Report The Obligate Intracellular Pathogen Chlamydia trachomatis Targets Host Lipid Droplets. Curr Biol 16:1646–1651.
49. Dai W, Li Z. 2014. Conserved type III secretion system exerts important roles in Chlamydia trachomatis. Int J Clin Exp Pathol 7:5404–5414.
50. Feliciano L-FP, Plotkowski M-C, Bozza PT, Freitas C, Raymond B, Zahm JM, Brandão BA, Touqui L, de Assis M-C, Saliba AM. 2008. Lipid body mobilization in the ExoU-induced release of inflammatory mediators by airway epithelial cells. Microb Pathog 45:30–37.
51. Almeida PE, Silva AR, Maya-Monteiro CM, Torocsik D, D'Avila H, Dezso B, Magalhaes KG, Castro-faria-neto HC, Nagy L, Bozza PT, Clarissa M, Töröcsik D, Ávila HD, Dezsö B, Magalhães KG, Castro-faria-neto HC, Nagy L, Bozza PT, Almeida PE, Silva AR, Maya-Monteiro CM, Magalha KG. 2009. Mycobacterium bovis Bacillus Calmette-Guérin Infection Induces TLR2-Dependent Peroxisome Proliferator-Activated Receptor γ Expression and Activation: Functions in Inflammation, Lipid Metabolism, and Pathogenesis. J Immunol 183:1337–1345.
52. Cao F, Castrillo A, Tontonoz P, Re F, Byrne GI. 2007. Chlamydia pneumoniae-Induced Macrophage Foam Cell Formation Is Mediated by Toll-Like Receptor 2. Infect Immun 75:753–759.
53. Mattos KA, Lara FA, Oliveira VGC, Rodrigues LS, D'Avila H, Melo RCN, Manso PPA, Sarno EN, Bozza PT, Pessolani MC V. 2011. Modulation of lipid droplets by Mycobacterium leprae in Schwann cells: A putative mechanism for host lipid acquisition and bacterial survival in phagosomes. Cell Microbiol 13:259–273.
54. Yu XJ, McGourty K, Liu M, Unsworth KE, Holden DW. 2010. pH Sensing by Intracellular Salmonella Induces Effector Translocation. Science (80-) 328:1040–1043.
55. Chakraborty S, Winardhi RS, Morgan LK, Yan J, Kenney LJ. 2017. Non-canonical activation of OmpR drives acid and osmotic stress responses in single bacterial cells. Nat Commun 8.
56. Zhan R, Han Q, Zhang C, Tian Z, Zhang J. 2015. Toll-Like Receptor 2 (TLR2) and TLR9

Play Opposing Roles in Host Innate Immunity against Salmonella enterica Serovar Typhimurium Infection. Infect Immun 83:1641–1649.
57. Weiss DS, Raupach B, Takeda K, Akira S, Zychlinsky A. 2004. Toll-Like Receptors Are Temporally Involved in Host Defense. J Immunol 172:4463–4469.
58. Seibert SA, Mex P, Köhler A, Kaufmann SHE, Mittrücker H-W. 2010. TLR2-, TLR4- and Myd88-independent acquired humoral and cellular immunity against Salmonella enterica serovar Typhimurium. Immunol Lett 127:126–134.
59. Mulye M, Zapata B, Gilk SD. 2018. Altering lipid droplet homeostasis affects Coxiella burnetii intracellular growth. PLoS One 13:e0192215.
60. Reens AL, Nagy TA, Detweiler CS. 2020. Salmonella enterica requires lipid metabolism genes to replicate in proinflammatory macrophages and mice. Infect Immun 88.
61. D'Avila H, Freire-de-Lima CG, Roque NR, Teixeira L, Barja-Fidalgo C, Silva AR, Melo RCN, DosReis GA, Castro-Faria-Neto HC, Bozza PT. 2011. Host Cell Lipid Bodies Triggered by Trypanosoma cruzi Infection and Enhanced by the Uptake of Apoptotic Cells Are Associated With Prostaglandin E2 Generation and Increased Parasite Growth. J Infect Dis 204:951–961.
62. D'Avila H, Roque NR, Cardoso RM, Castro-Faria-Neto HC, Melo RCN, Bozza PT. 2008. Neutrophils recruited to the site of Mycobacterium bovis BCG infection undergo apoptosis and modulate lipid body biogenesis and prostaglandin E2 production by macrophages. Cell Microbiol 10:2589–2604.
63. Sheppe AEF, Kummari E, Walker A, Richards A, Hui WW, Lee JH, Mangum L, Borazjani A, Ross MK, Edelmann MJ. 2018. PGE2 Augments Inflammasome Activation and M1 Polarization in Macrophages Infected With Salmonella Typhimurium and Yersinia enterocolitica. Front Microbiol 9:1–16.
64. McLaughlin PA, Bettke JA, Tam JW, Leeds J, Bliska JB, Butler BP, van der Velden AWM. 2019. Inflammatory monocytes provide a niche for Salmonella expansion in the lumen of the inflamed intestine. PLOS Pathog 15:e1007847.
65. Bosch M, Sánchez-álvarez M, Fajardo A, Kapetanovic R, Steiner B, Pereira-Dutra F, Moreira L, Lopez JA, Campo R, Mari M, Morales-Paytuni F, Tort O, Gubens A, Templin RM, Curson JEB, Martel N, Català C, Lozano F, Tebar F, Enrich C, Vazquez J, Del Pozo MA, Sweet MJ, Bozza PT, Gross SP, Parton RG, Pol A. Mammalian lipid droplets are innate immune hubs integrating cell metabolism and host defense. Science, in press.

Legends

Figure 1: *S. typhimurium* induces a rapid and time-dependent lipid droplet formation in macrophages. BMDM cells was infected with *S.* Typhimurium (MOI of 10). One hour after infection, the culture medium was discarded and extracellular bacteria were killed by addition of gentamicin for 1 h. **(A)** Representative images of Oil Red O-labeled LDs (red) kinetics from BMDM infected with *S.* Typhimurium. The nucleus was stained by DAPI (blue). Scale bar: 10 μm. **(B)** Kinetics of *Salmonella*-trigged LD enumeration in BMDMs after infection, performed by using Fiji/ImageJ from confocal images. In each group, at least 100 cells were analyzed in the total of 10 fields by experiment. **(C)** Invasion and Replication Kinetics of Salmonella in BMDM. Cells were lysed and serial dilutions were plated on TSA plates for CFU enumeration. **(D-E)** Representative confocal images of apposition Oil Red O-labeled LD (red) and DAPI-labeled bacteria (blue) in 1 hour **(D)** and 24-hours **(E)** post-infection. The nucleus was stained by DAPI (blue). Scale bar: 10 μm. **(F)** Quantification of the distance between LD and bacteria. was performed by using Fiji/ImageJ software from confocal images. In each group, at least 50 cells were analyzed in the total of 5 fields by experiment. Mean SEM for three independent experiments. (*) indicates the value is significantly different ($p<0.05$) from values in respective non-infected groups.

Figure 2: The early lipid Salmonella-trigged lipid droplets biogenesis is depentende of bacterial viability and T3SS activation. BMDM cells was infected with *S.* Typhimurium (MOI of 10) or *E. coli* (MOI of 100). **(A)** LD enumeration in *S.* Typhimurium or *E. coli*-infected and non-infected macrophages in 1-hour and 24-hours post-infection. **(B)** Bacterial enumeration in *S.* Typhimurium or *E. coli*-infected macrophages in 1-hour and 24-hours post-infection. **(C)** LD enumeration in BMDM infected with *S.* Typhimurium overnight-culture (live) or radiation-killed *S.* Typhimurium (dead), and non-infected cells, in 1-hour and 24-hours post-infection. Treatment with radiation-killed *Salmonella* (dead) was performed identically as with live *Salmonella*. **(D)** Bacteria enumeration in BMDM infected with *S.* Typhimurium overnight-culture (live) or radiation-killed *S.* Typhimurium (dead). **(E)** Experimental design of inhibition of *Salmonella* T3SS (Created with BioRender). *Salmonella* cells was pretreated with 100 μM of cns-B or vehicle (DMSO) in LB medium for 1h before infection **(F)** LD and **(G)** bacteria enumeration in BMDM infected with *S.* Typhimurium pretreated with cytosporone B (cns-B) or vehicle. LD and bacteria enumeration in BMDMs after infection was performed by using Fiji/ImageJ from confocal images.

In each group, at least 100 cells were analyzed in the total of 10 fields by experiment. Mean SEM for three independent experiments. (*) indicates the value is significantly different ($p<0.05$) from values in respective control groups, and (#) from values in respective *Salmonella*-infected BMDM group ($p<0.05$).

Figure 3: The early *Salmonella*-trigged lipid droplets biogenesis is dependent of Toll-like receptor 2 (TLR2) signalling and counter-regulated by TLR4. iBMM cells was infected with *S.* Typhimurium (MOI of 10). **(A)** Representative images of Oil Red O-labeled LDs (red) from wild-type (WT), Myd88/TRIF, TLR2 and TLR4 knockout iBMM infected with *S.* Typhimurium in 1-hour post-infection. The nucleus was stained by DAPI (blue). Scale bar = 10 μm. **(B-C)** LD enumeration in wild-type (WT), and knockout iBMMs in **(B)** 1-hour and **(C)** 24-hours post *Salmonella* infection. LD analysis was performed by using Fiji/ImageJ software from confocal images. In each group, at least 100 cells were analyzed in the total of 10 fields by experiment. **(D)** Invasion (1-hour post-infection) and **(E)** Replication (24-hour post-infection) kinetics of *Salmonella* in iBMM cell lineages. Cells were lysed and serial dilutions were plated on TSA plates for CFU enumeration. Mean SEM for three independent experiments. (*) indicates the value is significantly different ($p<0.05$) from the respective non-infected groups and (#) from values in *Salmonella*-infected wild-type group ($p<0.05$).

Figure 4: Lipid droplets formation contributes for an optimal *Salmonella* proliferation, but not to inflammatory response induced by *Salmonella* infection. (A) Experimental design of inhibition of DGAT-1 (Created with BioRender). BMDM cells was infected with *S.* Typhimurium (MOI of 10), with or without pre-treatment with 5 μM of DGAT1 inhibitor (A922500). **(B)** Representative images of Oil Red O-labeled LDs (red) from BMDM infected with *S.* Typhimurium. The nucleus was stained by DAPI (blue) (scale bar: 10 μm) **(C)** LD enumeration in *S.* Typhimurium -infected and uninfected macrophages, after 1-hour and 24-hours post-infection. In each group, at least 100 cells were analyzed in the total of 10 fields by experiment. **(D)** Invasion (1-hour post-infection) and replication (24-hour post-infection) kinetics of *Salmonella* in iBMM. Extracellular bacteria were killed by addition of gentamicin for 1 h. Cells were lysed and serial dilutions were plated on TSA plates for CFU enumeration. **(E)** Levels of PGE_2 in cell-free supernatants collected from non-infected (NI) and infected cultures in 1-hour and 24-hour post-infection, performed by EIA detection system. **(F-H)** Levels of cytokines and chemokines in cell-free supernatants in 24-hour post-infection, performed by ELISA detection

system. **(I)** Lactate level in cell-free supernatants collected from non-infected (NI) and infected cultures in 24-hour post-infection. Mean SEM for three or four independent experiments. (*) indicates the value is significantly different ($p<0.05$) from the respective non-infected groups and (#) from values in *Salmonella*-infected wild-type group ($p<0.05$). Created with BioRender.

Figure 5: Model of LD biogenesis in macrophages induzed by *S. typhimurium* infection. *S.* Typhimurium is recognized by TLR2 and TLR4, then internalized. After internalization, TLR activation and downstream signaling through the adapter proteins MyD88 and TRIF lead to rapid acidification of the SCV, and consequent activation of T3SS and translocation of effector proteins into the host cell cytosol. As one of the consequences of this process, *Salmonella* stimulates the t increase of activity of DGAT-1 leads to neutral lipids accumulation of and LD biogenesis. On the other hand, TLR4 performs a counter-regulatory action LD biogenesis through the control of the bacterial killing. In later times, LDs can be a lipid source to *Salmonella* proliferation.

Figure S1: *Salmonella* infection not induce the increased of secretion IL-10 and TNF-α in murine macrophages. BMDM cells was infected with *S.* Typhimurium (MOI of 10), with or without pre-treatment with 5 μM of DGAT1 inhibitor (A922500). Level of **(A)** IL-10 and **(B)** TNF-α in cell-free supernatants in 24-hour post-infection, performed by ELISA detection system.

694 *Figure 1:*

695

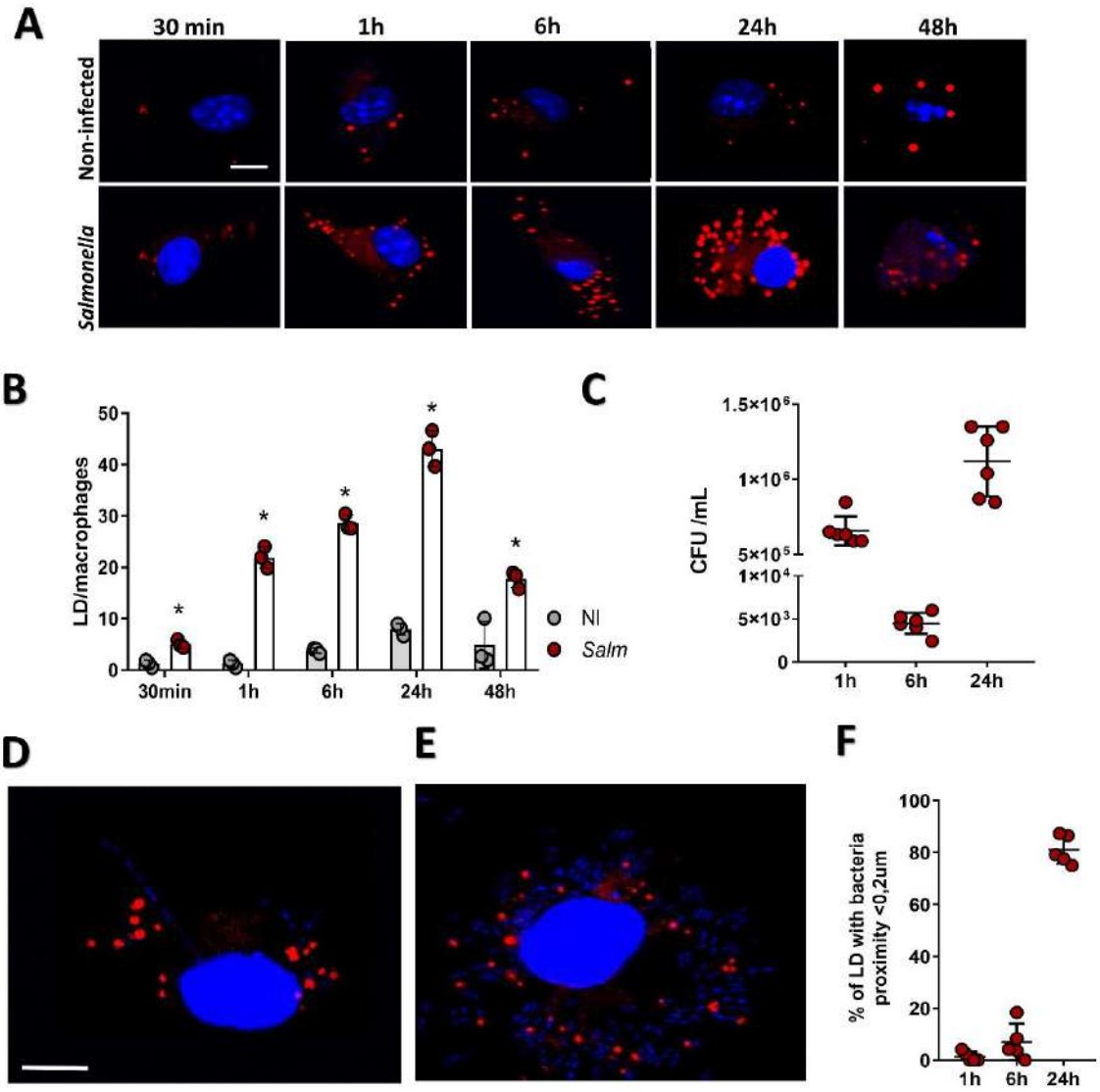

696

697

698 *Figure 2*

699

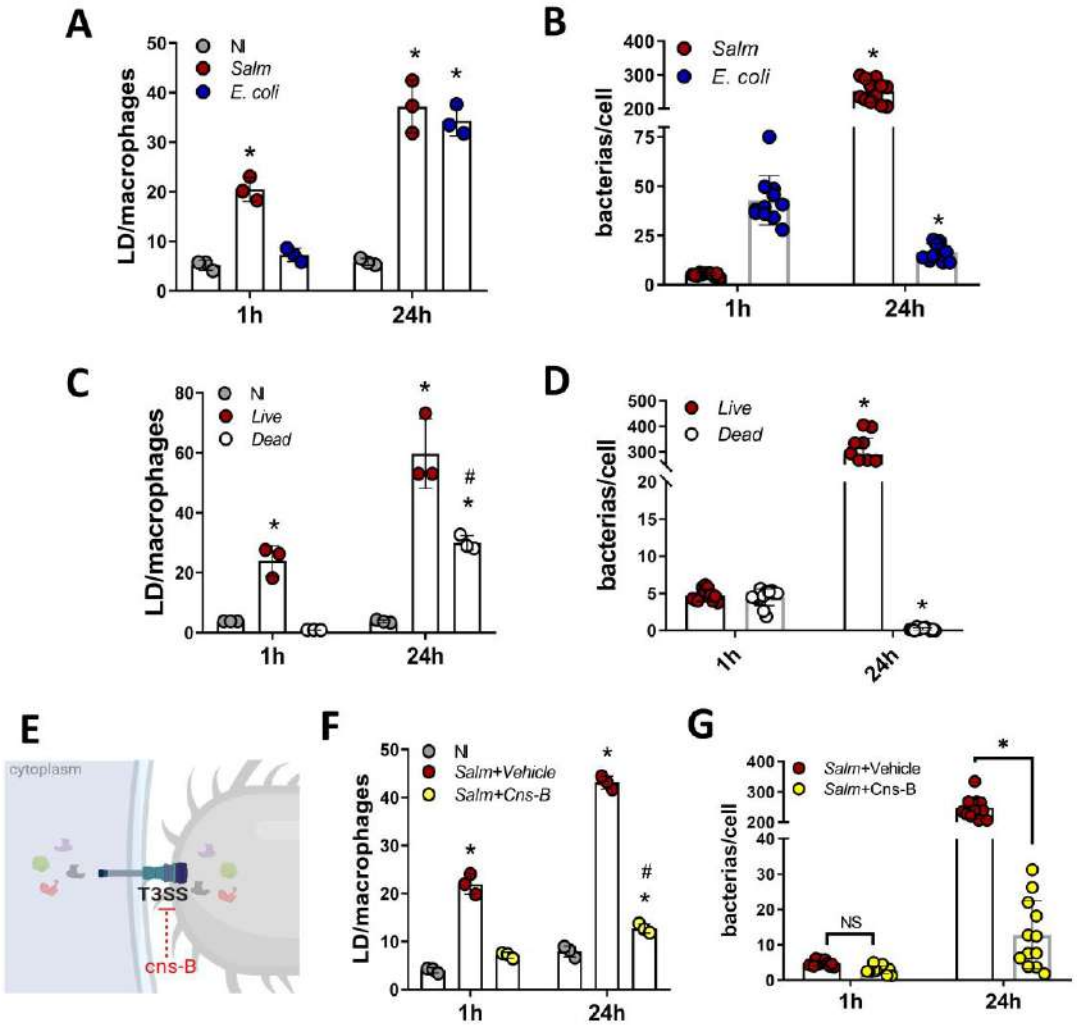

700

701

702 *Figure 3*

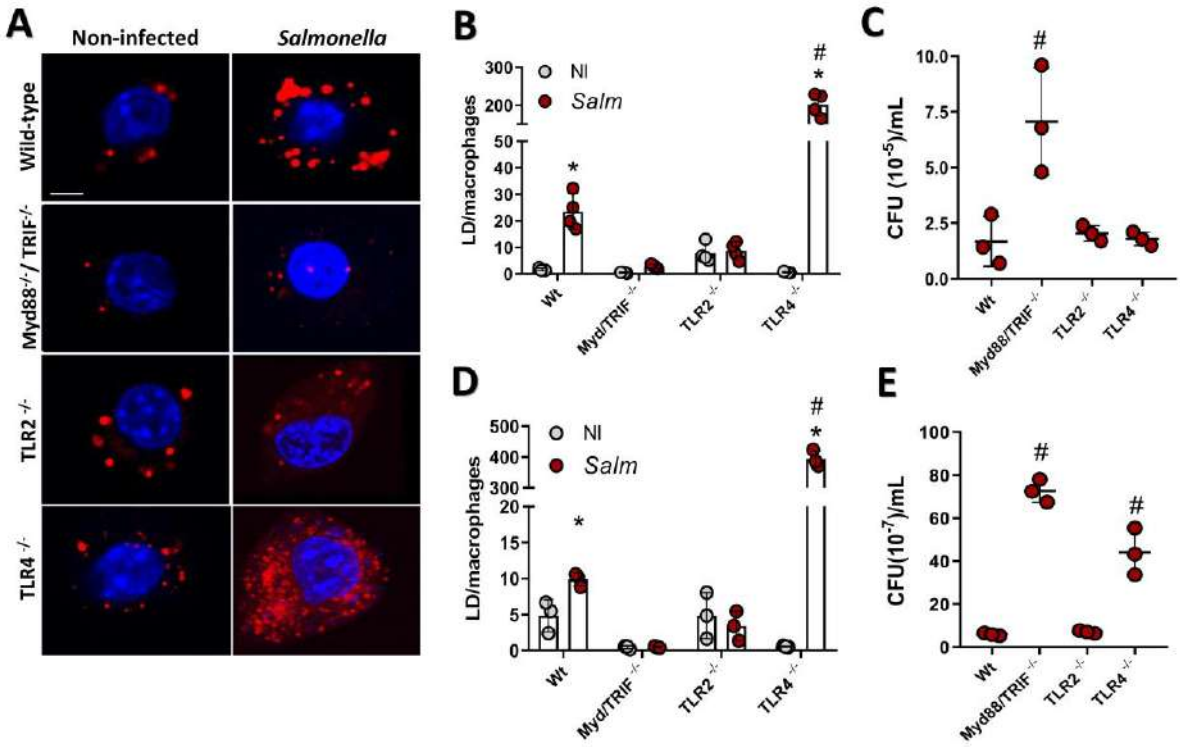

704

705

706 *Figure 4*

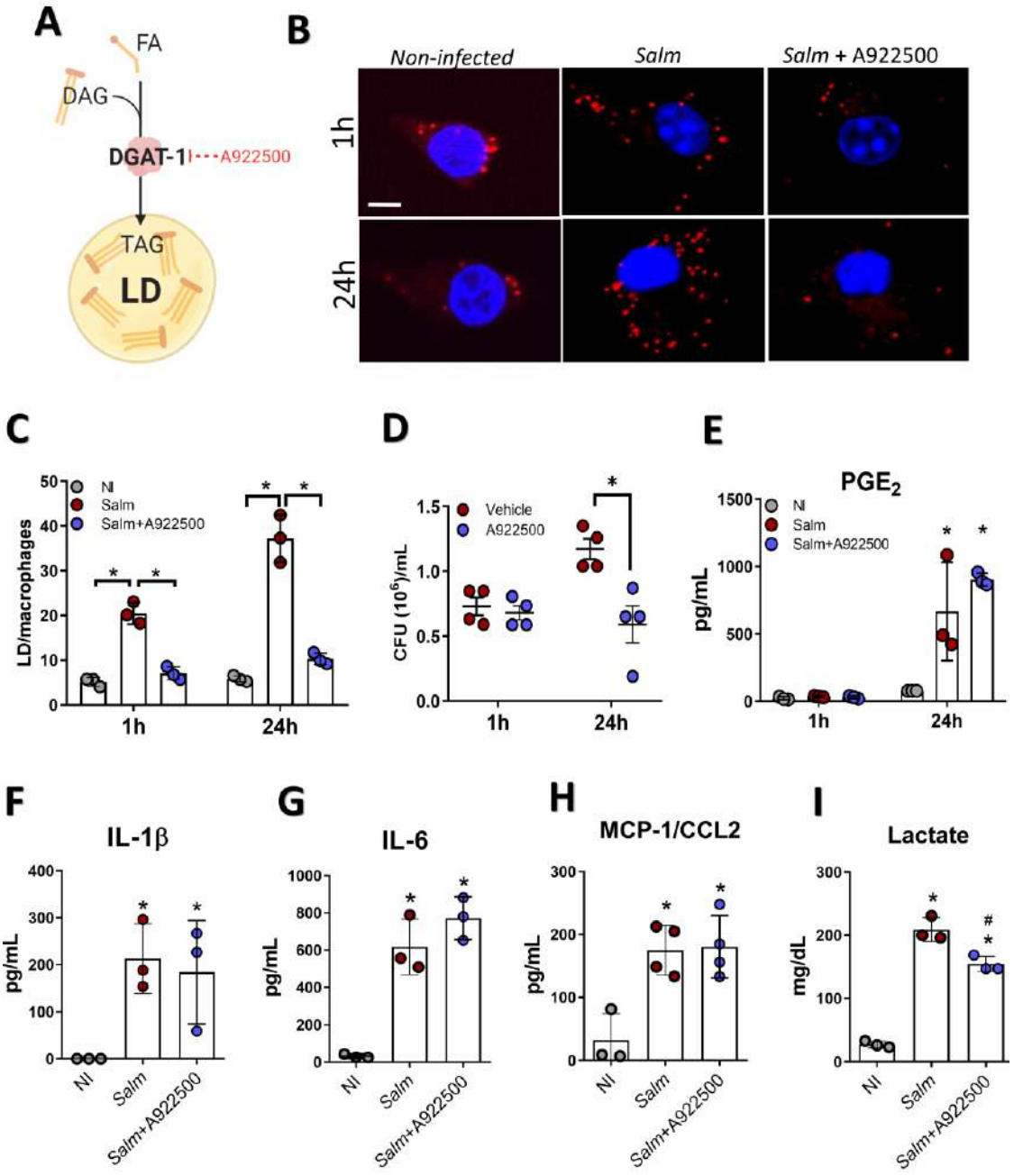

707

708

709 *Figure 5*

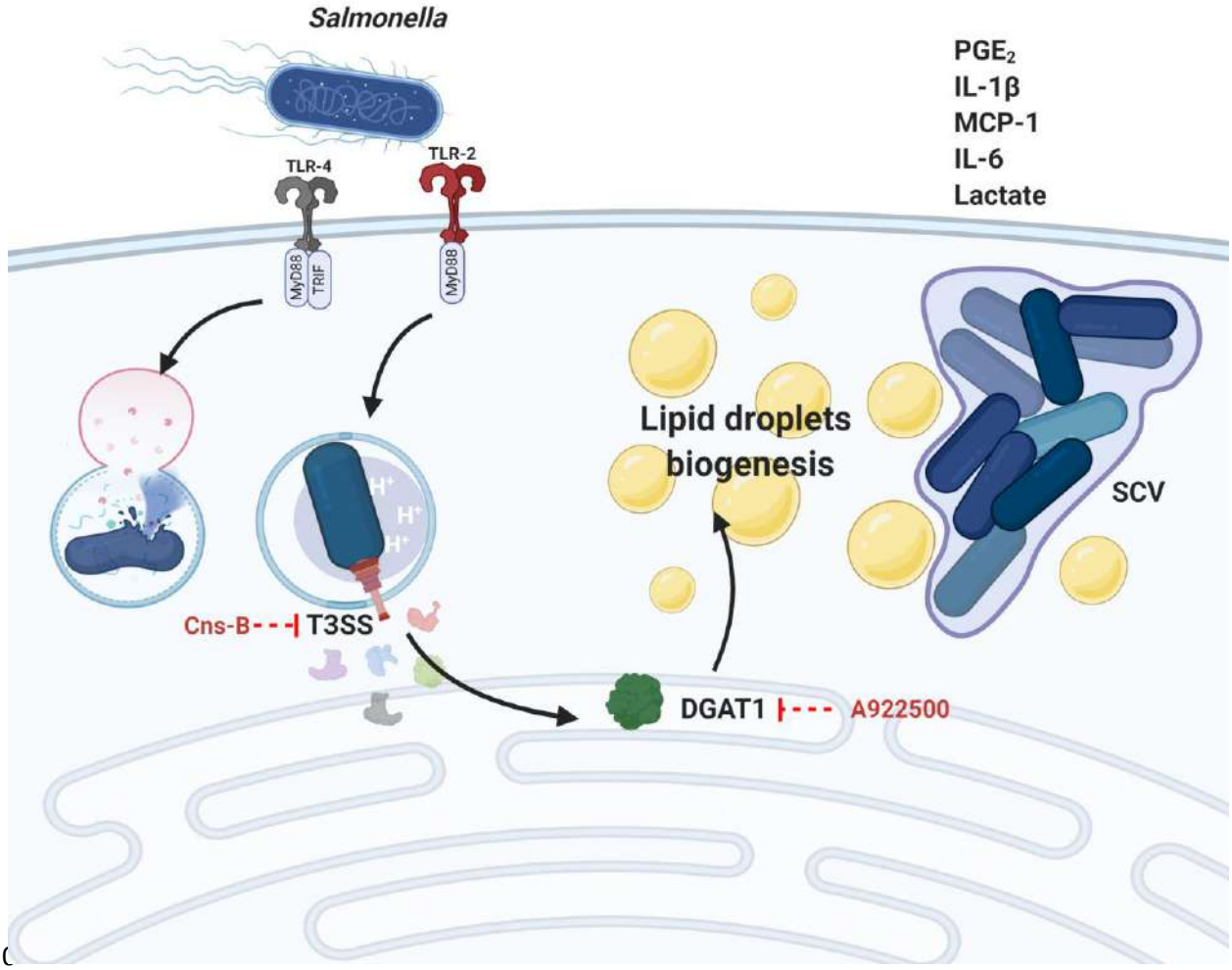

710

711

712 **Figure S1**

713

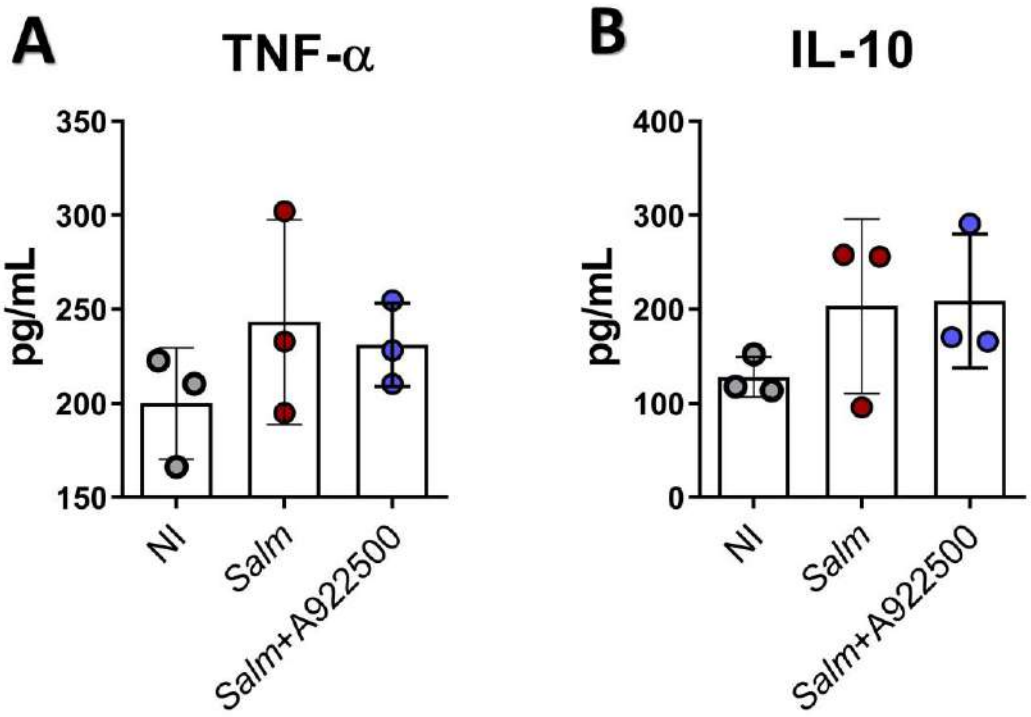

714

715

Anexo 4

TEIXEIRA, L.; SOUZA-MOREIRA, L.; PRESTES, E.; REIS, P.A.; **PEREIRA-DUTRA, F.S.**; ALBURQUERQE, C.; SILVA, T.P.; HOTTZ, E.D.; ESPINHEIRA-SILVA, H.; MAYA-MONTEIRO, C.M., ANTUNES, M. M.; MENEZES, G.B.; BOZZA, M.T.; BOZZA, F.A.; MELO, R.C.N.; BOZZA, P.T. **Lipid droplets contribute to sepsis-associated organ dysfunction by disrupting tissue tolerance through the amplification of inflammation and lipid peroxidation.** Manuscrito em revisão.

Lipid droplets contribute to sepsis-associated organ dysfunction by disrupting tissue tolerance through the amplification of inflammation and lipid peroxidation

Lívia Teixeira[1], Luciana Souza-Moreira[1], Elisa Prestes[2], Patrícia Alves Reis[1], Filipe S. Pereira-Dutra[1], Cassiano Albuquerque[1], Thiago P. Silva[3], Eugenio D. Hottz[1, 4], Hugo Espinheira-Silva, Clarissa M. Maya-Monteiro[1], Maísa Mota Antunes[7], Gustavo B. Menezes[7] Marcelo T. Bozza[2], Fernando A. Bozza[5,6], Rossana C. N. Melo[3], Patrícia T. Bozza[1]*

1. Laboratório de Imunofarmacologia, Instituto Oswaldo Cruz, Fundação Oswaldo Cruz, Rio de Janeiro, Brazil.
2. Laboratório de Inflamação e Imunidade, Departamento de Imunologia, Instituto de Microbiologia, Universidade Federal do Rio de Janeiro (UFRJ), Rio de Janeiro, Brazil.
3. Laboratório de Biologia Celular, Departamento de Biologia, Instituto de Ciências Biológicas (ICB), Universidade Federal de Juiz de Fora (UFJF), Minas, Gerais, Brazil
4. Departamento de Bioquímica, Instituto de Ciências Biológicas (ICB), Universidade Federal de Juiz de Fora (UFJF), Minas Gerais, Brazil
5. Laboratório de Medicina Intensiva, INI, FIOCRUZ, Rio de Janeiro, Brazil.
6. Instituto D'Or de Pesquisa e Ensino (IDOr), Rio de Janeiro, Brazil.
7. Center for Gastrointestinal Biology, Departamento de Morfologia, Instituto de Ciências Biológicas, Universidade Federal de Minas Gerais, Belo Horizonte, Brazil.

*Corresponding author: Patrícia T. Bozza, Laboratório de Imunofarmacologia, Instituto Oswaldo Cruz, Fundação Oswaldo Cruz, Avenida Brasil, 4365, Manguinhos, Rio de Janeiro, RJ, CEP 21045–900, Brazil. Email: pbozza@ioc.fiocruz.br, pbozza@gmail.com.

Abstract

Sepsis is a complex life-threatening syndrome caused by dysregulated inflammatory and metabolic host response to infection. Alterations in lipid metabolism and an increased number of lipid droplets (LDs) are observed during sepsis; however LD involvement in maladaptive tissue tolerance that culminates in organ dysfunction during sepsis is poorly understood. Here we show that increased accumulation of LDs is associated with peroxidized lipid production, liver dysfunction and sepsis severity. Through the use of antioxidants or CRISPR/Cas9 deletion of the NADPH oxidase subunit $p22^{phox}$ we demonstrate that ROS induced LD biogenesis and oxidatively altered LD content. Moreover, the LDs associated with mitochondria and peridroplet mitochondria in cells from the septic mice showed increased ultrastructural damage. Strikingly, dampening LD accumulation by DGAT1 inhibition decreased the production of inflammatory mediators, reduced lipid peroxidation while improving tissue function. Altogether, we demonstrate that LDs contribute to sepsis-associated organ dysfunction by disrupting tissue tolerance through the amplification of lipid peroxidation, suggesting that LD and changes in lipid metabolism in sepsis may be a target for therapy.

Key words: metabolism, inflammation, innate immunity, sepsis, MODS, lipid droplets, ROS, lipid peroxidation.

Introduction

Sepsis is a complex syndrome defined as a life-threatening organ dysfunction caused by a dysregulated host response to infection (Singer et al., 2016). Sepsis affects an estimated 30 million individuals per year worldwide, and remains the leading cause of death in the ICU (Fleischmann et al., 2016). Although outcomes have improved in recent years, mortality remains higher than 25–30%, even 40–50% when shock is present. Furthermore, sepsis also results in an impaired quality of life and decreased life-span for survivors (Hotchkiss et al., 2013; Vincent et al., 2014).

The success of host defense strategies to pathogen infection relies on a delicate balance between the ability to detect and eliminate pathogens (resistance) and the capacity to cope with the tissue damage caused by the pathogen and/or by the host immune response (tissue tolerance) (McCarville and Ayres, 2018; Wang et al., 2019; Weis et al., 2017). The development of organ dysfunction is the most serious outcome during sepsis, and is directly related to morbidity and mortality (Singer et al., 2016; Vincent et al., 2014).The mechanisms involved in sepsis-induced multiple organ dysfunction (MODS) are multifactorial and still incompletely understood, but maladaptive inflammation in response to infection and disrupted mechanisms of tissue tolerance are believed to be the main causes of tissue damage and mortality (Angus and van der Poll, 2013; Wang et al., 2019). Recent studies have indicated that alterations in metabolism during infection play central roles in tolerance (Gomez et al., 2017; Rao et al., 2017; Wang et al., 2016; Weis et al., 2017). Along this line, numerous studies have indicated that sepsis-induced organ dysfunction is associated with fundamental changes in organismal and cellular metabolism (Langley et al., 2013; Mickiewicz et al., 2015).

Lipids are important sources of energy in individuals with infections and adaptations to lipid metabolism are a requirement to survive bacterial sepsis (Wang et al., 2019). Recent integrated data based on metabolomics and proteomics analyses identified lipid metabolism processes as the main change in the septic patients when compared to healthy volunteers, and also as predictors of poor prognosis and death (Langley et al., 2013; Sharma et al., 2019). Increased LD accumulation in macrophages, neutrophils, liver and other cells and

tissues has been demonstrated in experimental models of sepsis as well as in samples from septic patients (Garofalo et al., 2019; Koskinas et al., 2008; Pacheco et al., 2002; Pacheco et al., 2007). Although pronounced alterations in lipid metabolism and an increased number of LDs are observed during sepsis, their involvement in the mechanisms of disrupted tissue tolerance and organ dysfunction in sepsis is poorly understood.

LDs are dynamic organelles that play major functions in lipid and energy homeostasis, inflammation and signaling (Bozza and Viola, 2010; Olzmann and Carvalho, 2019; Welte and Gould, 2017). LDs may participate in the infectious processes at multiple levels of innate and adaptative host immune responses (Pereira-Dutra et al., 2019). The biogenesis of LDs is tightly regulated during the immune response against pathogens including bacteria, viruses, fungi and protozoa, in some cases favoring the establishment of infection, and in others host resistance (Pereira-Dutra et al., 2019). We have recently described that in response to LPS, LDs act as immunometabolic hubs integrating local and systemic metabolic adaptation to infection and assembling host defense pathways including interferon-inducible GTPases and the antimicrobial cathelicidin (Bosch et al., 2020). During sepsis LDs in leukocytes were demonstrated to participate in the amplification of inflammatory mediator production (Pacheco et al., 2002; Pacheco et al., 2007), however the contributions of ectopic LDs to organ dysfunction in sepsis have not been addressed.

The current view is that LDs act as cellular mechanisms involved in the prevention of tissue damage because of their ability to buffer excess lipids in stressful situations and release them gradually to meet cellular need (Olzmann and Carvalho, 2019; Welte and Gould, 2017). LDs prevent the damage generated by high concentrations of FFAs, by storing them in their esterified forms within the neutral lipid core (Herms et al., 2013; Listenberger et al., 2003). Additionally, LDs protect cells from lipotoxicity by hijacking toxic lipid intermediates (Bosma et al., 2014; Liu et al., 2014; Nguyen et al., 2017). However, the role played by LDs in the lipotoxic events mediated by peroxidized lipids is still under intense investigation. Recent studies have suggested that polyunsaturated fatty acids in LDs are more protected from lipid peroxidation than fatty acids associated with

membranes. As such, LDs would provide a protective environment that minimizes lipid peroxidation chain reactions (Bailey et al., 2015; Jarc et al., 2018). Glial sequestration of toxic lipids within LDs has been proposed as a mechanism to protect neurons from lipotoxic damage (Liu et al., 2015). However upon mitochondrial dysfunction and excessive ROS production, LDs are sites of lipid peroxidation and/or peroxidized lipid accumulation, amplifying lipotoxic cell damage and neurodegeneration (Liu et al., 2017; Liu et al., 2015).

Here we investigate the mechanisms and consequences of lipid droplet formation during sepsis. Our results demonstrate that sepsis triggers increased accumulation of LDs in immune and liver cells, a cellular event associated with peroxidized lipid production, liver dysfunction and sepsis severity. Here we challenge the current view of LD accumulation in tissues as a conserved mechanism of tolerance that prevents lipotoxicity to propose that under an intense inflammatory and oxidative stress environment this mechanism of tissue tolerance is disrupted and LDs contribute to cellular damage and tissue dysfunction during experimental sepsis.

Results

Excessive LD formation observed in the hepatic tissue during experimental sepsis is associated with liver dysfunction

Liver dysfunction is an early outcome of sepsis often detected in the first 24h after disease onset in patients (Kramer et al., 2007). Hepatic lipid metabolism is profoundly altered during sepsis with increased synthesis and uptake of fatty acids and decreased beta-oxidation leading to liver steatosis (Pacheco et al., 2002; Van Wyngene et al., 2018). Experimental sepsis was induced in mice by cecal ligation and puncture (CLP). CLP is the most frequently used experimental model of sepsis induction since it closely mimics many aspects of human polymicrobial peritonitis, including immunological, hemodynamic and metabolic responses (Dejager et al., 2011). In the present study, the severity of the sepsis varied according to the number of cecum punctures, with 2 punctures leading to mild sepsis and 9 punctures inducing severe sepsis. By labeling hepatic tissue sections with the neutral lipid probe Bodipy, we detected increased accumulation of TAGs and LDs in the livers of animals submitted to mild and severe sepsis (**Figure 1**), the accumulation of LDs in the liver (i.e. hepatic steatosis) correlated with sepsis severity. To evaluate whether peroxidation of lipids in LDs is a pathophysiological contributor to liver dysfunction during sepsis, we evaluated the LD lipid content and peroxidation levels in livers, as well as classic markers of hepatic function such as serum transaminases (ALT and AST) and albumin. For these purposes, we isolated whole liver LDs from sham and CLP mice through sucrose gradient ultracentrifugation and measured the levels of TAG and total 8-isoprostane (i.e., free and esterified forms). 8-isoprostane is a prostanoid generated by non-enzymatic oxidation and extensively used as a lipid peroxidation marker (Roberts and Fessel, 2004). Twenty-four hours after surgery, we observed a large increase in liver TAG content in the CLP group compared with that in the sham group, with a further increment in TAG levels 48h after surgery (**Figure 1A**). Increased peroxidation of the lipids in the LDs, inferred by 8-isoprostane levels, was also observed as early as 24 h post induction of sepsis and, reaching even higher rates 48h of induction (**Figure 1B**). Similarly, an

enhancement in the serum levels of AST and ALT hepatic enzyme levels, and a reduction in albumin indicated liver dysfunction in the animals subjected to CLP (**Figure 1 D-E**). Considered together, the cytotoxic potential of the peroxidized lipids and the observations that LD oxidative changes occurred in parallel to liver damage support the hypothesis that LDs may play a role in tissue damage during sepsis.

Sepsis-induced LDs exhibit signs of oxidative changes and interact with mitochondria

Quantitative ultrastructural analysis of macrophage-like peritoneal cells 48h after CLP revealed an increase in both LDs number and area (**Figure 2A-D**). By assessing 8-isoprostane levels in the cell-free peritoneal wash we observed that lipid peroxidation correlated with sepsis severity (**Figure 2E**). The impact of LD oxidative damage on the cellular machinery is largely unknown, especially in sepsis. LDs and mitochondria establish close interactions in physiological and pathological conditions (Benador et al., 2018; Wang et al., 2011). We hypothesized that these interactions may be implicated in cell damage incurred during sepsis. We wondered if mitochondrial ROS could mediate the peroxidation of LDs and/or if lipotoxic potential effects of peroxidized lipids in LDs could lead to mitochondrial dysfunction. To address these questions, we performed a detailed ultrastructural study using transmission electron microscopy (TEM) to evaluate mitochondrion interactions and mitochondrial ultrastructural alterations in peritoneal cells 48 h after CLP induction. Our results showed that sepsis induced profound changes in mitochondrial ultrastructure including disruption of and reduction in mitochondrial cristae, emptying of the mitochondrial matrix, vacuolization, swelling of mitochondria (enlargement) and disruption of the mitochondrial envelope (**Figure S1 and Figure 2F, G**). Additionally, quantitative analyses demonstrated that the frequency of LD-mitochondrion interactions was augmented twice during experimental sepsis induction (**Figure 2I**). Interestingly, peridroplets mitochondria in the CLP group presented with higher frequencies of ultrastructural alterations than did peridroplets mitochondria in the control group (**Figure 2G, J**), suggesting that the associations between mitochondria and LDs may favor mitochondrial dysfunction and cellular oxidative damage during sepsis.

ROS induce LD biogenesis upon proinflammatory stimulation

It is widely known that ROS have a central role in LD formation, preadipocytes enlargement and stem cell differentiation into adipocytes (Atashi et al., 2015). However, the roles of ROS in LD biogenesis in immune cells and how they contributes to sepsis pathogenesis is far less explored.To study the dynamics of ROS generation and LD formation after proinflammatory stimuli *in vitro*, bone marrow-derived macrophages (BMDM) were stimulated with LPS+IFNγ (500ng/mL+10ng/mL) and analyzed for mitochondrial and total ROS production by MitoSox Red and DHE labeling, respectively; the LDs were stained with Oil Red O (ORO) for enumeration at different time-points (**Figure 3A-C**). The LPS+IFNγ treatment rapidly induced both cytoplasmic and mitochondrial ROS, which were detected as soon as 30 minutes after stimulation (**Figure 3A**). LD accumulation, on the other hand, occurred significantly later, 24hafter stimulation (**Figure 3B-C**). Therefore, augmented ROS production temporally precedes the increase of LDs upon proinflammatory signaling.

Since mitochondrial dysfunction is an important component in the pathogenesis of sepsis and a major source of intracellular ROS, we tested whether increasing mitochondrial ROS generation by blocking the electron transport chain (ETC) could also trigger LD biogenesis in macrophages. For this purpose, we treated BMDMs with antimycin A, a selective inhibitor of complex III, and evaluated ROS production and LD biogenesis at different time points. As expected, antimycin A induced a rapid increase in ROS generation (**Figure 3A**). Antimycin A also proved to be a potent trigger of LD formation, with a pronounced induction as early as 2h after treatment (**Figure 3C**). In line with the enhancement in LD biogenesis, LPS+IFNγ stimulation or antimycin A treatment also increased the expression ofPlin2/ADRP (**Figure 3D-E**), the major structural protein of macrophage LDs. Similarly, treatment with rotenone (an inhibitor of complex I) and oligomycin (an ATP synthase inhibitor) also increased Plin2/ADRP expression (**Figure 3E**). In contrast, treatment with the proton ionophore FCCP, which induces mitochondrial dysfunction without increasing ROS generation, did not increase ADRP expression (**Figure 3E**). These data show that LD biogenesis is triggered by mitochondrial-induced ROS.

To further investigate the association of dysfunctional mitochondria and LD biogenesis during macrophage proinflammatory activation, we costained BMDMs with Bodipy for LDs, and MitoTracker or MitoSox Red for mitochondria or mitochondrial-derived ROS, respectively. After BMDMs treatment with LPS+IFNγ, the LDs were observed in close association with mitochondria (**Figure 3F, 3Fi**), including those generating high levels of ROS (**Figure 3G, 3Gi**). Altogether, these data point out to spatial and functional interactions between mitochondria and LDs after macrophage proinflammatory activation.

Reduced ROS levels downregulate LD biogenesis

To confirm the central role of ROS in LD accumulation in proinflammatory macrophages, we employed pharmacological approaches to reduce mitochondrial- and cytoplasmic-generated ROS, followed by evaluation of LD formation. First, we pretreated the BMDMs with 100μM Mito-TEMPO, a mitochondria-targeted antioxidant, 1h before LPS+IFNγ stimulation and during the 24 h incubation period. Pretreatment with Mito-TEMPO significantly prevented the increase in LD formation after LPS+IFNγ stimulation, indicating a role for mitochondria derived ROS in proinflammatory stimuli-induced LDs (**Figure 4A**). In addition, we investigated the contribution of NADPH oxidase (NOX), an enzymatic complex centrally involved in cytoplasmic ROS generation and a major source of ROS during sepsis (Hernandes et al., 2014). Apocynin has been widely used to inhibit NADPH oxidase enzymatic activity by blocking the translocation of the $p47^{phox}$ cytosolic subunit to the plasma membrane, thus inhibiting NOX complex activation (mainly NOX1 and NOX2). The results from the flow cytometry analysis of DHE probe oxidation confirmed that apocynin pretreatment reduced ROS generation in the LPS+IFNγ, but not the antimycin A-treated BMDMs (**Figure 4B**). In our model, the BMDMs were pretreated with increasing concentrations of apocynin 1h before LPS+IFNγ stimulation, Gram-negative bacterial infection (*Escherichia coli*, MOI 5) or antimycin A treatment (1μg/mL). Twenty-four hours after initial cell stimulation, we observed dose-dependent pharmacological inhibition of NADPH oxidase which prevented the enhancement of LD biogenesis induced by LPS+IFNγ stimulation (**Figure 4C-D**) and *E. coli* infection (**Figure 4E**), but not by antimycin A treatment (**Figure 4F**).

The redundancy of NADPH oxidase- and mitochondrial-derived ROS in driving LD biogenesis in macrophages during proinflammatory activation is consistent with recent findings indicating that NADPH oxidase activation is upstream mitochondrial dysfunction induced by LPS and sepsis (Hernandes et al., 2014; Joseph et al., 2017). Thus, our results suggest that both mitochondrial and cytoplasmic ROS are involved in infection/inflammation-elicited LD biogenesis and highlight NADPH oxidase as a central enzyme in this process.

Macrophages p22$^{phox-/-}$ has impaired LD biogenesis and PPAR gamma expression

To gain insights into the mechanisms by which NADPH oxidase-derived ROS trigger LD biogenesis in macrophages, we used CRISPR/Cas9 gene editing to generate immortalized bone marrow macrophages (IBMM) deficient in p22^{phox}, a transmembrane subunit of the NOX1-4 complex. As expected, p22$^{phox-/-}$ cells produced lower levels of ROS when stimulated with LPS+IFNγ compared to the levels produced by the WT cells (**Figure 5A**). Since nitric oxide (NO) production is a redox-sensitive pathway(Wu et al., 2008), the p22$^{phox-/-}$ clones also downregulated iNOS expression and reduced NO synthesis as determined by the reduced nitrite detected in response to LPS+IFNγ stimulation (**Figure 5B and E**). Importantly, in alignment with our results from the apocynin treatment experiments, p22$^{phox-/-}$ clones showed no increase in LD biogenesis after stimulation with LPS+IFNγ (**Figure 5C-D**).

To gain insights into the mechanisms underlying the NADPH-oxidase-mediated increase in LD formation, we evaluated the expression of the transcription factors PPARγ and SREBP-1, which are crucial to the regulation of lipid metabolism and known to be sensitive to redox signaling (Chawla et al., 2001; Im et al., 2011). While genetic ablation of p22^{phox} did not affect SREBP-1 expression in LPS+IFNγ-activated macrophages, p22$^{phox-/-}$ clones had a marked reduction in PPARγ expression (**Figure 5E**). Since PPARγ regulates several genes encoding lipid uptake, transport, and storage pathways (Chawla et al., 2001), its reduced expression in p22$^{phox-/-}$ cells may explain the inability of these cells to accumulate LDs after proinflammatory stimulation. Our results show that NADPH-oxidase activity regulates key inflammatory and metabolic pathways in

LPS+IFNγ-activated inflammatory macrophages, and is required for LD biogenesis in these cells.

LD components are susceptible to oxidative damage depending on NADPH oxidase activity

During sepsis, upregulated production of ROS and inadequate recruitment of antioxidant defenses lead to deleterious effects in cellular machinery. Lipid peroxidation is considered the process that induces the most severe cellular oxidative damage in several pathologies and is responsible for lipotoxicity-mediated cell death (Dixon et al., 2012; Gaschler and Stockwell, 2017). To investigate whether LDs in sepsis play cytoprotective or lipotoxic roles, we firstly determined whether the molecular components of the LDs were susceptible to peroxidation or if these organelles protected lipids from oxidation. Staining with Bodipy 581/591 C11, a lipid peroxidation sensor, revealed intense labeling of both the reduced and oxidized forms of the probe in the LPS+IFNγ-or antimycin A-treated groups compared to the levels of in the control (**Figure 6A**). In the LDs of these groups, an abundance of peroxidized lipids was observed, suggesting that these organelles are sites of lipid peroxidation and/or the accumulation of peroxidized lipids (**Figure 6A**). Peroxidized lipids are potent second messengers active in cytotoxic events that change various cellular functions mainly through intramolecular and intermolecular adduct formation with biomolecules, including proteins. To evaluate whether lipid peroxidation alters LD protein content we used Click-iT® LAA Kit which detects proteins containing alkyne groups in side chains. Interestingly, many ring-shaped patterns were stained in the cytoplasm of the LPS+IFNγ stimulated BMDMs (**Figure 6B**). After counterstaining the cells with Nile red, neutral lipid stain, we confirmed that these stained ring-shape were located at the periphery of LDs (**Figure 6C**), in the most protein-rich site of these organelles. Importantly, even in cases of mild sepsis peritoneal cells exhibited the same pattern of stained ring around the LDs when subjected to peroxidized lipid-modified protein labeling (**Figure 6D**), demonstrating that LDs are sensitive to oxidative damage during experimental sepsis *in vivo*. In addition to ring-shaped staining, antimycin A-treated BMDM showed diffuse subcellular staining indicating more ostensive oxidative damage

(**Figure 6B**). Supernatants from LPS+IFNγ-activated macrophage cultures also presented with increased levels of 8-Isoprostane (**Figure 6F**). Importantly, apocynin pretreatment reduced 8-Isoprostane levels in a dose-dependent manner (**Figure 6F**), and reversed all the evaluated LD peroxidative alterations induced by LPS+IFNγ (**Figure 6E, G and FigureS2A-B**). These data show that the molecular components of LDs are highly susceptible to LPS+IFNγ-induced oxidative damage, and that NADPH oxidase activation is required in this process.

Dampening LD accumulation leads to recovery of septic mice from liver damage, lipid peroxidation and inflammation

Even though liver dysfunction is commonly observed in sepsis, the role played by LD accumulation in sepsis-associated hepatic tissue damage is still not clear. Thus, we searched for a strategy to reduce sepsis-induced hepatic steatosis. DGAT enzymes isoforms (DGAT1 and DGAT2) which catalyze the final and fully committed step to TAG synthesis, have differential role in the remodeling (DGAT1) and *de novo* pathways (DGAT2) of TAG synthesis (Villanueva et al., 2009). During sepsis, steatosis progression in the liver is more closely related to intense mobilization of TAG stocks and remodeling in peripheral tissues than to *de novo* lipid synthesis (Van Wyngene et al., 2018), therefore we proceeded to pharmacologically inhibit the DGAT1 enzyme. We treated septic mice with A922500, a DGAT1 inhibitor (DGAT1i), in addition to antibiotics given to CLP mice. We performed intravital confocal microscopy as described by Marques et al. (Marques et al., 2015) to visualize the progression of liver steatosis in live animals after Bodipy staining. The livers of the septic animals developed pronounced steatosis characterized by an increase in LDs in the tissue 48h after CLP surgery, which was prevented by treatment with DGAT1i **(Figure 7A-C)**. No difference in steatosis level was found in the DGAT1i and untreated mice after 6h from CLP **(Figure S3A, B)**. As expected, the same pattern was observed in hepatic tissue sections stained with ORO **(Figure 7C)**. Thin layer chromatography (TLC) analysis confirmed the reduction of TAGs in the liver of the DGAT1i-treated CLP mice without increasing diacylglycerol accumulation **(Figure 7D and Figure S3C)**. We then assessed whether preventing LD accumulation in the liver protected mice from hepatic damage. CLP mice

presented with higher levels of serum AST and ALT, indicating increased hepatic dysfunction. Importantly, treatment with DGAT1i significantly reduced the levels of both transaminases **(Figure 7E-7F)**. Albumin levels were reduced in septic mice compared to mice subjected to the sham surgery, and treatment with DGAT1i led to a trending recovery of albumin concentrations in the serum **(Figure 7G)**. Altogether, these results imply that dampening LD accumulation by DGAT1inhibition prevents hepatic injury during severe sepsis.

Importantly, DGAT1 inhibition ameliorated sepsis-associated liver damage independently on the pathogen load, as evidenced by similar bacterial counts in the peritoneal wash from treated and untreated mice **(Figure 7H)**. Considering the role played by lipid peroxidation in damage on cellular structures during sepsis, we evaluated the effect of DGAT1i on the levels of the lipid peroxidation adduct malondialdehyde (MDA) in the livers of CLP mice. The levels of MDA were higher in the livers from mice subjected to sepsis and treatment with DGAT1i significantly reduced MDA accumulation in these livers **(Figure 7I)** indicating that the inhibition of LD accumulation protects the organ from lipid peroxidation. In addition, the proinflammatory mediators leukotriene B4 (LTB4) and interleukin-6 (IL-6), were reduced in the DGAT1i-treated septic animals **(Figure 7J, K)**, while the chemokine MCP-1 and the anti-inflammatory cytokine IL-10 were not affected by the DGAT1i treatment **(Figure S3D, E).** Taken together, these data suggest that LD accumulation modulates both oxidative stress and the inflammatory response, with a great impact on tissue damage and liver dysfunction during sepsis.

Discussion

Sepsis is the major cause of death in ICUs, mainly attributed to multiple organ dysfunction syndrome (MODS) (Angus and van der Poll, 2013; Singer et al., 2016). Associated with uncontrolled inflammatory responses, evidence indicates that sepsis-induced organ dysfunction occurs due to bioenergetic metabolism alterations (Abraham and Singer, 2007; Brealey et al., 2002). LD accumulation in non-adipose tissues and oxidative stress are recurrent consequences of sepsis-induced metabolic reprogramming (Pacheco et al., 2002; Van Wyngene et al., 2018). Current view, place LD accumulation in tissues as an evolutionary conserved mechanism of tolerance that prevents lipotoxicity. Here we challenge this concept to propose that under an intense inflammatory and oxidative stress environment this mechanism of tissue tolerance is disrupted and LDs contribute to cellular damage.

Herein, we report a crosstalk between oxidative stress and LD biogenesis upon induction by endotoxic stimuli. In this regard, NADPH oxidase-derived ROS play pivotal roles in these mechanisms. Additionally, ROS induce oxidative changes in the lipid and protein contents of LDs, making them carriers of harmful oxidized molecules. The results from our ultrastructural study showed that sepsis intensified the interplay between LDs and mitochondria resulting in deleterious consequences to the mitochondrial machinery. Reciprocally, mitochondria-derived ROS amplify LD biogenesis. The accumulation of LDs was proven to have an amplifying effect on liver injury. Dampening LD accumulation in mice subjected to a polymicrobial sepsis-induction model (CLP) by pharmacological inhibition of DGAT1 reduced lipid peroxidation and protected the treated animals from hepatic dysfunction. Taken together, our results demonstrate a role for oxidative stress in LD biogenesis and the oxidative changes in LD components, thereby supporting to the hypothesis that LDs contribute to cell damage and organ dysfunction during sepsis.

The involvement of ROS in the LD formation process during infection and sepsis was largely unknown. We demonstrated that LPS+IFNγ-induced ROS from either mitochondrial or NADPH oxidase activity were able to induce LD formation. The relationship between mitochondrial ROS and the biogenesis of

LDs was demonstrated in *Drosophila* model of neurodegeneration. In this study, the increase in ROS production induced by mitochondrial gene mutations was accompanied by an intense accumulation of LDs in glial cells, which was abolished by antioxidant treatment or over expression of the SOD enzyme (Liu et al., 2015). However, our data support a prevalent role for NADPH oxidase in sepsis-triggered LD formation. While antioxidant-targeted mitochondrial ROS only partially blocked LD biogenesis, pharmacological or genetic intervention on NADPH oxidase activity completely reversed this phenotype. These findings are in agreement with recent data showing that NADPH oxidase activation during sepsis is up stream mitochondrial dysfunction and induces mitochondrial superoxide production through pathways dependent on calcium overload (Joseph et al., 2017). NADPH oxidase activity also reduces the expression of several genes involved in fatty acid oxidation via JNK activation, compromising mitochondrial function (Drosatos et al., 2011; Paumelle et al., 2019).

We shed light upon the molecular link between NADPH oxidase activity and LD formation. Impaired production of ROS derived from the NADPH oxidase complex had a profound impact on PPARγ expression. PPARγ is a redox sensitive transcription factor that coordinates lipid metabolism and inflammation(Corona and Duchen, 2016; Varga et al., 2011). PPARγ can be upregulated and selectively activated by oxidized-fatty acids, which promote the binding of PPARγ to specific target genes such as CD36, PLIN2, including PPARγ itself (Almeida et al., 2009; Chawla et al., 2001). Previous study from our group and others showed that PPARγ activation is associated with increased LD biogenesis in macrophages during infection(Almeida et al., 2014; Almeida et al., 2009; Diaz Acosta et al., 2018; Mei et al., 2009). Therefore, the reduction in ROS production in macrophages lacking the $p22^{phox}$subunit may lead to fewer oxidized-fatty acids impacting in PPARγ ligand availability. This mechanism might be critical for the decrease in PPARγ expression and the inability of these cells to form LDs in response to LPS + lFNγ.

In both *in vitro* and *in vivo* models, the LD content was oxidatively altered, which also depended on NADPH oxidase activation as indicated by pretreatment with apocynin that reversed all oxidative changes observed in these organelles. LDs are dynamic organelles that interact with different cellular components,

including mitochondria (Olzmann and Carvalho, 2019; Welte and Gould, 2017), these oxidative alterations could be implicated in the amplifying of cell damage since mitochondria are sensitive to excessive peroxidized lipids (Anderson et al., 2012; Bindoli, 1988). Here we show that upon LPS stimulation and sepsis, LDs interact with mitochondria including those producing large amounts of ROS. This close association may favor the process of peroxidation of LD content. Experimental sepsis increased the frequency of LD-mitochondrion interactions, which was correlated with an increased mitochondrial ultrastructural damage. Thus, LD and mitochondria interplay might be an important mechanism to induce mitochondrial dysfunction during sepsis. We also confirmed that LD accumulation is also deleterious at the organ level. Sepsis triggered a progressive increase in LDs in hepatic tissue and a simultaneous alongside with increase information of lipoperoxides within these organelles. These changes were associated with the sepsis model severity and an increased markers of liver dysfunction. Oral treatment with DGAT1inhibitor completely reversed sepsis-induced hepatic steatosis. The TLC results showed that TAG synthesis inhibition did not result in the accumulation of DAG, a lipid specimen with cytotoxic potential.This result is in agreement with the description indicating that the enzyme DGAT1 also has acyl CoA: monoacylglycerol acyltransferase (MGAT) activity, thus blocking DGAT1 can also affect DAG production (Yen et al., 2005). Low hepatic TAG levels result in decreased supply of oxidizable lipids within the LDs. Accordingly, the depletion of sepsis-induced LDs reduced tissue MDA levels, which are close to those of the control group. Previous studies have shown that the liver could compartmentalize peroxidized lipids during sepsis (Toufekoula et al., 2013). Our data indicate that LDs are among the main intracellular sites of hepatic peroxidized lipids accumulation. Damping LDs formation improves sepsis-induced liver dysfunction, supporting our hypothesis that LDs play a role in tissue damage during sepsis.

In sepsis, tissue damage is the results of a maladaptive inflammatory and metabolic response induced to resist infection and is associated with inadequate tissue tolerance mechanisms that prevent collateral damage caused by the immunometabolic response (Luan et al., 2019; Medzhitov et al., 2012). The protection against liver damage achieved by DGAT1 inhibition is not related

494 to the resistance mechanism, as shown by its dissociated from the control of
495 bacterial burden. In fact, our data indicate that DGAT1 inhibitor treatment actually
496 improves the mechanism of tissue tolerance against infection-induced
497 immunometabolic changes. Although Dgat1 overexpression in some tissues has
498 been suggested to confer cytoprotection by channeling toxic lipid intermediates
499 to LDs (Koliwad et al., 2010; Liu et al., 2009; Liu et al., 2007), Dgat1 deletion does
500 not necessarily lead to a deleterious phenotype (Chen and Farese, 2005). In
501 addition to the protection afforded by the reduction in LD formation and lipid
502 peroxidation described in our work, deletion or inhibition of DGAT1 can protect
503 tissue by altering the gene expression profile involved in glycolytic metabolism,
504 lipid uptake and fatty acid oxidation, thus reducing toxic lipid intermediate
505 formation (Liu et al., 2011; Smith et al., 2000; Villanueva et al., 2009; Zhang et
506 al., 2010).
507 DGAT1 inhibition also modulated the sepsis-induced inflammatory
508 response by downregulating the important LTB_4/IL-6 axis. This finding is in
509 agreement with the well established role of LDs in inflammatory mediator
510 production (Bozza and Viola, 2010; Pereira-Dutra et al., 2019). The bioactive lipid
511 LTB_4 is a potent leukocyte chemoattractant, that promotes cell activation and
512 enhances of antimicrobial functions (Brandt and Serezani, 2017). LTB_4 induces
513 transcription of the IL-6 gene and synthesis of IL-6 during experimental sepsis
514 (Uozumi et al., 2008), which may explain why they are synergistically regulated
515 in our model. Reduced LTB_4 and IL-6 levels were shown to protect against sepsis-
516 induced multiple organ dysfunction (Collin et al., 2004; Lee et al., 2018; Monteiro
517 et al., 2014). Therefore, modulation of these mediators can also contribute to the
518 liver protection achieved by the inhibition of DGAT1.
519 In conclusion, the synergistic effects of inflammation along with increased
520 lipid synthesis and/or LD accumulation in combination with elevated ROS and
521 lipid peroxidation contribute to tissue damage and organ dysfunction. Our
522 findings demonstrate that under intense oxidative stress, the LD accumulation is
523 a maladaptive mechanism of tolerance against lipotoxicity and becomes a
524 component of liver dysfunction pathogenesis triggered by sepsis. Finally, we
525 show that inhibition of LD accumulation decreased the production of inflammatory
526 mediators and lipid peroxidation while improving tissue function, suggesting that

LD and changes in lipid metabolism in sepsis may be a promising target for therapy.

Methods

Antibodies and reagents: Recombinant Murine IFN-γ was obtained from PeproTech. From Sigma-Aldrich (St Louis, MO) were obtained Lipopolysaccharides from Escherichia coli (serotype O111:B4, cat.# L4931), Antimycin A from Streptomyces sp. (cat.# A8674), Oligomycin A (cat.# 75351), Rotenone (cat.# R8875), Carbonylcyanide 4-(trifluoromethoxy)phenylhydrazone (cat.# C2920), Apocynin (cat.# W508454) and diacylglycerol acyltransferase-1 (DGAT-1) inhibitor (cat.# A92250). MitoTempo was obtained from Enzo Life Sciences (Farmingdale, NY - cat.# ALX – 430150 M005). Antibodies used in the study were the following: anti-ADRP (cat.# sc-32888), anti-PPARγ (cat.# sc-7196), anti-SREBP-1(cat.# sc-8984) from Santa Cruz Biotechnology (Dallas, TX); β-actin from Sigma-Aldrich (St Louis, MO – cat.# 5316); anti-INOS (cat.# 610333) from BD (New Jersey, USA); anti-p22phox (cat.# ab80896) from Abcam (Cambridge, USA). Anti-mouse IgG horseradish peroxidase (HRP), anti-rabbit IgG HRP, and anti-goat IgG HRP were purchase from Jackson ImmunoResearch Laboratories, (West Grove, PA).

Mice: C57BL/6 and Swiss mice were supplied by the Oswaldo Cruz Foundation's Central Animal House and used at 8–12 weeks of age. All experiments were approved by the Animal Welfare Committee of the Oswaldo Cruz Foundation under license number LW32/12 (CEUA/FIOCRUZ). Mice were maintained with rodent diet and water available *ad libitum* with 12-h light–dark cycle under controlled temperature (23 ± 1 °C).

Bone marrow-derived macrophages (BMDMs): Bone marrow-derived macrophages (BMDM) were obtained by isolation from C57/BL6 and differentiation in RPMI-1640 medium supplemented with 20% (v/v) fetal bovine serum, 1% penicillin-streptomycin (v/v), and 30% (v/v) L929 culture supernatant. Differentiated macrophages were cultured in RPMI-1640 supplemented with 1% L-glutamine(v/v), 1% penicillin/streptomycin (v/v) and 10% fetal bovine serum(v/v).

Immortalized BMDMs (iBMM): iBMM cells were cultured in RPMI 1640 supplemented with 10% fetal bovine serum and penicillin/streptomycin with 5% CO_2 at 37°C. iBMM cells were maintained at a density of $0.1x10^6$ – $1x10^6$ cells/ml.

Establishment of $p22^{phox\ -/-}$ knockout iBMM lines by CRISPR-Cas9 system: Immortalized bone marrow macrophages (iBMMs) were cultured in DMEM (Gibco) with 10% FCS. To generate p22-deficient iBMMs, a target sequence for mouse p22/CYBA (5'-GCTGGAGTATCCCCGGGGAAAGAGG-3') was inserted into the Cas9/gRNA expressing vector pX330 (Addgene #42230). Then, 10^6 iBMMs were co-transfected with 3µg of p22-pX330 and 1µgpmaxGFP (Lonza) using Nucleofector Kit V in a Nucleofector II B equipment (Lonza). 48h later, GFP-positive cells were sorted in a MoFlo XDP sorter (Beckman Coulter). Single clones of sorted cells were obtained by serial dilutions. Clones were screened for p22phox deficiency by western blotting using a full length p22 antibody (Santa Cruz, sc-20781) and nucleotide deletion in the gene was confirmed by sequencing.

Macrophages stimulation and treatments: BMDMs and iBMMs cells were seeded at 1 x 10^5cells per well in 24-well places and stimulated with LPS serotype 0111: B4 (500 ng/mL) plus murine interferon γ recombinant (10 ng/mL) for 24h, at 37°C in 5% CO_2. To study the effect of electrons flow modulation across the electron transport chain on LD formation were used antimycin A (1 µg/mL), rotenone (1 µg/mL), oligomycin A (2µg/mL) or FCCP (1µM) for 24h, at 37°C in 5% CO_2. To reduce ROS levels were used mitochondrial-target antioxidant Mito-TEMPO (100µM) or NADPH oxidase inhibitor apocynin (500µM), all added 1h before LPS + IFNγ and remained for24h, at 37°C in 5% CO_2.

In selected experiments, BMDM seeded at 1 x 10^5 cells per well in 24-well places were infected with *E. coli* at MOI 5 and incubated for 1 h at 37 °C in a humidified atmosphere of 5% CO_2. Extracellular bacteria were washed off with HBSS added 100 µg/mL of gentamicin and BMDMs were incubated for 1h with culture medium supplemented with 100 µg/ml gentamicin, at 37° C in humidified atmosphere of 5% CO_2. After, the medium was changed, fresh

medium was added without antibiotic and the cells were cultured for 24h at 37° C in humidified atmosphere of 5% CO_2.

Flow Cytometry: BMDMs and iBMMs were cultured in non-adherence tubes (BD Falcon, 149592A) at $1x10^6$ cells per tube. After stimuli and treatments, cells were washed in HBSS (without $Ca^{2+}$and Mg^{2+}/0.1% NaN_3) and then resuspended in 100µL of HBSS at final concentration of 1×10^6cells/100 µL. The following indices were assessed: Total ROS was detected using Dihydroethidium – DHE (Molecular probes, D11347) (2.5 µM at 37°C for 30 minutes). Alternatively, total ROS production was measured replacing DHE by CellROX Green (Molecular probes, C10444) (2.5 µM at 37°C for 30 minutes). Mitochondrial-derived ROS (ROSm) was detected using the cationic probe MitoSOX Red (Molecular Probes) (2.5 µM at 37°C for 10 minutes). Cells were distinguished by characteristic forward and side scattering and a gate excluding cell debris was utilized. A minimum of 10 000 events per gate was acquired using a FACScalibur flow cytometer (BD Bioscience) and analysis were performed in FlowJo™ Software.

ROS detection by fluorescence microscopy: BMDMs cells were cultured in 8-well Chambered Cover glass labtek (Thermo Fisher Scientific, 155411) at concentration of $1x10^5$ cells/ well. After time of stimulation with LPS (500 ng/mL) plus interferon γ (10ng / mL) or antimycin a (1µg / mL), cells were stained. For detection of total ROS was used the probe Dihydroethidium – DHE (Molecular probes, D11347) (2.5 µM at 37°C for 30 minutes) and for mitochondrial ROS was used MitoSOX Red (Molecular Probes, M36008) (0.5 µM at 37°C for 30 minutes). Live cell imaging was obtained on Olympus Fluoview FV1000 confocal microscope (Olympus America) with FV10-ASW acquisition software.

Mitochondria staining: BMDMs cells were cultured in 8-well Chambered Coverglass labtek (Thermo Fisher Scientific, 155411) at concentration of $1x10^5$ cells/well. After 24h stimulation, cells were incubated with 25nM of MitoTracker Red CMX Ros (Molecular Probes, M7512) in serum-free RPMI medium for 30 min at 37° C in humidified atmosphere of 5% CO_2, protected from the light. After labeling, the cells were washed with warm RPMI medium and immediately

analyzed. Live cell imaging was obtained on Olympus Fluoview FV1000 confocal microscope (Olympus America) with FV10-ASW acquisition software.

Lipid Droplets staining: BMDMs and iBMMs cells were fixed with 3.7% formaldehyde for 10 min and LDs were stained with 1 µM BODIPY 493/503 (Molecular Probes, D3922) or 500nM of HCS LipidTOX™ Red neutral lipid stain (Molecular Probes, H34476) for 10 min. Alternatively, cells were stained with Nile Red (Sigma-Aldrich, N3013) by diluting stock solution (1 mg/mL in acetone) at ratio of 1:20.000 in PBS and incubated for 15 min. Subsequently, cells were rinsed with PBS and immediately mounted with Vectashield (Vector Labs) for same-day imaging. Images were obtained with Olympus Fluoview FV1000 confocal microscope. To LDs quantification, cells were staining with Oil red O (Sigma-Aldrich, O0625) as previously described (Melo et al., 2011).

Lipid Peroxidation detection: BMDMs cells were cultured in 8-well Chambered Coverglass labtek (Thermo Fisher Scientific, 155411) at concentration of $1x10^5$ cells/well. Simultaneously to stimuli, 10 µM of C11-BODIPY$^{581/591}$ (Molecular Probes, C10445) was added to culture and remained throughout all experiment time (24h). Posteriorly, cells were washed three times with warm PBS, fresh RPMI medium was added and cells were immediately analyzed. Live cell imaging was obtained on Olympus Fluoview FV1000 confocal microscope (Olympus America) with FV10-ASW acquisition software.

Protein peroxidation detection: Click-iT® Lipid Peroxidation Detection Kit (Molecular probes, C10446) was used as manufacturer's instructions. Briefly, BMDMs were cultured in 8-well Chambered Coverglass labtek (Thermo Fisher Scientific, 155411) at concentration of $1x10^5$ cells/ well. Simultaneously to stimuli 25 µM of LAA reagent was added to culture and remained throughout all experiment time. After 24h stimuli, cells were fixed in 3% formalin for 20 min, washed 3x with PBS and then permeabilized with 0.05% Triton® X-100 for 10 min and blocked with 1% BSA for 30 min. Click reaction was performed by incubating cells with manufacturer-supplied reagent cocktail containing 5 µM Alexa 488 Fluor® azide for 30 min. Subsequently, cells were rinsed with PBS and

immediately mounted with Vectashield (Vector Labs) for same-day imaging. Images were obtained with Olympus Fluoview FV1000 confocal microscope (Olympus America) with FV10-ASW acquisition software.

Western blotting: BMDMs and iBMMs were seeded at 1 x 10^6 cells per well in 6-well plates. The cells were washed with ice-cold PBS, scraped and lysed in lysis buffer (150 mM NaCl, Triton 0.1% (v/v) and glycerol 10% (v/v) 10 mM Tris-HCl pH 8.0) in the presence of inhibitors of proteases and phosphatases (Roche). After centrifugation at 13 000 g for 5 min, cell lysates were prepared in reducing and denaturing conditions and subjected to SDS-PAGE. Equal concentrations of proteins were fractionated by electrophoresis on 10% or 15% acrylamide gels and were transferred onto a nitrocellulose membrane (Millipore, Billerica, MA, USA), followed by blockage with 5% nonfat milk in TBST (50 mM Tris-HCl (pH 7.4), 150 mM NaCl, 0.05% Tween 20) and blotting with primary antibodies in TBST with 1% nonfat dry milk. Proteins of interest were then identified by incubating the membrane with HRP-conjugated secondary Abs in TBST, followed by the detection of Ag-Ab complexes by Supersignal Chemiluminescence (Thermo Scientific, EUA).

Plin-2/ADRP immunofluorescence: BMDMs and iBMMs were cultured in 24-well at concentration of 1x10^5 cells/well. After 24h stimulation, cells were fixed in 3% formalin for 10 min washed with PBS and permeabilized with 0.2% triton in PBS for 20 min. After, cells were incubated with blocking solution composed by 1% donkey serum (Jackson Laboratories, 017-000-121) in PBS for 1 h and then incubated with guinea pig primary antibody against Plin2/ADRP (Fitzgerald, 20R-AP002) at 5µg/ml in PBS for 24 h at 4 °C. After this period, cells were washed 3x with PBS for 10 min then incubated with Alexa-488-conjugated secondary antibody (Molecular Probes, A-11073) 1:1000 diluted in PBS for 1 h, washed 3x with PBS and mounting with Vectashield medium containing DAPI (Vector Laboratories - H-1,200). The labeling specificity was confirmed replacing primary antibody with control isotype.

Measurement of 8-Isoprostane: Total 8-Isoprostane was measured in cell-free culture supernatant or in isolated hepatic LDs by enzyme-linked immunoassay - EIA (Cayman Chemical, Cat. # 516351) according to the manufacturer's instructions.

Measurement of nitric oxide: Nitrite levels in cell-free culture supernatant were measured using Griess reagent system according to the manufacturer's instructions (Promega cat.# G2930).

Measurement of Lactate: Lactate levels in cell-free culture supernatant were measured using enzymatic lactate kit (Labtest, cat.# 138-1/50) performed as manufacturer's instruction.

Polymicrobial sepsis model (CLP): Sepsis was induced by Cecal Ligation and Puncture (CLP). Briefly, C57BL/6 and Swiss mice were anesthetized with intraperitoneal injections of ketamine (100 mg/kg) and xylazine (10 mg/kg) and a 1 cm incision was made on the abdomen. The cecum was exposed and ligated below the ileocecal junction. The number of puctures made varied according to the degree of severity sought, with 2 perforations (moderate sepsis) and 9 perforations (severe sepsis) using a 22-gauge needle. Sham-operated animals (control) underwent an identical laparotomy but without ligation and punctures. All mice received 1 ml of sterile saline subcutaneously as fluid resuscitation and antibiotic therapy by subcutaneous injection of meropenen (10 mg/kg) (Merck) at 6h and 24h hours after surgery.

DGAT-1 inhibition *in vivo:* The Diacylglycerol acyltransferase-1 (DGAT-1) inhibitor was first dissolved in DMSO at proportion of 10mg / 200µL as stock solution then diluted in saline. Sham and CLP mice were orally treated withDGAT-1i solution at dose of 3 mg/kg or vehicle at 6h and 24h post surgery.

Transmission Electron microscopy (TEM): Peritoneal cells from Swiss mice subject to CLP or Sham operated were prepared to TEM as described(D'Avila et al., 2006). Briefly, peritoneal wash was centrifuged and cell pellet was immediately fixed in 0.1 M phosphate buffer solution containing 1%

paraformaldehyde and 1% glutaraldehyde, pH 7.3, for 4 h at room temperature and washed in the same buffer. The samples were post-fixed in a mixture of phosphate buffer containing 1% osmium tetroxide and 1.5% potassium ferricyanide for 1 h before dehydration in a gradual series of ethanol. Subsequently, they were infiltrated and included in propylene oxide - Epon (PolyBed 812). After polymerization at 60°C for 16 h, ultrathin sections were made using ultramicrotome diamond razor (Sorvall MT2) and collected on 200 mesh grids (Ted Pella) before staining with uranyl acetate and lead citrate. The samples were analyzed under transmission electron microscope (EMI, Zeiss) at 60KV and JEOL-JEM-1011 at 80 KV.

Hepatic LD isolation: Mice from CLP and Sham group were euthanized 24 or 48 hours post surgery. After liver perfusion with 0.9% NaCl and 0.1% EDTA solution, the tissue was macerate into a dounce tissue grinder at proportion of 1g / 3mL of homogenization buffer (25 mM Tris-HCl, pH 7.5, 100 mMKCl, 1 mM EDTA, 5mM EGTA) supplemented with antioxidant (BHT, 0,1%), protease and phosphatase inhibitor cocktail (Roche). After, the liver homogenate was centrifuged at 500 g for 10 minutes at 4°C. The resulting post-nuclei supernatant was collected and applied to a sucrose gradient (1.08 M, 0.27 M and 0.135 M) and subjected to ultracentrifugation (150,000 x g for 70 min). After ultracentrifugation was collect the first fraction rich in isolated LDs. To the first fraction was added TEE-KCl buffer and LDs were isolated a second time by a centrifugation at 14,000 g for 15 min. As control of properly cell fractionation, the activity of cytoplasmic enzyme lactate dehydrogenase - LDH (Promega, G1780) was assayed.

Thiobarbituric acid-reactive species assay (TBARS): TBARS, an index of lipid peroxidation, were determined according to the method described by Buege and Aust, (1978) with some modifications. Trichloroacetic acid and thiobarbituric acid were added to samples and incubated for 1 h at 100°C. A calibration curve was performed using 1,1,3,3-tetramethoxypropane. The absorbance was read at 535 mm, the results were reported as nmol TBARS/mg protein.

Measurement of triglycerides: Triglycerides levels in isolated LDs was measured using enzymatic triglycerides liquiform kit (Labtest, cat.# 87-2/100) according to manufacturer's instruction.

Thin-layer chromatography (TLC): Hepatic lipid fractions from 1mg of tissue samples were extracted applying the Bligh and Dyer method (BLIGH and DYER, 1959). TLC was performed on silica gel 60 plates (Merck) according to Horwitz and Perlman (1987). Plates were developed in hexane/ ethyl ether/ acetic acid solution (60:40:1, v/v) until the solvent front has reached the upper line. Neutral lipids were identified by comparison with standard lipids (1 mg/ml): cholesterol (CHO), cholesterol ester (CE), fatty acid (FA), monoacylglycerol (MAG), diacylglycerol (DAG), triacylglycerol (TAG), obtained from Sigma. For visualization of lipids, the TLC plates were stained by spraying with Charring reagent (3% $CuSO_4$ and 8% H_3PO_4 v/v) and heating at 110°C for 10 min. Triacylglycerol level were quantified by densitometry using the software ImageJ.

Measurements of liver function markers: Serum levels of aspartate transaminase (AST), alanine transaminase (ALT) and albumin were performed in a Metrolab2300® autoanalyzer, according to the manufacturer's instructions (Wiener Lab Group, Argentina).

Leukotriene B_4 level measurements: Levels of LTB_4 in cell-free peritoneal wash were measured using an enzyme-linked immunosorbent assay kit according to manufacturer's instructions (Cayman, **cat.#** 520111).

Cytokine level measurements: Levels of IL-6, MCP-1, and IL-10 in cell-free peritoneal wash were measured using an enzyme-linked immunosorbent assay kit according to manufacturer's instructions (R&D systems).

Statistical analysis: Data obtained in this study were presented as mean ± SEM and compared by analysis of variance (ANOVA). In case of significant interaction, Bonferroni post-test was used unless otherwise noted. For all analyzes was adopted $p \leq 0.05$ as the significance level.

References

Abraham, E., and Singer, M. (2007). Mechanisms of sepsis-induced organ dysfunction. Crit Care Med *35*, 2408-2416.

Almeida, P.E., Roque, N.R., Magalhaes, K.G., Mattos, K.A., Teixeira, L., Maya-Monteiro, C., Almeida, C.J., Castro-Faria-Neto, H.C., Ryffel, B., Quesniaux, V.F.*, et al.* (2014). Differential TLR2 downstream signaling regulates lipid metabolism and cytokine production triggered by Mycobacterium bovis BCG infection. Biochim Biophys Acta *1841*, 97-107.

Almeida, P.E., Silva, A.R., Maya-Monteiro, C.M., Torocsik, D., D'Avila, H., Dezso, B., Magalhaes, K.G., Castro-Faria-Neto, H.C., Nagy, L., and Bozza, P.T. (2009). Mycobacterium bovis bacillus Calmette-Guerin infection induces TLR2-dependent peroxisome proliferator-activated receptor gamma expression and activation: functions in inflammation, lipid metabolism, and pathogenesis. J Immunol *183*, 1337-1345.

Anderson, E.J., Katunga, L.A., and Willis, M.S. (2012). Mitochondria as a source and target of lipid peroxidation products in healthy and diseased heart. Clin Exp Pharmacol Physiol *39*, 179-193.

Angus, D.C., and van der Poll, T. (2013). Severe sepsis and septic shock. N Engl J Med *369*, 2063.

Atashi, F., Modarressi, A., and Pepper, M.S. (2015). The role of reactive oxygen species in mesenchymal stem cell adipogenic and osteogenic differentiation: a review. Stem Cells Dev *24*, 1150-1163.

Bailey, A.P., Koster, G., Guillermier, C., Hirst, E.M., MacRae, J.I., Lechene, C.P., Postle, A.D., and Gould, A.P. (2015). Antioxidant Role for Lipid Droplets in a Stem Cell Niche of Drosophila. Cell *163*, 340-353.

Benador, I.Y., Veliova, M., Mahdaviani, K., Petcherski, A., Wikstrom, J.D., Assali, E.A., Acin-Perez, R., Shum, M., Oliveira, M.F., Cinti, S.*, et al.* (2018). Mitochondria Bound to Lipid Droplets Have Unique Bioenergetics, Composition, and Dynamics that Support Lipid Droplet Expansion. Cell Metab *27*, 869-885 e866.

Bindoli, A. (1988). Lipid peroxidation in mitochondria. Free Radic Biol Med *5*, 247-261.

Bosch, M., Sánchez-Álvarez, M., Fajardo, A., Kapetanovic, R., Steiner, B., Dutra, F., Moreira, L., Lopez, J.A., Campo, R., Mari, M.*, et al.* (2020). Mammalian lipid droplets are innate immune hubs integrating cell metabolism and host defense. Science *in press*.

Bosma, M., Dapito, D.H., Drosatos-Tampakaki, Z., Huiping-Son, N., Huang, L.S., Kersten, S., Drosatos, K., and Goldberg, I.J. (2014). Sequestration of fatty acids in triglycerides prevents endoplasmic reticulum stress in an in vitro model of cardiomyocyte lipotoxicity. Biochim Biophys Acta *1841*, 1648-1655.

Bozza, P.T., and Viola, J.P. (2010). Lipid droplets in inflammation and cancer. Prostaglandins Leukot Essent Fatty Acids *82*, 243-250.

Brandt, S.L., and Serezani, C.H. (2017). Too much of a good thing: How modulating LTB4 actions restore host defense in homeostasis or disease. Semin Immunol *33*, 37-43.

Brealey, D., Brand, M., Hargreaves, I., Heales, S., Land, J., Smolenski, R., Davies, N.A., Cooper, C.E., and Singer, M. (2002). Association between mitochondrial dysfunction and severity and outcome of septic shock. Lancet *360*, 219-223.

Chawla, A., Barak, Y., Nagy, L., Liao, D., Tontonoz, P., and Evans, R.M. (2001). PPAR-gamma dependent and independent effects on macrophage-gene expression in lipid metabolism and inflammation. Nat Med *7*, 48-52.

Chen, H.C., and Farese, R.V., Jr. (2005). Inhibition of triglyceride synthesis as a treatment strategy for obesity: lessons from DGAT1-deficient mice. Arterioscler Thromb Vasc Biol *25*, 482-486.

Collin, M., Rossi, A., Cuzzocrea, S., Patel, N.S., Di Paola, R., Hadley, J., Collino, M., Sautebin, L., and Thiemermann, C. (2004). Reduction of the multiple organ injury and

847 dysfunction caused by endotoxemia in 5-lipoxygenase knockout mice and by the 5-
848 lipoxygenase inhibitor zileuton. J Leukoc Biol *76*, 961-970.
849 Corona, J.C., and Duchen, M.R. (2016). PPARgamma as a therapeutic target to rescue
850 mitochondrial function in neurological disease. Free Radic Biol Med *100*, 153-163.
851 D'Avila, H., Melo, R.C., Parreira, G.G., Werneck-Barroso, E., Castro-Faria-Neto, H.C.,
852 and Bozza, P.T. (2006). Mycobacterium bovis bacillus Calmette-Guerin induces TLR2-
853 mediated formation of lipid bodies: intracellular domains for eicosanoid synthesis in vivo.
854 J Immunol *176*, 3087-3097.
855 Dejager, L., Pinheiro, I., Dejonckheere, E., and Libert, C. (2011). Cecal ligation and
856 puncture: the gold standard model for polymicrobial sepsis? Trends Microbiol *19*, 198-
857 208.
858 Diaz Acosta, C.C., Dias, A.A., Rosa, T., Batista-Silva, L.R., Rosa, P.S., Toledo-Pinto,
859 T.G., Costa, F., Lara, F.A., Rodrigues, L.S., Mattos, K.A.*, et al.* (2018). PGL I expression
860 in live bacteria allows activation of a CD206/PPARgamma cross-talk that may contribute
861 to successful Mycobacterium leprae colonization of peripheral nerves. PLoS Pathog *14*,
862 e1007151.
863 Dixon, S.J., Lemberg, K.M., Lamprecht, M.R., Skouta, R., Zaitsev, E.M., Gleason, C.E.,
864 Patel, D.N., Bauer, A.J., Cantley, A.M., Yang, W.S.*, et al.* (2012). Ferroptosis: an iron-
865 dependent form of nonapoptotic cell death. Cell *149*, 1060-1072.
866 Drosatos, K., Drosatos-Tampakaki, Z., Khan, R., Homma, S., Schulze, P.C., Zannis, V.I.,
867 and Goldberg, I.J. (2011). Inhibition of c-Jun-N-terminal kinase increases cardiac
868 peroxisome proliferator-activated receptor alpha expression and fatty acid oxidation and
869 prevents lipopolysaccharide-induced heart dysfunction. J Biol Chem *286*, 36331-36339.
870 Fleischmann, C., Scherag, A., Adhikari, N.K., Hartog, C.S., Tsaganos, T., Schlattmann,
871 P., Angus, D.C., Reinhart, K., and International Forum of Acute Care, T. (2016).
872 Assessment of Global Incidence and Mortality of Hospital-treated Sepsis. Current
873 Estimates and Limitations. Am J Respir Crit Care Med *193*, 259-272.
874 Garofalo, A.M., Lorente-Ros, M., Goncalvez, G., Carriedo, D., Ballen-Barragan, A.,
875 Villar-Fernandez, A., Penuelas, O., Herrero, R., Granados-Carreno, R., and Lorente, J.A.
876 (2019). Histopathological changes of organ dysfunction in sepsis. Intensive Care Med
877 Exp *7*, 45.
878 Gaschler, M.M., and Stockwell, B.R. (2017). Lipid peroxidation in cell death. Biochem
879 Biophys Res Commun *482*, 419-425.
880 Gomez, H., Kellum, J.A., and Ronco, C. (2017). Metabolic reprogramming and tolerance
881 during sepsis-induced AKI. Nat Rev Nephrol *13*, 143-151.
882 Herms, A., Bosch, M., Ariotti, N., Reddy, B.J., Fajardo, A., Fernandez-Vidal, A., Alvarez-
883 Guaita, A., Fernandez-Rojo, M.A., Rentero, C., Tebar, F.*, et al.* (2013). Cell-to-cell
884 heterogeneity in lipid droplets suggests a mechanism to reduce lipotoxicity. Curr Biol *23*,
885 1489-1496.
886 Hernandes, M.S., D'Avila, J.C., Trevelin, S.C., Reis, P.A., Kinjo, E.R., Lopes, L.R.,
887 Castro-Faria-Neto, H.C., Cunha, F.Q., Britto, L.R., and Bozza, F.A. (2014). The role of
888 Nox2-derived ROS in the development of cognitive impairment after sepsis. J
889 Neuroinflammation *11*, 36.
890 Hotchkiss, R.S., Monneret, G., and Payen, D. (2013). Sepsis-induced
891 immunosuppression: from cellular dysfunctions to immunotherapy. Nat Rev Immunol *13*,
892 862-874.
893 Im, S.S., Yousef, L., Blaschitz, C., Liu, J.Z., Edwards, R.A., Young, S.G., Raffatellu, M.,
894 and Osborne, T.F. (2011). Linking lipid metabolism to the innate immune response in
895 macrophages through sterol regulatory element binding protein-1a. Cell Metab *13*, 540-
896 549.
897 Jarc, E., Kump, A., Malavasic, P., Eichmann, T.O., Zimmermann, R., and Petan, T.
898 (2018). Lipid droplets induced by secreted phospholipase A2 and unsaturated fatty acids
899 protect breast cancer cells from nutrient and lipotoxic stress. Biochim Biophys Acta Mol
900 Cell Biol Lipids *1863*, 247-265.

Joseph, L.C., Kokkinaki, D., Valenti, M.C., Kim, G.J., Barca, E., Tomar, D., Hoffman, N.E., Subramanyam, P., Colecraft, H.M., Hirano, M.*, et al.* (2017). Inhibition of NADPH oxidase 2 (NOX2) prevents sepsis-induced cardiomyopathy by improving calcium handling and mitochondrial function. JCI Insight *2*.

Koliwad, S.K., Streeper, R.S., Monetti, M., Cornelissen, I., Chan, L., Terayama, K., Naylor, S., Rao, M., Hubbard, B., and Farese, R.V., Jr. (2010). DGAT1-dependent triacylglycerol storage by macrophages protects mice from diet-induced insulin resistance and inflammation. J Clin Invest *120*, 756-767.

Koskinas, J., Gomatos, I.P., Tiniakos, D.G., Memos, N., Boutsikou, M., Garatzioti, A., Archimandritis, A., and Betrosian, A. (2008). Liver histology in ICU patients dying from sepsis: a clinico-pathological study. World J Gastroenterol *14*, 1389-1393.

Kramer, L., Jordan, B., Druml, W., Bauer, P., Metnitz, P.G., and Austrian Epidemiologic Study on Intensive Care, A.S.G. (2007). Incidence and prognosis of early hepatic dysfunction in critically ill patients--a prospective multicenter study. Crit Care Med *35*, 1099-1104.

Langley, R.J., Tsalik, E.L., van Velkinburgh, J.C., Glickman, S.W., Rice, B.J., Wang, C., Chen, B., Carin, L., Suarez, A., Mohney, R.P.*, et al.* (2013). An integrated clinico-metabolomic model improves prediction of death in sepsis. Sci Transl Med *5*, 195ra195.

Lee, E.K.S., Gillrie, M.R., Li, L., Arnason, J.W., Kim, J.H., Babes, L., Lou, Y., Sanati-Nezhad, A., Kyei, S.K., Kelly, M.M.*, et al.* (2018). Leukotriene B4-Mediated Neutrophil Recruitment Causes Pulmonary Capillaritis during Lethal Fungal Sepsis. Cell Host Microbe *23*, 121-133 e124.

Listenberger, L.L., Han, X., Lewis, S.E., Cases, S., Farese, R.V., Jr., Ory, D.S., and Schaffer, J.E. (2003). Triglyceride accumulation protects against fatty acid-induced lipotoxicity. Proc Natl Acad Sci U S A *100*, 3077-3082.

Liu, L., MacKenzie, K.R., Putluri, N., Maletic-Savatic, M., and Bellen, H.J. (2017). The Glia-Neuron Lactate Shuttle and Elevated ROS Promote Lipid Synthesis in Neurons and Lipid Droplet Accumulation in Glia via APOE/D. Cell Metab *26*, 719-737 e716.

Liu, L., Shi, X., Bharadwaj, K.G., Ikeda, S., Yamashita, H., Yagyu, H., Schaffer, J.E., Yu, Y.H., and Goldberg, I.J. (2009). DGAT1 expression increases heart triglyceride content but ameliorates lipotoxicity. J Biol Chem *284*, 36312-36323.

Liu, L., Trent, C.M., Fang, X., Son, N.H., Jiang, H., Blaner, W.S., Hu, Y., Yin, Y.X., Farese, R.V., Jr., Homma, S.*, et al.* (2014). Cardiomyocyte-specific loss of diacylglycerol acyltransferase 1 (DGAT1) reproduces the abnormalities in lipids found in severe heart failure. J Biol Chem *289*, 29881-29891.

Liu, L., Yu, S., Khan, R.S., Ables, G.P., Bharadwaj, K.G., Hu, Y., Huggins, L.A., Eriksson, J.W., Buckett, L.K., Turnbull, A.V.*, et al.* (2011). DGAT1 deficiency decreases PPAR expression and does not lead to lipotoxicity in cardiac and skeletal muscle. J Lipid Res *52*, 732-744.

Liu, L., Zhang, K., Sandoval, H., Yamamoto, S., Jaiswal, M., Sanz, E., Li, Z., Hui, J., Graham, B.H., Quintana, A.*, et al.* (2015). Glial lipid droplets and ROS induced by mitochondrial defects promote neurodegeneration. Cell *160*, 177-190.

Liu, L., Zhang, Y., Chen, N., Shi, X., Tsang, B., and Yu, Y.H. (2007). Upregulation of myocellular DGAT1 augments triglyceride synthesis in skeletal muscle and protects against fat-induced insulin resistance. J Clin Invest *117*, 1679-1689.

Luan, H.H., Wang, A., Hilliard, B.K., Carvalho, F., Rosen, C.E., Ahasic, A.M., Herzog, E.L., Kang, I., Pisani, M.A., Yu, S.*, et al.* (2019). GDF15 Is an Inflammation-Induced Central Mediator of Tissue Tolerance. Cell *178*, 1231-1244 e1211.

Marques, P.E., Antunes, M.M., David, B.A., Pereira, R.V., Teixeira, M.M., and Menezes, G.B. (2015). Imaging liver biology in vivo using conventional confocal microscopy. Nat Protoc *10*, 258-268.

McCarville, J.L., and Ayres, J.S. (2018). Disease tolerance: concept and mechanisms. Curr Opin Immunol *50*, 88-93.

954 Medzhitov, R., Schneider, D.S., and Soares, M.P. (2012). Disease tolerance as a
955 defense strategy. Science *335*, 936-941.
956 Mei, C.L., He, P., Cheng, B., Liu, W., Wang, Y.F., and Wan, J.J. (2009). Chlamydia
957 pneumoniae induces macrophage-derived foam cell formation via PPAR alpha and
958 PPAR gamma-dependent pathways. Cell Biol Int *33*, 301-308.
959 Melo, R.C., D'Avila, H., Bozza, P.T., and Weller, P.F. (2011). Imaging lipid bodies within
960 leukocytes with different light microscopy techniques. Methods Mol Biol *689*, 149-161.
961 Mickiewicz, B., Tam, P., Jenne, C.N., Leger, C., Wong, J., Winston, B.W., Doig, C.,
962 Kubes, P., Vogel, H.J., and Alberta Sepsis, N. (2015). Integration of metabolic and
963 inflammatory mediator profiles as a potential prognostic approach for septic shock in the
964 intensive care unit. Crit Care *19*, 11.
965 Monteiro, A.P., Soledade, E., Pinheiro, C.S., Dellatorre-Teixeira, L., Oliveira, G.P.,
966 Oliveira, M.G., Peters-Golden, M., Rocco, P.R., Benjamim, C.F., and Canetti, C. (2014).
967 Pivotal role of the 5-lipoxygenase pathway in lung injury after experimental sepsis. Am J
968 Respir Cell Mol Biol *50*, 87-95.
969 Nguyen, T.B., Louie, S.M., Daniele, J.R., Tran, Q., Dillin, A., Zoncu, R., Nomura, D.K.,
970 and Olzmann, J.A. (2017). DGAT1-Dependent Lipid Droplet Biogenesis Protects
971 Mitochondrial Function during Starvation-Induced Autophagy. Dev Cell *42*, 9-21 e25.
972 Olzmann, J.A., and Carvalho, P. (2019). Dynamics and functions of lipid droplets. Nat
973 Rev Mol Cell Biol *20*, 137-155.
974 Pacheco, P., Bozza, F.A., Gomes, R.N., Bozza, M., Weller, P.F., Castro-Faria-Neto,
975 H.C., and Bozza, P.T. (2002). Lipopolysaccharide-induced leukocyte lipid body formation
976 in vivo: innate immunity elicited intracellular Loci involved in eicosanoid metabolism. J
977 Immunol *169*, 6498-6506.
978 Pacheco, P., Vieira-de-Abreu, A., Gomes, R.N., Barbosa-Lima, G., Wermelinger, L.B.,
979 Maya-Monteiro, C.M., Silva, A.R., Bozza, M.T., Castro-Faria-Neto, H.C., Bandeira-Melo,
980 C.*, et al.* (2007). Monocyte chemoattractant protein-1/CC chemokine ligand 2 controls
981 microtubule-driven biogenesis and leukotriene B4-synthesizing function of macrophage
982 lipid bodies elicited by innate immune response. J Immunol *179*, 8500-8508.
983 Paumelle, R., Haas, J.T., Hennuyer, N., Bauge, E., Deleye, Y., Mesotten, D., Langouche,
984 L., Vanhoutte, J., Cudejko, C., Wouters, K.*, et al.* (2019). Hepatic PPARalpha is critical
985 in the metabolic adaptation to sepsis. J Hepatol *70*, 963-973.
986 Pereira-Dutra, F.S., Teixeira, L., de Souza Costa, M.F., and Bozza, P.T. (2019). Fat,
987 fight, and beyond: The multiple roles of lipid droplets in infections and inflammation. J
988 Leukoc Biol *106*, 563-580.
989 Rao, S., Schieber, A.M.P., O'Connor, C.P., Leblanc, M., Michel, D., and Ayres, J.S.
990 (2017). Pathogen-Mediated Inhibition of Anorexia Promotes Host Survival and
991 Transmission. Cell *168*, 503-516 e512.
992 Roberts, L.J., 2nd, and Fessel, J.P. (2004). The biochemistry of the isoprostane,
993 neuroprostane, and isofuran pathways of lipid peroxidation. Chem Phys Lipids *128*, 173-
994 186.
995 Sharma, N.K., Ferreira, B.L., Tashima, A.K., Brunialti, M.K.C., Torquato, R.J.S., Bafi, A.,
996 Assuncao, M., Azevedo, L.C.P., and Salomao, R. (2019). Lipid metabolism impairment
997 in patients with sepsis secondary to hospital acquired pneumonia, a proteomic analysis.
998 Clin Proteomics *16*, 29.
999 Singer, M., Deutschman, C.S., Seymour, C.W., Shankar-Hari, M., Annane, D., Bauer,
1000 M., Bellomo, R., Bernard, G.R., Chiche, J.D., Coopersmith, C.M.*, et al.* (2016). The Third
1001 International Consensus Definitions for Sepsis and Septic Shock (Sepsis-3). JAMA *315*,
1002 801-810.
1003 Smith, S.J., Cases, S., Jensen, D.R., Chen, H.C., Sande, E., Tow, B., Sanan, D.A.,
1004 Raber, J., Eckel, R.H., and Farese, R.V., Jr. (2000). Obesity resistance and multiple
1005 mechanisms of triglyceride synthesis in mice lacking Dgat. Nat Genet *25*, 87-90.
1006 Toufekoula, C., Papadakis, V., Tsaganos, T., Routsi, C., Orfanos, S.E., Kotanidou, A.,
1007 Carrer, D.P., Raftogiannis, M., Baziaka, F., and Giamarellos-Bourboulis, E.J. (2013).

Compartmentalization of lipid peroxidation in sepsis by multidrug-resistant gram-negative bacteria: experimental and clinical evidence. Crit Care *17*, R6.
Uozumi, N., Kita, Y., and Shimizu, T. (2008). Modulation of lipid and protein mediators of inflammation by cytosolic phospholipase A2alpha during experimental sepsis. J Immunol *181*, 3558-3566.
Van Wyngene, L., Vandewalle, J., and Libert, C. (2018). Reprogramming of basic metabolic pathways in microbial sepsis: therapeutic targets at last? EMBO Mol Med *10*.
Varga, T., Czimmerer, Z., and Nagy, L. (2011). PPARs are a unique set of fatty acid regulated transcription factors controlling both lipid metabolism and inflammation. Biochim Biophys Acta *1812*, 1007-1022.
Villanueva, C.J., Monetti, M., Shih, M., Zhou, P., Watkins, S.M., Bhanot, S., and Farese, R.V., Jr. (2009). Specific role for acyl CoA:Diacylglycerol acyltransferase 1 (Dgat1) in hepatic steatosis due to exogenous fatty acids. Hepatology *50*, 434-442.
Vincent, J.L., Marshall, J.C., Namendys-Silva, S.A., Francois, B., Martin-Loeches, I., Lipman, J., Reinhart, K., Antonelli, M., Pickkers, P., Njimi, H.*, et al.* (2014). Assessment of the worldwide burden of critical illness: the intensive care over nations (ICON) audit. Lancet Respir Med *2*, 380-386.
Wang, A., Huen, S.C., Luan, H.H., Yu, S., Zhang, C., Gallezot, J.D., Booth, C.J., and Medzhitov, R. (2016). Opposing Effects of Fasting Metabolism on Tissue Tolerance in Bacterial and Viral Inflammation. Cell *166*, 1512-1525 e1512.
Wang, A., Luan, H.H., and Medzhitov, R. (2019). An evolutionary perspective on immunometabolism. Science *363*.
Wang, H., Sreenivasan, U., Hu, H., Saladino, A., Polster, B.M., Lund, L.M., Gong, D.W., Stanley, W.C., and Sztalryd, C. (2011). Perilipin 5, a lipid droplet-associated protein, provides physical and metabolic linkage to mitochondria. J Lipid Res *52*, 2159-2168.
Weis, S., Carlos, A.R., Moita, M.R., Singh, S., Blankenhaus, B., Cardoso, S., Larsen, R., Rebelo, S., Schauble, S., Del Barrio, L.*, et al.* (2017). Metabolic Adaptation Establishes Disease Tolerance to Sepsis. Cell *169*, 1263-1275 e1214.
Welte, M.A., and Gould, A.P. (2017). Lipid droplet functions beyond energy storage. Biochim Biophys Acta Mol Cell Biol Lipids *1862*, 1260-1272.
Wu, F., Tyml, K., and Wilson, J.X. (2008). iNOS expression requires NADPH oxidase-dependent redox signaling in microvascular endothelial cells. J Cell Physiol *217*, 207-214.
Yen, C.L., Monetti, M., Burri, B.J., and Farese, R.V., Jr. (2005). The triacylglycerol synthesis enzyme DGAT1 also catalyzes the synthesis of diacylglycerols, waxes, and retinyl esters. J Lipid Res *46*, 1502-1511.
Zhang, X.D., Yan, J.W., Yan, G.R., Sun, X.Y., Ji, J., Li, Y.M., Hu, Y.H., and Wang, H.Y. (2010). Pharmacological inhibition of diacylglycerol acyltransferase 1 reduces body weight gain, hyperlipidemia, and hepatic steatosis in db/db mice. Acta Pharmacol Sin *31*, 1470-1477.

Acknowledgments

This work was supported by grants from Conselho Nacional de Desenvolvimento Científico e Tecnológico (CNPq), Fundação de Amparo a Pesquisa do Estado do Rio de Janeiro (FAPERJ), Fundação de Amparo a Pesquisa do Estado de Minas Gerais (FAPEMIG), Coordenação de Aperfeiçoamento de Pessoal de Nível Superior (CAPES) and Human Frontier Science Program (HFSP).

Authors Contributions

L.T. performed the majority of the experiments, data analyses and manuscript drafting; L. S-M., E. P., P. A. R., F. S. P-D., H. E., C. A., T. P. S., E. D. H., C. M. M-M,M. M. A. performed part of the experiments and data analyses. G.B. M.; M.T.B., F.A.B., R.C.N.M. designed and analyzed experiments. P.T.B. performed the experimental design, manuscript reviewing and directed all aspects of the study; and all authors reviewed and critically edited the manuscript.

Conflict-of-interest disclosure

The authors declare no competing interests.

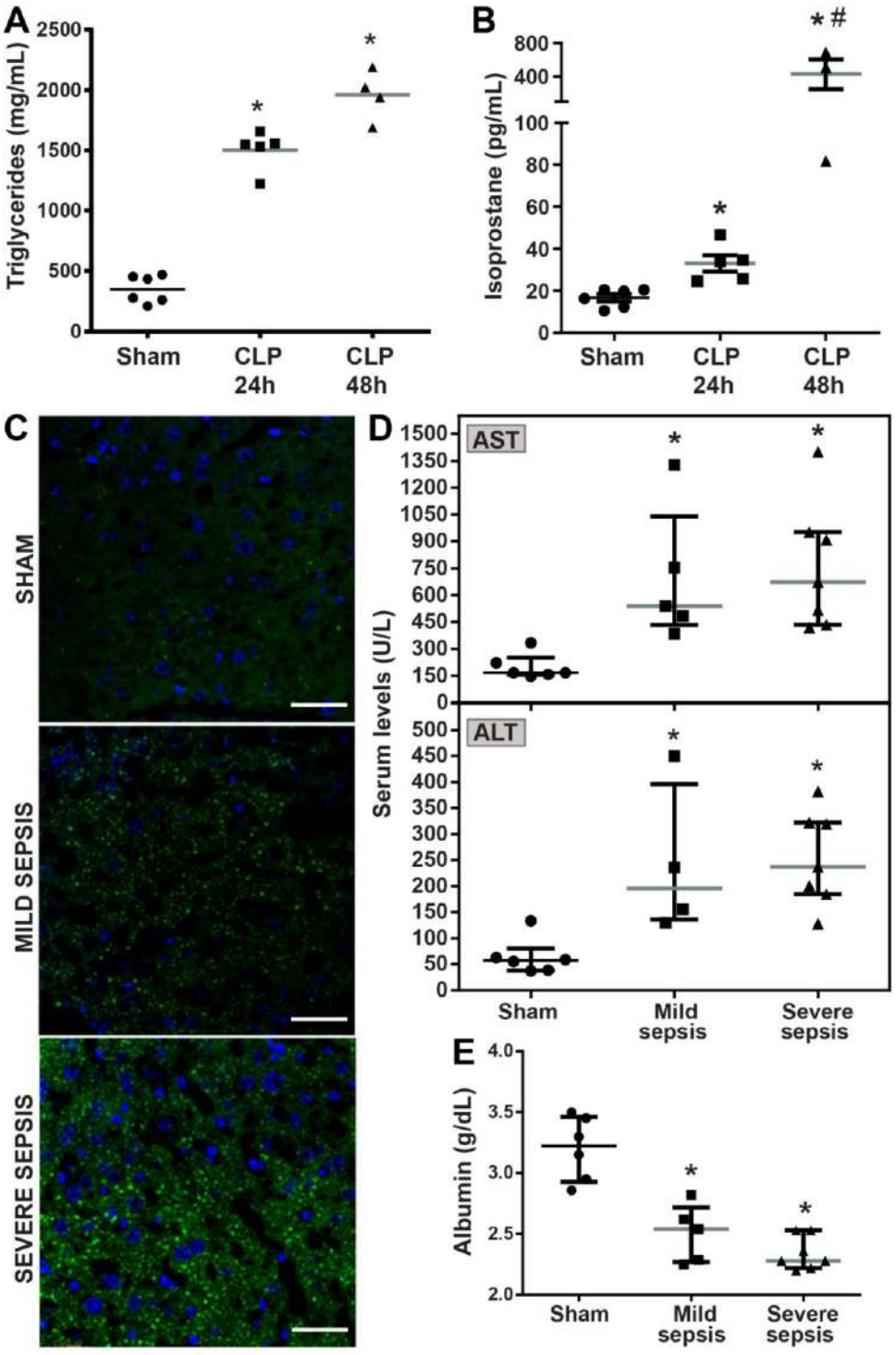
A
Triglycerides (mg/mL)
2500
2000
1500
1000
500
0
Sham
CLP 24h
CLP 48h
B
Isoprostane (pg/mL)
800
400
100
80
60
40
20
0
Sham
CLP 24h
CLP 48h
C
SHAM
MILD SEPSIS
SEVERE SEPSIS
D
AST
ALT
Serum levels (U/L)
Sham
Mild sepsis
Severe sepsis
E
Albumin (g/dL)
4.0
3.5
3.0
2.5
2.0
Sham
Mild sepsis
Severe sepsis

Figure 1: Accumulation and peroxidation of hepatic LDs induced by sepsis occur simultaneously to hepatic dysfunction. Lipid droplets level of **(A)** total triglycerides and **(B)** 8-isoprostane measured in isolated LDs (the F1 fraction of sucrose gradient) from livers of sham or septic (mild sepsis - 2 punctures) mice at 24 or 48h after CLP. **(C)** Representative images of Bodipy-labeled LDs (green) in the liver of Sham, mild (2 punctures) or severe (9 punctures) sepsis at 24h after CLP. Nuclei were visualized by DAPI staining (scale bar: 70µm). Serum level of **(D)** oxalacetic transaminase (AST), pyruvic transaminase (ALT) and **(E)** albumin were assayed 24h after CLP. **(A, B, D, E)** Data show mean ± SEM (n= 4–6 mice per group) *$p < 0.05$ versus control group, #$p < 0.05$ versus CLP 24h, One-way ANOVA followed by Bonferroni' test.

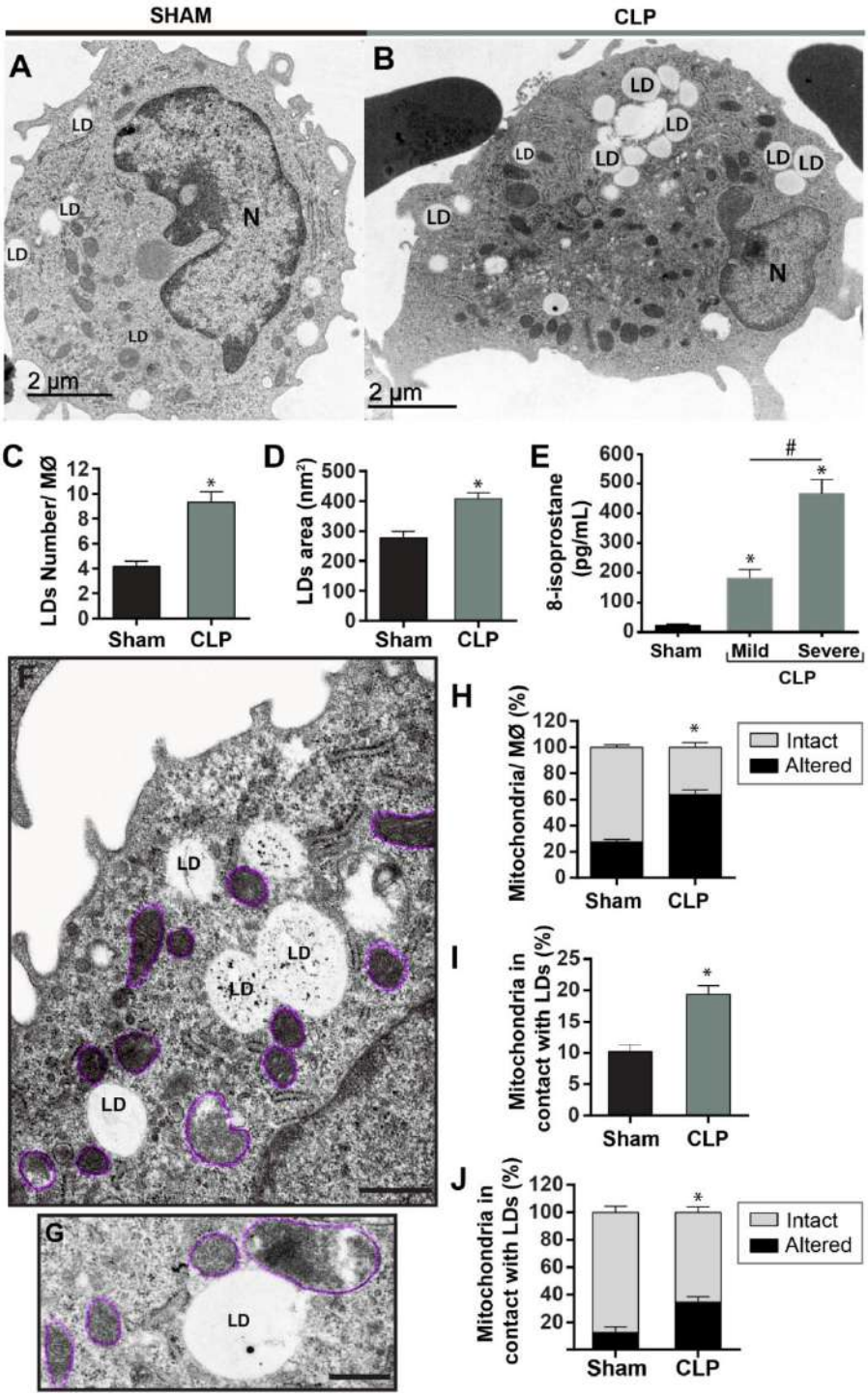
SHAM
CLP
A
B
LD
N
2 µm
C
LDs Number/ MØ
Sham
CLP
D
LDs area (nm²)
E
8-isoprostane (pg/mL)
Mild
Severe
F
G
H
Mitochondria/ MØ (%)
Intact
Altered
I
Mitochondria in contact with LDs (%)
J

Figure 2: Experimental sepsis increased the frequency of LDs-mitochondria interaction, which was correlated with mitochondria ultrastructural damage. Representative electron micrographs of peritoneal cells from **(A)** control group (Sham) and **(B)** septic group (CLP), 48 h post surgery. **(C)** and **(D)** show LDs number and area per cell, respectively, for each group. A total of 30 electron micrographs per group were evaluated. Data are expressed as mean ± SEM. (*) indicates differences considered significant compared to the control group (unpaired t test), $p < 0.05$. Analysis of number and area were made using the software imageJ® 1.41. In **(E),** measurement of 8-isoprostane levels in supernatants harvested from peritoneal wash of mice submitted or not to mild sepsis (2 punctures in the cecum) and severe (9 punctures), 24h post surgery. For statistical analysis, ANOVA was performed, followed by Bonferroni's post-test. The differences were considered significant when $p \leq 0.05$. The differences in relation to the control group were indicated by (*) n=6 animals per group. **(F, G)** Representative electron micrographs showing mitochondria-LD interaction events. Scale bar**:**1,2 µm. **(H)** Percentage of mitochondria morphologically intact or altered. In **(I),** percentage of mitochondriain interaction with LDs, in each group. In **(J),** percentage of ultrastructurally damaged mitochondria (as illustrated in **G)** in interaction with LDs. Scale bar**:** 1.2 µm. A total of 398 mitochondria were analyzed in the control group and 393 in the CLP. (*) indicates differences considered significant in relation to the control group (unpaired t test), $p < 0.05$. LDs = Lipid droplets, N = nucleus.

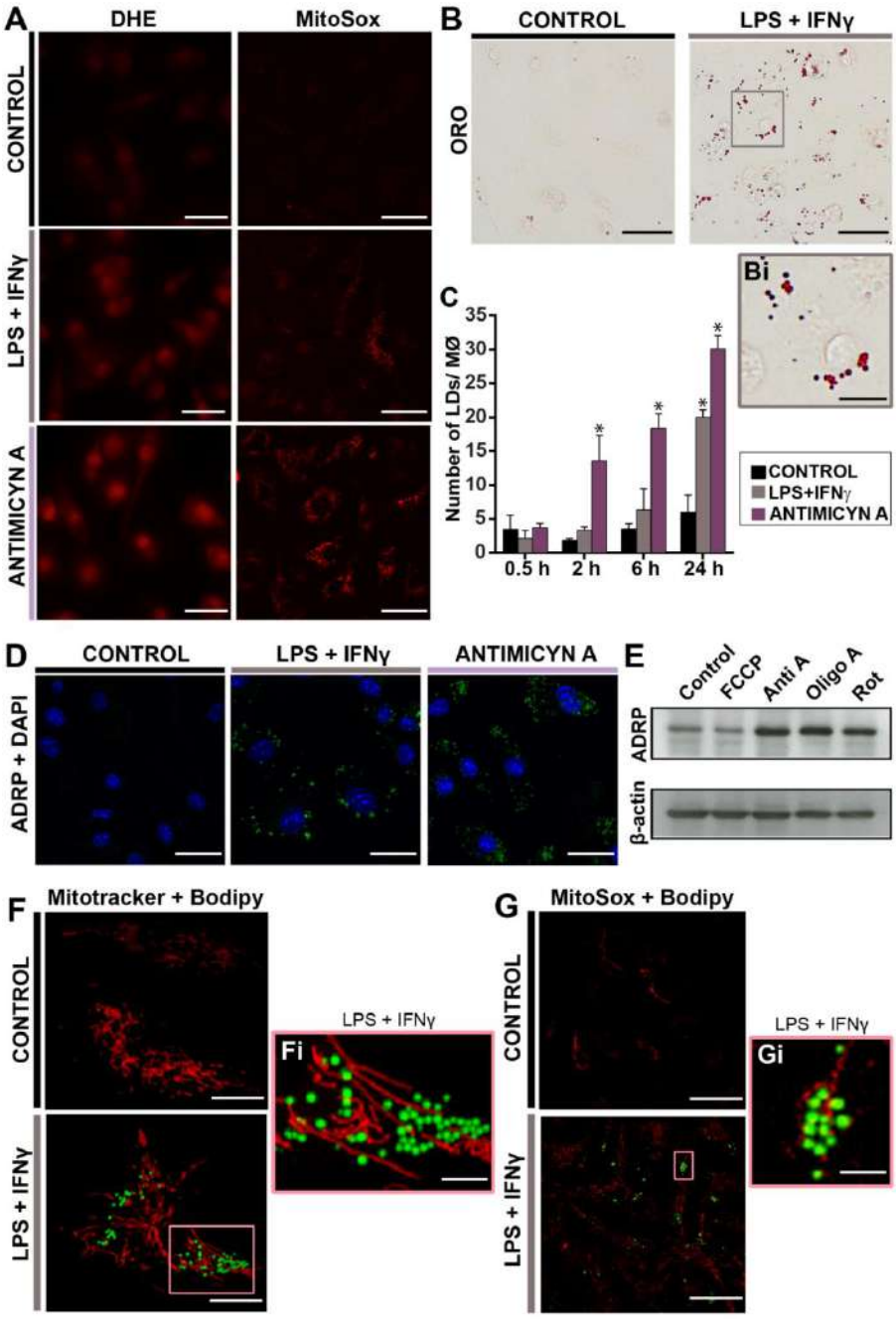
A
DHE
MitoSox
CONTROL
LPS + IFNγ
ANTIMICYN A
B
CONTROL
LPS + IFNγ
ORO
Bi
C
Number of LDs/ MØ
0.5 h
2 h
6 h
24 h
CONTROL
LPS+IFNγ
ANTIMICYN A
D
CONTROL
LPS + IFNγ
ANTIMICYN A
ADRP + DAPI
E
Control
FCCP
Anti A
Oligo A
Rot
ADRP
β-actin
F
Mitotracker + Bodipy
CONTROL
LPS + IFNγ
Fi
G
MitoSox + Bodipy
CONTROL
LPS + IFNγ
Gi

Figure 3: ROS induce lipid droplet (LD) biogenesis in macrophages. (A) Fluorescence microscopy images from dihydroethidium (DHE) or MitoSox Red-labeled BMDMs after 30 min of stimulation by LPS (500 ng/mL) + IFNγ (10 ng/mL) or treatment with Antimicyn A (Anti A, 1µg/mL) (n=3, scale bar: 50 µm). **(B)** Representative images of Oil Red O-labeled LDs (red) of BMDMs after 24h of stimulation (n=3, scale bar: 50 µm). **(Bi)** Higher magnification, scale bar: 3.5 µm. **(C)** Kinetics of LD formation after stimulation (0.5, 2, 6, and 24 h) with LPS + IFNγ or antimicyn A treatment. Data were represented as mean ± SEM, n=3, *$p < 0.05$, ANOVA One-Way followed by Bonferroni's test. **(D)** Representative images of BMDM immunolabeled with anti-Plin2/ADRP antibody (green) after 24h of stimulation (n=3, scale bar: 20µm). Nuclei were visualized by DAPI staining (blue). **(E)** Western blot analysis of Plin2/ADRP and β-actin in BMDMs treated with antimicyn A (Anti A - 1µg/mL), rotenone (rot -1 µg/mL), oligomycin A (Oligo A - 2 µg/mL) or FCCP (1 µM) for 24h. (**F, G)** Representative confocal images from live BMDMs showing **(F, Fi)** Bodipy $^{493/503}$-labeled LDs (green) and Mitotracker CMXRos Red-labeled mitochondria (Scale bar: 10 µm. Higher magnification: scale bar: 3.5 µm). In (**G, Gi**) Bodipy $^{493/503}$-labeled LDs (green) and mitochondrial ROS stained by MitoSox (red) (Scale bar: 20 µm. Higher magnification: scale bar: 6.5 µm. n=3).

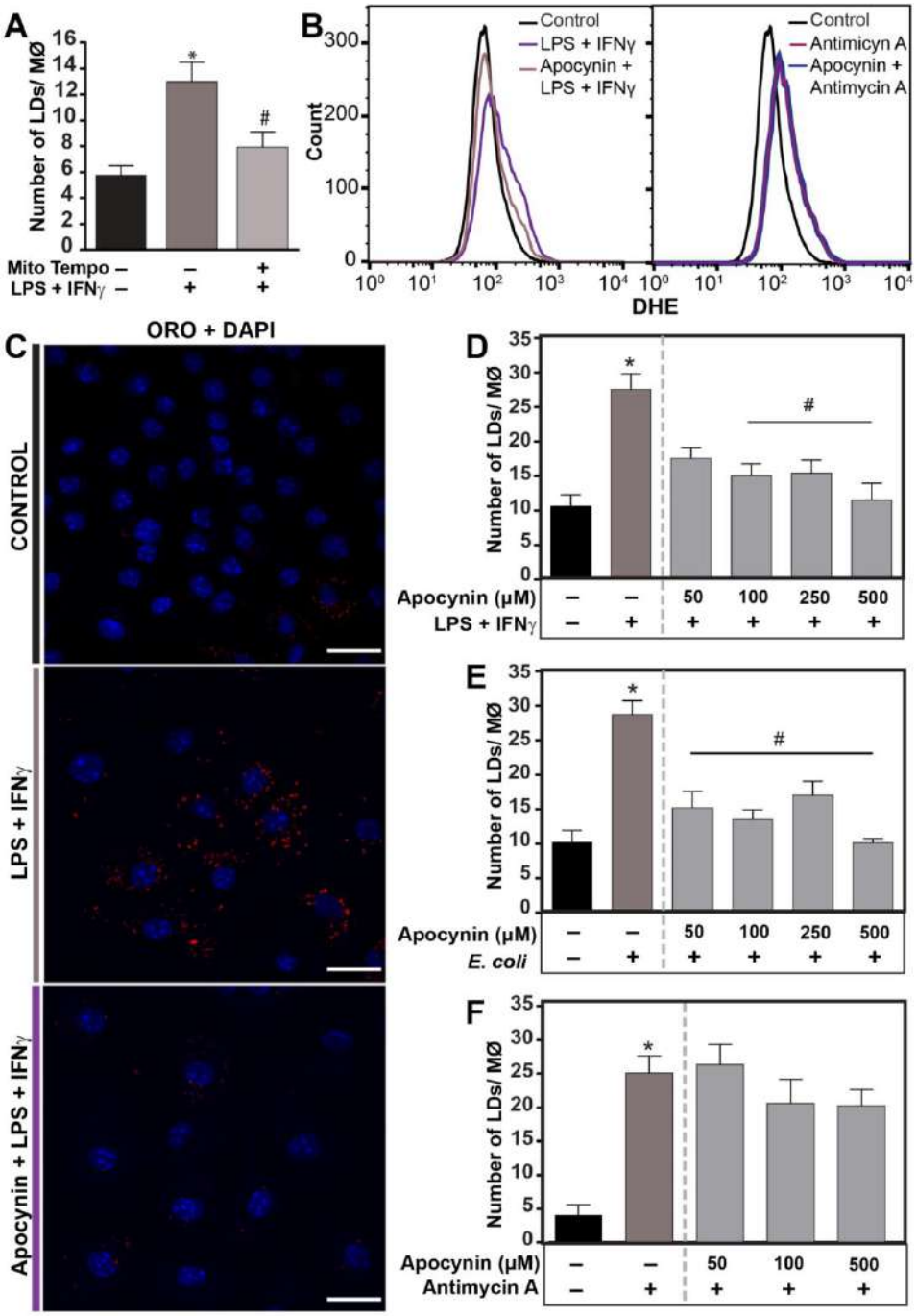
A
Number of LDs/ MØ
Mito Tempo
LPS + IFNγ
B
Control
LPS + IFNγ
Apocynin + LPS + IFNγ
Antimicyn A
Apocynin + Antimycin A
Count
DHE
C
ORO + DAPI
CONTROL
LPS + IFNγ
Apocynin + LPS + IFNγ
D
Apocynin (μM)
E
E. coli
F
Antimycin A

Figure 4: Antioxidants inhibit lipid droplet (LD) biogenesis in proinflammatory macrophages. (A) LD counting in BMDMs after in vitro incubation for 24h with LPS + lFNγ alone or in the presence of Mito-TEMPO (100 μM). **(B)** The MFI for DHE in BMDMs stimulated by LPS + lFNγ or treated with antimicyn A, for 24h, alone or in the presence of apocynin (500 μM). Representative histograms are shown (n=3). **(C)** Confocal images from Oil Red O-labeled LDs (red) in BMDMs. The nucleus was stained by DAPI (blue). (Scale bar: 20μm). **(D-F)** LD counting in BMDMs after 24h of **(D)** LPS + lFNγ stimulation, **(E)** *E. coli* infection or **(F)** antimycin A treatment, with or without pre-treatment with apocynin. **(A, D, E, F)** Cells were stained by Oil Red-O and then 50 cells were counted consecutively under bright field microscope. Each bar represents the mean ± SEM. For statistical analysis it was performed ANOVA, followed by the Bonferroni's post-test. The differences were considered significant when $p \leq 0.05$, n=3. Differences from the respective control groups were indicated by (*) and between the groups stimulated with LPS + lFNγ or infected by *E. Coli* were indicated by (#)

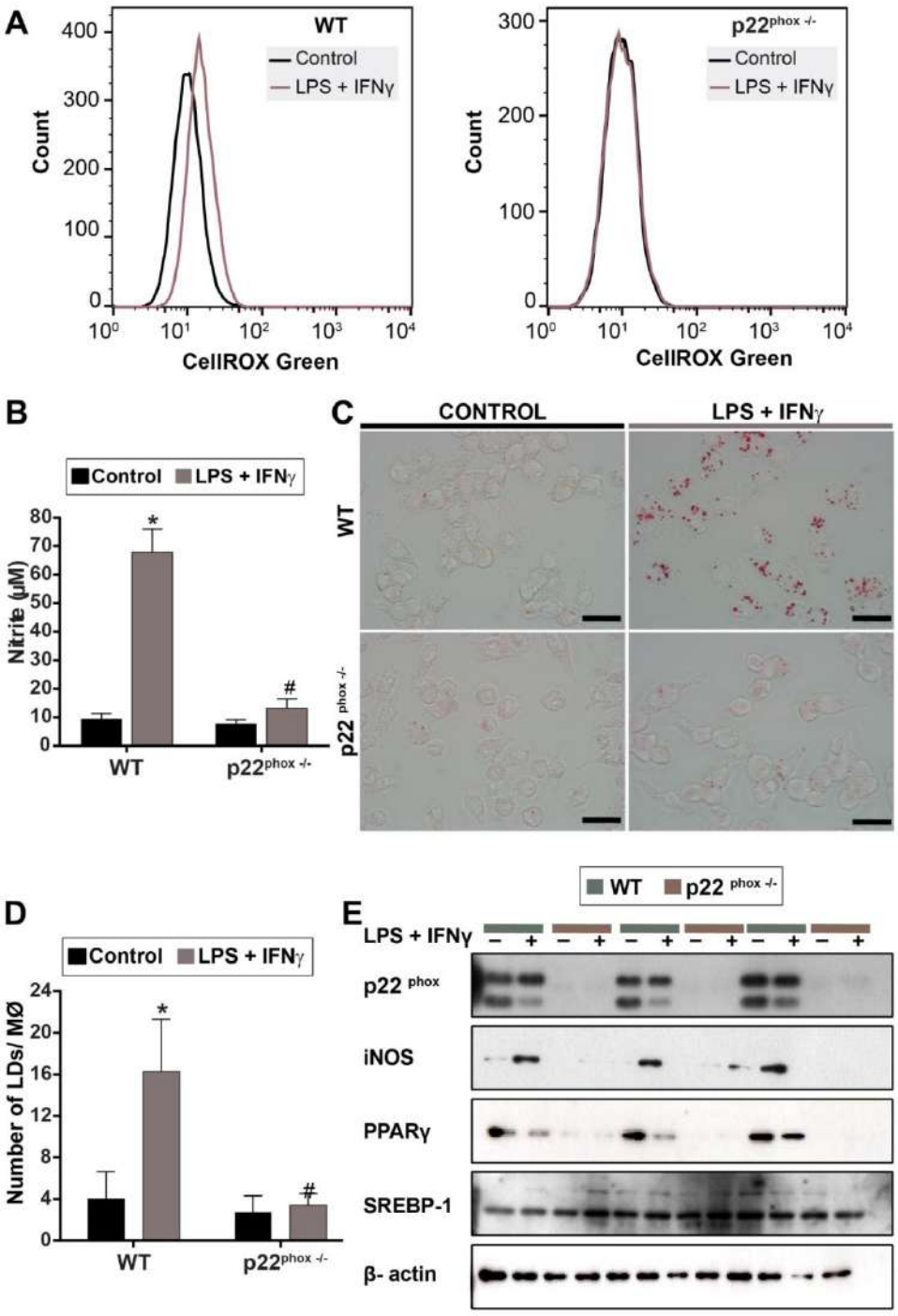
A
WT
Control
LPS + IFNγ
Count
CellROX Green
p22phox -/-
B
Control
LPS + IFNγ
Nitrite (μM)
WT
p22phox -/-
C
CONTROL
LPS + IFNγ
WT
p22 phox -/-
D
Number of LDs/ MØ
E
WT
p22 phox -/-
LPS + IFNγ
p22 phox
iNOS
PPARγ
SREBP-1
β- actin

Figure 5: LD biogenesis induced by LPS + IFNγ is dependent on NADPH oxidase activity. (A) The MFI for Cell Rox green from wild-type and $p22^{phox-/-}$ lBMMs clones stimulated by LPS (500 ng/mL) + IFNγ (10 ng/mL) for 24h. Representative histograms are shown. (n=3). **(B)** Levels of nitrite were measured by Griess method in supernatant of lBMM cultures after 24h of stimulus. Each bar represents the mean ± SEM. Statistical analysis were performed with one-way ANOVA followed by Bonferroni's post-test. The differences were considered significant when $p \leq 0.05$, n=3. Differences from the respective control groups were indicated by (*) and between wild-type stimulated with LPS + IFNγ were indicated by (#) (n=4). **(C)** Representative images of Oil Red O-labeled LDs (red) from wild-type and $p22^{phox-/-}$ lBMMs clones stimulated or not by LPS + IFNγ for 24h (scale bar:20μm). **(D)**LDs counting in wild-type and $p22^{phox-/-}$ lBMMs clones stimulated or not by LPS + IFNγ for 24 h. After Oil Red-O staining 50 cells were counted consecutively under bright field microscope. Each bar represents the mean ± SEM. Statistical analysis were performed ANOVA followed by the Bonferroni's post-test. The differences were considered significant when $p \leq 0.05$, n=3. Differences from the respective control groups were indicated by (*) and between wild-type stimulated with LPS + IFNγ were indicated by (#). **(E)** Western blot analysis for $p22^{phox}$, iNOS, PPAR-γ, SREBP-1and β-actin. n=3.

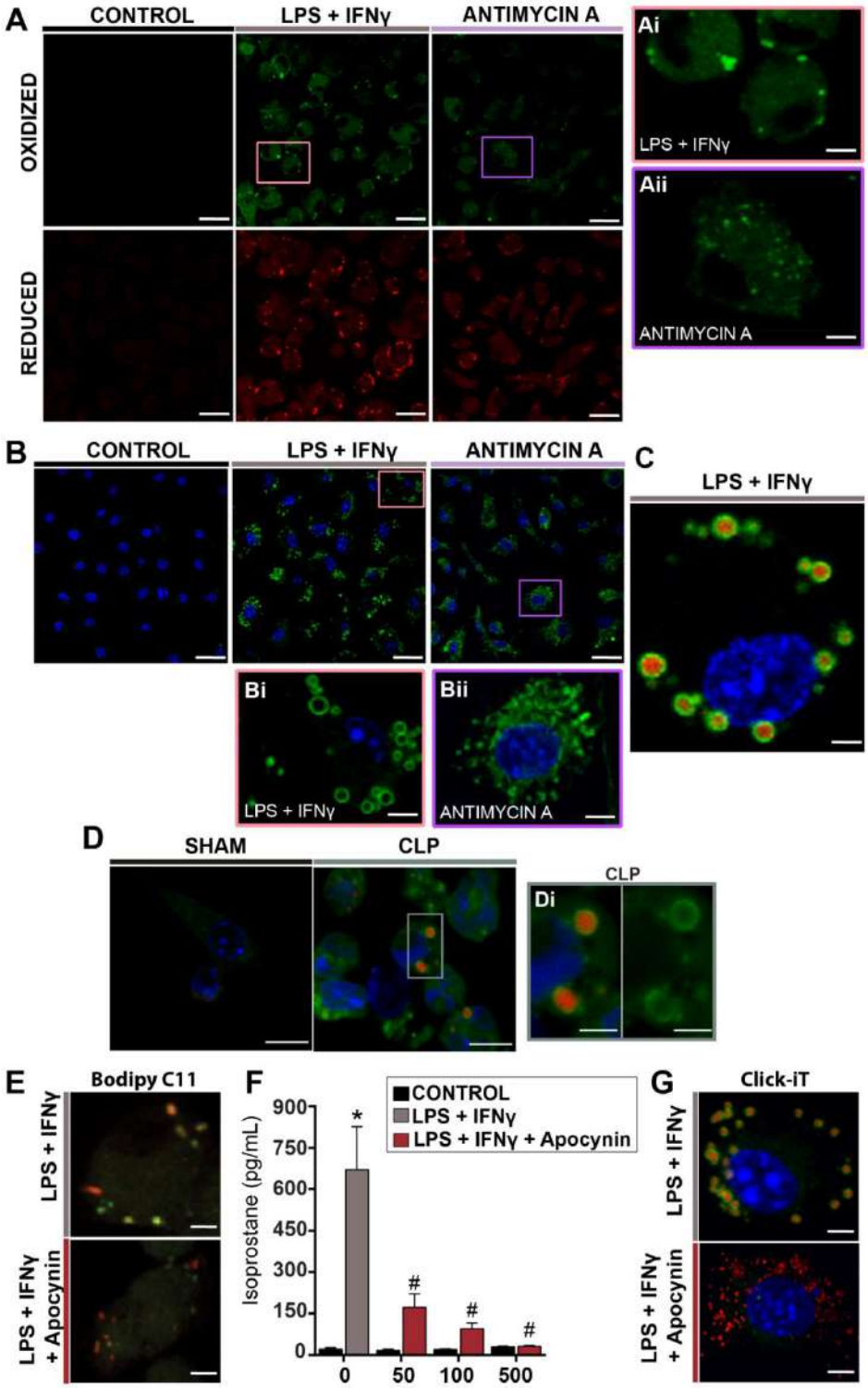
A
CONTROL
LPS + IFNγ
ANTIMYCIN A
OXIDIZED
REDUCED
Ai
LPS + IFNγ
Aii
ANTIMYCIN A
B
CONTROL
LPS + IFNγ
ANTIMYCIN A
Bi
LPS + IFNγ
Bii
ANTIMYCIN A
C
LPS + IFNγ
D
SHAM
CLP
CLP
Di
E
Bodipy C11
LPS + IFNγ
LPS + IFNγ + Apocynin
F
CONTROL
LPS + IFNγ
LPS + IFNγ + Apocynin
Isoprostane (pg/mL)
900
750
600
450
300
150
0
*
#
#
#
0
50
100
500
G
Click-iT
LPS + IFNγ
LPS + IFNγ + Apocynin

Figure 6: Lipid and protein content of LDs are susceptible to oxidation. (A, E) Representative confocal images from live BMDMs stained with lipid peroxidation sensor Bodipy$^{581/591}$-C11. Oxidized probe emission in green while reduced form in red. (n=3, scale bar: 20µm. **Ai, Aii** Higher magnification - scale bar: 10 µm).**(B, G**) Representative confocal images from BMDMs stained by Click-iT® Lipid Peroxidation Imaging Kit for detection of lipid peroxidation-derived protein modifications (green). Nuclei were visualized by DAPI staining (blue). (n=3, scale bar: 20µm. **Bi, Bii** Higher magnification - scale bar: 10 µm). Counterstaining with neutral lipid probe Nile red was performed in **(C)**. Scale bar: 5 µm. **(D, Di)** Lipid peroxidation-derived protein modifications detected in cells from peritoneal wash of septic mice 48 h after mild CLP model. **(E)** Measurement of 8-isoprostane levels in supernatants harvested from BMDM cultures. For statistical analysis ANOVA was performed followed by Bonferroni's post-test. The differences were considered significant when $p \leq 0.05$. n=4. The differences related to the control group were indicated by (*) and in relation to the groups stimulated with LPS + lFNγ were indicated by (#).

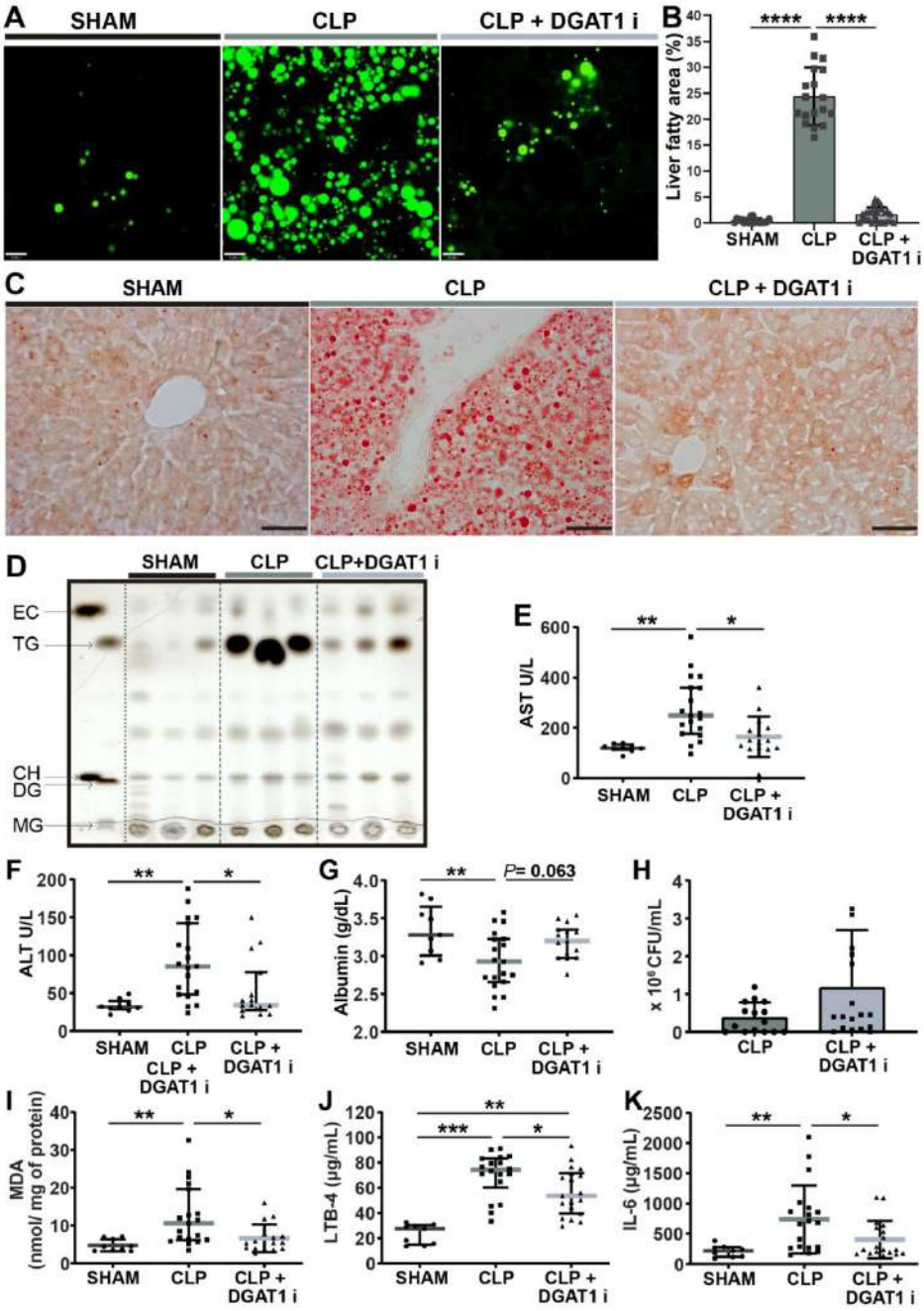
A
SHAM
CLP
CLP + DGAT1 i
B
Liver fatty area (%)
****
****
SHAM
CLP
CLP + DGAT1 i
C
SHAM
CLP
CLP + DGAT1 i
D
SHAM
CLP
CLP+DGAT1 i
EC
TG
CH
DG
MG
E
AST U/L
**
*
SHAM
CLP
CLP + DGAT1 i
F
ALT U/L
**
*
SHAM
CLP
CLP + DGAT1 i
G
Albumin (g/dL)
**
P= 0.063
SHAM
CLP
CLP + DGAT1 i
H
x 10⁶ CFU/mL
CLP
CLP + DGAT1 i
I
MDA (nmol/ mg of protein)
**
*
SHAM
CLP
CLP + DGAT1 i
J
LTB-4 (µg/mL)
**
***
*
SHAM
CLP
CLP + DGAT1 i
K
IL-6 (µg/mL)
**
*
SHAM
CLP
CLP + DGAT1 i

Figure 7: Oral treatment with DGAT1 inhibitor reduces hepatic LD accumulation, tissue lipid peroxidation and prevents sepsis-induced liver dysfunction. Sham or septic (2 punctures in the cecum) mice were orally treated or not with A922500 (DGAT1 inhibitor, 3mg/kg) and euthanized48h after surgery **(A)** Hepatic LD deposition *in vivo* evidenced by intravital confocal microscopy after Bodipy$^{493/503}$ staining (green). **(B)** Percentage of bodipy fluorescence area (LDs) per field. The graph shows averages of the analyzed images of 3 animals per group. For statistical analysis, ANOVA was performed followed by Bonferroni's post-test. The differences were considered significant when $p \leq 0.05$. **(C)** Representative micrograph from cryosections of liver tissue stained with Oil Red O (red). Scale bar: 80 µm. **(D)** Representative thin layer chromatography (TLC) of liver neutral lipids extract (n=6 mice/group). Standards: Cholesterol ester (CE), cholesterol (C), triacylglycerol (TG), diacylglicerol (DG) and monoacylglicerol (MG). **(E)** Serum level of oxaloacetic transaminase (AST), **(F)** pyruvic transaminase (ALT) and **(G)** albumin were assayed at 48h after CLP. **(H)** Bacterial load was assayed at 48h after CLP. **(I)**Hepatic MDA content levels were assayed at 48h after CLP. Measurement of **(J)** Leukotriene B_4 (LTB_4) and **(K)** IL-6 levels in supernatants harvested from peritoneal wash of mice submitted or not to CLP. For statistical analysis of **(E-K)**, ANOVA were performed followed by Bonferroni's post-test. (Sham n=9, CLP n=19, CLP-DGAT1-i n=18, $*p < 0.05$, $**p < 0.01$, $***p < 0.001$).

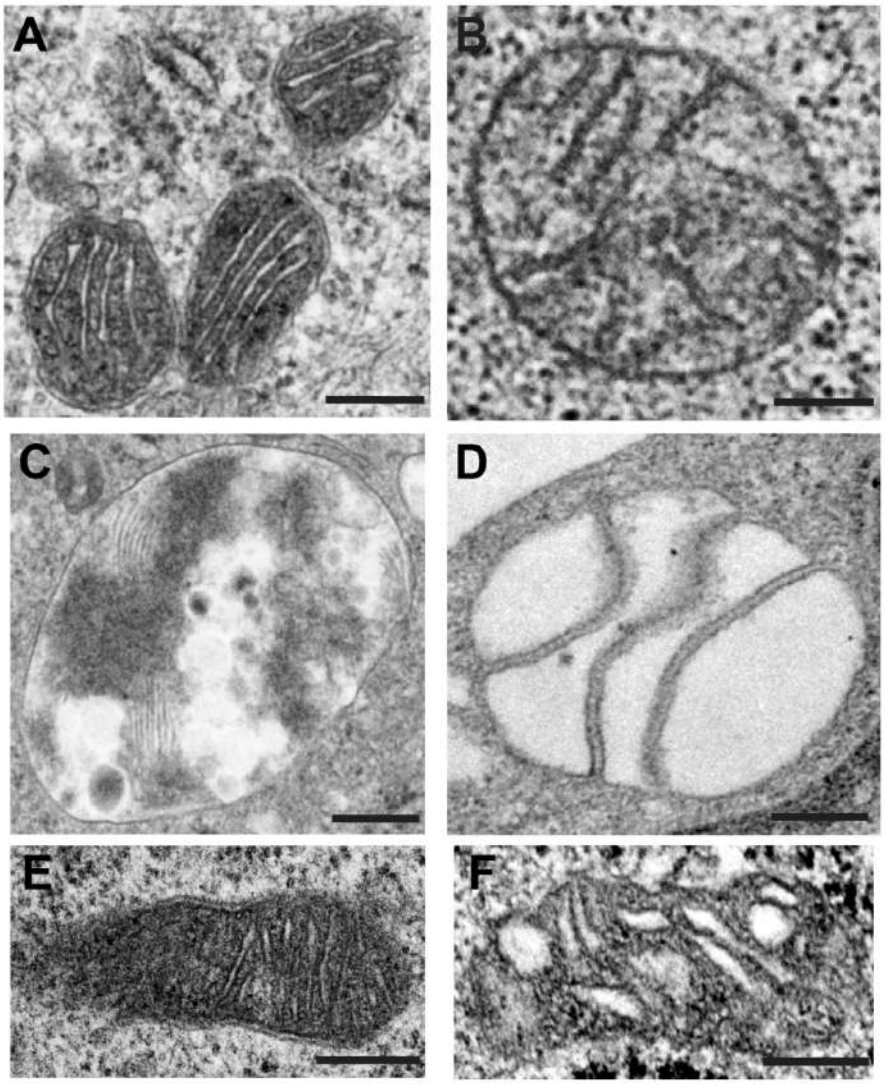

Figure S1: Mitochondrial ultrastructural changes induced by sepsis in peritoneal cells. **(A-F)** Representative electron micrographs of mitochondria highlighting the ultrastrutural parameters used to classify mitochondria as **(A)** intact or **(B-F)** altered. The major mitochondrial changes were: **(B-D)** swelling; **(B, D)** reduction in the number of mitochondrial cristae; **(C)** disarrangement of the mitochondrial cristae; **(D)** emptying of the mitochondrial matrix; **(E)** disruption of the mitochondrial envelope (arrowheads), and **(F)** vacuolization (asteriscs). Note in **(F)** that the mitochondrion is in process of degeneration. Cells were fixed and processed for transmission electron microscopy as before (Melo et al., 2006). Scale bar: **(A, B)** 400 nm, **(C, D)** 1.5 μm, **(E, F)** 350 nm.

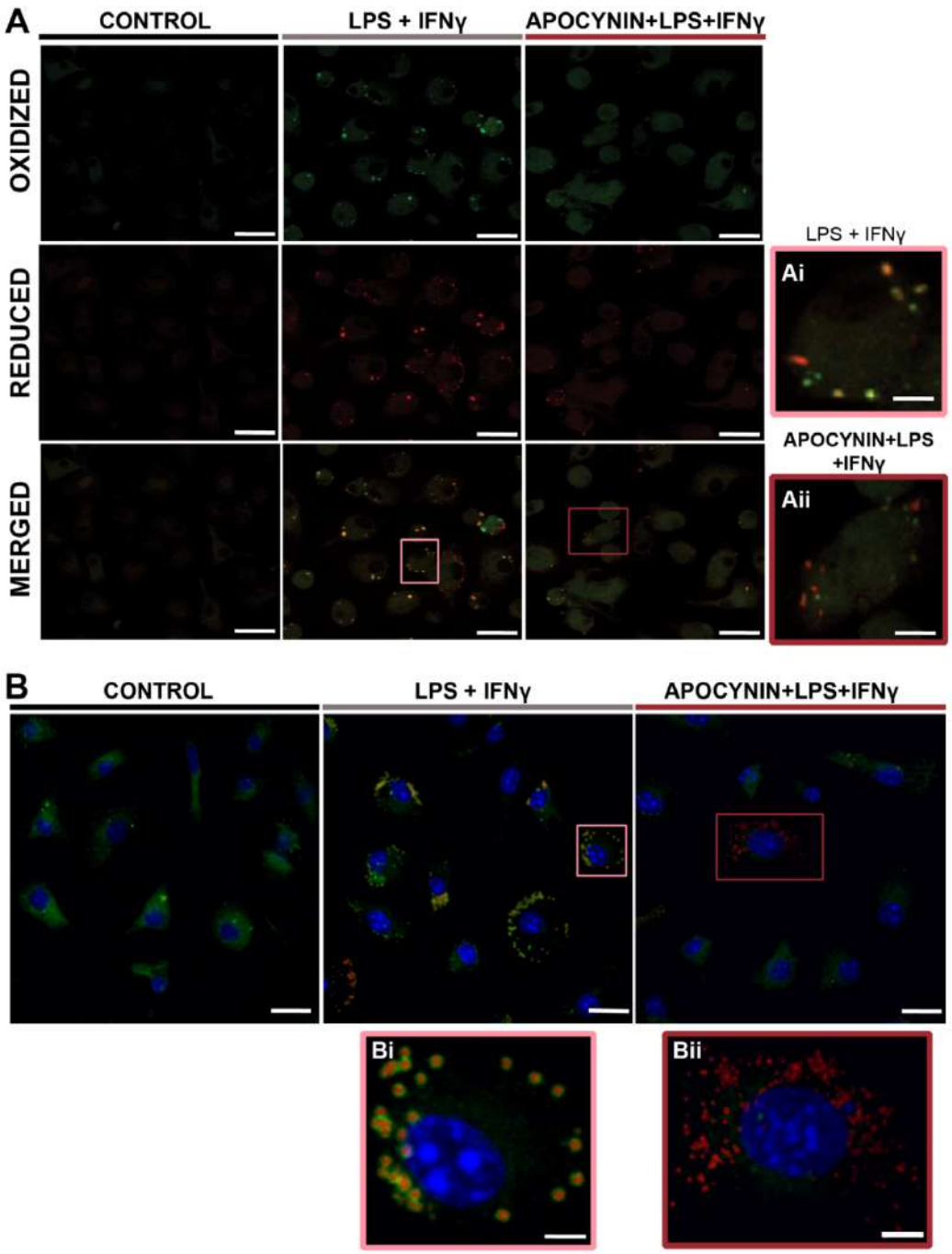

Figure S2: Apocynin inhibit the oxidation of lipid and protein content of LDs in macrophages. (A) *Full panel of* representative confocal images from live BMDMs stained with lipid peroxidation sensor Bodipy$^{581/591}$-C11. Oxidized probe fluoresce in green while in reduced form fluoresce in red. (n=3, scale bar: 20 μm. **Ai, Aii** - Higher magnification - scale bar: 10 μm).**(B**) Full panel of representative confocal images from BMDMs stained by Click-iT® Lipid Peroxidation Imaging Kit for detection of lipid peroxidation-derived protein modifications (green) Counterstaining with neutral lipid probe Nile red. Nuclei were visualized by DAPI staining (blue). (n=3, scale bar: 20 μm. **Bi, Bii -** Higher magnification - scale bar: 10 μm).

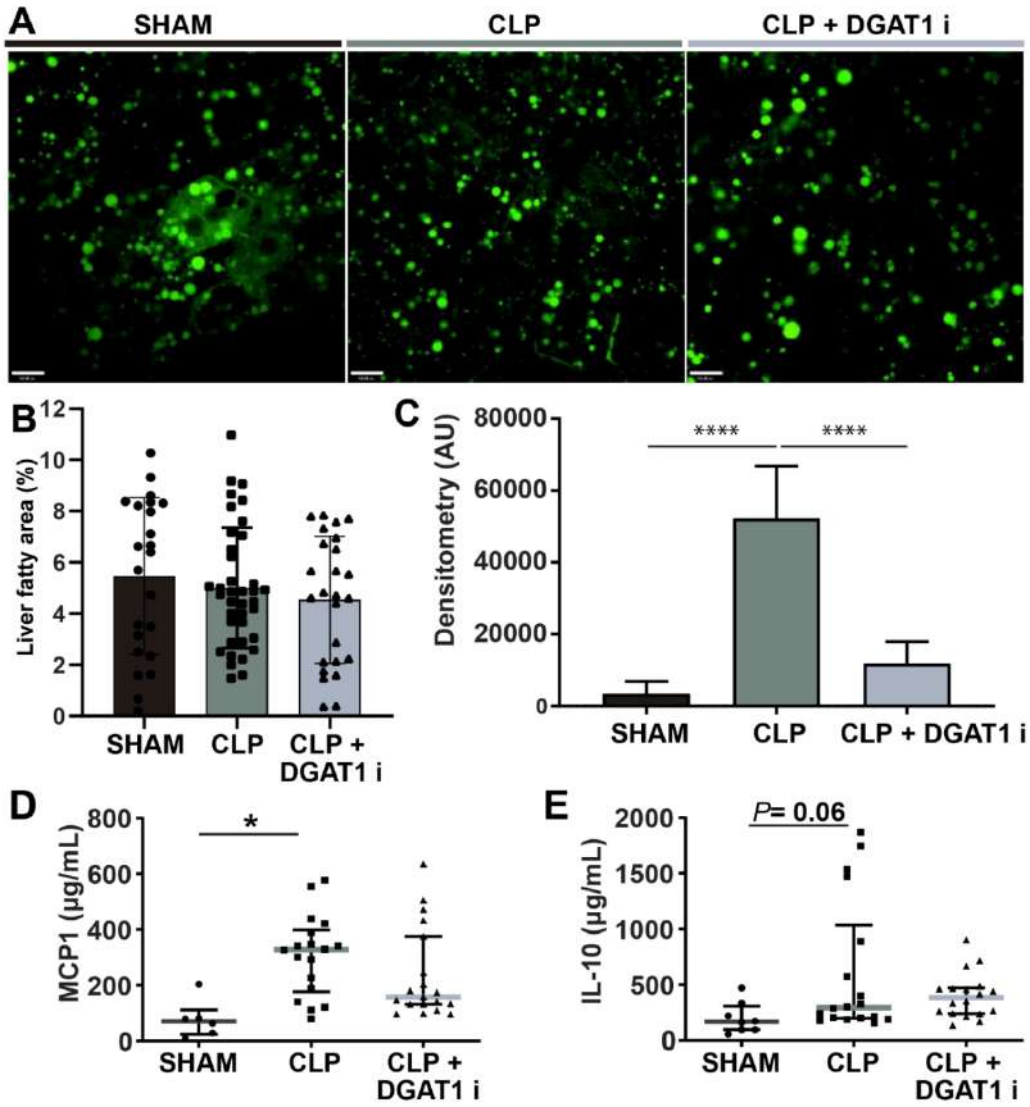

Figure S3: Effects of oral treatment with DGAT1 inhibitor in septic mice. Sham or septic (2 punctures in the cecum) mice were orally treated or not with A922500 (DGAT1 inhibitor, 3mg/kg) and euthanized 6h after surgery **(A)** Hepatic LD deposition *in vivo* evidenced by intravital confocal microscopy after Bodipy $^{493/503}$staining (green). **(B)** Percentage of bodipy fluorescence area (lipid droplets) per field. The graph shows averages of the analyzed images of 3 animals per group. **(C)** Densitometry from TLC of liver neutral lipids extract collect 48 h post surgery (n=6 mice/group). Measurement of **(D) MCP-1** and **(E)** IL-10 levels in supernatants harvested from peritoneal wash of mice submitted or not to CLP. For statistical analysis of **(B-E)**, ANOVA were performed followed by Bonferroni's post-test. *$p < 0.05$, **$p < 0.01$, ***$p < 0.001$. For **(D, E)** sample were collect 48 h post surgery from Sham group n=9 mice, CLP n=19 mice, CLP-DGAT1-i n=18 mice